U.PORTO

FEUP FACULDADE DE ENGENHARIA
UNIVERSIDADE DO PORTO

DYNAMIC BEHAVIOUR AND FATIGUE ASSESSMENT OF RAILWAY BRIDGE DECK SLABS

Joel Pedro da Conceição Malveiro

2017

A dissertation presented to the Faculty of Engineering of the University of Porto
for the degree of Doctor in Civil Engineering.

Supervisor: Prof. Rui Calçada (FEUP, Portugal)
Co-Supervisor: Prof. Carlos Sousa (FEUP, Portugal)

POPH PROGRAMA OPERACIONAL POTENCIAL HUMANO
QREN QUADRO DE REFERÊNCIA ESTRATÉGICO NACIONAL PORTUGAL 2007.2013
GOVERNO DA REPÚBLICA PORTUGUESA
UNIÃO EUROPEIA Fundo Social Europeu

"All of our days are numbered.
We cannot afford to be idle.
To act on a bad idea is better than to not act at all.
Because the worth of the idea never becomes apparent,
until you do it.
Sometimes, this idea can be the smallest thing in the world,
a little flame that you hunch over and cup with your hand...
and pray will not be extinguished
by all the storm that howls about it.
If you can hold on to that flame,
great things can be constructed around it...
things that are massive and powerful and world changing.
All held up by the tiniest of ideas."

Nick Cave (in 20,000 days on Earth)

"Há tempo para tudo e há um tempo para tudo."

Maria da Conceição Malveiro

Aos meus pais e avó

Abstract

A considerable growth in the railway system has been made during the last decade, either due to the introduction of new high-speed lines, and the modernisation of the existing ones, or due to the improvement of freight trains service on the classical network. This development only has been possible owing the construction of a significant number of bridges and viaducts, where distinct structural solutions have been implemented in its construction. Among them are I-shaped or U-shaped girders connected on the top by a reinforced concrete slab. This type of structures is related to the use of prestressed concrete or steel plates as main girders in the longitudinal direction. Furthermore, these reinforced concrete slabs present a low thickness and a low reinforcement rate, reason why they appear as being the most susceptible structural element to the occurrence of cracking and consequently to fatigue damage.

Since a high number of loading cycles can occur, due to the passage of railway traffic at different speeds, which typically exceeds 10 million over the total life of the structure, this thesis focuses on the evaluation of the local behaviour of these reinforced concrete slabs in railway viaducts. The analysis of this local behaviour reveals to be more complex rather than the analysis of the main girders, the latter associated with a global behaviour of the structure and usually being dominated by the first global vibration modes. Bearing this in mind, this thesis aims at giving a contribution to understand the real performance of this structural element. Particular attention was given to the development and validation of numerical models, based on the measurement of real responses, for the calculation of internal efforts in the slab. A realistic estimate of these internal efforts is a paramount step for carrying out a fatigue assessment of the structure.

Two different railway viaducts, with typical solutions widely employed in the construction of railway structures, are considered in the present thesis: i) a U-shaped precast and

prestressed concrete girder with an upper slender reinforced concrete slab, forming a single-cell box girder; ii) a steel-concrete composite structure, composed by two I-shaped steel plate girders connected on the top by a reinforced concrete slab.

In both cases, detailed numerical analyses are performed. For that purpose, three-dimensional numerical models of the viaducts and trains are used. A calibration methodology of numerical models is used, taking into account an optimisation method through a genetic algorithm and based on modal information experimentally obtained. The natural frequencies and mode shapes, both related to the global behaviour of the structures and to the local behaviour of the upper slabs, obtained via ambient vibration tests, are compared with the calculated ones.

Dynamic numerical responses, taking into account the interaction between the train and the bridge, are experimentally validated through the comparison with the real structural performances that are measured under railway traffic. Throughout the thesis, the influence of some relevant parameters is analysed and discussed, such as the modal damping coefficients, the stiffness of the bearings, the track irregularities, the train speed and the cut-off frequency considered in the analysis of each response variable.

In order to get more realistic results, a static correction procedure is employed, and validated, to account for the static contribution of vibration modes of higher frequencies, which are not explicitly considered in the basic modal-superposition method (used to solve the dynamic problem). Concerning the modal damping coefficients of local vibration modes of the RC deck slabs, a methodology based on the measurement of the slab's dynamic responses under railway traffic is implemented to identify accurate damping values, related to the vibration levels corresponding to the passage of trains, instead of using the values provided by ambient vibration tests.

Finally, based on the results of different train-bridge interaction dynamic analyses, the assessment of the fatigue resistance in the transverse reinforcement bars of upper deck slabs is performed. Taking into account the effects of the aforementioned parameters, the fatigue damage is calculated as well as the required reinforcement area to get a fatigue life equal to 100 years.

Resumo

Na última década tem-se registado um crescimento considerável no que diz respeito ao transporte ferroviário, seja devido ao desenvolvimento de novas linhas de alta velocidade, ou mesmo a modernização das existentes, ou devido à melhoria do serviço de transporte de mercadorias nas linhas convencionais. Este desenvolvimento só tem sido possível com recurso à construção de um significativo número de pontes e viadutos, nas quais diversas soluções estruturais têm sido empregues. Entre elas há a destacar a construção de tabuleiros com vigas I ou vigas U, ligadas superiormente por lajes de betão armado. Este tipo de estruturas está associado ao uso de longarinas de betão pré-esforçado ou vigas metálicas na direção longitudinal. Para além disso, estas lajes de betão armado apresentam uma espessura reduzida e uma baixa taxa de armadura, razão pela qual aparecem como sendo o elemento mais suscetível à ocorrência de fendilhação e, consequentemente, de dano por fadiga.

Uma vez que estas estruturas podem estar sujeitas a um elevado número de ciclos de carregamento, que normalmente excede os 10 milhões de ciclos ao longo de toda a vida da estrutura, a presente tese foca-se na avaliação do comportamento local destas lajes de betão armado em tabuleiros ferroviários. A análise deste comportamento local revela-se mais complexa do que a análise das vigas principais, estas últimas associadas a um comportamento global da estrutura e geralmente dominado pelos primeiros modos de vibração globais. Neste sentido, esta tese tem como objetivo contribuir para a interpretação do desempenho real deste elemento estrutural. Foi dada particular atenção ao desenvolvimento e validação de modelos numéricos, com base em respostas realmente medidas, a usar no cálculo dos esforços internos da laje. Uma estimativa realista destes esforços internos é um passo fundamental para uma avaliação cuidada da fadiga da estrutura.

Dois viadutos ferroviários, com soluções amplamente empregues na construção deste tipo de estruturas, são analisados no presente estudo: i) viga U pré-fabricada e pré-esforçada, a

qual serve de suporte a uma esbelta laje de betão armado, formando assim uma viga em caixão unicelular; ii) ponte mista aço-betão composta por duas vigas I metálicas ligadas superiormente por uma laje de betão armado.

Em ambos os casos procedeu-se à realização de cuidadas análises numéricas. Para tal, recorreu-se ao uso de complexos modelos tridimensionais tanto das pontes como do comboio. A calibração dos modelos numéricos foi realizada com base na aplicação de um algoritmo genético e recorrendo a informação modal obtida experimentalmente. Quer as frequências naturais quer a configuração dos modos de vibração, relativas tanto ao comportamento global da estrutura como ao comportamento local da laje, foram obtidas através de ensaios de vibração ambiental e comparadas com os resultados obtidos por via numérica.

As respostas dinâmicas obtidas por via numérica, tendo em conta a interação entre ponte e comboio, foram validadas através da comparação com as respostas medidas experimentalmente sob ação de tráfego ferroviário. De forma a otimizar esta comparação, ao longo deste trabalho foi avaliada e discutida a influência de diversos parâmetros, tais como os coeficientes de amortecimento modais, a rigidez dos aparelhos de apoio, as irregularidades da via, a velocidade do comboio e a frequência de corte a considerar nas demais análises.

De forma a obter resultados mais realistas, procede-se à implementação e validação de um procedimento de correção estática de forma a assegurar pelo menos a contribuição estática dos modos de vibração com frequências mais elevadas, os quais não são explicitamente considerados na usual aplicação do método de sobreposição modal (usado para a resolução do problema dinâmico). No que diz respeito aos coeficientes de amortecimento dos modos de vibração locais, foi implementada uma metodologia, baseada na medição da resposta dinâmica da laje sob acção de tráfego ferroviário, com vista à identificação de valores mais precisos, os quais estão relacionados com níveis de vibração correspondentes à passagem de comboios em vez de recorrer a valores associados a níveis de vibração ambiental.

Finalmente, com base nos resultados das demais análises dinâmicas com interação ponte-comboio, é realizada a avaliação da resistência à fadiga da armadura transversal da laje superior do tabuleiro. Tendo em conta os efeitos dos parâmetros anteriormente referidos, procede-se ao cálculo do dano por fadiga assim como da área de armadura necessária para obter uma vida útil de fadiga igual a 100 anos.

List of Publications

The following publications were performed throughout the development of the present work:

International scientific journals

- Malveiro, J., Ribeiro, D., Calçada, R., Delgado, R. (2014). Updating and validation of the dynamic model of a railway viaduct with precast deck. Structure and Infrastructure Engineering, 10 (11), 1484-1509.
- Malveiro, J., Sousa, C., Ribeiro, D., Calçada, R. (2017). Impact of track irregularities and damping on the fatigue damage of a railway bridge deck slab. Structure and Infrastructure Engineering, DOI:10.1080/15732479.2017.1418010 (published online).
- Malveiro, J., Ribeiro, D., Sousa, C., Calçada, R. (2018). Model updating of a dynamic model of a composite steel-concrete railway viaduct based on experimental tests. Engineering Structures, 164, 40-52.

International conference proceedings

- Malveiro, J., Ribeiro, D., Calçada, R. (2011). Dynamic monitoring of a railway viaduct with precast deck. In EVACES'11 – International Conference on Experimental Vibration Analysis for Civil Engineering Structures. Varenna, Italy.
- Malveiro, J., Ribeiro, D., Calçada, R., Delgado, R. (2013). Updating and validation of the finite element model of a railway viaduct based on dynamic tests. In IOMAC'13 – 5th International Operational Modal Analysis Conference. Guimarães, Portugal.

- Ribeiro, D., Malveiro, J., Meixedo, A., Calçada, R., Delgado, R. (2014). Calibração e validação experimental de modelos dinâmicos de pontes ferroviárias. In CILAMCE2014 – XXXV Iberian Latin American Congress on Computational Methods in Engineering. Fortaleza, Brasil.
- Malveiro, J., Sousa, C., Ribeiro, D., Calçada, R. (2015). Dynamic analysis for fatigue assessment of reinforced concrete slabs in railway viaducts. In MSLB2015 – Multi-span Large Bridges Conference. Porto, Portugal.
- Malveiro, J., Sousa, C., Ribeiro, D., Calçada, R. (2016). Influence of track irregularities in the global and local dynamic response of precast decks under railway traffic loads. In IABMAS2016 – 8th International Conference on Bridge Maintenance, Safety and Management. Foz do Iguacu, Brasil.

National conference proceedings

- Malveiro, J., Ribeiro, D., Sousa, C., Calçada, R, (2011). Identificação experimental dos parâmetros modais de um viaduto ferroviário com tabuleiro pré-fabricado. In ASCP'11 – Congresso Nacional sobre Segurança e Conservação de Pontes. Coimbra, Portugal

Acknowledgments/Agradecimentos

I would like to take this opportunity to express my gratitude to everyone who supported me throughout this academic accomplishment, which was only possible with their powerful guidance, invaluably constructive criticism and friendly advices during these years. To all of them I convey my sincere thanks:

To my supervisor, Professor Rui Calçada, to whom I am grateful for the encouragement and support given to develop this work. His enthusiasm about the railways and his huge knowledge about the dynamic behaviour of structures guided me since my first steps in this research field;

To my co-supervisor, Professor Carlos Sousa, for all the dedication, availability and willingness to help during these years. I am also really thankful for all the teachings in the area of the fatigue of structures. His clarity and pragmatism were undoubtedly strong pillars in the different stages of this work and his incentive words, especially to overcome the most difficult moments and tasks during this thesis, will never be forgotten;

To both of them I would like to thank for providing me with all the conditions to develop this work, for all the technical discussions and teachings related with all the covered topics and for the accurate revision of this document;

To my colleague and friend Diogo Ribeiro that highly contributed to my scientific growth in the areas of numerical and experimental characterisation of the dynamic behaviour of structures. I would also to thank all the help and fruitful discussions during the work developed together;

To the Portuguese Foundation for Science and Technology (FCT), for the funding of this work through the research grant SFRH/BD/79816/2011;

To IP – Infraestruturas de Portugal, in particular to Eng. Hugo Patrício and Eng. Francisco Ganhão, for providing me all the data about the case studies and giving me the opportunity and conditions to carry out all the experimental tests;

To LESE, the Structural and Seismic Engineering Laboratory research group of CONSTRUCT - Institute of R&D in Structures and Construction, for providing me all the equipment and human resources that I needed in the experimental campaigns;

To Nuno Pinto for all his patience, availability and knowledge to support me in the development of the monitoring systems. The good mood that is also crucial to spend several days in experimental campaigns will never be forgotten;

To my friends and colleagues André Paixão, Carlos Albuquerque, Diogo Ribeiro, Guilherme Alencar, João Xico, Ladislao Melo, Marco Fonseca and Nuno Ribeiro for spending their time to help me during the experimental campaigns. I regret the times that I could not offer them even a proper dinner as gratification at the end of those hard days;

To the other friends and colleagues from our research group for their availability to share their experience and knowledge, for all the discussions and for all the awesome moments spent together: Alejandro de Miguel, Andreia Meixedo, Cristiana Bonifácio, Cristina Ribeiro, Joana Delgado, João Rocha, Nuno Santos, Pedro Jorge, Pedro Montenegro and Sérgio Neves;

To the other friends and colleagues whom I had the great pleasure to meet at FEUP: Adam Zsarnoczay, André Monteiro, Despoina Skoulidou, Diogo Figueira, Jiang Yadong, José Pedro Silva, Luis Macedo, Mário Marques, Miguel Araújo, Miriam Lopez, Nuno Pereira and Rui Barros;

To all my colleagues at Network Rail for the warm welcome to a new country and work environment. Their enthusiastic words when, for several times, found me working at the office on weekends, writing this thesis, were a huge support to carry on. I would also like to thank Alex Allen, Benjamin Lewis, João Rocha, Milad Behbin, Richard Crew and Stephen Delderfield for taking the time to review all the grammar in this document;

Aos vários amigos que tão bem me acolheram nesta minha mudança para Londres: João, Joana, David, Miguel, Susana, Marta, Leandro, Patrícia e Daniel. Apesar da minha constante

ausência nos tempos em que me dedicava à escrita desta tese, foram incansáveis em me incluir nas suas atividades, a mostrar o seu apoio, atenção e encorajamento;

A todos os meus amigos que, mais perto ou mais longe, de forma mais ou menos intensa, sempre estiveram a meu lado, a demonstrar o seu carinho, força e motivação. Peço desculpa pela minha ausência mas cá estarei para vos recompensar. Uma palavra especial para a Ana, Isa e Pedro, pelo seu apoio incondicional na altura de decidir avançar para estes anos de investigação.

Aos meus irmãos Carlos e Alberto, à minha cunhada Paula e às minhas sobrinhas Ana, Paula e Jéssica. Foi doloroso este tempo longe de vós, especialmente ver as pequeninas crescer à distância. Mas muito obrigado por cada abraço reconfortante no regresso a casa, pelas gargalhadas cativantes e por fazerem sentir que, quando estamos juntos, nem o tempo nem a distância passou por nós.

Finalmente, mas de todo menos importante, aos meus pais e à minha avó. Apesar dos momentos difíceis por que ambos passámos nos últimos dois anos, foram incansáveis em me transmitir força, confiança e determinação. Muitas das vezes quando devia ser eu a estar ao lado deles… peço-lhes também desculpa pela minha ausência e pelos momentos de menor paciência da minha parte. Não há definitivamente muitas palavras para descrever o seu apoio. O seu amor é incondicional e são sem dúvida os grandes responsáveis por tudo o que tenho alcançado, razão pela qual lhes dedico inteiramente esta tese.

Table of contents

List of symbols and abbreviations

Symbols and abbreviations are defined upon their first appearance in the text. The following list is presented in alphabetic order and does not include some symbols and notations of a secondary order.

ABBREVIATIONS

2D	Two Dimensional
3D	Three Dimensional
AP	Alfa-Pendular
CWR	Continuously Welded Rails
D.I.	Newmark's Direct Integration method
DOF	Degree Of Freedom
EFDD	Enhanced Frequency Domain Decomposition
EMAC	Energy-based Modal Assurance Criterion
FDD	Frequency Domain Decomposition
FE	Finite Element
FL	Fatigue Life
FRA	American Federal Railroad Administration
HSLM	High Speed Load Models
IEPE	Integrated Electronic Piezoelectric
LVDT	Linear Variable Differential Transformer
M.S.	Modal-Superposition method
MAC	Modal Assurance Criterion
NI	National Instruments
PP	Peak Picking
PSD	Position Sensitive Detector
PSD	Power Spectral Density
RC	Reinforced Concrete

RT	Real Trains
SLS	Serviceability Limit States
SNCF	Société Nationale des Chemins de Fer Français
SSI-COV	COVariance-driven Stochastic Subspace Identification
SSI-DATA	DATA-driven Stochastic Subspace Identification
TBI	Train-Bridge Interaction
TSI	Technical Specifications for Interoperability
ULS	Ultimate Limit States

LATIN SYMBOLS

A	Parameter that depends on the track quality
A	Influence surface
a, b	Weighing factors of the objective function's terms
a, b	Smallest and the largest plan dimensions of the bearings
A_{brac}/I_{brac}	Area / Inertia of bracings
A_{diap}/I_{diap}	Area / Inertia of diaphragms
A_{rail}/I_{rail}	Area / inertia of the rail UIC 60
A_s	Cross-sectional area of transverse reinforcement
c	Damping constant
c_p	Damping of primary suspension of the train
c_s	Damping of secondary suspension of the train
D	Total fatigue damage
D_{1year}	Fatigue damage corresponding to one year of traffic
E	Neoprene equivalent elasticity modulus
E_{bal}	Ballast elasticity modulus
E_c	Concrete elasticity modulus
$E_{cd,max,i}$	Maximum compressive stress level, to define the fatigue strength of concrete under compression
$E_{cd,min,i}$	Minimum compressive stress level, to define the fatigue strength of concrete under compression
E_{cm}	Concrete elasticity
$E_{cm}(t)$	Mean value of concrete elasticity modulus at age *t*
E_{hm}	Mean value of the elasticity modulus of the homogenised section

E_{neop}	Neoprene elasticity modulus
E_{pad}	Rail pad elasticity modulus
E_{rail}	Steel (rail) elasticity modulus
E_s	Steel elasticity modulus
$E_{sleeper}$	Concrete (sleeper) elasticity modulus
E_{Tef}	Teflon elasticity modulus
f	Objective function
f	Vector of wheel loads applied to the nodes of the rail path
f	Natural frequency
F_b^k	Moving load applied to the bridge (*b*) in iteration *k*
$f_{cd,fat}$	Fatigue reference strength for concrete under compression (design value)
f_{ck}	Characteristic value of concrete compressive strength
f_{cm}	Mean value of concrete cylinder compressive strength
$f_{cm}(t)$	Mean value of concrete cylinder compressive strength at age *t*
F_{dyn}	Dynamic component of the interaction load
f_i^{exp}, f_i^{num}	Experimental and numerical frequencies for mode *i*
f_{max}	Frequency of the highest vibration mode considered in the analysis
F_{stat}	Static component of the interaction load
F_t^k	Reaction force at a contact node, in iteration *k*
G	Neoprene shear modulus
G_a	Time-record of any parameter (displacement, stress, bending moment, etc.) in the node a
G_{an}	Parameter value in the node a and in the *n*-th vibration mode
$G_{a,s}$	Total static response of the structure for each node a
h_{bal}	Additional height of the ballast
i	Number of axles in the train
i, n	Referred to two orthogonal vibration modes with different natural frequency
k	Number of iteration
$\mathrm{k}_1, \mathrm{k}_2$	Parameters to define the slopes of the S-N curve
k_1	Wavenumber
k_1	Reduction factor to define the design fatigue strength of concrete
k_h	Longitudinal bearing stiffness
$\mathbf{K}_{kl}$	Stiffness submatrix which connects the DOFs of *clusters k* and *l*

k_p	Stiffness of primary suspension of the train
k_{pad}	Vertical rail pads stiffness
k_{rc}	Stiffness of wheel-rail connection
k_s	Stiffness of secondary suspension of the train
k_v	Vertical bearing stiffness
L	Span of the bridge
L_Φ	Determinant length, which represents the length of the influence line for deflection of the element being analysed
LM71	Traffic load model LM71 as defined by EN 1991-2
m	Total number of nodes in the load path
$M(t)$	Time record of the transverse bending moment
M, C, K, F	Mass, Damping, Stiffness and Load related to a specific vibration mode
$\mathbf{M}, \mathbf{C}, \mathbf{K}, \mathbf{F}$	Mass, Damping, Stiffness and Loads matrices of the structure
$M_{A,B,C,D}$	Bending moment obtained by static analysis (A), moving load analysis (B) and TBI analysis without (C) or with (D) the inclusion of track irregularities
M	Carbody translational mass
MC90	Model Code 1990
n	Number of modes considered in the analysis
n	Total number of *clusters*
n	Number of applied stress cycles
n	Number of neoprene layers
N	Number of permissible load cycles, before fatigue failure
N	Total number of vibration modes
$N(t)$	Time record of the transverse axial force
n_0	Natural frequency related to a vertical bending vibration mode
n_T	Natural frequency related to a torsional vibration mode
N^*	Total number of vibration modes considered in the analysis
N^*	Number of load cycles at fatigue failure at the trasition between slopes of the S-N curve for reinforcing and prestressing steel
P_k	Static load per axle *k*
p_s	Reinforcement percentage in the homogenised section
r	Rail irregularities
r	Residue of the objective function's terms
R_i	Stress ratio, to define the fatigue strength of concrete under compression

r_{xy}^{S}	Spearman's correlation coefficient between vectors x and y
S_0	Dynamic signature of a train
S_j	Sensitivity coefficients
t	Time step
t	Concrete age (in days)
t_{bal}	Thickness of the ballast layer
t_c	Thickness of the reinforced concrete slab
t_i	Thickness of each bearing's neoprene layer
u, u̇, ü	Displacement, velocity and acceleration vectors (nodal coordinates)
u_b^k	Displacement of the bridge (*b*) under a contact node, in iteration *k*
u_t^k	Displacement of the train (t) at each contact node, in iteration *k*
v	Train speed
v_3	Value that depends on the bearing's shape
v_{max}	Maximum train speed
x_j	Initial numerical parameters
x_k	Distance between axle *k* and the first axle of the train
$y, \dot{y}, \ddot{y}$	Displacement, velocity and acceleration vectors (modal coordinates)
y_{dyn}	Maximum value of the dynamic response for a specific location of the structure
y_n	Record of the modal coordinate for the *n*-th vibration mode
y_{sn}	Static component of the record of the modal coordinate for the *n*-th vibration mode
y_{stat}	Maximum value of the dynamic response for a specific location of the structure
z	Internal lever arm
z_j	Response values for the initial numerical parameters
$\prod_{jk}$	Relative modal strain energy representing the portion of total energy mobilised by vibration mode *j* considering only the DOFs of *cluster k*

GREEK SYMBOLS

α	Factor for quantification of classified railway traffic loads
$\beta_{cc}(t_0)$	Coefficient to define the concrete compressive strength at the time t_0
γ, β	Parameters that control stability and precision of Newmark's method
$\gamma_{F,fat}$	Partial factor for cyclic actions

$\gamma_{S,fat}$	Partial factor for fatigue verification of reinforcing and prestressing steel
Δt	Time step
$\Delta\sigma_{equiv}$	Damage equivalent stress range
$\Delta\sigma$	Stress range
$\Delta\sigma_s$	Specific stress amplitude
ε	Tolerance
η	Ratio between fundamental frequencies of the primary suspension of the train and the bridge
λ	Factor related to track maintenance
λ	Wavelength
λ_0 to λ_4	Correction factors for calculation of damage equivalent stress ranges
μ_{neop}	Neoprene-steel friction coefficient
μ_{Tef}	Teflon-steel friction coefficient
ν_{bal}	Ballast Poisson's ratio
ν_c	Concrete Poisson's ratio
ν_{neop}	Neoprene Poisson's ratio
ν_{rail}	Steel (rail) Poisson's ratio
ν_s	Steel Poisson's ratio
$\nu_{sleeper}$	Concrete (sleeper) Poisson's ratio
ν_{Tef}	Teflon Poisson's ratio
ξ	Modal damping ratio
ρ_{bal}	Ballast density weight
ρ_c	Concrete density weight
ρ_{rail}	Steel (rail) density weight
ρ_s	Steel density weight
$\rho_{sleeper}$	Concrete (sleeper) density weight
σ	Standard deviation
$\sigma_{cd,max,i}$	Upper stress in a cycle, to define the fatigue strength of concrete under compression
$\sigma_{cd,min,i}$	Lower stress in a cycle, to define the fatigue strength of concrete under compression
$\sigma_s(t)$	Time record of the steel stress
$\boldsymbol{\varphi}$	Mode shape vector

φ_n	Vector containing the coordinates of the *n*-th vibration mode for the nodes of the rail path
$\varphi_{dyn}{}'$	Factor to describe the dynamic enhancement
φ''	Factor to describe the dynamic enhancement due to track defects and vehicle imperfections
Φ	Dynamic factor
$\mathbf{\Phi}_i$	Vector containing the experimental information of the vibration mode *i*
$\mathbf{\Phi}_j$	Vector containing the coordinates of the numerical mode *j*
$\mathbf{\Phi}_{jk}$	Matrix containing the modal information of numerical modes *j*, corresponding to the DOFs of *cluster k*
$\mathbf{\Phi}_{jl}$	Matrix containing the modal information of numerical modes *j*, corresponding to the DOFs of *cluster l*
$\boldsymbol{\phi}_i^{exp}$, $\boldsymbol{\phi}_i^{num}$	Vectors containing the experimental and numerical modal information
ω_j	Angular frequency of numerical mode *j*

Chapter 1

Introduction

1.1 Scope of the thesis

During the last decades railway system has shown a major influence over the economic and social development of our society. In Europe, the railway transport assumes an important role to achieve the 2020 strategy, a strategy towards to the development of a smarter, more sustainable and more competitive economy (European Commission 2008). The introduction of new high-speed lines, or the modernisation of the existing ones, has contributed largely to this growth, reducing journey times, improving the passenger riding comfort and reducing congestion on the overall transport infrastructure network. It has created opportunities for a modal shift from air and road to rail which has brought environmental gains. As consequence, this has also become beneficial for the rail freight since high-speed lines have freed up essential capacity for more freight trains on the classical network, which have been increasingly used in the transport of heavy bulky goods, consumer goods and construction materials, connecting the main ports with the major cities and reducing considerably the number of lorries and congestion on the main roads.

Although road remains the most used mode of transport in Europe, the demand for passenger rail transport grew by 17 % between 2000 and 2012, partially driven by the expansion of the European high-speed railway network (ECORYS 2014). However, rail freight volumes dropped considerably during the period from 2007 to 2009, as a result of the economic and financial crisis, but subsequently recovered between 2009 and 2011 [Figure 1.1 a)]. In

terms of modal share, rail transport supplied 11.0 % of freight and 6.3 % of passenger transport in 2011 [Figure 1.1 b)].

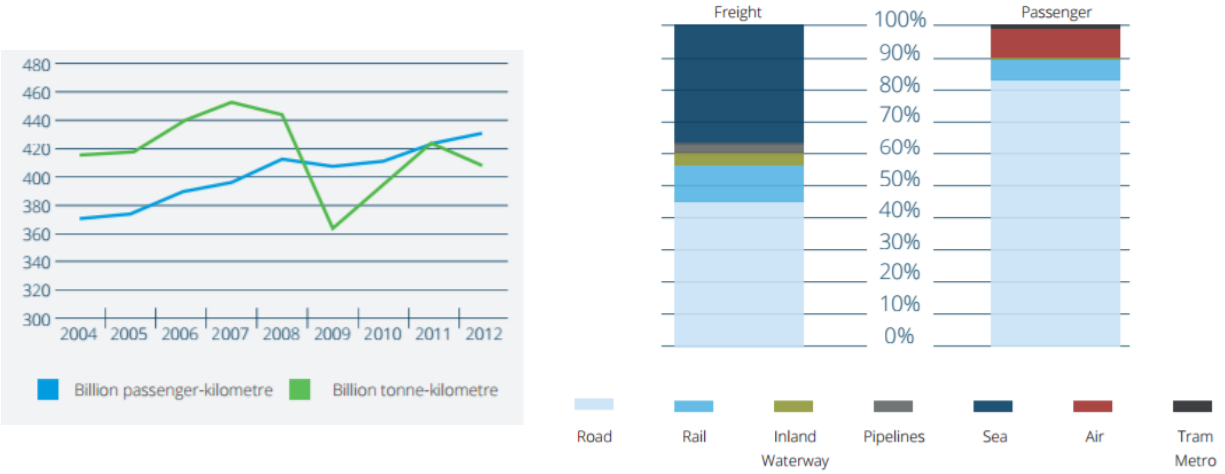

a) b)

Figure 1.1 – Development of passenger/freight transport in the EU: a) passenger/tonnes-kilometres between 2004 and 2012; b) modal split in 2011 (ECORYS 2014)

This development in the railways has been possible due to the construction of a significant number of bridges and viaducts. Taking into account the specific characteristics of the railway traffic, the design of railway bridges must address to some technical constraints, which have led to the adoption of structural solutions with higher stiffness levels when compared to the ones adopted to road bridges. Several and distinct structural solutions have been widely used, depending on the material (steel, reinforced or prestressed concrete and composite steel-concrete solutions) or the deck configuration (slab, I girders or box girders). Generically, the increase in the stiffness levels has been achieved essentially through the main girders, using either I-shaped or U-shaped girders connected by an upper reinforced concrete deck or, alternatively, using cast-in-place box girders.

In Spain, U-shaped prefabricated girders connected by an upper concrete slab were widely employed in the construction of bridge decks with one or more box girders. According to Aparicio (2004), simply supported schemes present good performance for spans between 10 and 30 m and continuous schemes up to 38 m. Two examples are the Martorella viaduct [Figure 1.2 a)], constructed in high-speed line between Madrid and Barcelona, and the Ricla viaduct [Figure 1.2 b)], constructed in the high-speed line between Madrid and Zaragoza.

In Italy, more than 90 % of new railway viaducts included in the high-speed network were made with simply-supported integrally prestressed concrete decks. However, other solutions were adopted as the use of several prestressed U-shaped girders or I-shaped girders connected by an upper slab cast in situ (Evangelista and Vedova 2004).

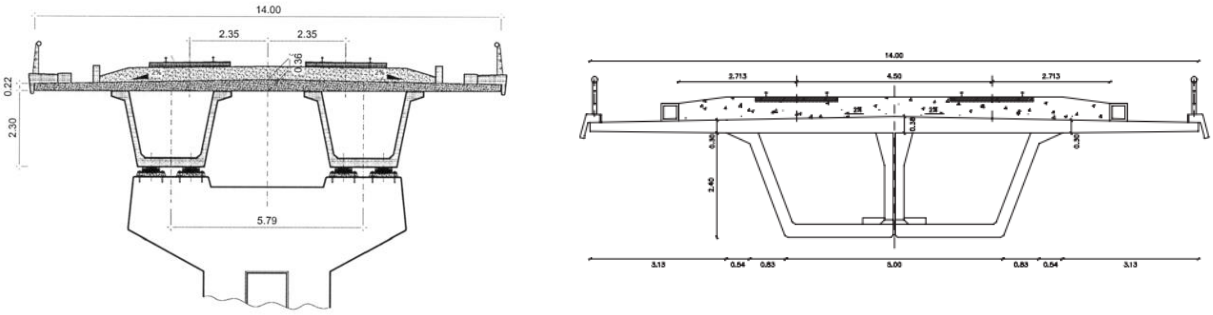

a) b)

Figure 1.2 – U-shaped girders connected on the top by a reinforced concrete slab, used in high-speed lines: a) Martorella viaduct; b) Ricla viaduct (Aparicio 2004)

Composite solutions have also been employed, essentially composed of two steel plate girders connected on the top by a reinforced concrete slab. An example of this structural solution was applied in the construction of the *Haute-Colme* viaduct, in France, a remarkable work of *TGV Nord* taking into account its total development of 1827 m (Figure 1.3).

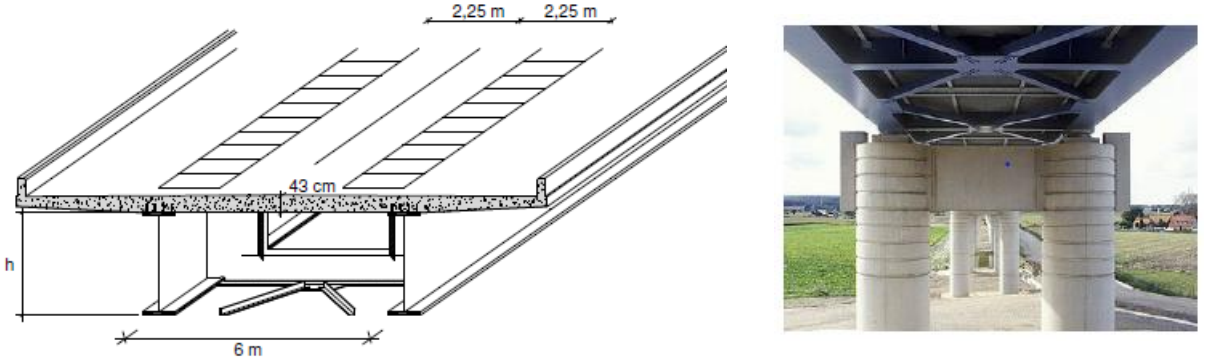

a) b)

Figure 1.3 – Composite steel-concrete railway viaduct: a) typical cross-section; b) bottom view of the *Haute-Colme* viaduct (Figueiredo 2007)

Bearing in mind the aforementioned growth in the use of railways, and the evolution expected for a near future, this type of structures is nowadays subjected to high intensity moving loads, where the dynamic effects can reach significant values. Reinforced concrete

(RC) deck slabs in railway bridges and viaducts can be particularly sensitive to these dynamic effects, which increase due to higher train speeds and higher axle loads can lead to excessive bridge vibrations, giving rise to fatigue damage and setting in risk the traffic safety (ERRI D214/RP9 2001, Gabaldón et al. 2004).

Several authors (Schlafli and Bruhwiler 1998, Pimentel et al. 2008, Zanuy et al. 2011) pointed out that these are the bridges' structural elements most susceptible to the occurrence of fatigue phenomena. A high number of loading cycles can occur, which typically exceeds 10 million and, in some structures, reaches 100 million over the total life of the structure. This is due to the fact that they often present a low thickness and a low reinforcement rate, in order to comply with the standard's recommendations as far as static behaviour is concerned.

As aforementioned, one of the specificities of this type of structures is related to the use of prestressed concrete or steel plates as main girders in the longitudinal direction, reason why there is generally no cracking related with the stresses in this direction. The fatigue resistance of deck slabs is usually controlled by the fatigue damage of transverse tensile reinforcement and not by the fatigue damage of concrete. In fact, as mentioned by Johansson (2004), in slab plates subjected to significant cyclic bending moments, fatigue of concrete under compression is not observed in experiments, due to the redistribution of concrete stresses within the cross-sections that prevents the fatigue failure of concrete and results in fatigue of the reinforcement.

The evaluation of the fatigue behaviour plays an important role in the design of new structures subjected to cyclic loading. This becomes even more crucial when has been proved that several existing railway bridge decks do not comply with the requirements of actual design codes in terms of fatigue resistance (Bogaert 2009). A carefully assessment of fatigue strength in railway bridge decks should be performed, reason why this thesis aims to contribute to the knowledge about the real performance of these structures, in terms of dynamic behaviour and fatigue resistance, and also to give a contribution in terms of numerical methods for its assessment.

1.2 Main objectives and contributions

The main motivation for the research work presented in this dissertation is the paucity of studies carried out to evaluate the dynamic behaviour and fatigue resistance of reinforced

concrete slabs used in the construction of railway bridges or viaducts. As previously highlighted, the specific loading related to railway traffic leads to important dynamic effects, due to higher train speeds, higher axle loads and the existence of track irregularities or wheel defects, which can lead to excessive bridge vibrations. However, most of the work developed in this field takes into account only the global performance of the structure or lacks experimental evidence. So, bearing in mind that the fatigue phenomenon is strongly dependent on the dynamic behaviour of the structure, the main objectives of this thesis are both the study of the local dynamic behaviour and the fatigue assessment of RC deck slabs, based on numerical and experimental information. For this purpose, two real structures are analysed: the Alverca railway viaduct and the access viaduct to the Alcácer do Sal bridge.

With the final objective of an accurate fatigue analysis, even without using some of the complex methodologies that can be found in the literature, in the present dissertation powerful and accurate numerical tools are used firstly to evaluate the dynamic behaviour of slabs. Advanced three-dimensional numerical models of the bridges and trains are used. A calibration methodology of numerical models is used, taking into account an optimisation method through a genetic algorithm and based on modal information experimentally obtained. Dynamic numerical responses taking into account the interaction between the train and the bridge, either the global responses of the structures or the local responses of the reinforced slabs, are validated through the comparison with the real structural performances measured under railway traffic.

The specific contributions of this thesis are as follows:

- an interconnection of the aforementioned numerical tools in order to obtain accurate numerical responses, regarding the dynamic behaviour of the RC deck slabs, in order to perform its fatigue assessment;
- the use of a static correction procedure within the train-bridge interaction methodology, which leads to obtain the static contribution of vibration modes of higher frequencies, which are not explicitly considered in the basic modal-superposition method (used to solve the dynamic problem);
- the experimental approach for the identification of modal parameters (natural frequencies, mode shapes and damping coefficients), based on ambient vibration tests, specifically related to the local behaviour of the RC deck slabs;

- the development of a methodology to identify accurate modal damping coefficients, related to local vibration modes of the RC deck slabs, for vibration levels corresponding to the passage of trains instead of using the values provided by ambient vibration tests;
- the evaluation of the effects of distinct track irregularities (different real profiles and space variability), modal damping coefficients and trains' speed in the dynamic behaviour and fatigue resistance of RC deck slabs of railway bridges.

1.3 Layout of the thesis

The present dissertation is divided into 7 chapters, whose content is briefly summarised in the following paragraphs.

The current Chapter 1 presents the scope of this thesis, describes the motivation for its development and the main contributions to the research field, and outlines the organisation of the document.

Chapter 2 is dedicated to the review of the state of the art concerning the dynamic behaviour of railway bridges. The most typical approaches that can be used to evaluate the numerical evaluation of bridges' dynamic response are analysed, with particular focus on the train-bridge interaction method. Some of the recommendations defined in the European standards, in order to guarantee both the structural and operational safety of railway bridges in high-speed railway lines, are also presented.

Chapter 3 starts with a brief presentation of the fatigue behaviour of reinforcing steel, concrete and reinforced concrete structures. The methods suggested on European Standards for the fatigue-strength verification are presented, with particular attention to the damage accumulation method, used in the present work.

Given the great importance of the real response of structures, Chapter 4 starts with an overview of some experimental techniques widely used to obtain the dynamic response of bridges, either to identify its modal parameters or to measure its dynamic behaviour under railway traffic. Afterwards, regarding the calibration of finite element numerical models, the steps involved in an iterative method based on an optimisation algorithm are presented, namely, the sensitivity analysis, the vibration modes' pairing and the optimisation phase.

Chapters 5 and 6 are dedicated to the study of the local dynamic behaviour and fatigue resistance in two real railway bridges, the Alverca railway viaduct and the access viaduct to Alcácer do Sal bridge, respectively. In both chapters, three-dimensional finite element numerical models are developed, calibrated and validated based on experimental tests. Detailed calculations of internal forces are performed through train-bridge interaction numerical analyses. A static correction procedure is also implemented, and validated, in these dynamic analyses to take into account the static contribution of higher-frequency vibration modes. The effects of different track irregularities, modal damping coefficients and trains' speed on the dynamic behaviour of the upper deck slab are discussed. Finally, based on the results of different train-bridge interaction dynamic analyses, the assessment of the fatigue damage in the transverse reinforcement bars of the upper deck slab is performed.

In Chapter 7 the main conclusions of the present work are summarised as well as some future research topics.

Chapter 2

Dynamic behaviour of railway bridges

2.1 Introduction

The railway system and its infrastructures have over the last decades played a key role in the process of economic development of our society. On one hand, the introduction of high-speed trains has contributed largely to this growth, reducing travel time and improving the passenger comfort. On the other hand, freight trains have been increasingly used in the transport of heavy bulky goods, consumer goods and construction materials, connecting the main ports with the major cities, reducing considerably the number of lorries and congestion on the main roads.

This development has been possible due to the construction of a significant number of bridges and viaducts. This type of structures is nowadays subjected to high intensity moving loads, where the dynamic effects can reach significant values. Due to higher train speeds, higher axle loads and the existence of track irregularities or wheel defects, particular attention has been given to these dynamic effects, since they can lead to excessive bridge vibrations and consequently may put in risk the traffic safety. Some research works (ERRI D214/RP9 2001, Gabaldón et al. 2004) have highlighted that the resonance phenomenon, originated by periodic loading associated with the passage of regularly spaced train's axles groups, may occur in these structures at speeds above 200 km/h. This phenomenon can lead to problems such as the ballast instability, the loss of contact between the wheel and the rail, fatigue damage or affect the passenger comfort. In order to evaluate such effects and evaluate the dynamic behaviour of the

structure, numerical analyses are usually performed. Some representative researches can be cited.

Museros et al. (2004) studied the evolution of the wheel-rail contact forces in high-speed simply supported railway bridges during resonance situations, comparing the theoretical model with a real case scenario. The authors found oscillations in the wheel-rail contact forces during the passage of the axles over the bridge, which become more severe during resonance, especially for the rear wheels rather than the front ones. Xia et al. (2006) also evaluated the resonance effects on a railway bridge subjected to the passage of high-speed trains by means of theoretical methodologies, numerical simulations and experimental tests. According to the authors, the resonance of the train-bridge system is essentially affected by the span, total length of the bridge as well as its vertical and transverse stiffness, and also by the characteristics of the trains, namely, load distribution scheme and natural frequency of the trains.

Regarding the evaluation of the ballast layer instability, Norris (2005) and Zacher and Baeβler (2009) have carried out several experimental tests. In both cases, the authors found that the limit to the maximum vertical acceleration of the deck, imposed by the European Standard EN1990-A2 in order to avoid the ballast instability, is very conservative and have suggested more suitable values. Later on, Baeβler et al. (2012) also evaluated the maximum frequency that should be considered in the dynamic analyses. These authors revealed that, in a way to prevent ballast instability, which is associated with higher frequency vibration modes, it would be advisable to consider the maximum frequency threshold equal to 60 Hz.

The effects of several parameters on the response's dynamic amplification of railway bridges, such as the train speed, wheelbase, frequency range and structural damping to be considered in the analyses, were evaluated by Majka and Hartnett (2008). As an example, one can observe in Figure 2.1 the considerable decrease in the vertical acceleration, in the mid-span section of the bridge, to increasing values of the structural damping coefficient, revealing the importance in the correct quantification of this parameter.

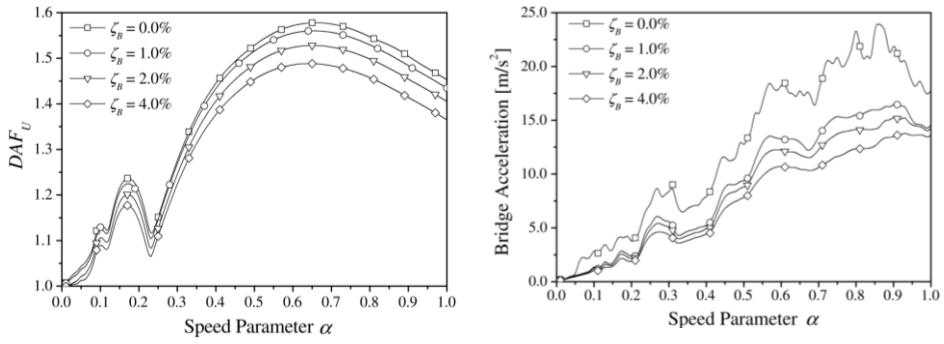

a) b)

Figure 2.1 – Influence of damping on the structural response in: a) the dynamic amplification factor (DAF); b) the acceleration of the bridge (Majka and Hartnett 2008)

Other authors, such as Ülker-Kaustell & Karoumi (2012) and Leander & Karoumi (2013), also carried out some studies to understand how structural damping affects the global dynamic behaviour of railway bridges. Leander and Karoumi (2013) carried out a numerical study considering modal damping coefficients between 0 % and 3 % (keeping a constant value for all of the 50 vibration modes considered in analyses), showing that lower damping coefficients give rise to considerably higher fatigue damages, especially in the case of simply supported structures. They also showed that damping strongly affects the bridge response after the train leaves the structure.

Ribeiro et al. (2012), resorting to ambient vibration tests carried out in a bowstring-arch railway bridge, identified the modal damping coefficients of several global and local vibration modes of the structure (Figure 2.2). These authors showed that the experimentally identified damping coefficients can be very different from the value of 0.5 %, which is proposed by EN 1991-2 (2003) for the design of bridges with steel-concrete deck and spans greater than 20 m. The authors also presented values for damping coefficients of the local vibration modes of the hangers and diagonals of the arch, which have a low dispersion and are generally located between 0.10 % and 0.30 %.

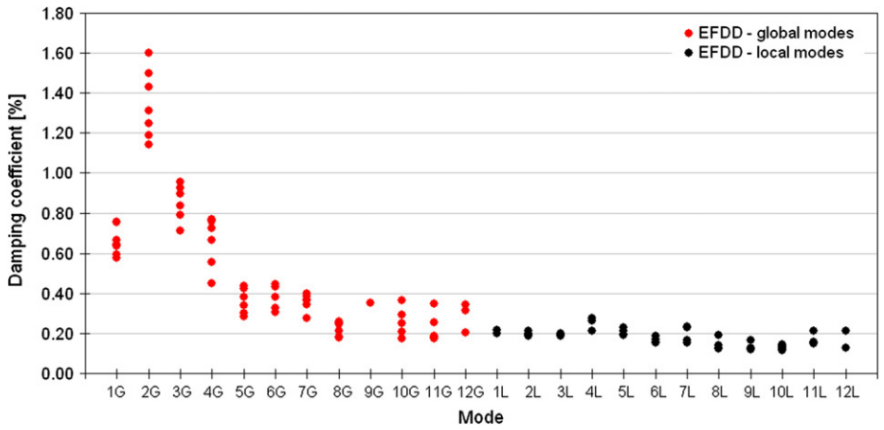

Figure 2.2 – Damping coefficients estimates for global and local vibration modes for different experimental setups (Ribeiro et al. 2012)

Track irregularities are an important source of excitation that may affect the ride comfort, the train response and safety and also the bridge dynamic response. There are two different ways to define the track irregularities to be used in the numerical analyses: using experimentally measured values or through random generation using power spectral density (PSD) functions. Concerning the latter approach, Rocha et al. (2014), performing dynamic analysis considering irregularities wavelengths between 3 m and 25 m, have shown significant differences in the global behaviour of a railway bridge, in terms of vertical accelerations in different cross-sections, by comparing the results for a perfect track and a track with irregularities.

Cantero et al. (2016) have also discussed the effect of different wavelength ranges (3-25 m, 25-70 m and 70-150 m) on global bridge deck acceleration, for different train speeds. These authors showed that the major contribution to the increase of the dynamic response (with respect to the response for a smooth rail without irregularities) comes from the lower wavelength range (3-25 m), as can be seen in Figure 2.3. Within the scope of the Rivas research project (2013), where the importance of experimentally measured track irregularities for ground-borne vibrations was analysed, the relevance of irregularities with smaller wavelength (in the interval 0.5 m to 3 m) has also been demonstrated.

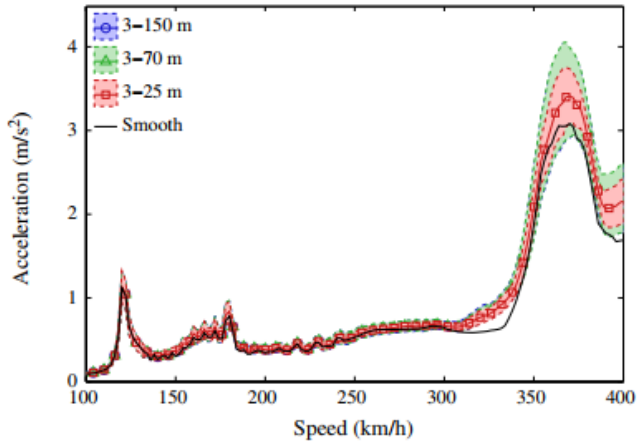

Figure 2.3 – Effect of track irregularity wavelengths in the vertical acceleration of a bridge (Cantero et al. 2016)

Herwig & Bruhwiler (2011), found that track irregularities may be one of the main causes for dynamic effects for fatigue relevant bridge elements, leading to amplifications of the bridge dynamic response and that the wheel-force variation leads to an almost immediate bridge response. Based on measurements and simulations from a prestressed concrete bridge girder, the authors obtained dynamic amplification factors that vary with varying train velocity. A maximum occurs at the resonance speed for maximum vehicle excitation due to track irregularities. The authors pointed out that high contact force amplitude leads to high action effect amplitudes but the maximum dynamic wheel forces do however not necessarily occur always at the location leading to maximum action effect (such as the bending moment).

Sousa (2012) developed a numerical methodology to evaluate the fatigue behaviour of cracked reinforced concrete elements subjected to cyclic loading, validating the results through laboratory tests and applying it in a railway bridge case-study. The author verified that the existence of cracks can be considered in linear dynamic analysis through a reduction of the bending stiffness, and that this reduction leads to an increase in the vertical displacements of the structure, to a decrease in the frequencies of vibration and to a decrease of the resonant speeds during the passage of high-speed trains [see Figure 2.4 related to the latter effect].

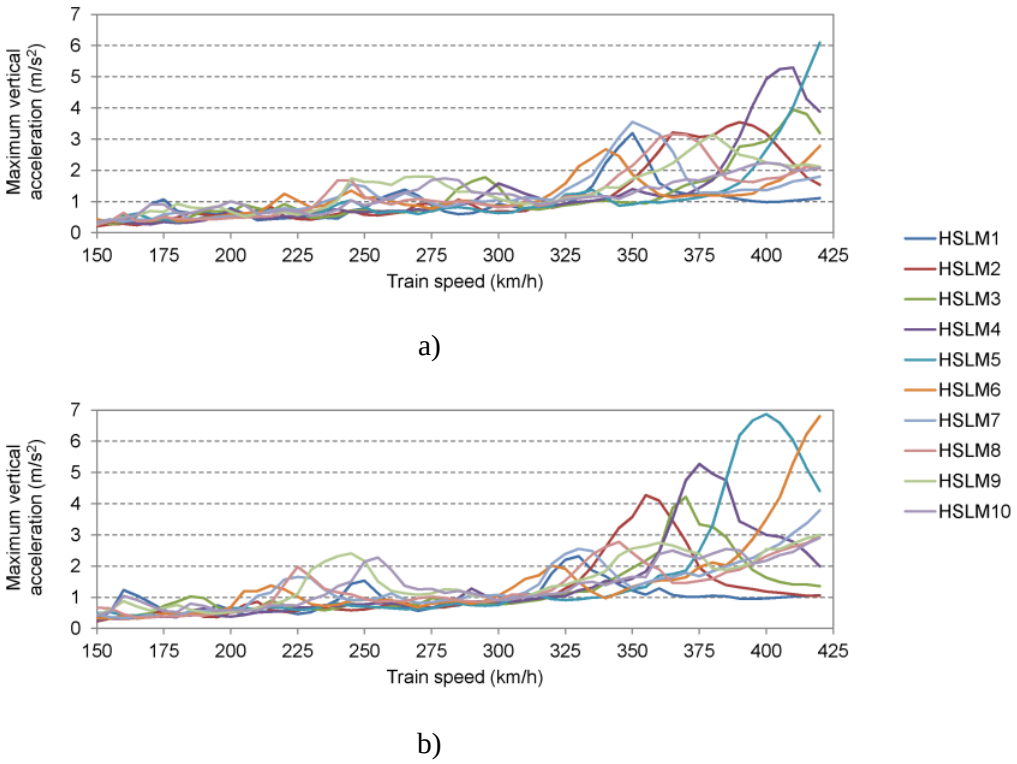

Figure 2.4 – Maximum vertical acceleration in the mid-span section of the bridge as function of the train speed: a) without the influence of cracks; b) with the influence of cracks (adapted from Sousa (2012))

Dynamic analysis is thus of particular importance, essentially due to several parameters that should be taken into account in order to obtain accurate results. In this Chapter, the most important aspects regarding the dynamic behaviour of railway bridges are presented and discussed. The most typical approaches that can be considered to perform the numerical evaluation of the dynamic response are analysed, with particular focus on the train-bridge interaction method which allows obtaining the most realistic results. Finally, some of the recommendations defined in the European standards, in order to guarantee both the structural and operational safety of railway bridges in high-speed railway lines, are presented.

2.2 Numerical evaluation of the dynamic behaviour

There are several methodologies that can be used to analyse the bridge dynamic response regarding the passage of trains, namely, numerical, simplified, analytical or empirical methods. A detailed description of different methods can be found in Barbero (2001). The numerical

analysis methodologies are nowadays among the most used techniques to verify the dynamic behaviour of structures, and for this reason they are the only ones detailed in the present section. Two main methods for studying the dynamic behaviour of a railway structure are discussed: moving loads (section 2.2.1) and train-bridge interaction (section 2.2.2). These methods vary in complexity, computational cost and accuracy as will be discussed in the following subsections.

2.2.1 Moving loads method

The moving loads method do not consider the interaction between bridge and trains since the latter are characterised by a set of moving loads spaced apart according to trains' geometry. Each load is defined by a value related to the static load of each axle, as shown in Figure 2.5.

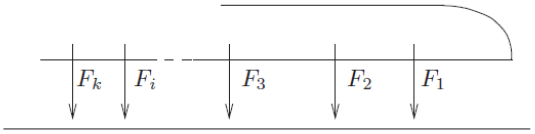

Figure 2.5 – Schematic representation of the moving loads method

The dynamic response of the structure can be calculated, in each time step *t*, by solving the following dynamic equation of motion:

$$\mathbf{M}\ddot{\mathbf{u}}(t) + \mathbf{C}\dot{\mathbf{u}}(t) + \mathbf{K}\mathbf{u}(t) = \mathbf{F}(t) \tag{2.1}$$

where $\mathbf{M}$, $\mathbf{C}$ and $\mathbf{K}$ are the mass, damping and stiffness matrices of the structure, respectively and $\mathbf{F}$ is the vector of external loads applied to the structure (generic external loads and time-dependent moving loads of the train). Equation 2.1 can be solved using direct integration techniques, such as the Newmark method (Clough and Penzien 1993), the Wilson-θ method and the Hilber-Hughes-Taylor (HHT) method (Cruz 1994, Calçada 1995, Neves 2008), or using the modal superposition method (Chopra 1995, Clough and Penzien 1993).

This method can be used with sufficient accuracy in cases where the train-bridge interaction does not significantly influence the dynamic response of the structure, such as where the train's mass is considerably lower when compared to the bridge's mass (Martínez-Rodrigo 2009, Goicolea and Gabaldon 2012). Short to medium span bridges are not within these cases. They

should be carefully analysed since the moving loads method may sometimes underestimate the real bridge's deck response.

It thus becomes a methodology of greater simplicity to apply, with reduced effort and computational times, but limited to the study of the dynamic response of the structure. Furthermore, this method does not allow considering the effect of track irregularities. Examples of the application of this method can be found in the works of Albuquerque et al. (2010) and Rocha et al. (2012).

2.2.2 Train-bridge interaction method

2.2.2.1 Overview

The methodology based on the consideration of the train-bridge interaction (TBI) is a method of greater complexity in terms of computational implementation but more realistic regarding to the results obtained, since it takes into account both the dynamic characteristics of the bridge and the train, by considering the effects associated with the interaction forces that develop with the passage of the train over the structure. Due to the explicit modelling of the bridge, track and train, this methodology allows not only an accurate assessment of the dynamic behaviour of railway bridges but also the evaluation of the ride comfort, the wheel-rail stability or the effects of track irregularities.

In order to evaluate the TBI effects, ERRI's D214 (2001) expert committee conducted a number of analyses considering distinct bridges and two types of trains, the conventional ICE2 and the articulated EUROSTAR trains. Concerning large-span bridges, the commission found that the response of the structure is very similar whether or not the TBI is considered. The main differences were observed in small-span bridges but only in the proximity of resonance speeds, where considering the interaction leads to lower displacements and accelerations. This commission also defined an additional value for structural damping in order to take into account the interaction effects in analyses according to the moving loads method, thus allowing for simpler analyses without explicit consideration of this phenomenon.

Museros et al. (2002) also compared the dynamic behaviour of several simply supported bridges using both the moving loads and the TBI methods, concluding that the interaction effects lead to a significant reduction (around 25%) of the maximum dynamic response.

The dynamic problem, considering now the interaction between the bridge and the train, can be solved considering the two systems, bridge and train, in coupled or uncoupled sets of equations. The uncoupled consideration of the dynamic equilibrium equations of the two systems requires less computational effort than the coupled resolution, since in the latter case the matrices are generated together and subsequently solved together as well, requiring to be constantly updated at each time step. Examples of application of the coupled approach can be found in Yang et al. (2004) and Neves et al. (2012).

In the case of uncoupled dynamic equilibrium equations, the compatibilisation of the two systems, bridge and train, can be done based on iterative methods (Cruz 1994, Calçada 1995, Lei and Noda 2002) or through direct methods, as developed by Neves et al. (2012). Dynamic equilibrium equations can be solved based on direct integration methods, such as the Newmark or Wilson-θ methods, or based on the modal-superposition method.

In the iterative methods, the two systems are solved simultaneously over time, resorting to an iterative process in each time step in order to obtain the compatibility of the two structural systems, in terms of the dynamic component of the interaction force and the displacement in the contact nodes. The dynamic equilibrium equations of both systems can be written separately as follows (Calçada 1995):

$$\begin{bmatrix} \mathbf{M}_b & 0 \\ 0 & \mathbf{M}_t \end{bmatrix} \begin{bmatrix} \ddot{\mathbf{u}}_b(t) \\ \ddot{\mathbf{u}}_t(t) \end{bmatrix} + \begin{bmatrix} \mathbf{C}_b & 0 \\ 0 & \mathbf{C}_t \end{bmatrix} \begin{bmatrix} \dot{\mathbf{u}}_b(t) \\ \dot{\mathbf{u}}_t(t) \end{bmatrix} + \begin{bmatrix} \mathbf{K}_b & 0 \\ 0 & \mathbf{K}_t \end{bmatrix} \begin{bmatrix} \mathbf{u}_b(t) \\ \mathbf{u}_t(t) \end{bmatrix} = \begin{bmatrix} \mathbf{F}_b(t) \\ \mathbf{F}_t(t) \end{bmatrix} \tag{2.2}$$

where $\mathbf{M}$, $\mathbf{C}$ and $\mathbf{K}$ are the mass, damping and stiffness matrices, respectively. $\mathbf{F}$ is the load vector and $\ddot{\mathbf{u}}$, $\dot{\mathbf{u}}$, and $\mathbf{u}$ are the vectors of accelerations, velocities, and displacements, respectively. The subscripts "*b*" and "*t*" stand for bridge and train, respectively.

Each time step (Δt) involves the following operations:

1. In the iteration *k,* the moving loads in correspondence to the axles of the train are applied in the structure. Each moving $F_b^k(t)$ load is given by:

$$F_b^k(t) = F_{stat} + F_{dyn}^{k-1}(t) \tag{2.3}$$

where F_{stat} is the static load, constant over time, and $F_{dyn}^{k-1}(t)$ is the dynamic component of the interaction force calculated in the previous iteration (equal to $F_{dyn}(t - \Delta t)$ in the first iteration). By solving the system of equations related to the bridge (see Equation 2.2), the nodal displacements are computed and consequently also the displacements of the structure under the contact nodes, $u_b^k(t)$.

2. At the same time, in each contact node of the train a displacement ($u_t^k(t)$), corresponding to the sum between the displacement $u_b^k(t)$ and the track irregularity $r(t)$ that may exist between the wheel and the rail, is imposed. By solving the system of equations related to the train (see Equation 2.2), the reaction forces $F_t^k(t)$ at the contact nodes are computed. These forces are the dynamic components of the interaction forces $F_{dyn}^k(t)$ to be applied to the structure in the following iteration.

3. At the end of each iteration a convergence criterion is used, which takes into account the dynamic components of the interaction forces of the current and previous iterations. For each moving load, the convergence is verified based on the following equation:

$$\frac{\left\|F_{dyn}^k(t) - F_{dyn}^{k-1}(t)\right\|}{\left\|F_{dyn}^{k-1}(t)\right\|} \leq \varepsilon \tag{2.4}$$

where ε is a specified tolerance. If the desired degree of convergence is achieved, the procedure may advance to the next time step $(t + \Delta t)$, otherwise the iterative process continues to the next iteration. The process starts by assuming that the dynamic component of the interaction force at the initial instant of time, $F_{dyn}(t = 0)$, are zero.

The iterative procedure described above is generically schematized in Table 2.1.

Table 2.1 – Iterative method to solve the TBI dynamic problem (Ribeiro 2012)

	Bridge	Train
Scheme	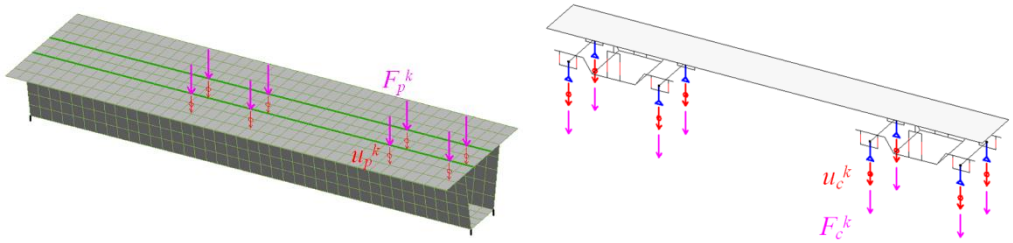	
Load	$F_b^k(t) = F_{stat} + F_{dyn}^{k-1}(t)$	$u_t^k(t) = u_b^k(t) + r(t)$
Result	$u_b^k(t)$	$F_{dyn}^k(t) = F_t^k(t)$
Convergence criterion	$\frac{\left\|F_{dyn}^k(t) - F_{dyn}^{k-1}(t)\right\|}{\left\|F_{dyn}^{k-1}(t)\right\|}$	If $\leq \varepsilon \rightarrow t + \Delta t$ If $> \varepsilon \rightarrow k + 1$

Based on the iterative procedure used by Cruz (1994) and Calçada (1995), in which both systems were solved through a direct integration method, Ribeiro (2012) proposed another development by combining the modal-superposition and Newmark's direct integration method to solve the bridge and train systems, respectively. The modal-superposition method has proved to be more efficient from a computational point of view, reducing considerably the total analysis time. However, Ribeiro (2012) points out that the existence of dampers on the trains does not allow obtaining a set of uncoupled equations, so for that reason the Newmark's direct integration method is used to solve the train's system. In this dissertation the approach introduced by Ribeiro (2012) is used.

In these iterative procedures the computational effort can be critical when a large number of contact nodes is used, leading to a slow convergence rate (Yang and Y.S.Wu 2001). Some techniques, such as relaxation coefficients (Yang and Fonder 1996), have been used to accelerate the convergence process and reduce the total number of iterations.

Bearing this in mind, Neves et al. (2012) developed a direct method in which the compatibilisation of the dynamic equilibrium equations of both systems is performed without iterations. In this approach, for each time step, compatibility equations between the displacements in the contact nodes of the bridge and the train have to be defined. The efficiency of this method consists essentially in changing, at each time step, only the terms of the set of equations (composed by dynamic equilibrium equations and compatibility equations) involving interaction forces, keeping the remaining terms unchanged.

2.2.2.2 Bridge numerical modelling

Nowadays, due to a huge development and evolution of calculation methods and computer technology, powerful numerical models can be developed and very often these models can reproduce quite closely the real behaviour of structures. Depending on the complexity of the problem to be solved and the desired level of detail to be obtained in analyses, different numerical models can be developed. If the main objective is to evaluate a global performance of a bridge the development of a simple 2D numerical model can be suitable. However, if a more complex analysis is required, for example to evaluate local phenomena in a bridge, or even in a train considering the train-bridge interaction, the use of 3D numerical models is more appropriate (Nguyen et al. 2014).

Dieleman and Fournol (2003) reported that simplified bridge modelling could lead to a great difference between the numerical and real acceleration results, especially for small-span bridges. Aspects like the definition of the real span, the incorrect definition of the abutments' stiffness or the non-inclusion of the railway track in the numerical modelling were pointed out as the main issues in the numerical modelling.

Calçada et al. (2002) developed 2D and 3D numerical models of a metallic arch railway bridge which were calibrated based on experimental tests. The 2D model (Figure 2.6) was mainly used to analyse the dynamic response of the bridge under new traffic loads while the 3D model was used essentially to evaluate its seismic response.

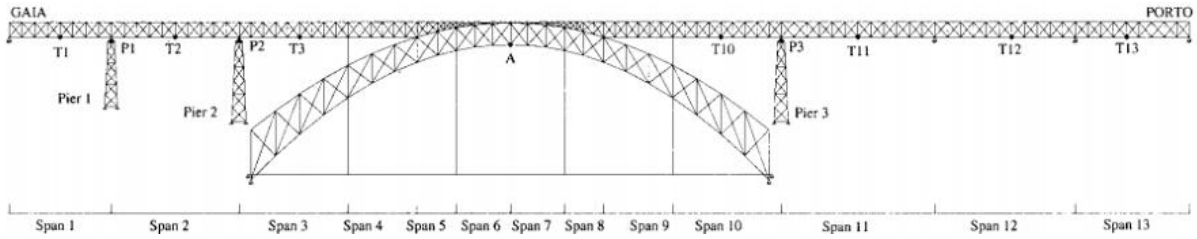

Figure 2.6 – 2D numerical model of the Luiz I railway bridge (Calçada et al. 2002)

Rocha et al. (2012) developed a 2D numerical model in order to evaluate the sensitivity of the global dynamic response of a small span bridge due to the variability of the main structural parameters. Figure 2.7 show the numerical model, which included the ballast and the rail modelled as beam elements and the bearings modelled by means of spring elements. As noted by the detailed picture, horizontal springs were used to reproduce the frictional behaviour of the ballast.

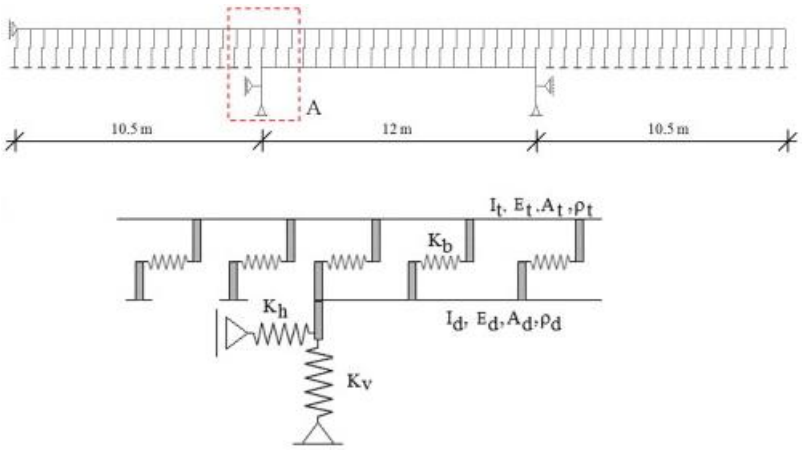

Figure 2.7 – 2D numerical model of Canelas railway bridge (Rocha et al. 2012)

Due to higher train speeds, higher axle loads and the existence of track irregularities or wheel defects, particular attention has been given to the increase of the dynamic effects, reason why 3D finite element numerical models with growing complexity have been widely used. Despite that, the process of developing a FE model of a structure always involves assumptions and simplifications that may cause some errors, such as uncertainties in geometry and boundary conditions and changes in the material properties.

Chellini et al. (2011) showed how important is the influence of the continuity of long welded rails and the ballast layer, to a full understanding of a railway bridge dynamic behaviour, highlighting how simplified structural models can lead to a wrong estimate of the dynamic response. Ribeiro (2012) also showed how the inclusion of the track in the numerical model changes the modal parameters of the bridge, due to the composite effect resulting from the transmission of shear stresses between the deck and the rail through the ballast layer. For that purpose, the author developed a 3D model of a bowstring-arch railway bridge, which is presented in Figure 2.8.

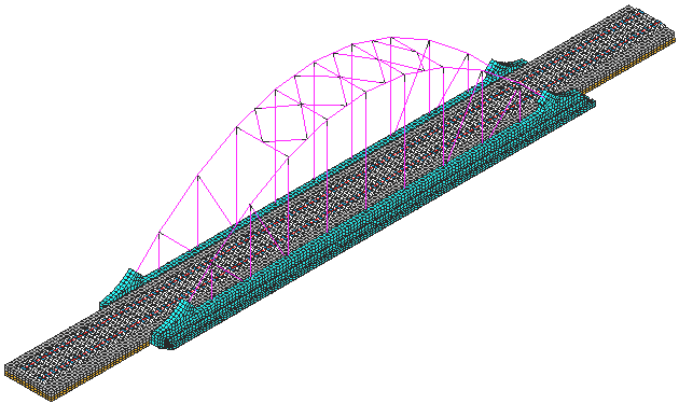

Figure 2.8 – 3D numerical model of the bowstring-arch Sao Lourenco railway bridge (Ribeiro 2012)

Costa et al. (2016) revealed the importance of experimental results, obtained from material mechanical characterization tests made in a centenary stone-arch bridge and in laboratory, to ensure a better estimate of the initial values of the material mechanical parameters adopted in the FE model. Figure 2.9 shows a generic and detailed view of the 3D numerical model of Durraes bridge.

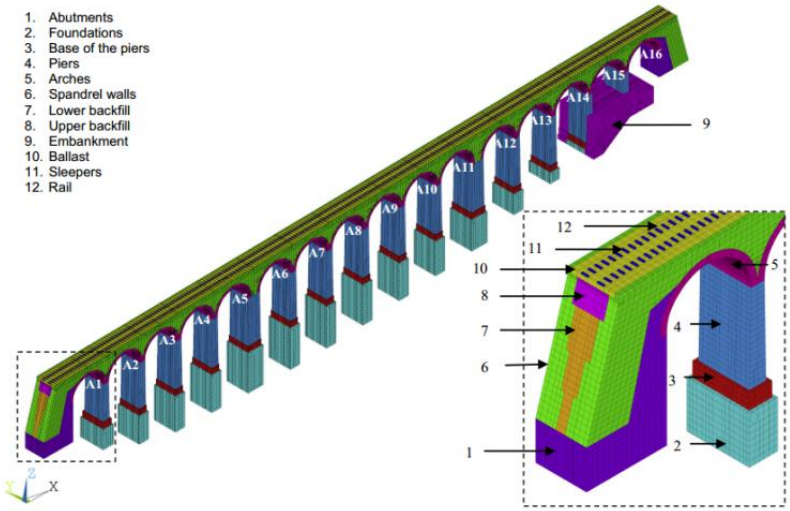

Figure 2.9 – 3D numerical model of Durraes railway bridge (Costa et al. 2016)

Lin et al. (2015) also pointed out that some details of the structures cannot be disregarded, suggesting that expansion joints and accessory structures, such as parapets and footways, need to be considered in the numerical modelling for the evaluation of the real performance of existing or new railway bridges. Otherwise, ignoring these elements can lead to a significant underestimation of the bridge stiffness.

2.2.2.3 Train numerical modelling

In the same way that the evolution of the computational performance enabled increased accuracy in the development of the numerical models of structures, the numerical models of trains to be used in TBI dynamic analyses have had a great development over the last years.

These numerical models may present different degrees of complexity and can be generally classified as simplified models or complete models. The latter involves modelling the main structural elements of the train, namely the car body, the bogies, the elements of the suspensions, the axles and also the wheel-rail connection, while the simplified models do not consider all the structural elements. A concise resume of the different level of complexity that can be found in the numerical models, such as moving masses or the different suspended mass models, is presented by Ribeiro (2012).

Liu et al. (2009) also evaluated the effect of using different train models, using moving loads and numerical models with different degrees-of-freedom (DOF) as presented in Figure 2.10, on

the dynamic response of a simply supported bridge. The authors concluded that the dynamic amplification factors and the maximum accelerations in the mid-span section tend to be overestimated when the moving loads approach is used, while the complete model leads to the most accurate prediction of the dynamic response.

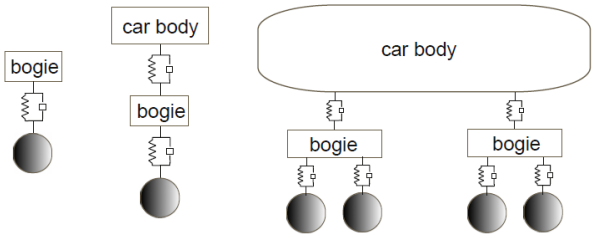

Figure 2.10 – Train numerical models: a) 1 DOF; b) 2 DOF; c) complete model

The complete model has been widely used in TBI dynamic analyses (Lou 2007, Wu et al. 2010, Rocha et al. 2014) since the dynamic response of the train can also be evaluated with higher precision. The assessment of the passenger riding comfort has been crucial to the fact that more complex train models have been proposed. These models involve the widest knowledge of the mechanical and geometric parameters of the structural and suspension elements of the train. However, this information is in most situations difficult to find in the literature or it is not provided by the manufacturers for confidentiality reasons.

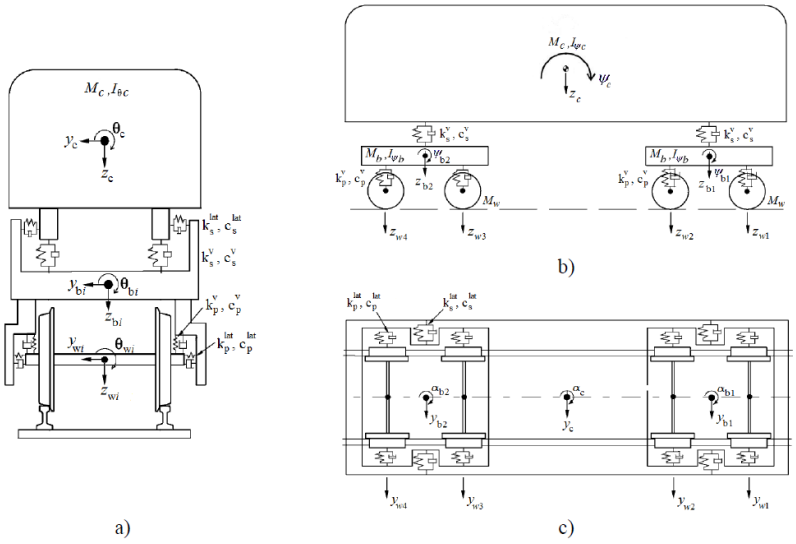

Figure 2.11 – Schematic representation of complete train: a) front view; b) elevation view; c) plan view [adapted from Xia and Zhang (2005)]

The numerical models can be either 2D (Goicolea et al. 2004, Rocha et al. 2014) or 3D (Xia and Zhang 2005, Ribeiro 2012), depending on the type of analysis and required level of accuracy. The 2D models are essentially used for evaluation of the vertical behaviour of the train-bridge system, and include the DOF associated with the vertical displacement and rotation in the plane of the different structural elements. The 3D models involve a greater number of DOF and allow obtaining the dynamic response in any element of the train. These models are used when a more complex analysis is required, for example when the lateral and torsional effects are important or when it is desired to evaluate the local behaviour of some bridge's elements and the use of a 2D model is not suitable.

The train models can still be modelled based on the multibody dynamics concept (Pombo 2004, Tomioka and Takigami 2010) or on the finite element method (Li et al. 2010, Ribeiro 2012). According to Pombo (2004), the models based on multibody dynamics concept have the potential to reduce the computational effort in the dynamic analyses, since only some DOF of reference are analysed. However, the non-consideration of the flexibility of some structural elements, in particular of the car body, is usually reported as the main disadvantage.

In terms of the models based on the finite element method, beam and shell element are the most widely used, especially to model the bogies and the car body, respectively. Li et al. (2010) developed a complete model of a train, modelling the car body and the bogies through beam FE elements [Figure 2.12 a)] and using spring-dashpot elements to simulate the primary and secondary suspensions. Ribeiro et al. (2013) also developed a 3D numerical model for the Alfa Pendular (AP) train, the fastest passenger train in circulation on the Portuguese rail network, using the same approach to model the bogies. However, the car body of the motor vehicle of this conventional tilting train was modelled with shell FE elements [Figure 2.12 b)]. This author took yet into account the passenger-seat interface which allowed assessing the passenger riding comfort.

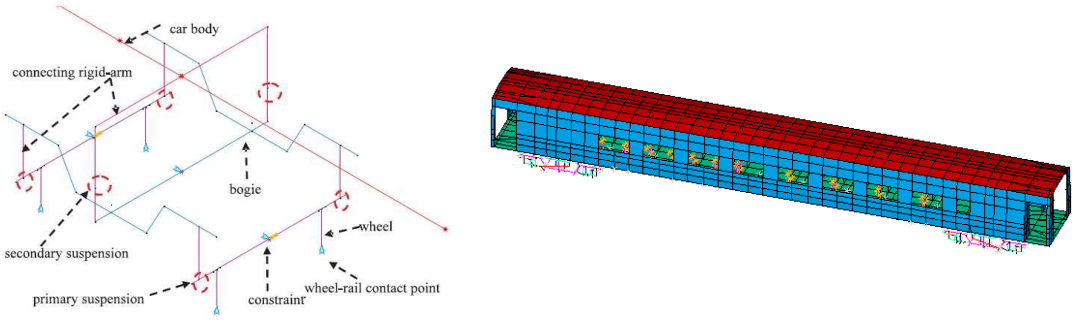

a) b)

Figure 2.12 – Train models based on the finite element method: a) bogie (Li et al. 2009); b) car body (Ribeiro et al. 2013)

Based on the work developed by Ribeiro et al. (2013), a simplified model of the train, in which the car body was modelled by a rigid beam with concentrated mass and rotational inertia, was adapted by Meixedo et al (2014). Top and front views of this model are shown in Figure 2.13. Table 2.2 shows the main mechanical and geometrical parameters of the numerical model of a typical AP train's motor vehicle. In the present dissertation, this simplified FE model of the train was considered in the numerical analyses.

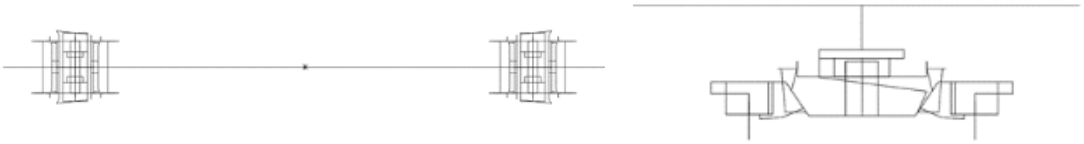

a) b)

Figure 2.13 – 3D numerical model of the AP train: a) top view; b) front view of a bogie

Table 2.2 – Mechanical and geometrical parameters of an AP train's motor vehicle

Parameter	Value
Stiffness of secondary suspension, k_s	367.4 kN/m (front) 343.1 kN/m (rear)
Damping of secondary suspension, c_s	35 kN.s/m
Stiffness of primary suspension, k_p	826.4 kN/m
Damping of primary suspension, c_p	16.7 kN.s/m
Stiffness of wheel-rail connection, k_{rc}	1.5674×10^9 N/m
Carbody translational mass, M	3261 kg

2.2.2.4 Track irregularities modelling

It is well-known, in the field of railway vehicle dynamics, that track irregularities are an important source of excitation, which affect the ride comfort, the train response and safety and also the bridge dynamic response (Cantero et al. 2016). Track irregularities are deviations in the geometry from the smooth track (Fryba 1996) and can be divided into isolated irregularities and distributed irregularities.

The isolated irregularities may be derived from switches & crossings, structural joints, the difference of stiffness of adjacent sections in transition zones, among others. The distributed irregularities are mainly due to the deterioration of the track geometry, rail corrugation or settlements and deformations along the track or in the supporting structures (Fryba 1996, Rigueiro 2007).

There are two different ways to define the track irregularities: using experimentally measured values or through random generation using power spectral density (PSD) functions. The use of experimentally measured track irregularities is generally limited to the analysis of specific cases but, in those situations, it can lead to a better understanding of the train-bridge behaviour. PSD functions have been proposed by railway administrations to be used in the random generation of track irregularities since several measurements have shown that track irregularities represent a stationary and ergodic Gaussian random process that may be adequately described by such functions (Fryba 1996).

The PSD function provided by the French administration SNCF (Société Nationale des Chemins de Fer Français) is given by the following expression (Fryba 1996, Alves Costa 2011) for each wavenumber k_1 (corresponds to the inverse of the wavelength, given by $k_1 = 2\pi/\lambda$):

$$S_{rzz}(k_1) = \frac{10^{-6}A}{\left(1 + \frac{k_1}{k_0}\right)^3} \tag{2.5}$$

which leads to a good approximation to the measured results for wavelengths between 2 m and 40 m. The parameter A depends on the track quality, assuming the value 160 and 500 for a track in good and bad quality, respectively, and k_0 is equal to 0.307 rad/m.

A more detailed proposal is presented by the American Federal Railroad Administration (FRA), which considers six different classes of tracks. In the FRA proposal, the PSD function of the irregularity profile is given by (Fryba 1996, Alves Costa 2011):

$$S_{rzz}(k_1) = \frac{10^{-7} A k_3^2 (k_1^2 + k_2^2)}{k_1^4 (k_1^2 + k_3^2)} \tag{2.6}$$

where k_2 and k_3 are constants which take the values 0.1466 rad/m and 0.8168 rad/m, respectively. Table 2.3 presents the values of the parameter A for 6 distinct geometric quality classes of the track.

Table 2.3 – Parameter A proposed by FRA (Alves Costa 2011)

Class	1	2	3	4	5	6
A (m^3/rad)	660.079	376.229	208.841	116.856	65.929	37.505

Figure 2.14 illustrates the power spectral density functions provided by these two railway administrations. Regarding the suggestions provided by FRA, only the PSD functions related to classes of tracks 1 and 6 are depicted in this figure.

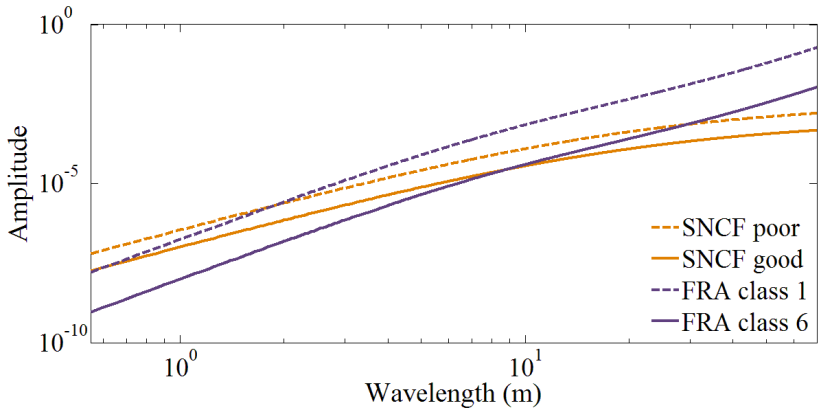

Figure 2.14 – PSD functions provided by two railway administrations – SNCF and FRA

2.2.3 Methods to solve the dynamic equilibrium equations

As mentioned before, there are different methods that can be used to solve the dynamic equilibrium equations in TBI analyses. Among others, the most common techniques are the Newmark's direct integration method and the modal-superposition method (Clough and Penzien 1993, Chopra 1995).

The Newmark method is an implicit method of direct integration of the set of dynamic equilibrium equations, in which the integration space is not changed and the contribution of all natural frequencies is taken into account. The stability and precision of this method are

controlled through the parameters γ e β (Clough and Penzien 1993). The Newmark method becomes unconditionally stable for $\gamma \geq 1/2$ and the maximum efficiency occurs to $\beta = (\gamma + 1/2)^2 / 4$. However, it is found that this method only shows 2nd order accuracy for $\gamma = 1/2$, which means to consider $\beta = 1/4$.

In order to solve the system of equilibrium equations using the Newmark method, it is important to define an appropriate structural damping matrix. Rayleigh damping matrix (**C**) is usually used, expressed as a linear combination of the mass (**M**) and stiffness (**K**) matrices, according to the following expression:

$$\mathbf{C} = \mathbf{M}c_1 + \mathbf{K}c_2 \tag{2.7}$$

The two damping factors, c_1 and c_2, are obtained by solving the following system of equations (Chopra 1995):

$$\frac{1}{2}\begin{bmatrix} 1/w_i & w_i \\ 1/w_j & w_j \end{bmatrix}\begin{Bmatrix} c_1 \\ c_2 \end{Bmatrix} = \begin{Bmatrix} \xi_i \\ \xi_j \end{Bmatrix} \tag{2.8}$$

where w_i and w_j correspond to the angular frequencies of the vibration modes i and j, respectively, and ξ_i and ξ_j are the corresponding structural damping ratios.

As an alternative to the direct integration methods, the modal-superposition method (Chopra 1995) has been widely used. This method is based on a transformation of general nodal coordinates (u) into modal coordinates (y), in order to proceed with the uncoupling of the general dynamic equilibrium equation [shown in Equation (2.1)]. This transformation is performed as follows:

$$\mathbf{u}(t) = \sum_{i=1}^{N} y_i(t) \cdot \boldsymbol{\varphi}_i \tag{2.9}$$

where $\boldsymbol{\varphi}_i$ is the i^{th} mode shape (does not vary with time), $y_i(t)$ is a scalar multiplier (modal coordinate) and N is the total number of mode shapes. Equation (2.1) can be re-written considering the orthogonality property of the mode shapes, and multiplying each term of this equation by $\boldsymbol{\varphi}_n^T$ (with n and i associated to different natural frequencies):

$$\boldsymbol{\varphi}_n^T\mathbf{M}\boldsymbol{\varphi}_n\ddot{y}_n(t) + \sum_{i=1}^{N} \boldsymbol{\varphi}_n^T\mathbf{C}\boldsymbol{\varphi}_i\dot{y}_i(t) + \boldsymbol{\varphi}_n^T\mathbf{K}\boldsymbol{\varphi}_n y_n(t) = \boldsymbol{\varphi}_n^T\mathbf{F}(t) \tag{2.10}$$

where it can be written as:

$$M_n\ddot{y}_n(t) + \sum_{i=1}^{N} \boldsymbol{\varphi}_n^T \mathbf{C} \boldsymbol{\varphi}_i \dot{y}_i(t) + K_n y_n(t) = F_n(t) \tag{2.11}$$

Equation (2.11) represents a system of N equations which are coupled through the damping terms. The modal equations can be uncoupled if $\boldsymbol{\varphi}_n^T \mathbf{C} \boldsymbol{\varphi}_i$ is taken as zero when $n \neq i$. Therefore it is possible, based on a new system of linearly independent equations, to obtain the individual response regarding each one of the vibration modes. The following expression illustrates the uncoupled equation regarding the vibration mode *i*:

$$M_i\ddot{y}_i + C_i\dot{y}_i + K_i y_i = F_i(t) \tag{2.12}$$

where M_i, C_i, K_i and F_i are the modal mass, damping, stiffness and load, respectively. Each differential equation of a single degree of freedom can be solved, for example, using the Newmark method. The global response of the structure is obtained by superposing the effects of each of the modal contributions.

Contrarily to the Newmark's direct integration method, in which all vibration modes of the structure are taken into account in the dynamic analysis, the great advantage of the modal-superposition method is the possible selection of the number of modes to be considered. This allows reducing the computational effort and has proved to be particularly useful to evaluate the effect of different range of frequencies in the global response of the structure.

Another advantage of the method is the possibility to define the damping ratio for each mode, which is more convenient and generally more reasonable since the modal damping ratios can normally be determined experimentally or estimated with adequate precision in many cases. One of the drawbacks of the method is the fact that it requires performing a modal analysis prior to the dynamic analysis in order to identify the structure mode shapes and the corresponding natural frequencies.

2.2.4 Time step selection

In order to perform a detailed evaluation of the dynamic response of the structure, the time step, Δt, to be considered in the numerical analyses should be carefully defined. Among others suggestions, ERRI (2001) pointed out that the selected time step should be the minimum of the following two values:

$$\Delta t = \frac{1}{8 f_{max}} \tag{2.13}$$

$$\Delta t = \frac{L}{4 n v_{max}} \tag{2.14}$$

where f_{max} is the frequency of the highest mode of vibration considered in the analysis, L is the span of the bridge, n is the number of modes considered in the analysis and v_{max} is the maximum train speed.

The criterion defined by Equation 2.10 guarantees that a cycle corresponding to the sinusoidal movement of highest vibration mode (highest frequency) is represented by a minimum of eight points. The criterion given by Equation 2.11 is intended to ensure that the excitation is sufficiently well characterised in the dynamic analyses, thus ensuring that the period of time of a given load moving at maximum speed over the structure is discretised into $4n$ intervals.

In some cases, the selection of the time step might also depend on the characteristics of the train and the track irregularities to be used in the numerical analyses. Generally, the train frequencies are lower than those related to the bridge, and for this reason this criterion is usually less limitative. However, when track irregularities are to be considered in the numerical analyses, special attention should be paid, since depending on the train speed and on the irregularities wavelengths under consideration, this might be the conditional criterion to reproduce an accurate response. Special attention is given to each case-study discussed in this thesis.

2.2.5 Quasi-static correction procedure

As mentioned before, the TBI methodology is considered in the present dissertation to evaluate the dynamic response of the bridge under the passage of railway traffic. The methodology presented by Ribeiro (2012), which combines the modal-superposition and Newmark's direct integration method to solve the bridge and train systems, respectively, is used.

The modal-superposition method has proved to be an efficient procedure from a computational point of view, reducing considerably the total analysis time. However, in the

study of structural elements with a localised behaviour, as in the case of RC slabs in railway bridges, their dynamic behaviour might strongly influenced by the contribution of local vibration modes, which are normally associated to smaller wavelengths and therefore to higher frequencies. Thus, it is common to consider a large number of vibration modes in the dynamic analysis to make sure that, at least, the static response of the structure can be ensured, which can lead again to a higher computational effort. If the structure response is dominated by local vibration modes, there is no guarantee that the correct structure response is obtained, even if a great number of vibration modes is considered in the analysis of the bridge subsystem (when the basic modal-superposition method is used).

Therefore, an improved formulation of the modal-superposition method is applied in the present dissertation, in the analysis of the bridge subsystem. It combines the modal-superposition method with a static correction procedure, using the influence surface to obtain the static contribution of vibration modes of higher frequencies, which are not explicitly considered in the basic modal-superposition method. This methodology guarantees that the static component of the structural response is properly captured, and is correctly added to the dynamic component of the response associated to all the vibration modes considered in the analysis.

The static correction procedure is reported in the literature (Clough and Penzien 1993, Chopra 1995) as a technique to consider the static contribution of vibration modes with higher frequency which are often not considered in the dynamic analysis using the basic modal-superposition method. Clough and Penzien (1993) and Chopra (1995) deal with load regimens whose magnitude varies in time, having a fixed space distribution. The case of loads for which both the magnitude and the space distribution vary in time can be dealt with as described in the following paragraphs. The relevance of considering a static correction procedure in the calculation of local effects in railway bridge decks has already been pointed out by Pimentel et al. (2008).

In the basic modal-superposition method, the time-record $G_a(t)$ for any parameter (displacement, stress, bending moment, etc.) in the node a and in the instant of time t is given by:

$$G_a(t) = \sum_{n=1}^{N^*} G_{an} \cdot y_n(t) \tag{2.15}$$

where N^* is the total number of vibration modes considered in the analysis, G_{an} is the parameter value in the node a and in the *n*-th vibration mode and $y_n(t)$ the time-record of the modal coordinate for the *n*-th vibration mode. As mentioned before, this method does not guarantee that the obtained results include the total static response to the applied forces, when the structural behaviour is governed by local effects.

The static correction procedure consists of considering, in the improved modal-superposition method, a limited number of vibration modes, N^* (those which are expected to have a significant contribution in terms of inertial forces, i.e., in terms of the dynamic amplification of internal forces). The static component (s) of the contribution of each of those vibration modes can be calculated, for each instant of time, by dividing the modal forces $F_n(t)$ by the modal stiffness K_n, as shown by Clough & Penzien (1993):

$$y_{sn}(t) = \frac{F_n(t)}{K_n} = \frac{\boldsymbol{\varphi}_n^T \mathbf{f}(t)}{\boldsymbol{\varphi}_n^T \mathbf{K} \boldsymbol{\varphi}_n} \tag{2.16}$$

where $\boldsymbol{\varphi}_n$ is the vector containing the coordinates of the *n*-th vibration mode for the nodes of the rail path, $\mathbf{f}(t)$ is the vector of wheel loads applied to the nodes of the rail path in the instant of time t and K is the structure's stiffness matrix.

On the other hand, the total static response of the structure (i.e., the total static component of the parameter G), for each node a, $G_{a,s}(t)$ can be calculated as a function of the influence surface A_{nk} (value of the parameter G in node a when the structure is subjected to a unit force in node k):

$$G_{a,s}(t) = \sum_{k=1}^{m} A_{nk} \cdot f_k(t) \tag{2.17}$$

where m is the total number of nodes in the load path.

Thus, an improved calculation of the time-record for $G_n(t)$ for any parameter can be determined by adding the total static component to the dynamic component of the response associated to the N^* modes considering in the improved modal-superposition analysis:

$$G_n(t) = \sum_{k=1}^{m} A_{nk} \cdot f_k(t) + \sum_{n=1}^{N^*} G_{an} \cdot y_n(t) - \sum_{n=1}^{N^*} G_{an} \cdot y_{sn}(t) \tag{2.18}$$

2.3 Standard's recommendations concerning the safety of railway bridges

The passage of rail traffic over a structure induces efforts and displacements, in general, greater than those caused by static loading. According to EN1991-2 (CEN 2003), the consideration of these dynamic effects can be performed in two ways: affecting the static effects through a dynamic factor Φ or performing dynamic analyses. The following subsections summarise the normative conditions for the application of each one.

2.3.1 Consideration of dynamic effects in static analyses

According to EN1991-2 (CEN 2003), a static analysis can be carried out based on the use of Load Models LM71, SW/0 and SW/2. In order to take into account the dynamic effects, the results obtained from the static analysis must be multiplied by a dynamic factor Φ. This factor takes account of the dynamic magnification of stresses and vibration effects but it does not allow reproducing the effects caused by the resonant phenomena.

This dynamic coefficient depends on the maintenance level of the track, whether it may be standard (Φ_3) or careful (Φ_2) and is given by the following expressions, respectively:

$$\Phi_3 = \frac{2{,}16}{\sqrt{L_\Phi} - 0{,}2} + 0{,}73 \text{ with } 1{,}00 \leq \Phi_3 \leq 2{,}00 \tag{2.19}$$

or

$$\Phi_2 = \frac{1{,}44}{\sqrt{L_\Phi} - 0{,}2} + 0{,}82 \text{ with } 1{,}00 \leq \Phi_2 \leq 1{,}67 \tag{2.20}$$

where L_Φ is the "determinant" length, which represents the length of the influence line for deflection of the element being analysed, and can be found in Table 6.2 of EN1991-2 (CEN 2003).

In cases where it is relevant to evaluate the structural response during the passage of real trains (RT), it can be achieved through the multiplication of the static effects, resulting of this passage, by the dynamic amplification factor $(1 + \varphi' + \lambda\varphi'')$, where φ' is given by the following expression:

$$\varphi' = \begin{cases} \dfrac{K}{1 - K + K^4} & \text{with } K < 0{,}76 \\ 1{,}325 & \text{with } K \geq 0{,}76 \end{cases} \tag{2.21}$$

where

$$K = \frac{\mathrm{v}}{2L_{\Phi}n_0} \tag{2.22}$$

The coefficient φ'' can be obtained by the following expression:

$$\varphi'' = \frac{\alpha}{100}\left[56e^{-\left(\frac{L_{\Phi}}{10}\right)^2} + 50\left(\frac{L_{\Phi}n_0}{80} - 1\right)e^{-\left(\frac{L_{\Phi}}{20}\right)^2}\right] \geq 0 \tag{2.23}$$

where

$$\alpha = \begin{cases} \frac{\mathrm{v}}{22} & para\ \mathrm{v} \leq 22\ m/s \\ 1 & para\ \mathrm{v} > 22\ m/s \end{cases} \tag{2.24}$$

where λ corresponds to a factor that accounts for the quality of the track maintenance, v corresponds to the train speed and n_0 is the natural frequency of the bridge.

2.3.2 Standard's criteria to perform dynamic analyses

According to EN1991-2 (2003), the decision on whether or not to perform a dynamic analysis of the structure is taken based on the flowchart shown in Figure 2.15. Essentially, dynamic analyses are needed in cases where resonance phenomena may occur, since the amplification that happens in these situations is not predicted in the aforementioned Equations (2.19) to (2.24).

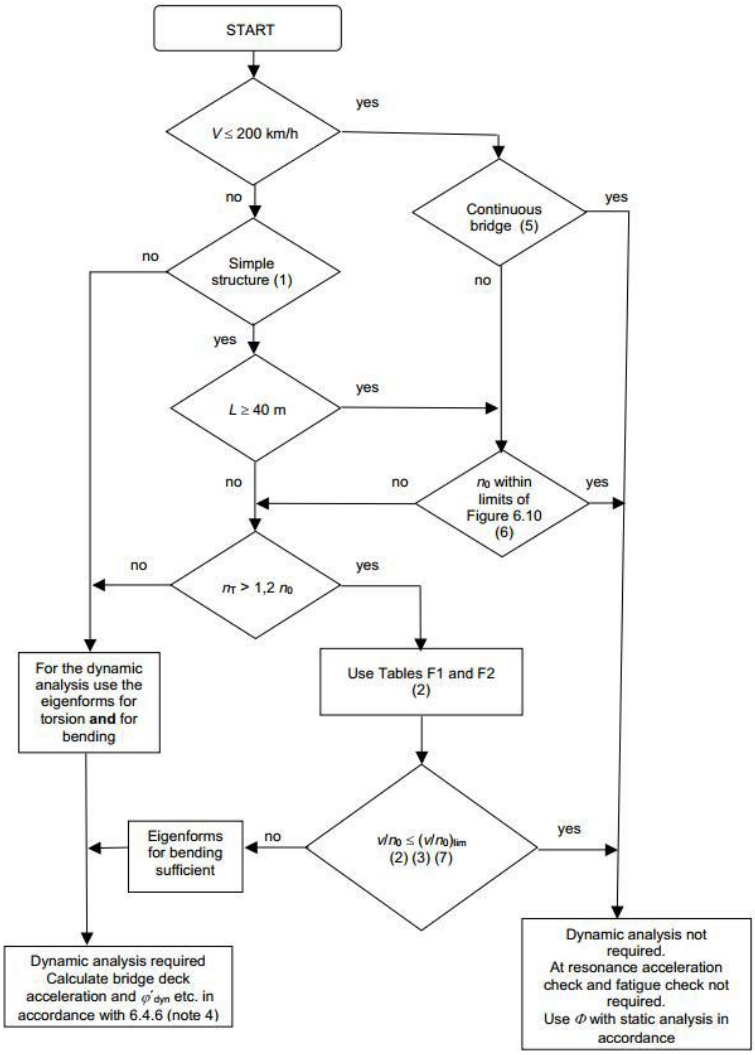

Figure 2.15 – Flowchart supporting the decision to perform a dynamic analysis [EN1991-2 (CEN 2003)]

In this flowchart, v (km/h) corresponds to the maximum train speed over the bridge, L (m) is the span of the bridge, n_0 (Hz) corresponds to the first natural frequency related to a vertical bending vibration mode, n_T is the first natural frequency related to a torsional vibration mode and $(v/n_0)_{lim}$ are the limits given in Annex F of EN1991-2. The upper and lower limits for the fundamental frequency of the bridge, as a function of the span, are also given in EN 1991-2.

The dynamic analyses are performed based on the characteristic values of the axle loads of various real trains specified for the particular design project and also on the High Speed Load Models (HSLM), the latter in the case of railway bridges on international lines to take into account the interoperability criteria defined in TSI (2002). The HSLM load model, indicated in Annex E of EN1991-2, was developed in order to ensure that the dynamic effects that occur

with the passage of the current high-speed trains, and with the passage of that come to circulate in the future, are covered by the defined envelope values.

EN1991-2 suggests that the efforts and/or displacements of the structure to be considered in its design can be obtained by multiplying the static effects, due to the passage of real trains, by a dynamic amplification factor $(1 + \varphi)$, which is given by the following expression:

$$1 + \varphi = 1 + \varphi_{dyn}{}' + \lambda\varphi'' \tag{2.25}$$

where $\varphi_{dyn}{}'$ corresponds to a dynamic amplification factor which can be obtained by expression (2.19) taking into account the quotient between the maximum value of the dynamic response y_{dyn} and the static response y_{stat} for a specific location of the structure, φ'' is a factor used to take into account the effect of track and wheel irregularities, and λ a factor related to track maintenance (1.0 for tracks with standard maintenance levels or 0.5 for tracks carefully maintained).

$$\varphi_{dyn}{}' = max\left|\frac{y_{dyn}}{y_{stat}}\right| - 1 \tag{2.26}$$

An important aspect to take into account in the numerical analyses is related with the speed range to be considered. Train speeds from 40 m/s (≈145 km/h) to 1.2 times the maximum speed allowed in the railway line under evaluation should be adopted as well as a suitable time step that allows to correctly identifying all the peaks of the response.

The standard EN1991-2 also defines the values of the damping coefficients to be considered, as a function of the type of bridge and corresponding span, which can be found in Table 2.4. This parameter has revealed great importance since an underestimation of this values leads to a considerable increase in the amplitude of the structural response. It is important to point out that the values presented in the table below were obtained taking into account only the global behaviour of bridges. In some cases, the local behaviour of some structural elements may be also preponderant, due to the existence of several local vibration modes, and special attention should be paid. However, the information about the damping coefficients that should be used in these local vibration modes is scarce and no recommendation is given by the standard EN1991-2.

Table 2.4 – Damping coefficients to railway bridges (adapted of EN1991-2 (CEN 2003))

Bridge type	Lower limit of the damping coefficient ξ (%)	
	Span L ≤ 20 m	Span L ≥ 20 m
Steel or composite	ξ = 0,5 + 0,125 (20 – L)	ξ = 0,5
Prestressed concrete	ξ = 1,0 + 0,07 (20 – L)	ξ = 1,0
"Filler-beam" and reinforced concrete	ξ = 1,5 + 0,07 (20 – L)	ξ = 1,5

2.3.3 Limit states

The Eurocodes establish the criteria that must be verified in the design of railway bridges, involving the Ultimate Limit States (ULS) for the bridge structures, Serviceability Limit States (SLS) for the bridge structure, as well as SLS to ensure adequate track behaviour, traffic safety and passenger comfort. The following subsections summarise the most relevant in the context of this research.

2.3.3.1 Structural safety

Concerning the structural safety, when a dynamic analysis is mandatory, the standard defines that the effects based on railway loads must be calculated for the most unfavourable of the following scenarios:

$$\left(1 + \varphi_{dyn}' + \lambda\varphi''\right) \times \begin{pmatrix} HSLM \\ \text{or} \\ RT \end{pmatrix} \tag{2.27}$$

or

$$\Phi \times (LM71" + " SW/0) \tag{2.28}$$

where $HSLM$ correspond to the load models previously mentioned in section 2.3.2, RT represents the several real trains operating in the line, $LM71$ and $SW/0$ stand for the static effects of vertical loading due to normal rail traffic in generic structures and in continuous structures, respectively, and φ_{dyn}' consists on a dynamic amplification factor that can be obtained by expression (2.19).

Another important verification on railway bridges is related with the fatigue safety assessment, whose specific recommendations are discussed further in Chapter 3.

2.3.3.2 Traffic safety

The EN1990 (Annex A2) standard defines a set of verifications needed to guarantee the safety of the railway track and to avoid phenomena of ballast instability, derailment of the trains by excessive twisting of the deck and excessive deformation of the track. Bearing this is mind, there are limits imposed to the vertical acceleration, torsion, vertical deformation and transverse deformation and vibration of the deck. Since the focus of this dissertation is the vertical behaviour of the bridge, only the verifications related to this behaviour will be presented in the following subsections.

2.3.3.2.1 Vertical acceleration of the deck

In order to avoid ballast instability, which leads to the loss of lateral resistance of the track and consequently affects the running safety of the trains, EN 1990-A2 [CEN 2005 a)] imposes the limit of 3.5 m/s^2 for the maximum vertical acceleration of the deck. This value must be verified on all structural elements that support the railway track, considering vibration frequencies up to the maximum value of: 30 Hz; 1.5 times the value of the frequency of the fundamental vibration mode; and the natural frequency of the third vibration mode of the element under evaluation.

The criteria for limiting the vertical acceleration have not been consensual and it is important to point out here the conclusions of some investigations. Norris (2005), based on experimental tests performed in more than 100 railway bridges across the United Kingdom, concluded that there are small areas that may be subjected to acceleration levels higher than 1g (see red zones in Figure 2.16), but with the ballast layer remaining stable as adjacent ballast provides confinement and prevents local instability. Based on these results Norris suggests new values for the acceleration limit: 5 m/s^2 for ballasted bridges and 6 m/s^2 for bridges that present higher structural damping levels.

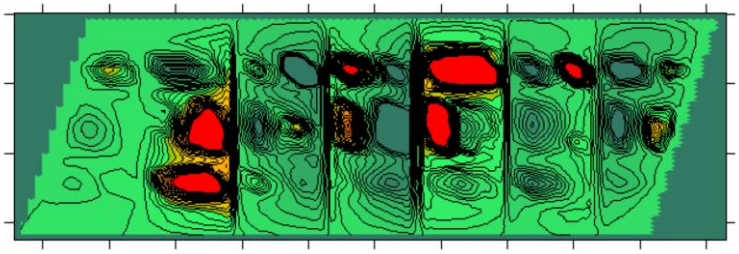

Figure 2.16 – Acceleration levels on a railway deck (Norris 2005)

By performing laboratory tests, Zacher and Baeβler (2009) also demonstrated that the ballast layer is significantly affected when acceleration values reach 7 m/s^2. These results point out that the limit value suggested in the standard for ballast tracks results from the application of a safety factor of 2. Since it seems to be a very conservative value, the authors suggest a smaller value, corresponding to 1.3, leading to a limit value of the acceleration equal to 5.5 m/s^2.

In recent studies, Baeβler et al. (2012) also evaluated the maximum frequency that should be considered in the dynamic analyses. It was found that the transfer function between the ballast layer and the sleeper continues to grow up to a frequency of 60 Hz, as shown in Figure 2.17. Considering this, the authors concluded that higher frequencies are not less critical than the lower frequencies, although being associated with smaller wavelengths their effects correspond to a more localised phenomena. In order to avoid the ballast instability, associated with higher frequency vibration modes, it would be advisable to change the maximum frequency threshold to a value equal to 60 Hz.

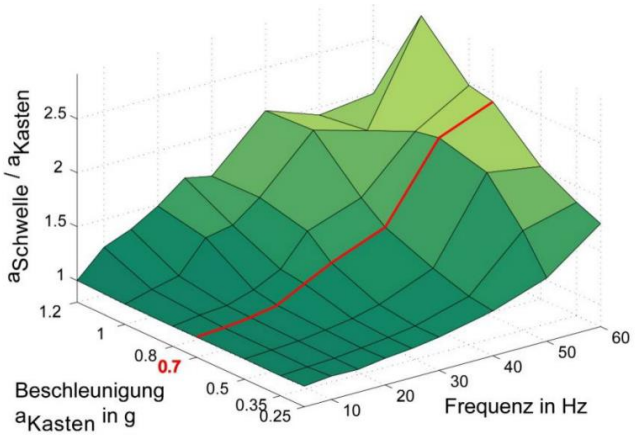

Figure 2.17 – Transfer function between ballast and sleeper (Baeβler et al. 2012)

2.3.3.2.2 Vertical deformation of the deck

In addition to the limit for the vibration of the deck, a limit for its vertical deformation is also imposed, in order to avoid excessive bending of the track.

The maximum vertical deformation of the deck due to the load model LM71 (or SW/0 and SW/2 in the bridges where these are applicable) should not exceed L/600, where L is the span of the bridge. The static effects of load models LM71, SW/0 and SW/2 should be multiplied by the aforementioned dynamic factor. In bridges with two tracks, the loads should be applied to both.

2.3.3.2.3 Transversal deformation of the deck

The transversal deformation of the deck has to be controlled in order to limit the angular variation and horizontal radius of curvature, according to the values presented in Table 2.5. The angular variations are related either to the transversal rotations at the end of the deck or to the relative transversal rotations between two adjacent spans. This values are to be evaluated based on the application of the Load Models LM71 and SW/0, multiplied by the dynamic factor Φ, wind loads, centrifugal forces and the temperature's transverse differential across the bridge.

Table 2.5 – Design limit values of angular and radius of curvature (EN 1990 – Annex A2, 2001)

Speed v (km/h)	Maximum angular variation (rad)	Minimum radius of curvature (m)	
		Single span	Multi-span
$v \leq 120$	0.0035	1700	3500
$120 < v \leq 200$	0.0020	6000	9500
$v > 200$	0.0015	14000	17500

2.3.3.2.4 Deck twist

The EN 1990-Annex A2 (2001) defines the maximum twist allowed in order to minimize the risk of train derailment, which should be calculated based on the characteristics values of the Load Models LM71, SW/0 or SW/2, as appropriate, and HSLM. In the Table 2.6 are

presented the maximum values for a track gauge of 1435 mm over a length of 3 m, depending on the train speed under analysis.

Table 2.6 – Design limit values of angular and radius of curvature (EN 1990 – Annex A2, 2001)

Speed v (km/h)	Maximum twist (mm/3m)
$v \leq 120$	4.5
$120 < v \leq 200$	3.0
$v > 200$	1.5

2.3.3.3 Passenger riding comfort

The passenger comfort level is directly related to the vertical accelerations to which they are subjected within the trains. This level of comfort can be considered very good, good or acceptable depending on the recorded value of the accelerations: 1.0, 1.3 or 2.0 m/s^2, respectively (CEN 2005 a)).

The numerical evaluation of the accelerations in the trains can only be performed based on dynamic analyses that consider the interaction between the bridge and the train, with the latter being explicit modelled. Alternatively, Annex A2 of EN1990 suggests a simplified methodology based on the maximum value of the vertical displacement of the deck, in the alignment of the loaded track, considering the LM71 load model affected of the respective dynamic amplification factor. Depending on the span of the bridge (L) and the speed of the train (V), the displacement value must be lower than the limit shown in Figure 2.18 in order to achieve a very good comfort level.

This abacus was defined for simply supported bridges with 3 or more spans. For bridges with less spans, the limit values in the figure should be multiplied by 0.7. In the case of continuous bridges with 3 or more spans, these values shall be multiplied by 0.9.

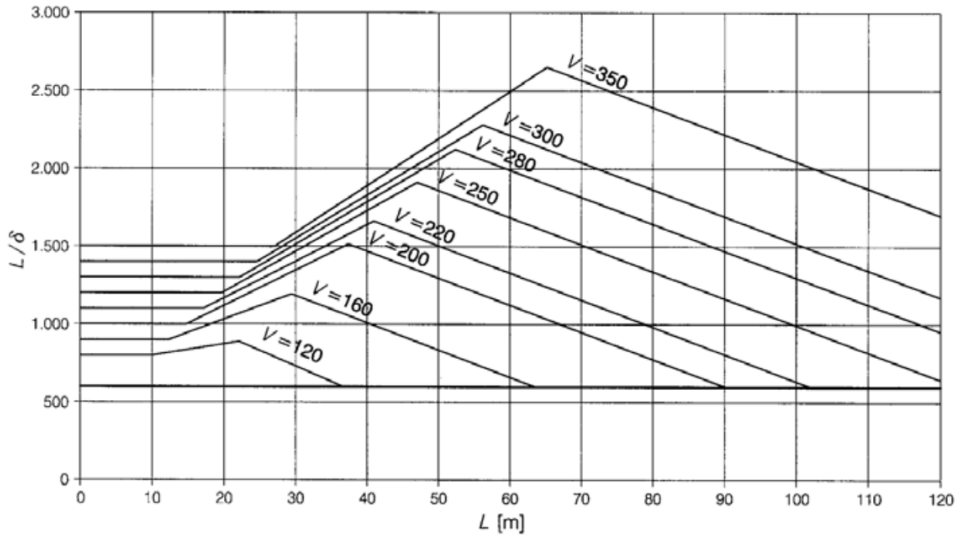

Figure 2.18 – Maximum acceptable vertical deflection to ensure a very good level of comfort (CEN 2005 a))

Chapter 3

Fatigue analysis of railway bridge deck slabs

3.1 Introduction

The geometrical and mechanical characteristics of structural materials change naturally over time as a result of the action of both environmental factors and traffic over the structures. In the case of railway bridges, the successive application of loads in a short period of time, although lower than those that could cause the structure collapse but with high repeatability over its useful life, can lead to the occurrence of fatigue phenomena. These usually give rise to the appearance and subsequent development of cracks in some elements of the structure.

Constructions composed by longitudinal girders and an upper reinforced concrete (RC) slab consists on a particular structural solution that have been widely used in the construction of railway bridge decks. RC deck slabs in railway bridges and viaducts can be particularly sensitive to dynamic effects induced by trains owing to the resonance phenomena originated by periodic loading associated with the passage of regularly spaced train's axles groups. The increase in these dynamic effects, due to higher train speeds, higher axle loads and the existence of track irregularities or wheel defects, can lead to excessive bridge vibrations, giving rise to fatigue damage.

According to Schlafli and Bruhwiler (1998) and Zanuy et al. (2011), RC deck slabs are the bridges' structural elements most susceptible to the occurrence of fatigue phenomena, since a high number of loading cycles can occur, which can exceed 100 million over the total life of

the structure. This is due to the fact that they often present a low thickness and a low reinforcement rate, in order to comply with the standard's recommendations as far as static behaviour is concerned.

The main girders of concrete bridges are usually prestressed in the longitudinal direction, reason why there is generally no cracking related with the stresses in this direction. So the fatigue resistance of deck slabs is usually controlled by the fatigue damage of transverse tensile reinforcement and not by the fatigue damage of concrete. In fact, in slab plates subjected to significant cyclic bending moments, fatigue of concrete under compression is not observed in experiments. This is because the redistribution of concrete stresses within the cross-sections prevents the fatigue failure of concrete, and results in fatigue of the reinforcement (Johansson 2004, Schlafli and Bruhwiler 1998, Zanuy et al. 2011, Zanuy et al. 2009).

It has also been shown that the fatigue life of slab elements is very sensitive to the value of applied stresses. Pimentel et al. (2008) have carried out a parametric study of the fatigue life of short-span RC bridges, concluding that it is drastically reduced when heavier axle loads are considered, even though the total traffic volume (tonnes/year) is not significantly changed. The authors also concluded that, in the design of new structures, a small increase in the slab's reinforcement rate can lead immediately to a better behaviour in terms of fatigue resistance.

The evaluation of the fatigue behaviour plays an important role in the design of new structures subjected to cyclic loading. This becomes even more crucial when has been proved that several existing bridge decks do not comply with the requirements of actual design codes in terms of fatigue resistance (Bogaert 2009). Bearing this in mind, a carefully assessment of fatigue strength in bridge decks should be performed, especially in railway bridges that are subjected to important cyclic loading. In fact, as the importance of cyclic loading increases, fatigue verifications become more critical, by comparison with other limit states. For that purpose, EN 1992-2 (CEN 2005) provides fatigue-strength verification procedures on RC structural elements, namely, the detailed damage accumulation method and the simplified damage equivalent stress method. In this chapter, these two methods are presented, with particular attention to the detailed one since it is the method used in the present work. Since RC consists of a composite material, the fatigue strength depends on the fatigue properties of each of the constituent materials, reason why this chapter starts with a brief presentation of the fatigue behaviour of the reinforcing steel, plain concrete and RC concrete structures. A

comprehensive description of the fatigue behaviour of RC structures can be found in both ERRI D216/DT386 (2000) and RILEM Committee 36 RDL (1984) reports.

3.2 Fatigue of reinforcement

Some experimental works have been done in order to understand the behaviour of reinforcing steel under cyclic loading.

Tilly (1979) performed axial and bending fatigue tests, under constant stress amplitude, on rebars in air and embedded in concrete, respectively. The results of these tests are on the basis of the standard S-N curves used still nowadays for fatigue safety evaluation.

More recently, Nunes (2014) performed several experimental high-cycle fatigue tests in distinct reinforcing bars (hot rolled, cold worked and quenched/self-tempered) in order to investigate its fatigue strength. Since fatigue cracks tend to initiate on the surface, the author found that surface imperfections were the determinant factor that led to the fracture of rebars, at similar stress ranges as applied for survival rebars. These imperfections are produced during the manufacturing process and located near the transversal ribs, in the zone of highest stress concentrations.

The extensive investigations that have been done during the last decades have provided a lot of knowledge about the behaviour of the reinforcement under cyclic loading. As occur in other metallic materials, the fatigue life of reinforcing steel comprises three phases (D216 2002): the crack initiation phase that usually appears at the places of stress concentration; a slow propagation phase; and the fracture of the cross section. Some particularities in the behaviour of the reinforcement, regarding this fatigue phenomenon, have been found (D216 2002, Fryba 2002):

- the stress range ($\Delta\sigma = \sigma_{max} - \sigma_{min}$) is the main factor affecting the fatigue damage of reinforcement, if the total loading does not lead to plastic deformation;
- the curvature of reinforcing bars can lead to a reduction of ≈ 30% in the fatigue strength;
- the fatigue strength weakly diminishes with the increasing diameter of reinforcing bars;

- mechanically joined bars have a small effect if the lapped joins are longer than 20 times the diameter of the bar while, in opposition, welded joins can lead to a reduction up to 50 % in fatigue strength;
- surface corrosion is negligible if it is lightly distributed but it can strongly affect the fatigue strength if it is concentrated.

Usually, the fatigue life of the reinforcement subjected to axial forces is expressed by means of Wöhler curves (also known as S-N curves), which provide the number of permissible load cycles N, before fatigue failure, for a given stress amplitude $\Delta\sigma_s$, as presented in Figure 3.1. EN1992-1-1 allows obtaining different S-N curves as function of the type of reinforcement, such as straight and bent bars, welded bars and splicing devices, by presenting different values for the parameters shown in Figure 3.1. Table 3.1 shows the S-N curves' parameters for reinforcing steel.

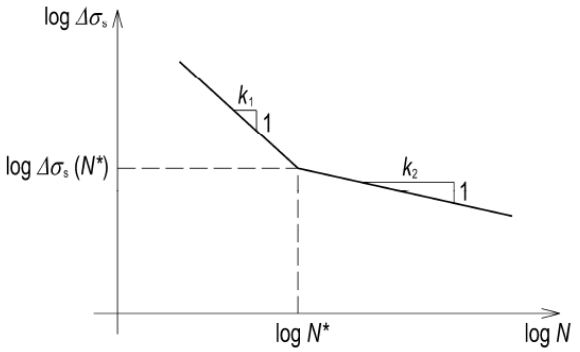

Figure 3.1 – Wöhler (S-N) curve for reinforcement

Table 3.1 S-N curves' parameters for reinforcing steel (EN 1992-1-1)

Type of reinforcement	N^*	k_1	k_2	$\Delta\sigma_{Rsk}(N^*)$ (MPa)
Straight and bent bars	10^6	5	9	162.5
Welded bars and wire fabrics	10^7	3	5	58.5
Splicing devices	10^7	3	5	35

Note: values for $\Delta\sigma_{Rsk}(N^*)$ are those for straight bars. Values for bent bars should be obtained using a reduction factor $\zeta = 0.35 + 0.026\ D/\varnothing$, where D is the diameter of the mandrel and $\varnothing$ is the bar diameter.

3.3 Fatigue of concrete

In contrast to reinforcing steel, plain concrete is a less homogeneous material due to the presence of cement paste and coarse aggregates of distinct dimensions. In this sense, fatigue cracks can present a complex behaviour, which can hardly be accurately predicted. The fatigue failure in concrete is usually attributed to the deterioration of the bond between the coarse aggregate and the cement paste, and also, to the presence of small cracks within the cement paste due to the shrinkage effect during hardening period and externally applied loads (Murdock and Kessler 1960, Antrim 1965).

Several experimental tests have been carried out in order to predict the fatigue behaviour of plain concrete, considering distinct types of loading or material properties. Tepfers (1979) evaluated the effect of different wave shapes, e.g. sinusoidal, triangular and rectangular shapes in the loading applied to concrete prisms, as shown in Figure 3.2. The number of cycles to failure as well as the wave shape is also shown. As seen, the rectangular wave proved to be the most damaging one.

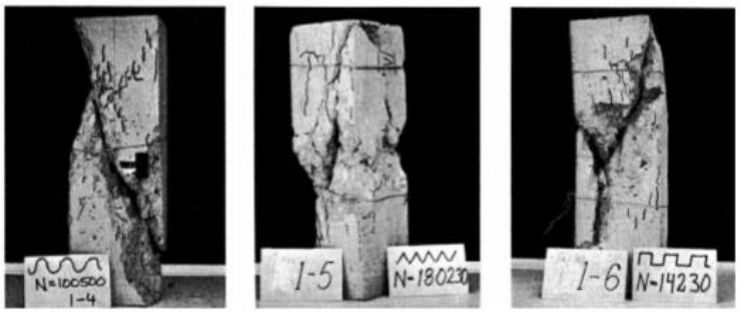

Figure 3.2 – Tests prisms after fatigue failure (Tepfers 1979)

Holmen (1982) performed static and dynamic tests in a total of 612 specimens of plain concrete. In addition to fatigue strength, special attention was paid to the deformation characteristics of the concrete. The author pointed out that the evolution of the concrete deformations due to fatigue phenomenon involves three stages: a first stage corresponding to the formation of the crack, with a fast increase of deformation; the intermediate stage where the deformations grow at a constant rate; and the last stage related to last cycles (typically the last 10% to 15% of fatigue life) where a rapid increase in deformation occurs, with an increasing rate that leads to the failure of the specimen.

Cachim (1999) evaluated the fatigue behaviour of plain and fibre-reinforced concrete under compressive and flexural fatigue tests. The author found that the addition of fibres to concrete increases the failure deformation, which may be important if stress redistribution is likely to occur in the structural system. Under compressive fatigue, it was observed that the 30 mm length fibres increased the fatigue life of concrete while the 60 mm fibres reduced it, showing the influence of the concrete properties in the overall fatigue performance of concrete.

Some factors have been found to influence the fatigue behaviour of plain concrete (D216 2003, RILEM 1984):

- mean stress (unlike steel, concrete strength depends on the maximum and minimum stress in each cycle);
- type of loading;
- loading frequency (a loading frequency between 1 Hz and 15 Hz only has a slight effect if the maximum stress does not exceed 75 % of the compressive strength; at higher stress levels, the fatigue strength decreases as the loading frequency decreases);
- concrete composition and curing conditions;
- confining stresses (confinement seems to prolong the fatigue life considerably);
- rest periods (the periods between blocks of cyclic loading seem to increase the fatigue life).

Usually, the fatigue strength of the concrete under a constant-amplitude cyclic loading is expressed by means of Wöhler curves, which provide the number of resisting load cycles *N*, before fatigue failure, as function of the minimum and maximum stress levels (Figure 3.3).

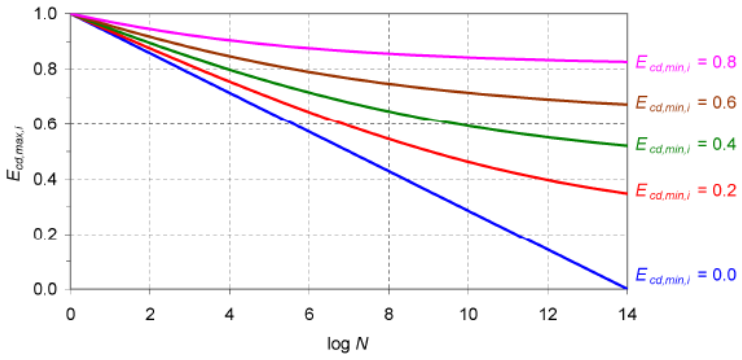

Figure 3.3 – Wöhler curves for concrete under compression [Sousa (2012), according EN 1992-2(CEN 2005)]

According to the EN 1992-2 (CEN 2005), the number of permissible load cycles for concrete under compression is given by the following expression:

$$N_i = 10^{14\frac{1-Ecd,max,i}{\sqrt{1-R_i}}} \tag{3.1}$$

where

$$R_i = E_{cd,min,i}/E_{cd,max,i} \tag{3.2}$$

$$E_{cd,min,i} = \sigma_{cd,min,i}/f_{cd,fat} \tag{3.3}$$

$$E_{cd,max,i} = \sigma_{cd,max,i}/f_{cd,fat} \tag{3.4}$$

and $\sigma_{cd,min,i}$ and $\sigma_{cd,max,i}$ correspond to the minimum and maximum stress in a cycle, respectively, and $f_{cd,fat}$ is the fatigue reference strength of concrete given by the following expression:

$$f_{cd,fat} = k_1 \cdot \beta_{cc}(t_0) \cdot \frac{f_{ck}}{1.5} \cdot \left(1 - \frac{f_{ck}}{250}\right) \tag{3.5}$$

where k_1 is a reduction factor to consider the actual frequencies of loading (whose recommended value is 0.85), $\beta_{cc}(t_0)$ is a coefficient to define the compressive strength at the beginning of the cyclic loading t_0 (given in EN1992-1-1) and $(1 - f_{ck}/250)$ consists on a factor to take into account the increasing fatigue sensitivity of concrete with increasing compressive strength (f_{ck} in MPa).

3.4 Fatigue of reinforced concrete structures

As shown before, plain concrete and reinforcing steel present different behaviour under cyclic loading. As the reinforced concrete consists of a composite material, the fatigue strength depends on the fatigue properties of each of the constituent materials as well as the connection between them. Given that the stress amplitudes in uncracked structures are quite reduced, significant fatigue damage only occurs after cracking, particularly in the cases of steel and of concrete under compression. Therefore, distinct modes of failure can occur in RC structures concerning the fatigue of the concrete or the reinforcement, as briefly presented in the following subsections.

3.4.1 Bending failure

Cyclic loading gives rise to an increase in bending deformations due to the progressive occurrence of cracking, a reduced stiffness of concrete under compression and a degradation of the bond connection between the concrete and tensile reinforcement (Sousa 2012).

In the case of structural elements with low reinforcement ratio, the fatigue failure usually occurs due to the failure of the reinforcement (RILEM 1984). However, in elements with high reinforcement ratios, the failure can occur by the concrete in the most compressed fibre. Important stress redistributions take place in the concrete compression zone, due to the transference of stresses from more loaded to less loaded fibres in the cross section (Zanuy et al. 2009, Zanuy et al. 2007). Fatigue failure of the concrete is preceded by greater deformations of the structure, giving rise to a ductile rupture, while the fatigue failure of tensile reinforcement might occur without advance warning, resulting in a brittle failure. In slab elements, the fatigue rupture of all the bars in the most stressed cross-section is usually not simultaneous (Johansson 2004).

3.4.2 Shear failure in members without stirrups

The fatigue failure by shear effect is strongly dependent on whether there are stirrups on the structural element. According to the RILEM Committee (1984), there are two modes of failure associated to cyclic shear forces in elements without shear reinforcement, as shown in Figure 3.4, by propagation of a diagonal crack along all cross section or by squeezing the concrete in the compressed zone above the crack. CEB (1988) also pointed out that after the development of the critical shear crack, when it reaches a high width, shear transference across the crack is prevented and the beam may fail due to fatigue of the compression strut, without being possible to predict the number of load cycles that can be resisted after the critical shear crack is formed.

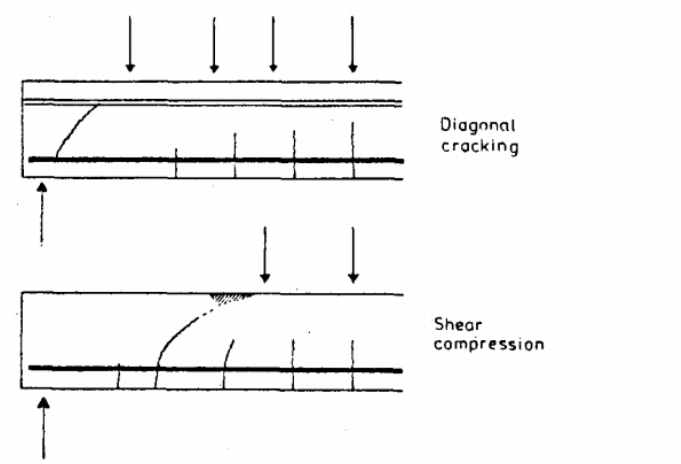

Figure 3.4 – Types of shear fatigue failure in beams without shear reinforcement (RILEM 1984)

3.4.3 Shear failure in members with stirrups

In structures with shear reinforcement, four fatigue failure scenarios can occur, as shown in Figure 3.5: failure of the shear reinforcement, the compressed concrete above the critical shear crack, the longitudinal reinforcement crossing the crack and the concrete compression strut in the middle of the beam.

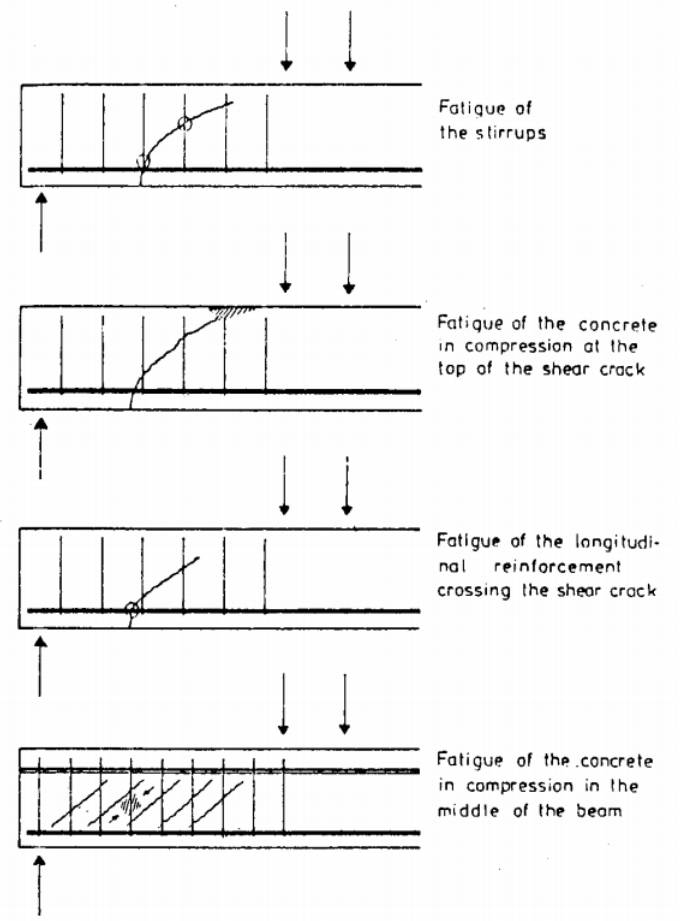

Figure 3.5 – Possible types of shear fatigue failure in beams with shear reinforcement (RILEM 1984)

3.4.4 Shear failure at the interface between concretes cast at different times

Another important aspect to be taken into account is the evaluation of the shear resistance of the connection between different structural elements, which usually present concrete of different ages, such as in concrete joints or in the connection between prefabricated elements and concrete elements cast *in situ*.

Several studies have been developed to investigate the ultimate shear resistance and the behaviour of these interfaces under monotonically increasing loads. Among others, Hanson (1960) studied the connections between prefabricated and cast *in situ* concrete structural elements, in order to evaluate the transference of shear stress at the bonding interface. Some investigations have also been carried out to evaluate the behaviour of these connections when subjected to cyclic loading of high amplitude but little repeatability (Walraven 1994). However, few studies have been performed in order to assess their behaviour when subjected to high-

cycle loading. In this field, the work of Pruijssers (1988) is highlighted, as well as the works recently carried out by Figueira et al (2016b, 2016a).

3.5 Normative recommendations for fatigue evaluation of RC railway bridges

The European standards present two approaches for the fatigue evaluation of RC structures subjected to important cyclic loading, such as railway bridge decks: the damage equivalent stress method and the damage accumulation method. The recommendations for fatigue verification are spread over three standards: EN 1991-2 (CEN 2003), EN 1992-1-1 (CEN 2004) and EN 1992-2 (CEN 2005). In this section the two procedures are presented, with special focus on the damage accumulation method that is the most detailed one and widely used.

3.5.1 Methods for fatigue analysis

3.5.1.1 Damage accumulation method

The damage accumulation method is a detailed approach and one of the most widely used for fatigue assessment of several types of structures. This method takes into account the loading applied on the bridge from which the stress history is obtained, allowing for the quantification of the fatigue damage through the damage linear accumulation rule and the S-N curves of the material. The steps involved in this method are listed below.

1. Definition of the traffic scenario (train types, number of trains per day and train speeds);

2. Calculation of the time records of internal forces due to the passage of each train;

   The calculation of internal forces is based on the results of transient analyses, which can be performed considering the moving loads method or the train-bridge interaction method, as mentioned before in Chapter 2. The latter is more suitable for analysis of structures sensitive to the effect of interaction between the train and the bridge or structures subjected to important local phenomena, such as those with shorter spans or the specific analysis of railway deck slabs, respectively.

Different approaches can be considered related to the numerical modelling of the structure. If the aim of the analysis is related to the global behaviour of the main girders, FE models with beam elements can be adopted. However, if shear forces and bending moments applied to the deck slab and webs are to be quantified, a FE model with shell elements should be employed.

Depending on the accuracy of the numerical modelling and the analysis to be carried out, there are different ways how train loads can be applied on FE models. In the case where the track is not explicitly modelled, the train loads can be directly applied on the beam or shell elements, considering or not the degradation of the forces through the ballast layer. When the railway track is modelled, the loads are applied directly in the rails, usually modelled by means of beam elements, and the forces are transmitted through all the connected elements. As shown before in Chapter 2, different approaches can be adopted for the track modelling.

Bearing in mind all these aspects, the nodal forces can be obtained for the passage of each train, which allow obtaining the internal forces. In the present work, a 3D numerical model with explicit track modelling is adopted and the TBI effects are considered in the dynamic analyses. A detailed explanation about the methodology used in TBI analyses and how the calculation of internal forces is performed can be seen in section 2.2.5 and 5.6.2.

3. Quantification of the stress history at the several critical locations of the structure for the passage of each train;

   The variation of stresses at each critical location of the structure due to the passage of each train assumes a crucial role in the fatigue strength assessment. Small variations in the amplitude of the stresses can lead to different evaluation results due to the logarithmic relationship between the applied stress range and the number of resisting load cycles, reason why stress calculations for fatigue analyses must be as accurate as possible.

   Generally, cracked cross sections should be considered since this is the location where the most unfavourable stresses occur. Complex non-linear models that account for the cyclic response in terms of both bond-slip and normal stress-crack opening relationships can be used, as adopted by Sousa (2012). Alternatively, approximate

stresses can be obtained ignoring the tensile strength of concrete and considering the compatibility of strains between the concrete under compression and the reinforcements. This is the typical approach for stress calculations in cracked RC elements (also known as calculations in state II), and usually takes the value 10 as the ratio of elasticity modulus, as suggested by the MC90.

4. Identification of the peak values of the stress history;

   The calculation of the accumulated fatigue damage is a function of the extreme values reached in each load cycle, only. The shape of the time-stress diagram between contiguous minimum and maximum stress values does not affect the calculated damage. For that reason, the local peak values in the time-stress function are identified in this step of the method.

5. Counting of the stress cycles;

   This step, together with step 4, allows the calculation of the stress range histograms, which provide the number of repetitions for each stress range. Among other methodologies for the counting of stress cycles, the Rainflow method is the most used by many authors, since it is based on the mechanics of materials such as steel and it generally leads to higher total damage than other methods, giving results on the safe side (Sousa 2012). In the present work, the Rainflow's cycles counting method described by Fryba (1996) was adopted and implemented.

6. Calculation of the total accumulated damage;

   Once the stress histograms have been computed, the total damage caused by traffic scenario can be calculated. The fatigue damage cannot be directly read from S-N curves as they represent the fatigue life for a constant amplitude cyclic loading. Due to its simplicity, the damage linear-accumulation rule of Palmgren-Miner (Miner 1945) is the procedure most commonly used to get the total fatigue damage, D, which is given by the following expression:

$$D = \sum_i \frac{n_i}{N_i} \tag{3.6}$$

where n_i is the number of applied cycles for a given stress range and N_i corresponds to the number of resisting cycles for the same stress range, according the respective S-N curve.

The design value of the number of resisting load cycles, N_i, is obtained by dividing the characteristic value by the safety factor $\gamma_{S,fat}$, which takes the value 1.15. For a given stress range $\Delta\sigma_s$, N_i is obtained by:

$$N_i = N^* \cdot \left(\frac{\Delta\sigma_{Rsk}(N^*)/1.15}{\Delta\sigma_s} \right)^k \tag{3.7}$$

where

$$k = \begin{cases} k_1 \text{ for } \Delta\sigma_s > \Delta\sigma_{Rsk}(N^*)/1.15 \\ k_2 \text{ for } \Delta\sigma_s \leq \Delta\sigma_{Rsk}(N^*)/1.15 \end{cases} \tag{3.8}$$

The parameters N^*, $\Delta\sigma_{Rsk}(N^*)$, k_1 and k_2 are given in Table 3.1 and are depicted in Figure 3.1. A value of the fatigue damage, D, greater than 1.0 indicates the fatigue failure of the structural element under analysis.

7. Quantification of the fatigue life;

   The fatigue life (FL), in years, is given by the following expression:

$$FL = \frac{1}{D_{1year}} \tag{3.9}$$

   where D_{1year} is the fatigue damage corresponding to one year of traffic. This expression takes into account that the characteristics of the structure and the traffic scenario remain unchanged throughout its life.

3.5.1.2 Damage equivalent stress method

The fatigue evaluation can be performed through a simplified method, based on the quantification of the damage equivalent stress range, $\Delta\sigma_{equiv}(N^*)$, which represents the constant amplitude stress range that, if repeated N^* times, causes the same fatigue damage to the structure as the total live load in its planned service life.

According to this approach, the fatigue safety verification on RC elements of railway bridges is ensured on the basis of the following expression:

$$\gamma_{F,fat} \cdot \Delta\sigma_{s,equiv}(N^*) \leq \frac{\Delta\sigma_{Rsk}(N^*)}{\gamma_{S,fat}} \tag{3.10}$$

where $\Delta\sigma_{Rsk}(N^*)$ is the fatigue strength for N^* cycles of constant amplitude according to the respective S-N curve. The safety factors $\gamma_{F,fat}$ and $\gamma_{S,fat}$ take the values 1.0 and 1.15, respectively.

According to EN 1992-2, the damage equivalent stress in tensile reinforcement of RC elements in railway bridges is given by the following expression:

$$\Delta\sigma_{s,equiv} = \lambda_s \cdot \Phi \cdot \Delta\sigma_{s,71} \tag{3.11}$$

where $\Delta\sigma_{s,71}$ is the stress range in the reinforcement due to the load model LM71 (and due to the load model SW/0 when applicable), obtained in the most unfavourable position for the structural element, Φ is the dynamic factor previously presented in section 2.3.3.1 and λ_s is a correction factor that can be quantified through the equation below:

$$\lambda_s = \lambda_{s,1} \cdot \lambda_{s,2} \cdot \lambda_{s,3} \cdot \lambda_{s,4} \tag{3.12}$$

that takes into account the structural and material performance and the type of loading ($\lambda_{s,1}$), the annual traffic volume ($\lambda_{s,2}$), the design service life ($\lambda_{s,3}$) and the number of tracks and the influence of simultaneous crossings ($\lambda_{s,4}$).

This methodology is the result of an extensive numerical research performed at the Technical University of Munich and sponsored by the UIC/ERRI (ERRI D183/DT346 1997). The main source of inaccuracies in the application of this method is related to the quantification of the factor that takes into account with the type of structural element and the characteristics of the railway traffic, $\lambda_{s,1}$. This factor was calibrated essentially for the longitudinal analysis of the main girders, either considered as continuous or simply supported. Moreover, a single formulation, applicable to any structural typology, is not able to provide precise results for all kind of structures, especially in the cases where local phenomena play a crucial role in the structural behaviour. Thus, for the analysis of the local behaviour of railway deck slabs, a careful quantification of this coefficient should be undertaken.

It is also important to point out that this methodology present two considerable limitations, namely, it is not applicable whenever dynamic analyses of the effect of the trains' passage are required and it is not valid for lines carrying railway traffic heavier than usual (if an α factor higher than 1.0 is required to simulate the real traffic). In these situations, the fatigue

verification must be carried out through the damage accumulation method, considering an adequate traffic scenario, as described in the previous subsection.

3.5.2 Basis for the fatigue assessment of railway structures

The Annex D of EN 1991-2 (CEN 2003) defines the basis for the fatigue assessment of railway structures. To take account of the average effect over the assumed 100 years life of the structure, the dynamic enhancement for each Real Train may be reduced by:

$$1 + 0.5 \cdot (\varphi' + 0.5\varphi'') \tag{3.13}$$

where φ' and φ'' are given by the following expressions:

$$\varphi' = \frac{K}{1 + K + K^4} \tag{3.14}$$

$$\varphi'' = 0.56e^{-\frac{L^2}{100}} \tag{3.15}$$

The factor K is given by the following expressions:

$$K = \frac{v}{160} \quad for\ L \leq 20m \tag{3.16}$$

$$K = \frac{v}{47.16L^{0.408}} \quad for\ L > 20m \tag{3.17}$$

where v is the maximum permitted vehicle speed (m/s) and L is the determinant length, as described as section 2.3.1.

The fatigue assessment should be carried out on the basis of the traffic mixes, “standard traffic”, “traffic with 250 kN-axles” or “light traffic mix” depending on whether the structure carries mixed traffic, predominantly heavy freight traffic or lightweight passenger traffic in accordance with the requirements specified. Details of the service and traffic mixes are given in Annex F of EN 1991-2.

It should be pointed out that Equations (3.13) to (3.17) can only be used in cases where a dynamic analysis is not required, according to the criteria summarised in subchapter 2.3.2, since these equations do not take resonance effects into account. As mentioned before, to take account of such effects, a dynamic analysis should be carried out.

Chapter 4

Experimental calibration and validation of numerical models

4.1 Introduction

The process of developing a FE model of a structure involves important assumptions and simplifications, such as the type of modelling and respective level of discretisation, uncertainties in geometry and boundary conditions and changes in the material properties of the structure. Such assumptions/simplifications can result in inaccuracies in the results of dynamic analyses of the structure. In this sense, the use of an accurate numerical model for the evaluation of the dynamic behaviour of a structure has revealed to be a step of particular importance in minimising these inaccuracies, reason why particular consideration to the calibration of numerical models has been shown in recent years (Jaishi and Ren 2005, Zabel and Brehm 2009b, Arora 2011, Ribeiro et al. 2012).

The accuracy of numerical models strongly depends on their experimental validation, in which the estimation of structural modal parameters has revealed to be a crucial step in this process. In this context, the comparison between experimentally identified and numerically calculated modal parameters allows the identification of inaccuracies in the numerical models. Distinct techniques have been used in order to experimentally identify structures' modal parameters (i.e. natural frequencies, mode shapes and damping coefficients) that are used in the calibration of numerical models, such as the use of external induced excitation (Morassi and

Tonon 2008, Zwolski and Bien 2011) or the use of ambient vibration tests (Cunha et al. 2003, Chellini et al. 2011, Benedettini and Gentile 2011, Cabboi et al. 2017), the latter with increasing use in recent years due to the ease of application.

Adjustments of the parameters of the initial model can be done manually, based on the engineer's structural sensitivity, or automatically, by means of numerical algorithms that allow the adjustment to be performed in a more efficient and optimised way. There are two main methodologies to develop an automatic calibration of the numerical models: direct (Yang and Chen 2009, Arora 2011) and iterative (Teughels et al. 2003, Ribeiro 2012, Zordan et al. 2014, Sarmadi et al. 2016). In the direct methods, the calibration is carried out in only a single step by updating only the stiffness and mass matrices, without changing the FE physical parameters. The iterative methods are generally related to the use of an objective function, successively updating the physical parameters until the FE model reproduces the experimental results with an adequate degree of accuracy.

Among the iterative methods, those based on optimisation algorithms are among the most recently used. Several methods are available to solve the optimisation problem, such as gradient-based methods (Teughels et al. 2003), response surface methods (Ren and Chen 2010b, Zhou et al. 2016) and nature inspired algorithms (e. g., genetic algorithm, evolutionary strategies, particle swarm optimization) (Zabel and Brehm 2009b, Deng and Cai 2010, Jafarkhani and Masri 2011). Concerning the application of a genetic algorithm in the scope of railway bridges, used in the present work, there has been an increase in the number of applications: Zabel and Brehm (2009) and (Ribeiro et al. 2012) performed the model calibration of railway bridges demonstrating the reliability of a genetic algorithm in estimating the optimal values of a large number of numerical parameters; Costa et al. (2016), performing an experimental calibration of a stone masonry arch railway bridge trough a genetic algorithm based on ambient vibration results, verified also that the material mechanical characterization tests made in situ and in laboratory revealed to be important to ensure a better estimate of the initial values of the material mechanical parameters adopted in the FE model.

Given the great importance of gauging the real response of structures, this chapter starts with an overview of some experimental techniques widely used to obtain the dynamic response of a bridge, either to identify its modal parameters or to measure its dynamic behaviour under railway traffic. Afterwards, the steps involved in an iterative method based on an optimisation algorithm are presented, namely, the sensitivity analysis, the modal analysis, the vibration

modes' pairing and the optimisation. A detailed explanation about this method, used in the present work, can be found in Ribeiro (2012).

4.2 Experimental evaluation of dynamic structural behaviour

As mentioned in the Introduction, the measured structural response provides the reference values to be used in the calibration and validation of numerical models. The most common types of experimental tests considered for this purpose are the experimental identification of modal parameters and the measurement of structural dynamic responses under railway traffic.

4.2.1 Experimental identification of modal parameters

The minimisation of the difference between numerical and experimental responses has been carried out based on the identification of modal parameters of the structure, such as natural frequencies, mode shapes and damping coefficients. It is usually carried out through two types of tests: ambient vibration tests (Magalhães 2004, Rodrigues 2004), in which the response of the structure is measured when it is subjected to ambient and service loads; and forced vibration tests (Cunha et al. 2003, De Roeck 2010), which are based on measuring the response of the structure when subjected to an artificial and controlled excitation.

In order to identify such parameters, "*input-output*" techniques were initially developed, which allowed the estimation of a set of frequencies relating the response of the structure to the corresponding measured artificial excitation. These techniques proved to be difficult to apply due to the difficulty in exciting large structures, both due to the inherent limitations of the equipment regarding its huge dimensions, and the need to restrict the normal operation of the structure. An overview of modal identification techniques as well as the equipment used can be found in Zhang (2004) and Cunha and Caetano (2006).

The considerable improvement in the characteristics of measurement systems (transducers, cables or wireless systems for data transmission, acquisition systems, etc.) has contributed to a better quality of the experimental records obtained and, consequently, to the enhancement of the modal identification techniques. New identification techniques, based on the measurement of only the structural response, usually denominated "*output-only*" techniques, have emerged

(Cunha et al. 2007). Liu et al. (2009) carried out the experimental identification of the modal parameters of the Sesia viaduct through environmental vibration tests. In Figure 4.1 a), the various measuring points where the accelerometers were installed are depicted. Figure 4.1 b) shows the configuration of the identified vibration modes.

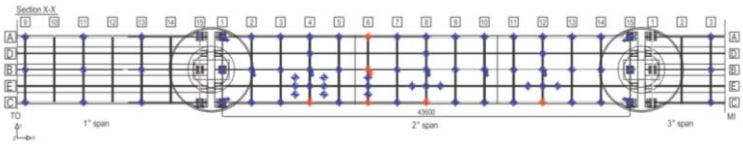

a)

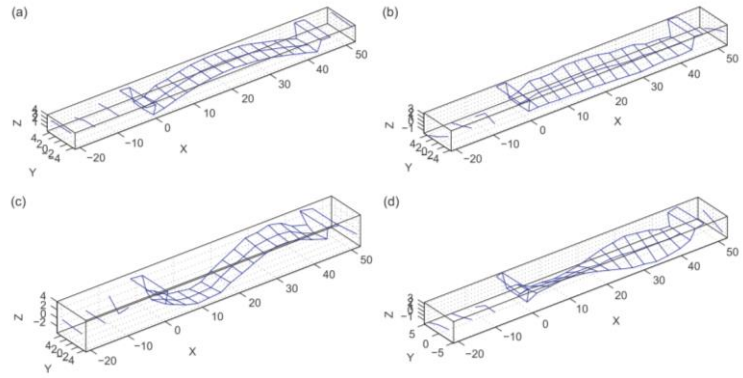

b)

Figure 4.1 – Ambient vibration test of the Sesia railway viaduct: a) measurement points; b) identified mode shapes (Liu et al. 2009)

These techniques are also referred to as stochastics since the unknown excitation (usually ambient excitation, from different sources such as wind, traffic or machines operating in the structure or in its vicinity) is idealized as a stochastic process (Magalhães 2004). These stochastic methods are generally divided into two main groups: analysis methods in the frequency domain, such as PP (Peak Picking), FDD (Frequency Domain Decomposition) and EFDD (Enhanced Frequency Domain Decomposition) and analysis methods in the time domain, namely SSI-COV (COVariance-driven Sthocastic Subspace Identification) and SSI-DATA (DATA-driven Sthocastic Subspace Identification). A more detailed description of each method can be found in Magalhães (2004) or Rodrigues (2004). The EFDD and SSI methods, which are used in the present dissertation, are presented below.

4.2.1.1 EFDD method

The FDD method was initially developed by Brincker et al. (2000). This is a simple method in terms of computational implementation, which later formed the basis of the development of the ARTeMIS (2009) commercial software. This is a very intuitive method that relates to the classic technique of *peak picking*.

According to Brincker et al. (2000), this method is based on the singular values decomposition of the spectral density matrix of each record, resulting in a set of power spectral density functions. The response is thus separated into a set of systems of one DOF, each one corresponding to a separate vibration mode. This result is accurate when the excitation corresponds to a white noise, in which the structure is poorly damped and the vibration modes with near frequencies are geometrically orthogonal. When these conditions are not satisfied, the decomposition into one DOF systems is approximate, but still leads to significantly more accurate results than those obtained by the *peak-picking* technique. As an example, Figure 4.2 shows the singular values spectra corresponding to the longitudinal acceleration records obtained in an ambient vibration test of a physical model of a 4-storey building (Rodrigues 2004).

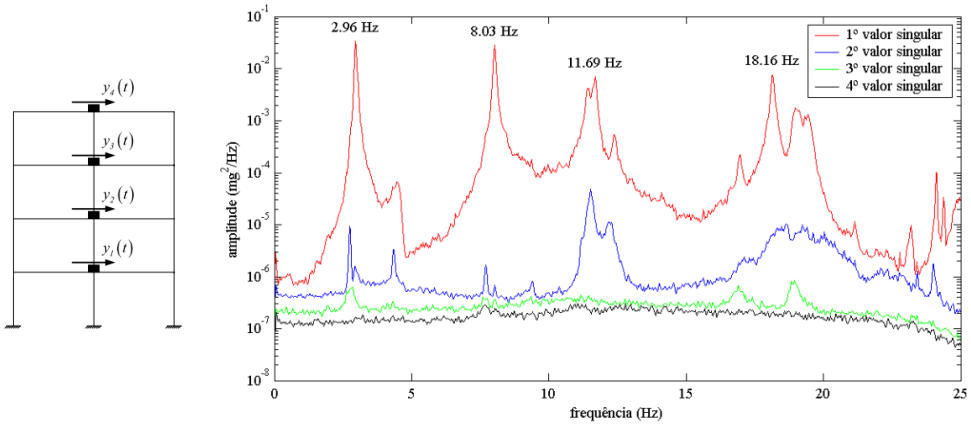

Figure 4.2 – Singular values spectra corresponding to the records of longitudinal accelerations (Rodrigues 2004)

The estimation of the damping coefficient was only possible to achieve through the EFDD method, also developed by Brincker et al. (2001). In this method, the spectral density function identified for each vibration mode is changed to the time domain through the inverse Fourier transform. An auto-correlation function of the response of a one DOF system is obtained, which, assuming that the excitation forces are idealised by a white noise process, is similar to the free regime response of that system. From this auto-correlation function the natural

frequencies and the damping coefficients can be estimated through the zero-crossing instants and through the logarithmic decrement, respectively.

The identification of the spectral density functions of one DOF systems is performed through the MAC (Modal Assurance Criteria) coefficient, relating the singular vector in a resonant peak with the singular vectors in the neighbouring frequencies of that peak. A limit in terms of the MAC value is previously defined and for all natural frequencies located outside that limit, a zero value for the spectral density function of that system is considered. Figure 4.3 illustrates the spectral density functions and the MAC coefficients for the first singular value of the example referred to in Figure 4.2.

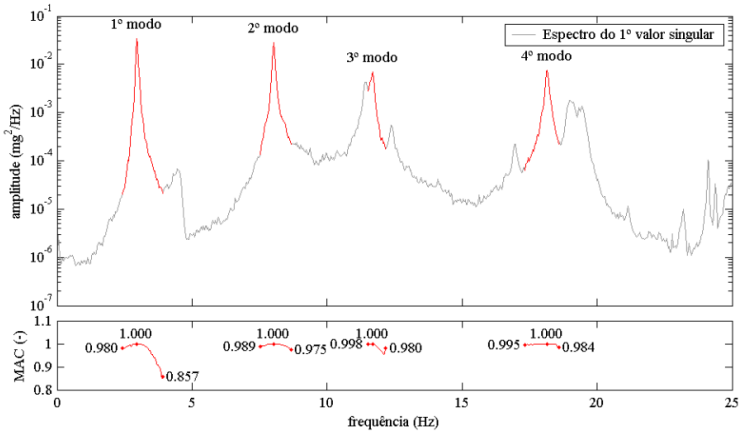

Figure 4.3 – Spectral density functions of each vibration mode and MAC coefficients (Rodrigues 2004)

4.2.1.2 SSI method

The SSI-DATA is a method that relies on a state model obtained directly from the time series of the structure's response. An advantage of this method in comparison to frequency-domain identification methods is that it does not require any pre-processing of the recorded information for the calculation of the correlation functions. In addition, this method involves numerical techniques that have proved to be very efficient, such as QR factorization and matrix decomposition in singular values, as well as the use of the least squares method (Magalhaes 2004).

This methodology is also implemented in the ARTeMIS (2009) commercial software and has allowed the achievement of very accurate results, revealing even greater precision in the identification of vibration modes with near frequencies.

Reynolds et al. (2004) evaluated the potential of the SSI method in the identification of modal parameters of an arch metal bridge, based on ambient vibration tests. In these tests tri-axial accelerometers were considered and eight experimental setups were performed. The results were compared with the ones obtained through the *peak-picking* method, where a similar result in the natural frequencies was obtained, although the SSI method gave rise to mode shapes with greater accuracy.

Chen et al. (2013) also evaluated the *peak-picking*, EFDD and SSI-DATA methods in the modal identification of the Newmarket viaduct in New Zealand, composed of 12 continuous spans. It was possible to identify 10 vibration modes using all methodologies, with insignificant differences between them. In this study, the comparison revealed that all the methods considered gave rise to reasonably consistent estimates of the natural frequencies and mode shapes. The authors also pointed out that, in opposition to the *peak-picking* method, SSI and EFDD methods allowed the identification of damping coefficients and, in this case, the latter method revealed to be faster in the modal identification.

a)

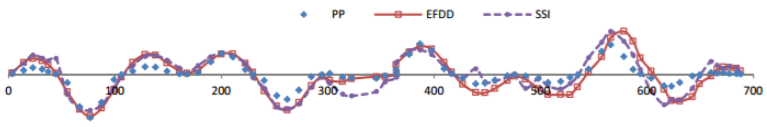

b)

Figure 4.4 – Newmarket viaduct: a) overview; b) global vibration mode (Chen et al. 2013)

4.2.2 Experimental measurement of dynamic structural response under railway traffic

The evaluation of the dynamic response of bridges under railway traffic has also been reported in the work of several authors, such as Liu et al. (2009), Ribeiro et al (2012), Guo et al. (2012) and Zhai et al. (2013). The focus of these experimental tests under railway traffic is essentially related to the measurement of dynamic responses in order to validate the bridge's numerical models. The measurements are usually performed in terms of displacements,

accelerations and deformations in several locations of the bridge, such as the deck, bearing zones or railway track.

Guo et al. (2012) described the numerical and experimental evaluation of the dynamic behaviour of the Sesia viaduct, which is located on the Italian high-speed line between Torino and Milano. Some accelerometers were installed in the intermediate span in order to measure the dynamic response of the bridge during the passage of an Italian high-speed ETR500Y train, although the focus of the authors in this work has been in locations A to D, which are presented in Figure 4.5 a). Figure 4.5 b) shows the computed and measured vertical acceleration time histories at point C, with the measured data filtered to 30 Hz. The authors highlighted a good agreement between the experimental and the predicted results.

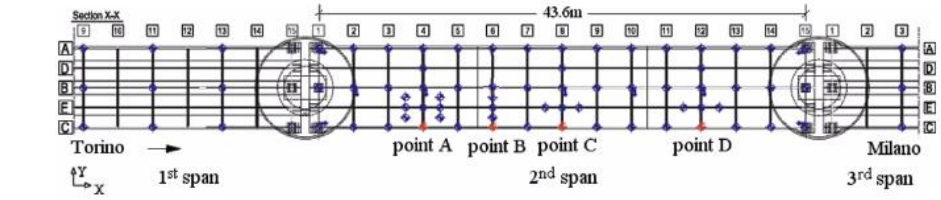

a)

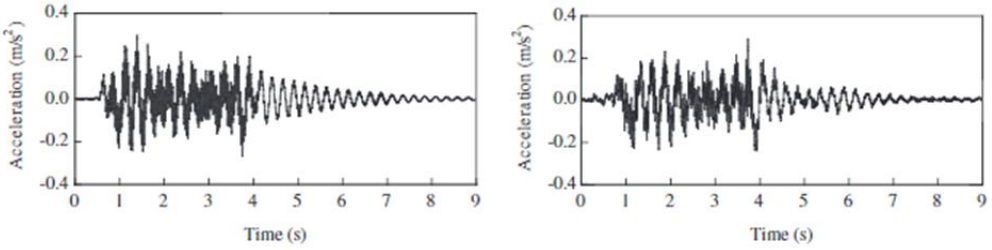

b)

Figure 4.5 – Measurement of vertical accelerations in the Sesia viaduct: a) structure and position of the accelerometers; b) measured (left) and computed results (right) (Guo et al. 2012)

Zhai et al. (2013) carried out experimental tests on the Jinan Yellow River Bridge [Figure 4.6 a)] located on the first high-speed railway line in China, for the passage of high-speed trains traveling between 200 km/h and 380 km/h. Figure 4.6 b) shows the measurement locations for the bridge and the railway track and Figure 4.6 c) shows the comparison between calculated and measured responses of the main girder in terms of vertical displacements and accelerations, respectively. Despite some differences, the authors pointed out that these experimental results allowed a validation of the previously developed TBI methodology, which could be used to

evaluate the dynamic performance of bridges as well as running safety and ride comfort of high-speed trains on bridges at the design stage.

a)

b)

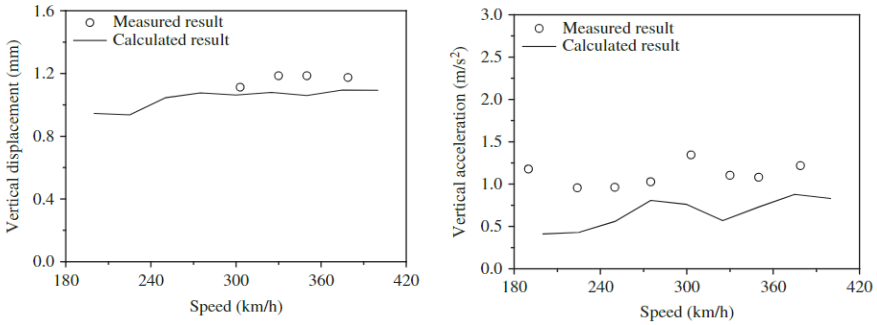

c)

Figure 4.6 – Experimental evaluation of the dynamic behaviour of the Jinan Yellow River Bridge: a) bridge; b) measured variables; c) calculated and experimental results [adapted from Zhai et al. (2013)]

4.3 Model calibration method based on an optimisation algorithm

In this section, the iterative method for model calibration used in this thesis, is presented. It is based on an optimisation algorithm, using the modal parameters of the structure. Figure 4.7 shows a flowchart that depicts the generic steps involved in this process. Particular attention is given to: the sensitivity analysis, used to identify the most sensitive numerical parameters that should be considered in the calibration process (section 4.3.1); the mode pairing, where the vibration modes obtained in the numerical modal analysis are compared with those experimentally identified (section 4.3.2); and the optimisation algorithm (a genetic algorithm is used in the present work) to minimise the differences between numerical and experimental

parameters and to estimate, if needed, a new set of numerical parameters to be introduced in the FE model (section 4.3.3).

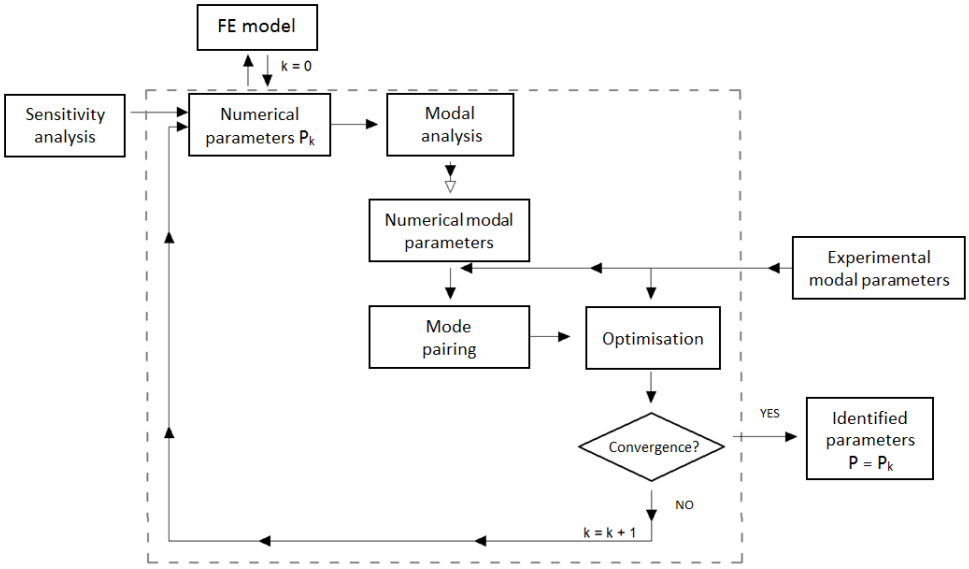

Figure 4.7 – Iterative method based on an optimisation technique [adapted from Ribeiro (2012)]

4.3.1 Sensitivity analysis

According to Brehm (2011), the sensitivity analysis can be local, carried out parameter by parameter, or global, based on the analysis of simultaneous correlation between all the parameters and responses of the numerical model.

Jaishi and Ren (2005) carried out a local sensitivity analysis in order to evaluate the most sensitive parameters to the calibration of the numerical model of a metal arch bridge with RC deck. For that purpose, the sensitivity coefficients S_j were obtained, based on the calculation of the first derivative of each response for each parameter, which are given by the following expressions:

$$\delta_z = S_j \delta_x \tag{4.1}$$

wherein

$$S_j = \frac{\delta_z}{\delta_x} = \frac{z - z_j}{x - x_j} \tag{4.2}$$

where z and x represent the values of both the response and each numerical parameter in the current iteration, respectively, z_j are the response values for the initial numerical parameters

and x_j are the initial numerical parameters. The sensitivity of the parameters is generally evaluated by comparing all sensitivity coefficients.

In opposition to the local sensitivity analysis that varies one parameter at a time, in global sensitivity analysis all parameters vary simultaneously. Zabel and Brehm (2009b) and Brehm et al. (2010) show the application of this methodology, the latter focusing in the study of the Erfttal railway bridge located on the high-speed line between Cologne and Brussels. This methodology is generically based on a set of initial numerical parameters, randomly generated through the application of sampling techniques, and on the correlation analysis between the input parameters (numerical parameters) and the output parameters (numerical responses).

The sampling techniques allow generating a set of samples, each one consisting on a set of parameters of the FE numerical model. The Monte Carlo and Latin Hypercube methods are the most widely used, which allow to generate, for each random variable (numerical parameter), a sample with *N* values according to the assumed probability distribution for that parameter (Henriques 1998).

Concerning the correlation analysis, it can be performed through parametric correlation coefficients, such as Pearson's linear coefficient or quadratic coefficient, or through non-parametric coefficients, namely the Spearman and Kendall coefficients (OptisLang 2008). The following expression shows the Spearman's correlation between two vector-shaped samples, x and y, based on their rank vectors $R(x_i)$ and $R(y_i)$:

$$r_{xy}^{S} = 1 - \frac{6\sum_{i=1}^{n} D_i^2}{n(n^2-1)} \tag{4.3}$$

where

$$D_i = R(x_i) - R(y_i) \tag{4.4}$$

with $i = 1,2,\ldots,n$, where n represents the number of sample variables. The rank vector results from assigning a value between 1 (element of the original vector with lower value) and n (element of the original vector with higher value) to each element of the original vector.

As indicated in OptisLang (2008), the Spearman correlation coefficients may take values in the interval [-1, 1], considering a weak correlation when the coefficients present values lower than 0.30. However, Zabel and Brehm (2009) recommend that only the parameters with correlation coefficients above 0.50 should be used in the calibration of the FE model.

Ribeiro et al. (2012) performed the calibration of the numerical model of a railway bridge, with a metallic *bowstring* arch and RC deck, using an iterative method based on the identification of modal parameters. The authors performed a global sensitivity analysis using the Spearman correlation coefficients, whose matrix is presented in Figure 4.8. In this case, the values located in the interval [-0.25, 0.25] were not considered. The authors verified that parameters such as the concrete and steel elasticity modulus, concrete and ballast density and vertical bearing stiffness had a significant influence on the frequencies and MAC coefficients of global vibration modes. On the other hand, the parameters related to the initial stress of the hangers and diagonals as well as the stiffness of the connections between these elements and the deck and arches have an important influence on the frequencies and MAC values of the local modes.

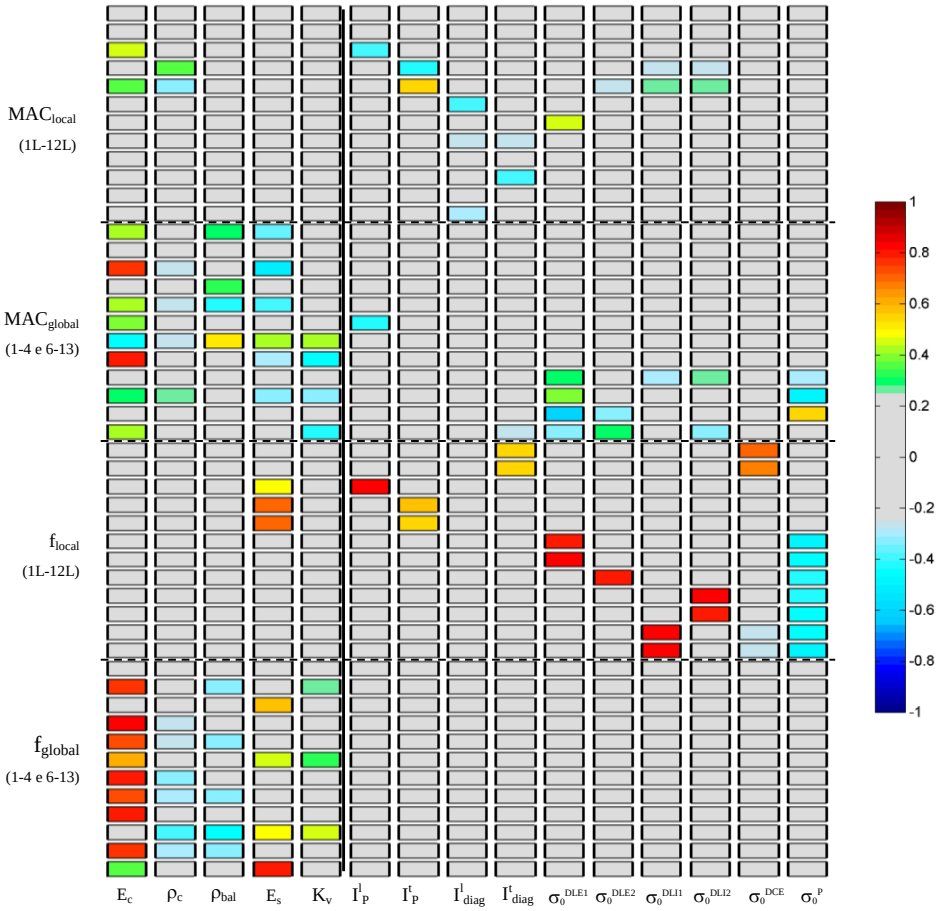

Figure 4.8 – Spearman correlation matrix (Ribeiro et al. 2012)

4.3.2 Mode pairing

The pairing of vibration modes establishes the correspondence between each experimental and numerical vibration mode. The mathematical concept of correlation between two vectors,

in this case the vectors of experimental and numerical vibration modes, is on the basis of this process (Allemang 2003).

The MAC (*Modal Assurance Criterion*) parameter is the approach most widely used (Calçada et al. 2002, Ren et al. 2005, Gentile and Saisi 2011) in the correlations between numerical and experimental vibration modes due to an easy computational implementation and for the fact that it is not necessary to obtain experimental information in all DOF of the numerical model. This parameter can be calculated by the following expression (Allemang 2003):

$$\mathrm{MAC}_{ij} = \frac{\left(\widehat{\boldsymbol{\Phi}}_i^T \widehat{\boldsymbol{\Phi}}_j\right)^2}{\left(\widehat{\boldsymbol{\Phi}}_i^T \widehat{\boldsymbol{\Phi}}_i\right)\left(\widehat{\boldsymbol{\Phi}}_j^T \widehat{\boldsymbol{\Phi}}_j\right)} \tag{4.5}$$

where $\boldsymbol{\Phi}_j$ is the vector containing the coordinates of the numerical mode *j* corresponding to the experimental DOFs and $\boldsymbol{\Phi}_i$ is the vector containing the experimental information of the vibration mode *i*.

The MAC parameter assumes values between 0 and 1, the latter corresponding to a perfect match between the numerical and experimental vibration mode. Values higher than 0.80 indicate that there is a good correlation between the two vectors. According to Allemang (2003), there may be values of the MAC coefficients close to zero due to: the inability of the numerical model to reproduce the dynamic behaviour of the structure; the presence of noise in the experimental measurements; an incorrect application of the modal parameters identification techniques; or a mismatch between the experimental measurement points and their respective locations in the FE numerical model. Ribeiro (2012) also points out that the value of the MAC parameter depends on the size of the modal vectors, where experimental vectors with a reduced number of elements, associated with a limited number of measurement points, tend to present high MAC values for a large number of numerical modes.

The EMAC (Energy-based *Modal Assurance Criterion*) parameter, recently developed by Brehm et al. (2010), brings together the information coming from the mathematical correlation between the modal vectors (MAC parameter) with the physical information of the DOFs observed in the experimental test and related to the distribution of stiffness and mass in the structure. This parameter involves the calculation of the modal strain energy associated with groups of DOFs of the numerical model, denominated *clusters*, using the following expression:

$$\mathrm{EMAC}_{ijk} = \prod_{jk} \mathrm{MAC}_{ij} \tag{4.6}$$

where $\prod_{jk}$ is the relative modal strain energy representing the portion of total energy mobilised by vibration mode *j* considering only the DOFs of cluster *k*, and is given by:

$$\prod_{jk} = \frac{\mathrm{MSE}_{jk}}{\omega_j^2} = \frac{\sum_{l=1}^{n} \boldsymbol{\Phi}_{jk}^T \mathbf{K}_{kl} \boldsymbol{\Phi}_{jl}}{\omega_j^2} \tag{4.7}$$

where $\boldsymbol{\Phi}_{jk}$ is the matrix containing the modal information of numerical modes *j*, corresponding to the DOFs of *cluster k*, $\mathbf{K}_{kl}$ is the stiffness submatrix which connects the DOFs of *clusters k* and *l* and $\boldsymbol{\Phi}_{jl}$ is the matrix containing the modal information of numerical modes *j*, corresponding to the DOFs of *cluster l*, *n* is the total number of *clusters* and ω_j is the angular frequency of numerical mode *j*.

According to Ribeiro (2012), who also used this approach, the success of the mode pairing based on the EMAC parameter strongly depends on the selection of the DOFs of the numerical model related to the *clusters* configuration. The *clusters* should be chosen in order to allow the separation of the experimentally measured DOFs from the unmeasured DOFs. In complex structures, the *clusters* must also take into account the different substructures composed of groups of elements with a distinct dynamic behaviour, when compared with the global structural behaviour.

4.3.3 Optimisation

The optimisation phase aims to obtain the parameter values of the numerical model that minimise the differences between numerical and experimental modal responses, and involves the definition of an objective function and the application of an optimisation technique.

4.3.3.1 Objective function

The objective function is obtained by summing the differences between the experimental and numerical modal responses, differences that are known as residues. The modal responses most commonly used in the objective function are natural frequencies and vibration modes, the

latter usually taken into account through the MAC parameter. The following expression shows the objective function adopted by Ribeiro (2012):

$$\mathrm{f} = a \sum_{i=1}^{n\,modes} \frac{\left|f_i^{exp} - f_i^{num}\right|}{f_i^{exp}} + b \sum_{i=1}^{n\,modes} \left|\mathrm{MAC}\left(\boldsymbol{\phi}_i^{exp}, \boldsymbol{\phi}_i^{num}\right) - 1\right| \tag{4.8}$$

where f_i^{exp} and f_i^{num} are the experimental and numerical frequencies for mode *i*, $\boldsymbol{\phi}_i^{exp}$ and $\boldsymbol{\phi}_i^{num}$ are the vectors containing the experimental and numerical modal information regarding mode *i*, a and b are weighing factors of the objective function's terms and $'n\,modes'$ is the total number of modes considered in the calibration process.

Regarding the frequencies' residue, given the greater uncertainty generally associated to the identification of natural frequencies with higher values, the use of relative differences allows an equal weight to be defined to the residue of each natural frequency, since in this case they are all limited to the range [0, 1].

In terms of mode shapes' residue, Brehm (2011) suggests a simple formulation in which its variation is also limited to the range [0, 1], as presented in the second term of the right-hand side of expression (4.8). However, there are other approaches for the quantification of these residues, r, such as those presented by Moller and Friberg (1998) and Gentile and Cabrera (2001), given by expressions (4.9) and (4.10), respectively.

$$r = \frac{\left(1 - \sqrt{\mathrm{MAC}(\boldsymbol{\phi}^{exp}, \boldsymbol{\phi}^{num})}\right)^2}{\mathrm{MAC}(\boldsymbol{\phi}^{exp}, \boldsymbol{\phi}^{num})} \tag{4.9}$$

$$r = \sqrt{\frac{1 - \mathrm{MAC}(\boldsymbol{\phi}^{exp}, \boldsymbol{\phi}^{num})}{\mathrm{MAC}(\boldsymbol{\phi}^{exp}, \boldsymbol{\phi}^{num})}} \tag{4.10}$$

As can be seen in the objective function presented in Equation (4.8), both terms on the right-hand side can be differently weighed, which allows to assign each term a lighter, or heavier, importance in reaching the optimum value of the objective function. According to Jaishi and Ren (2005), this assumes particular importance since if there is a greater precision in the experimental identification of natural frequencies, compared to the identification of mode shapes, a higher weight must be given to the residue related to this modal parameter.

4.3.3.2 Optimisation algorithm

Regarding optimisation techniques, two main approaches can be considered: a local optimisation, such as gradient-based algorithms (Brownjohn et al. 2010, Teughels et al. 2003, Wang et al. 2010); or a global optimisation, such as response surface (Ren and Chen 2010a, Zhou et al. 2016) or genetic algorithms (Zabel and Brehm 2009b, Deng and Cai 2010, Jafarkhani and Masri 2011, Ribeiro 2012).

The main difference between these approaches is related to the type of minimum value that can be identified. Global optimisation algorithms are more robust since they allow the identification of the global minimum value of the whole problem, regardless of both how many local minimum exist and the starting point chosen to solve the algorithm. However, since they are based on a stochastic process, and taking into account the huge number of points that have to be under evaluation in the objective function, this process can take more time and computational effort (Ribeiro 2012).

Regarding the gradient-based algorithms, Ribeiro (2012) points out both a good performance on problems characterised by convex functions and a reduced computational time as the main advantages of this method. However, the limitation in the number of numerical parameters (< 5) to be used, the possibility to detect local minimum instead of the global minimums and the dependence on the starting point are also reported as the main drawbacks.

The algorithms based on response surfaces are dependent on the construction of an approximation function to the objective function, from a set of support points that are generated only once and are distributed throughout the variables' space (Ren and Chen 2010a). The approximation function can be linear, quadratic or polynomial, with the quadratic functions being the most widely used in this scope. The success in the application of this methodology is directly related to the quality of the approximation function and, whenever possible, a comparison between the values obtained from both functions, the approximate and the objective, must be carried out. The fast convergence, the use of simple approximation functions and the competitive computational effort are usually reported as the main advantages while the lower number of variables (< 10) is depicted as the great disadvantage of the process (Zabel and Brehm 2009a).

Genetic algorithms are stochastic processes based on Darwin's theory of natural evolution of species and their stages of adaptation, selection and variation, following the survival principle of the fittest (OptisLang 2008). Figure 4.9 generically illustrates the process associated with a

genetic algorithm, which is based on the crossing, and punctually in the mutation, of an initial population of individuals looking for in all variables' space for the solution that is closest to the optimal solution.

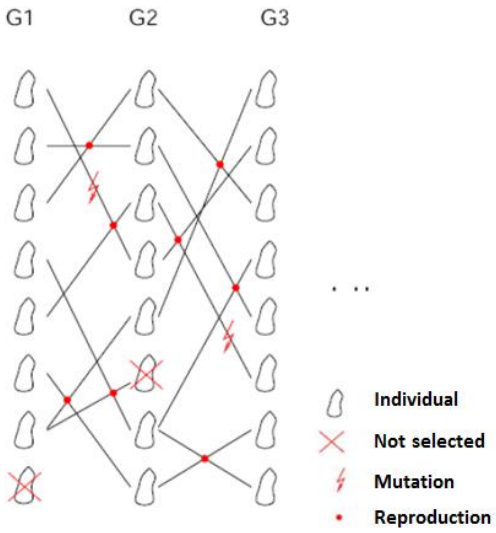

Figure 4.9 – Genetic algorithm [adapted from OptisLang (2008)]

The flowchart depicted in Figure 4.10 shows the distinct steps of genetic algorithms to be used in optimisation problems.

The process starts with the random generation of a certain number of individuals. Each of these individuals can be a probable solution to the optimisation problem and consist of a set of numerical parameters, which were previously selected according to the sensitivity analysis (see section 4.3.1). According to Ribeiro (2012), the evaluation of each individual is based on the value of the fitness function that is directly related to the value of the objective function of the problem. A high value in the fitness function means a good fit to the problem, leading to a reduced value of the objective function.

From the group of individuals initially generated, those that will constitute the initial population of the problem (generation 1) are then selected, which usually have the highest values of the fitness function. The next generation is then obtained based on four basic operators: selection, reproduction, mutation and substitution. In order to achieve the optimal solution of the problem, individuals of the $k+1$ generation result from the joining of some individuals of generation k with some of the best individuals of previous generations, who are temporarily placed in a waiting bag and replaced according by the substitution strategy

adopted. A detailed explanation about each of these steps and genetic operators, which transform the population over successive generations, can be found in Ribeiro (2012).

The process described above is repeated iteratively according to the maximum number of generations previously defined and according to the residue reached in the objective function.

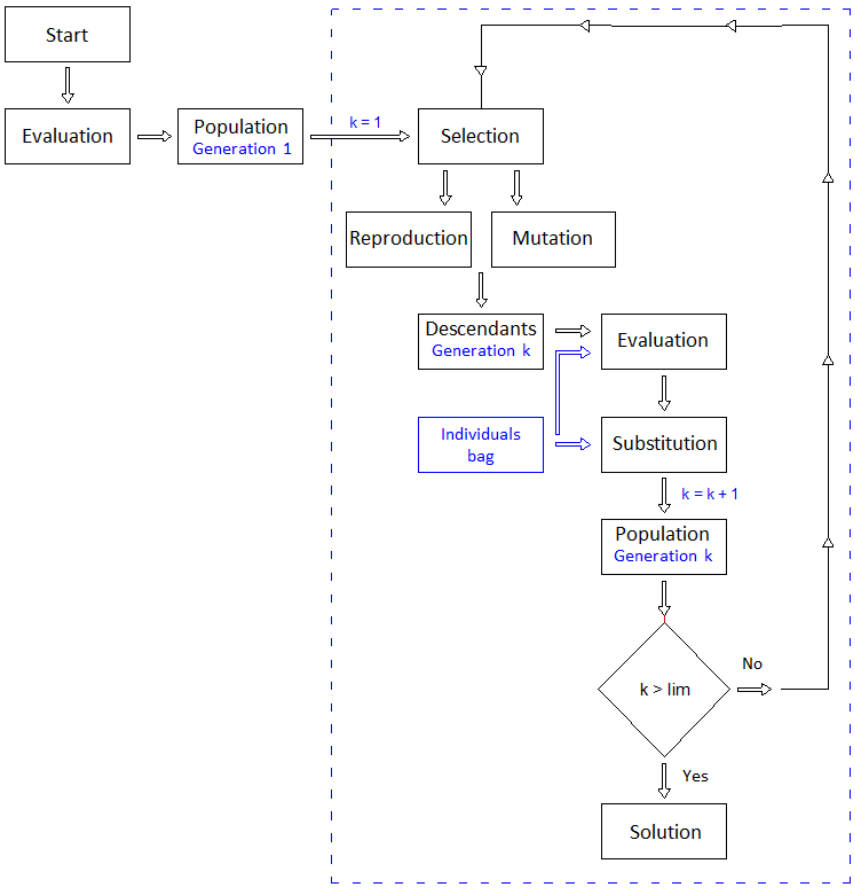

Figure 4.10 – Typical flowchart of a genetic algorithm [adapted from Ribeiro (2012)]

Few applications of genetic algorithms in the experimental calibration of numerical models of railway systems have been reported in literature. The works carried out by Cantieni et al. (2008), Xiankun et al. (2009), Zabel and Brehm (2009a) and Ribeiro (2012) should be highlighted. Ribeiro (2012) implemented an iterative method based on the application of an optimisation technique through a genetic algorithm, involving the use of three software packages: ANSYS (2007), MATLAB (2011) and OptiSlang (2008). This method, which is used in the present work, and the respective connections between the software are shown in the flowchart depicted in Figure 4.11.

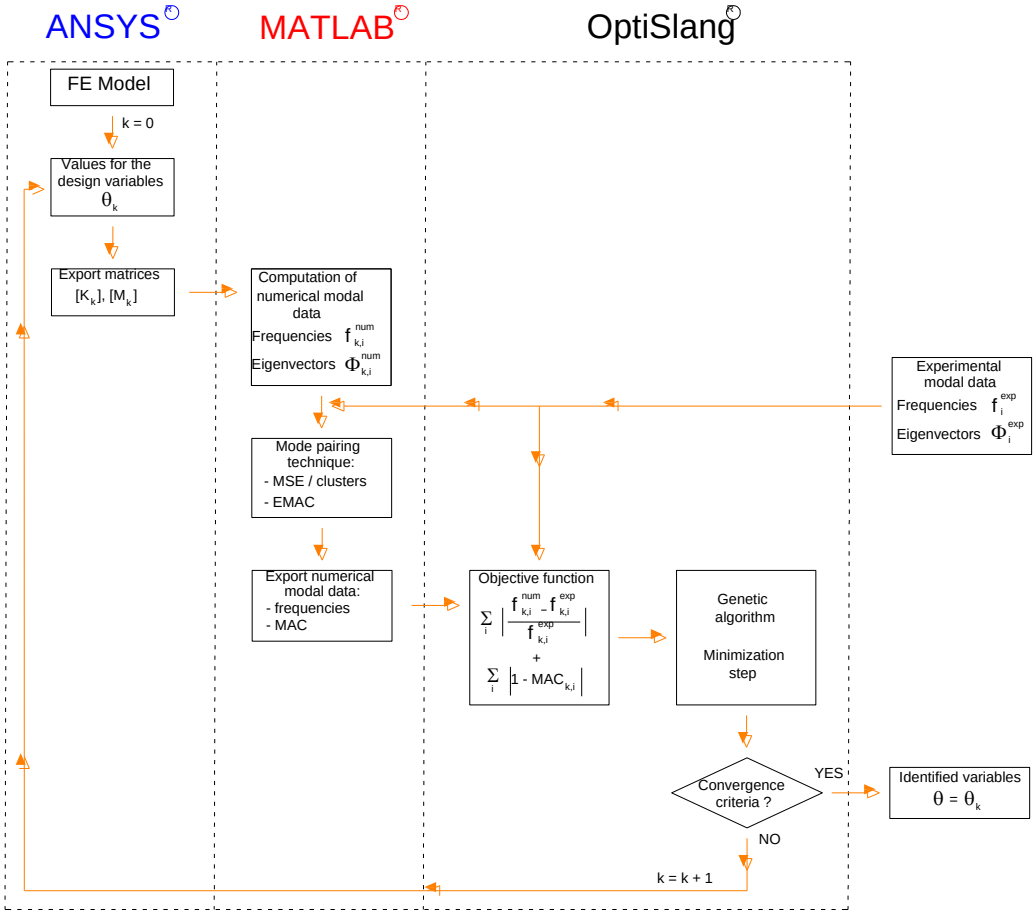

Figure 4.11 – Flowchart of the calibration process [adapted from Ribeiro (2012)]

Chapter 5

Case study I: Alverca viaduct

5.1 Introduction

In this chapter the dynamic behaviour and fatigue assessment of a reinforced concrete slab in a single-cell box girder railway viaduct are studied. The Alverca railway viaduct, located on the Portuguese railways' Northern Line, which presents a common structural form used on the European railway network, was chosen as a case study.

For that purpose, a three-dimensional finite element numerical model is developed, calibrated and validated based on experimental tests. The calibration of the numerical model is performed by applying an iterative methodology based on a genetic algorithm, taking into account the results obtained from an ambient vibration test, which allowed the identification of the modal parameters (natural frequencies, mode shapes and damping coefficients) of whole the structure and the upper deck slab as well. The validation of the numerical model is carried out through the comparison between numerical and experimental responses, in terms of displacements, accelerations and deformations measured in several locations on the viaduct, for the passage of AP trains with different running speeds.

For a realistic assessment of the fatigue strength of transverse reinforcement bars in the upper deck slab, detailed calculations of internal forces are needed. Bearing this is mind, train-bridge interaction analyses are performed considering the contribution of vibration frequencies up to 60 Hz. A static correction procedure is implemented, and validated, in these dynamic

analyses to take into account the static contribution of higher-frequency vibration modes (usually not explicitly considered in analyses using the basic modal-superposition method).

The effects of track irregularities and damping coefficients on the dynamic behaviour of the upper deck slab are discussed, when subjected to the passage of trains at speeds up to 240 km/h. Track irregularities, measured at different instants of time, and damping coefficients, determined based on accelerations records, are taken into account to evaluate the dynamic responses in terms of vertical accelerations and transverse bending moments.

The results of different train-bridge interaction dynamic analyses are the basis for the assessment of the fatigue damage in the transverse reinforcement bars of the upper deck slab. The fatigue damage is calculated based on the linear damage accumulation rule, considering the transverse bending moments and axial forces obtained for two different positions in the upper slab (positions of maximum sagging and hogging transverse bending moments).

5.2 Description of the Alverca viaduct

Alverca railway viaduct is a flyover structure that starts at 18.676 km on the Portuguese railways' Northern Line, which establishes the rail connection between Lisbon and Porto. It supports one single railway track and its construction allowed the separation of rail traffic that flows in the downstream and upstream directions and also to keep maximum train speed at 200 km/h.

Figure 5.1 depicts a map of the Portuguese railway network (Portugal 2017), highlighting the location of the Alverca viaduct and showing a general aerial view, with the *pergola* area that allows the intersection over the lines below. Figure 5.2 shows two perspective views of the viaduct.

Figure 5.1 – Location of the Alverca viaduct on the Portuguese railway network

a)

b)

Figure 5.2 – Perspective views of Alverca viaduct: a) lateral view; b) bottom view

The viaduct is composed of successive simply supported spans and has a total length of 1091 m divided into 3 parts: the south viaduct with 388 m (4×16.5 m + 4×17.5 m + 12×21.0 m), the *pergola* with 176 m and the north viaduct with 527 m (5×16.5 m + 5×17.5 m + 17×21.0 m). Figure 5.3 illustrates the elevation of the south and north ramps of the viaduct (Figure 5.3 a) and its respective cross section (Figure 5.3 b).

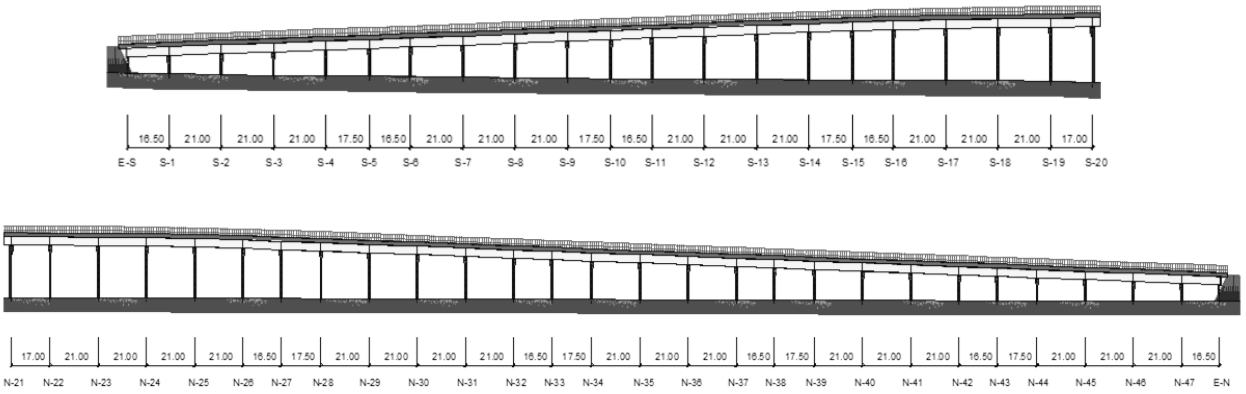

a)

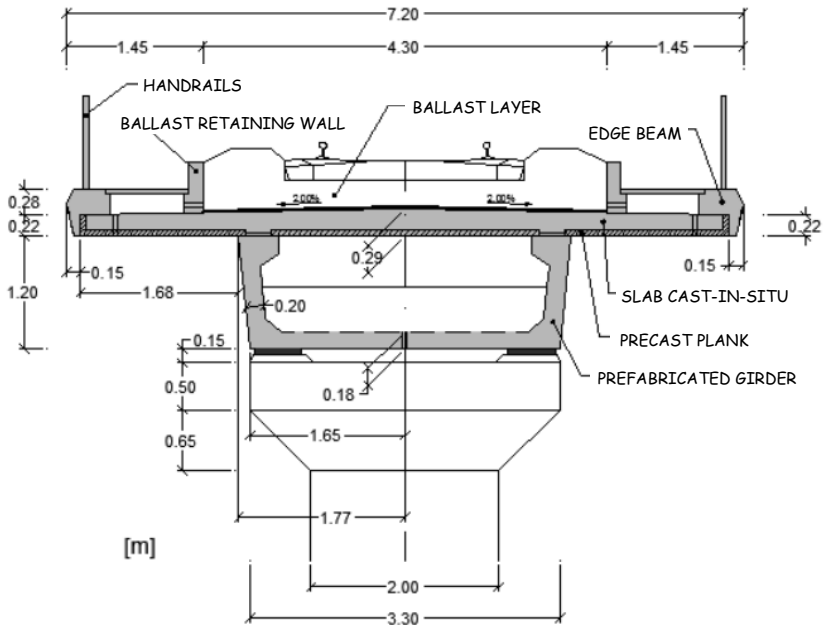

b)

Figure 5.3 – Alverca railway viaduct: a) elevation view of the north and south ramps; b) cross section of the deck over piers

Each span is composed of a single-cell box-girder deck trough a prefabricated and prestressed U-shaped girder, with thickness of 0.18 m and 0.20 m in the bottom slab and in the webs, respectively, and a concrete upper slab cast-in-situ over pre-slabs previously installed to

be used as formwork. The total height of the slab varies from 0.22 m to 0.29 m, in the outer edge of the cantilever footway and in central zone, respectively. It should be pointed out that there are ballast retaining walls, monolithically connected to the upper slab of the deck, with a height of 0.45 m and a width of 0.15 m.

The deck is directly supported in the piers and in the abutments by elastomeric reinforced bearings, each one composed of four layers of neoprene with plan dimensions of 500 mm × 300 mm and 8 mm thick, placed between steel plates with a thickness of 3 mm. In each span the bearings are fixed in one extremity and longitudinally guided in the other one. Figure 5.4 shows a schematic representation of the bearings system [Figure 5.4 a)] and an example of a longitudinally guided bearing over a pier [Figure 5.4 b)].

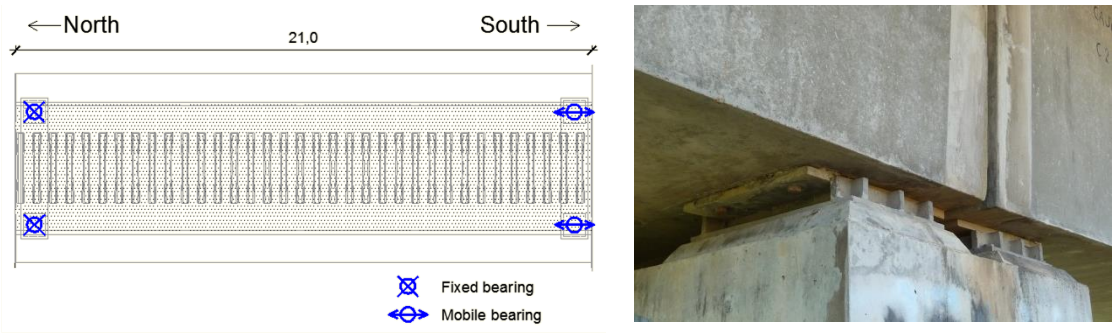

a) b)

Figure 5.4 – Bearings system: a) schematic representation; b) generic view of guided bearing

The track consists of UIC60 continuously welded rails (CWR) spaced apart by 1.688 m (Iberian gauge), elastomeric rubber pads, prestressed concrete monoblock sleepers and a ballast layer with a thickness of approximately 25 cm under sleepers.

Figure 5.5 – Overall view of railway track

5.3 Bridge FE numerical model

5.3.1 Description

The FE method was used in the numerical modelling of Alverca viaduct. A 3D numerical model was developed in ANSYS software (ANSYS 2007), considering three spans adjacent to the North abutment: one 16.5 m long span (Span 1) and two 21 m long spans (Spans 2 and 3). Figure 5.6 shows an overview of the numerical model with a detail of the track components [Figure 5.6 a)] and a cross section of the deck [Figure 5.6 b)].

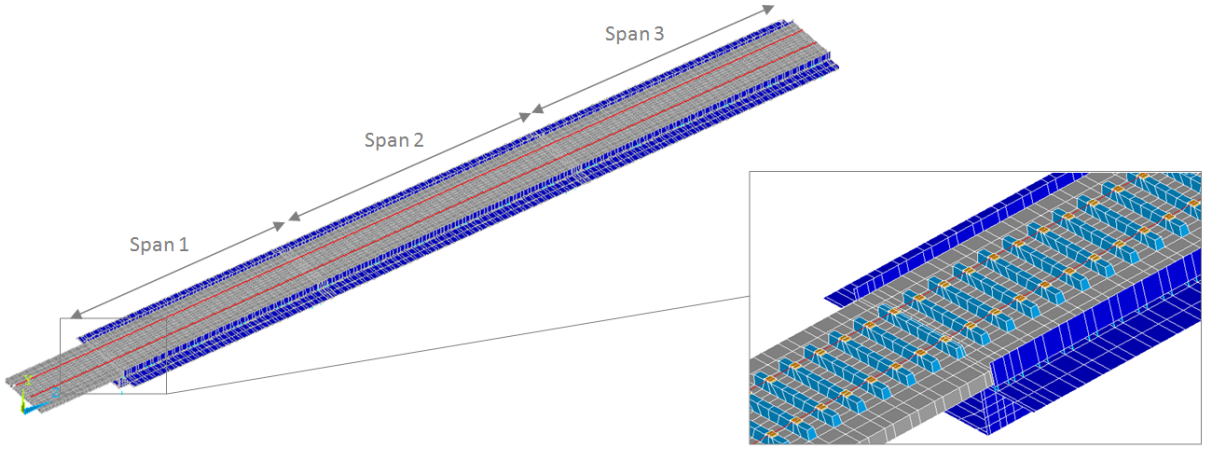

a)

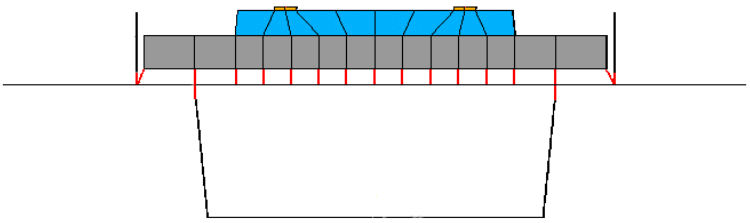

b)

Figure 5.6 – 3D numerical model: a) overview and track detail; b) cross section of the deck

Deck elements such as the prefabricated beam, the upper slab and the ballast retaining walls were modelled by shell FEs. Relating to the track modelling, the sleepers, the rail pads and the ballast layer were modelled by volume FEs while the rails were modelled as beam elements, positioned at their centre of gravity. Figure 5.7 shows a detailed view of the track FE numerical model. Additionally, an extension of the track, with a length of 6 m beyond the abutment, was

modelled in order to simulate the effect of the track over the adjacent embankment. The compatibility of displacements and rotations between the nodes of the precast beam and the nodes of the upper slab as well as the compatibility of displacements between the nodes of the upper slab of the deck and the lower nodes of the ballast layer were accomplished by rigid finite elements [see Figure 5.6 b)].

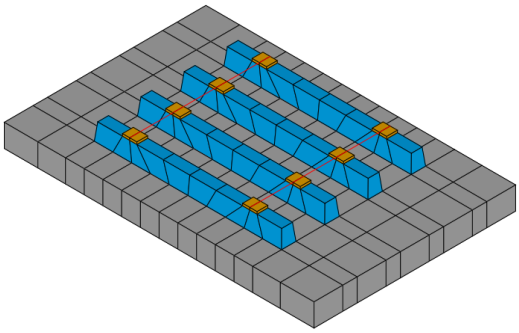

Figure 5.7 – Detailed view of the railway track FE numerical model

Each bearing was regarded as a single point and modelled by a spring element positioned at the corresponding centre of rotation. The non-structural elements such as handrails and edge beams were considered as additional masses, applied to the nodes of the FE mesh according to the real location of those elements. The global numerical model of the viaduct includes 19018 nodes and 20906 elements.

It should be pointed out that, although all concrete spans are simply supported, the railway track is continuous over successive spans, which can lead to some connection between them. Bearing this is mind, in order to evaluate the global behaviour of the viaduct and this composite effect between the structure and the track, three spans were initially modelled. However, in order to assess the dynamic behaviour and fatigue damage of the upper slab, a detailed refinement of the FEs should be adopted, reason why a new numerical model was considered, as explained further in section 5.6.1.

5.3.2 Geometrical and mechanical properties

The main geometrical and mechanical parameters of the various components of the finite element model are presented in Table 5.1, generically divided into deck and track parameters. Most of these parameters were defined based on design drawings while others were estimated

or obtained from local measurements such as elasticity modulus or thickness of the ballast layer, respectively. Detailed explanation about some parameters is presented below.

Table 5.1 – Geometrical and mechanical parameters of the numerical model

	Parameter	Designation	Adopted value	Unit
Deck	t_c	Thickness of the upper slab (cantilevers / central zone)	0.24 / 0.27	m
	E_{c1}	Concrete elasticity modulus of the upper slab (span 1)		
	E_{c2}	Concrete elasticity modulus of the upper slab (span 2)	35.4	GPa
	E_{c3}	Concrete elasticity modulus of the upper slab (span 3)		
	E_c	Concrete elasticity modulus of the prefabricated beam	40.9	GPa
	ρ_c	Concrete density	2548.4	kg/m^3
	ν_c	Concrete Poisson's ratio	0.2	-
	k_v	Vertical bearing stiffness	5200	MN/m
	k_{h1}	Longitudinal bearing stiffness (span 1)		
	k_{h2}	Longitudinal bearing stiffness (span 2)	3.6	MN/m
	k_{h3}	Longitudinal bearing stiffness (span 3)		
Track	t_{bal}	Thickness of the ballast layer	0.25	m
	E_{bal}	Ballast elasticity modulus	145	MPa
	ρ_{bal}	Ballast density	2039	kg/m^3
	ν_{bal}	Ballast Poisson's ratio	0.15	-
	E_{pad}	Rail pad elasticity modulus	500	MPa
	k_{pad}	Vertical rail pads stiffness	500	kN/mm
	A_{rail} / I_{rail}	Area / inertia of the rail UIC 60	76.7 / 3038	cm^2 / cm^4
	E_{rail}	Steel (rail) elasticity modulus	200	GPa
	ρ_{rail}	Steel (rail) density	7850	kg/m^3
	ν_{rail}	Steel (rail) Poisson's ratio	0.3	-
	$E_{sleeper}$	Concrete (sleeper) elasticity modulus	36	GPa
	$\rho_{sleeper}$	Concrete (sleeper) density	2890	kg/m^3
	$\nu_{sleeper}$	Concrete (sleeper) Poisson's ratio	0.3	-

5.3.2.1 Deck

5.3.2.1.1 RC upper slab

Concerning the thickness of the upper slab, although it is variable, a constant value was adopted in order to simplify its modelling: 0.24 m in the cantilevers zones and 0.27 m in the central zone between webs of the U-shaped girder.

The concrete elasticity modulus was indirectly estimated through the concrete compressive strength, f_{cm}, initially taken equal to 38 MPa considering a concrete class of C30/37 (CEN

2004). In order to take into account the age of the concrete at the date of the experimental tests (≈ 13 years ≈ 4745 days), the concrete compressive strength was corrected, using the following equation (CEN 2004):

$$f_{cm}(t) = e^{s\left[1-\left(\frac{28}{t}\right)^{0.5}\right]} \cdot f_{cm} \tag{5.1}$$

where *t* represents the concrete age (in days) and *s* is a coefficient that depends on the type of cement, which in the case of CEM 42.5N takes the value of 0.25. By applying this correction a concrete compressive strength equal to 47.86 MPa was obtained.

The variation of the concrete elasticity modulus with time correlates to the time variation of the compressive strength and is given by the following equation (CEN 2004):

$$E_{cm}(t) = \left(\frac{f_{cm}(t)}{f_{cm}}\right)^{0.3} \cdot E_{cm} \tag{5.2}$$

with

$$E_{cm} = 22 \cdot \left(\frac{f_{cm}}{10}\right)^{0.3} \tag{5.3}$$

where E_{cm} corresponds to the elasticity modulus at 28 days. By applying Equations 5.2 and 5.3, a corrected elasticity modulus equal to 35.4 GPa was obtained.

Due to the fact that the slab was cast-in-situ, it was considered that this parameter can assume distinct values in different spans, so their values are presented separately in Table 5.1.

5.3.2.1.2 U-shaped girder

Relating to the prefabricated U-shaped girder, the same approach presented above was used to obtain the elasticity modulus. According to the design project its concrete class is C55/67, whose compressive strength takes the value 63 MPa, corrected to the value 79.4 MPa to take into account the age of the concrete at the date of the experimental tests. By applying Equations 5.2 and 5.3, a corrected elasticity modulus equal to 40.9 GPa was obtained.

Following the guidelines of the standards EN1991-1-1 (CEN 2002) and EN1992-1-1 (CEN 2004), for both the upper slab and U-shaped girder, the concrete density and Poisson's ratio were adopted as equal to 2548.4 kg/m^3 (25 kN/m^3) and 0.20, respectively.

5.3.2.1.3 Bearings

As mentioned before, the deck is directly supported on the piers and on the abutments by elastomeric reinforced bearings. Figure 5.8 shows a schematic representation of a fixed bearing of the Alverca railway viaduct.

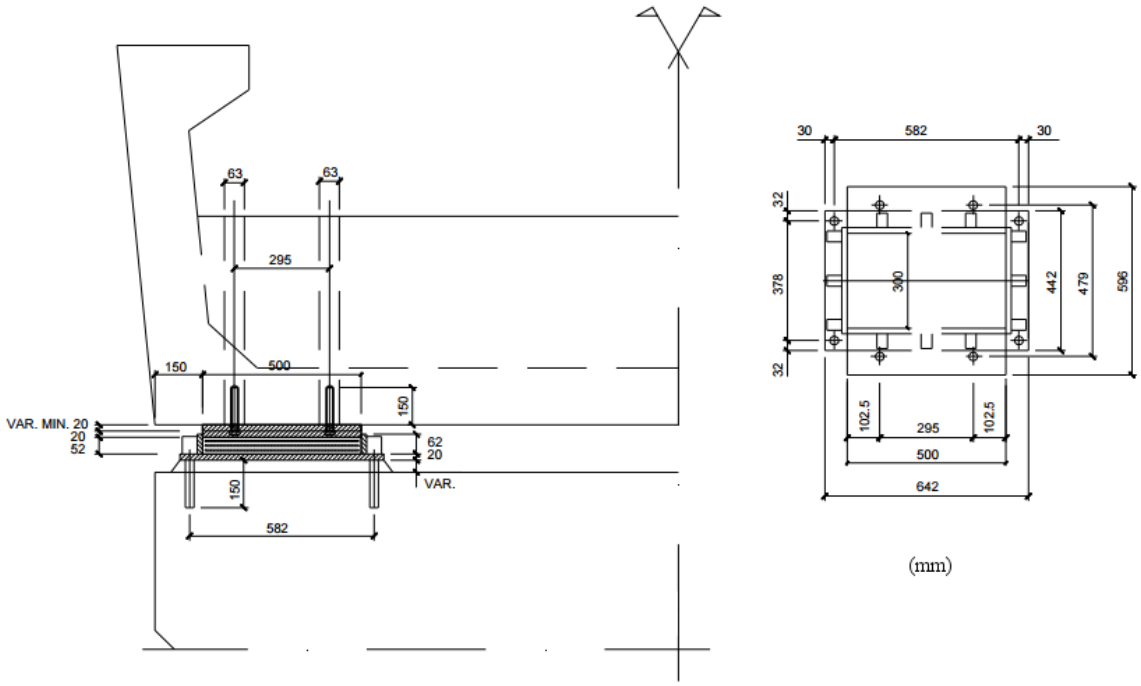

Figure 5.8 – Cross section and plan views of a fixed bearing

Due to the lack of information in the design project about the vertical bearings stiffness, this parameter was calculated based on a method proposed by Manterola (2006), which takes into account the confinement effect of neoprene layers provided by various steel plates. The bearing stiffness in the vertical direction (k_v) can be calculated considering a system of series-connected springs, each one simulating an individual neoprene layer, according to the following expression:

$$k_v = \frac{1}{\sum_{i=1}^{n} \frac{1}{k_{v,i}}} \tag{5.4}$$

with:

$$k_{v,i} = \frac{E \cdot a \cdot b}{t_i} \tag{5.5}$$

where E is the neoprene equivalent elasticity modulus, a and b are the smallest and the largest plan dimensions of the bearings, equal to 0.30 m and 0.50 m respectively, t_i is the thickness of each neoprene layer and n is the number of neoprene layers.

The longitudinal bearing stiffness (k_h) can be calculated by applying the following expression:

$$k_h = \frac{G \cdot a \cdot b}{\sum t_i} \tag{5.6}$$

with:

$$E = 3G\left(\frac{a}{t_i}\right)^2 v_3 \tag{5.7}$$

where G is the neoprene shear modulus, usually based on its Shore hardness (in this case considered equal to 60) and v_3 is a value that depends on the bearing shape which was considered equal to 0.202 . The possibility of distinct values of bearing stiffness in the longitudinal direction, in different spans, was also considered.

5.3.2.2 Railway track

The thickness of the ballast layer was obtained from several measurements taken during the experimental tests. In this modelling, a layer of constant thickness, equal to 0.25 m measured between the slab and the base of the sleepers, was adopted. The ballast between successive sleepers was considered as additional mass, which was concentrated at the nodes of the FEs of the upper face of the ballast layer. This FE model did not consider the explicit modelling of this additional ballast since it does not significantly influence the longitudinal stiffness of the track and, consequently, the composite effect between the deck and the track (ERRI 1997).

The adopted value for the ballast elasticity modulus comes from an experimental calibration of a railway track FE numerical model performed by Ribeiro (2012), studying also a bridge in the Portuguese railways' Northern line and using a similar modelling technique. The initial value for ballast density weight was adopted following the guidelines of standard EN1991-1-1.

The rail pads were modelled, taking into account plan dimensions equal to 0.15 m × 0.20 m, a thickness of 0.03 m and a modulus of elasticity equal to 500 MPa, leading to a vertical stiffness equal to 500 kN/mm. Due to the lack of information regarding the rail pads, these

dimensions were adopted in order to get a vertical stiffness similar to that used by Ribeiro (2012) for a rail pad model Vossloh ZW687.

The geometrical and mechanical properties of the UIC60 rail were adopted following the guidelines of the standard EN 13674-1:2003 and UIC 861-3. The steel elasticity modulus and density weight were taken equal to 200 GPa and 7850 kg/m^3, respectively.

The density value of the sleepers corresponds to an equivalent value, taking into account the simplified geometry of the sleepers adopted in the numerical model, namely, 2.60 m long and a trapezoidal cross section with the greater base equal to 0.20 m, the smaller base equal to 0.15 m and a height of 0.23 m. The concrete elasticity modulus and the Poisson's ratio were taken equal to 36 GPa (concrete strength class C45/55) and 0.3, respectively.

5.4 Calibration of the numerical model

The calibration of the FE numerical model of the viaduct was performed based on the results of ambient vibration tests, which allowed the identification of modal parameters. Such tests are described in this section. The calibration process involved two steps: sensitivity analysis and optimisation. The technique adopted for pairing numerical and experimental vibration modes is also discussed.

5.4.1 Identification of modal parameters

Ambient vibration tests were performed in order to identify the modal parameters of the viaduct, namely its natural frequencies, mode shapes and damping coefficients. As shown below, while natural frequencies and mode shapes are important information for the calibration process of the FE numerical model, damping coefficients are crucial for its validation process.

A preliminary numerical modal analysis revealed the existence of distinct vibration modes, among them vibration modes involving global movement of the structure and vibration modes of local structural elements such as the upper slab of the deck. Thus, the ambient vibration test was performed in two different phases: the first focused on the identification of global parameters (G) of the structure and the second focused on the identification of local parameters (L) of the upper slab of the deck.

A technique based on fixed reference points and mobile measuring points (Rodrigues 2004) involving the use of 12 piezoelectric accelerometers, model PCB 393A03, was conducted in both phases. The time series were acquired in periods of 4 minutes with a sampling frequency of 2000 Hz, which was then decimated to a frequency of 200 Hz. The data acquisition was performed using the cDAQ-9172 system from National Instruments, equipped with IEPE analog input modules (NI 9233).

Railway traffic was not considered as an ambient action since it introduces dominant frequencies, resulting from the passage of regularly spaced axles at a certain speed, which makes it difficult to use modal identification methods. So, due to the low acceleration levels of the deck under ambient conditions, a forced excitation of the structure was carried out by a group of people jumping randomly over the viaduct. This external action, which consists of the application of several random impulse loads, allowed significant improvements in signal-to-noise ratios and, therefore, an increase of the coherence between the measured signals. Figure 5.9 shows a view of the three instrumented spans, the type of accelerometer that was used in the test and a group of people jumping in one of the deck's spans.

a) b) c)

Figure 5.9 – Ambient vibration test: a) instrumented spans; b) typical accelerometer; c) group of people jumping on the viaduct deck

5.4.1.1.1 Phase 1: Identification of global modal parameters

During phase 1 of the ambient vibration test 60 measurement points were considered along the three analysed spans, specifically 50 measurement points located in the ballast retaining wall, 6 measurement points in the extremity of the footway cantilever and 4 in the webs of the prefabricated girder. The ambient response was evaluated in successive setups in terms of accelerations in the vertical, transverse and longitudinal directions. Figure 5.10 a) shows the

plan location of the measurement points and a detail of the location of the accelerometers near the structural joint between spans 1 and 2.

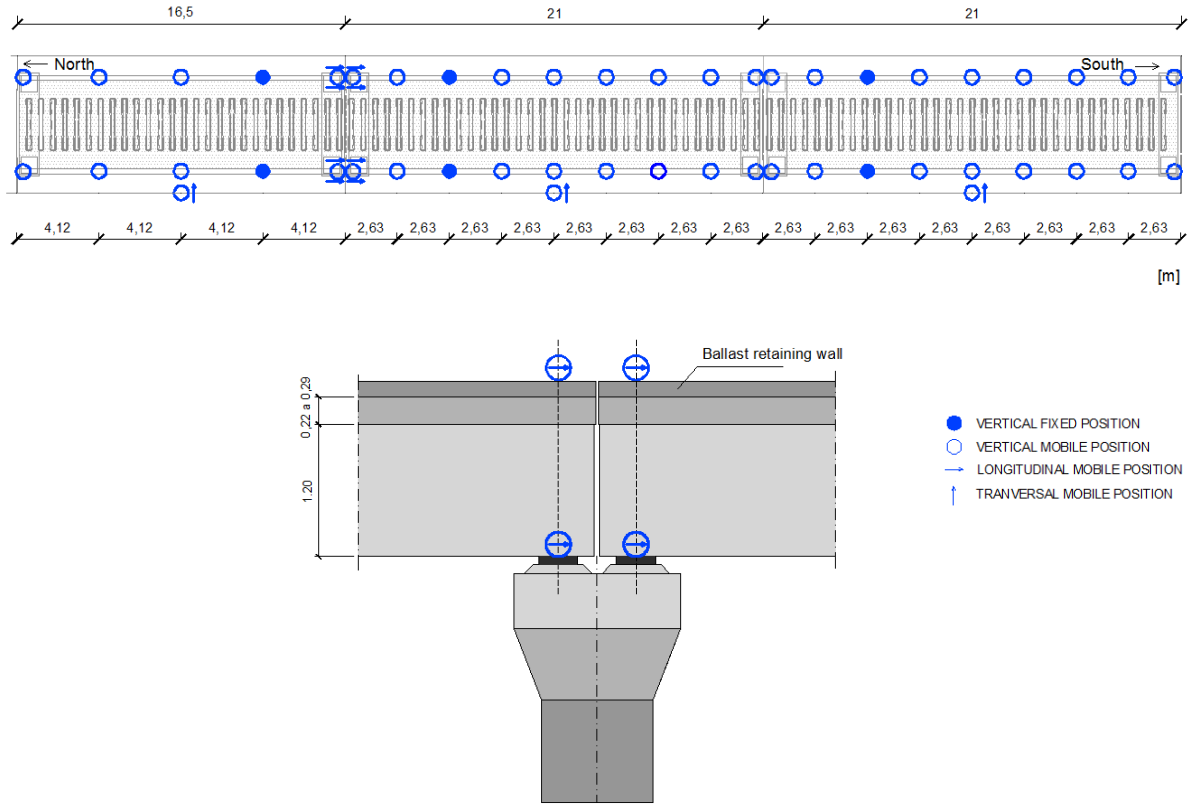

a)

b)

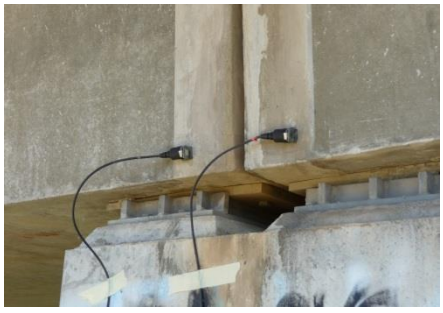

c)

d)

Figure 5.10 – Ambient vibration test – phase 1: a) measurement points; b) accelerometer in the top of ballast retaining wall; c) accelerometers near the joint at the supports level; d) accelerometers near the joint in the ballast retaining wall level

The accelerometers were placed on both ballast retaining walls, in the vertical direction, through metal plates bonded to the concrete surface [Figure 5.10 b)]. Due to the close proximity between the alignments of the ballast retaining walls and the girder's webs [see Figure 5.3 and Figure 5.6 b)], the measured responses at these locations allowed the identification of global vibration modes of the deck, especially those associated with bending

and torsion movements. A greater ease in repositioning the accelerometers between successive setups also contributed to their installation on ballast retaining walls rather than on the girder's webs.

Additionally, some accelerometers were also installed near the structural joint between spans 1 and 2, in the longitudinal direction at two different levels: at a lower level, on the webs of the prefabricated beam near the supports [Figure 5.10 c)] and at a higher level, on the ballast retaining walls [Figure 5.10 d)]. The results measured at these points allowed the characterization of the structural continuity between successive spans provided by the track.

The accelerometers in the transverse direction allowed the distinction between vertical vibration modes and transverse vibration modes of the deck. Since almost all accelerometers were installed in the vertical direction, in the possible presence of transverse vibration modes, although they might have some vertical component, looking at the amplitude of movement obtained by the accelerometers installed in the transverse direction it is possible to distinguish these vibration modes.

A Stochastic Subspace Identification method (SSI-DATA), UPC variant, available in the Ambient Response Testing and Modal Identification Software (ARTeMIS 2009) was used to identify modal parameters. Figure 5.11 shows a stabilization diagram of one of the experimental setups, using models of order between 1 and 150, for the range of frequencies between 0 and 25 Hz. Evaluating the abscissa corresponding to the peaks on the diagram allows one to identify the most relevant vibration frequencies. The same figure also includes a chart with the mean values of the coherence function for all experimental setups. A stabilization criterion that allows a maximum variation of 0.05 Hz for the frequency, 0.5 % for the damping coefficient and 0.05 for the Modal Assurance Criterion (MAC), was taken into account.

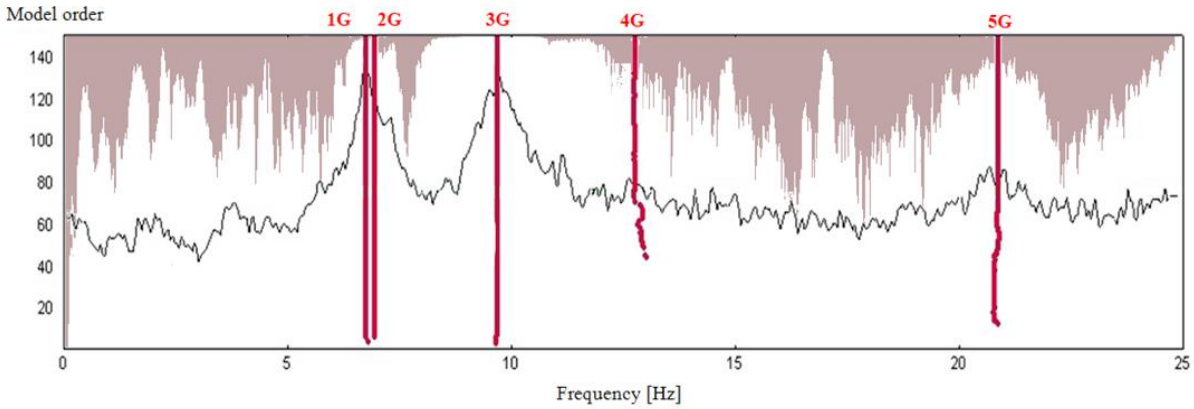

Figure 5.11 – Stabilization diagram of phase 1 of the ambient vibration test

Figure 5.11 shows five vertical alignments of poles according to the identified vibration modes (1G to 5G). The average value of the modal coherence function in the proximity of these alignments tends to the value 1.0, showing the high quality of the measured signals.

Figure 5.12 presents the identified mode shapes with the corresponding value of the natural frequency (f). The value of standard deviation (σ), estimated from different experimental setups, is presented in brackets. The same figure also presents the numerical vibration modes obtained from a previous modal analysis of the numerical model, before calibration, taking into account the adopted values indicated in Table 5.1.

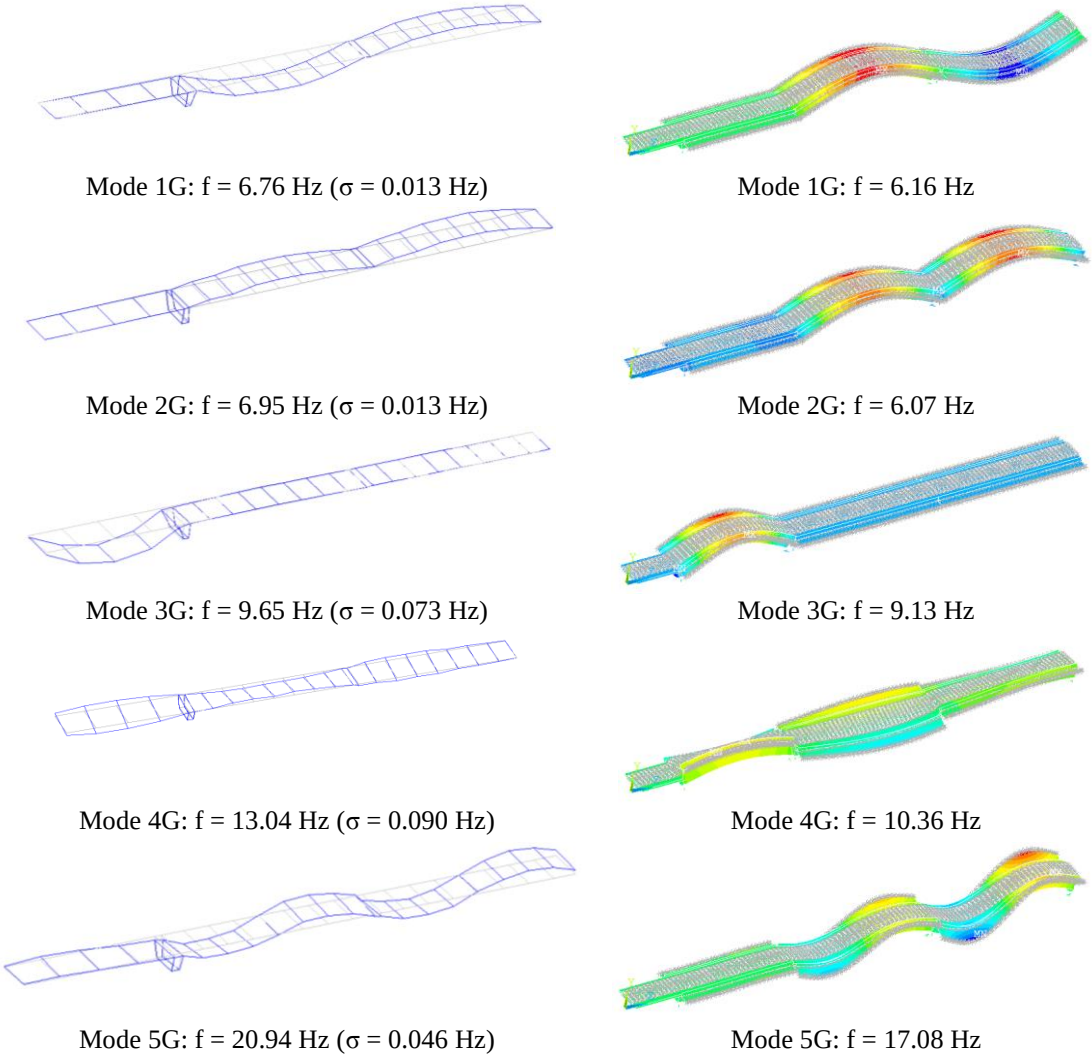

Figure 5.12 – Global vibration modes: a) experimental; b) numerical

Vibration modes 1G, 2G and 5G involve simultaneous bending of spans 2 and 3. In the particular case of modes 1G and 2G, the similar frequencies' values and the obtained modal

configurations are related to the coupling effect that occurs between the simply supported spans due to the continuity established by the track (rails, pads, sleepers and ballast layer). Mode 3G involves isolated bending of span 1. Mode 4G is associated with torsion movements of the different analysed spans.

It should be pointed out that the installation of accelerometers in the ballast retaining walls rather than directly in the girder has proved to be particularly efficient in the identification of global vibration modes. The installation near of the supports also has proved to have huge value in understanding the coupling effect between adjacent spans provided by the track.

Regarding the configuration of the vibration modes, it should be noted that the modal coordinates associated with the longitudinal movements of the supports are reduced, which means that, under ambient actions, all the supports operate like fixed supports.

Figure 5.13 shows the damping coefficient of each global vibration mode, estimated by the SSI-DATA method for each experimental setup. The mean values of the damping coefficients and corresponding values of the standard deviation are presented in Table 5.2. Experimental setups that mostly involve sensors placed in the transverse and longitudinal directions were not taken into consideration for the estimation of the damping coefficients, since the global vibration modes are mainly associated with vertical movements of the deck.

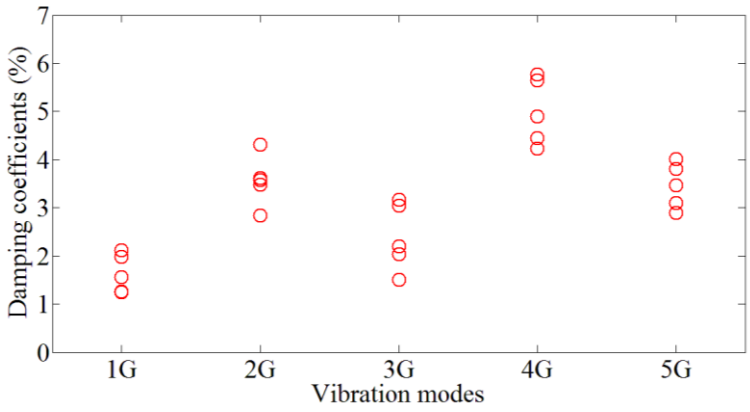

Figure 5.13 – Damping coefficients of the global vibration modes

Table 5.2 – Statistical properties of the damping coefficients of the global vibration modes

Vibration mode	Damping coefficient (%)	
	Mean value	Standard deviation
1G	1.63	0.403
2G	3.56	0.525
3G	2.39	0.705
4G	4.99	0.690
5G	3.46	0.469

The mean values of damping coefficient for the global vibration modes range between 1.6 % and 5.0 %. The distribution of damping coefficients' values for each experimental setup in relation to the average value is similar for all vibration modes.

5.4.1.1.2 Phase 2: Identification of local modal parameters

Since a great majority of the local vibration modes of the upper deck slab, seen in the previously performed numerical modal analysis, were predominantly associated with bending movements of the central zone of the upper slab, along the different spans of the viaduct, only one span was considered in this identification. So, during phase 2 of the ambient vibration test 84 measurement points were considered, located in span 2, with particular focus on the northern half of that span. The ambient response was evaluated in successive setups in terms of accelerations only in the vertical direction. Figure 5.14 a) shows the measurement points with the fixed reference points and the mobile measuring points.

The accelerometers were placed on the sleepers, on the ballast retaining walls, in the extremity of the footway cantilevers and on the lower slab of the deck, through metal plates bonded to the concrete surface. The installation of the accelerometers on the sleepers is due to the inaccessibility of the upper slab either internally, through the box-girder deck, or externally, by removing the ballast layer. Figure 5.14 b) and c) shows the installation of accelerometers on the sleepers and a detail of one accelerometer on the sleeper edge, respectively.

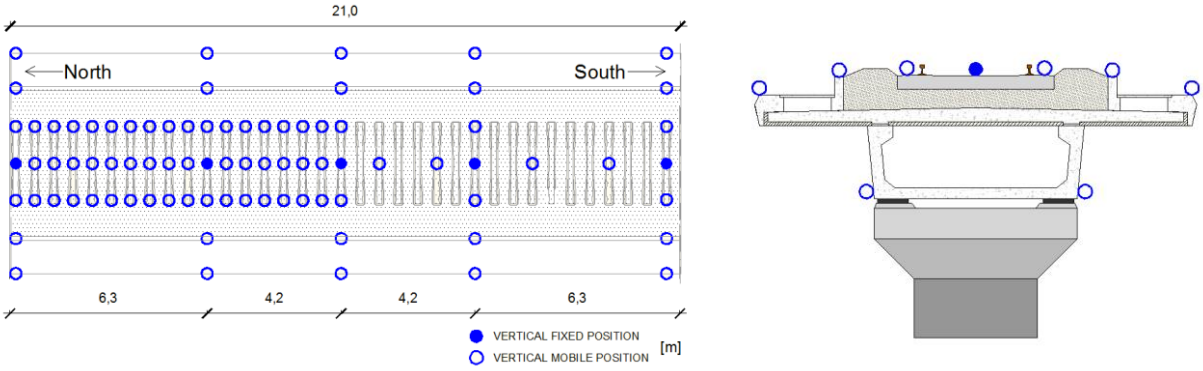

a)

b)

c)

Figure 5.14 – Ambient vibration test – phase 2: a) measurement points; b) installation process of the accelerometers on the sleepers; c) accelerometer on the sleeper edge

The identification of the modal parameters was performed resorting once more to the stochastic subspace identification method (SSI-DATA), UPC variant. Figure 5.15 shows the stabilization diagram of one of the experimental setups using models of order between 1 and 150, for the range of frequencies between 0 Hz and 80 Hz. Evaluating the abscissa corresponding to the peaks on the diagram allows one to identify the most relevant vibration frequencies. A chart with the mean values of the coherence function for all experimental setups is also included in the same figure. The stabilization criterion was the same as the one adopted in the first phase of the ambient vibration test.

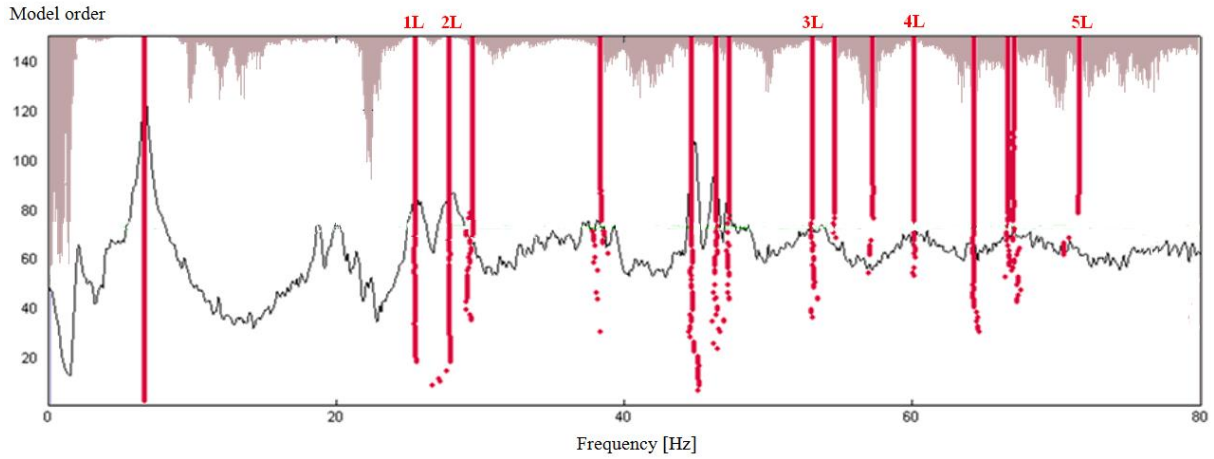

Figure 5.15 – Stabilization diagram of phase 2 of the ambient vibration test

Figure 5.15 shows the alignments of five local vibration modes of the upper slab of the deck (1L to 5L). The stabilization diagram also identifies other stable vibration modes but most of them presented deformed configurations without physical meaning. These configurations are probably related to local modes of the adjacent spans with reduced modal amplitudes in the instrumented span, which in most cases are not correctly reproduced.

Figure 5.16 presents the identified mode shapes with the corresponding value of the natural frequency. The value of the standard deviation, estimated from various experimental setups, is presented in brackets. The same figure also presents the numerical vibration modes obtained from a modal analysis of the numerical model, before calibration, taking into account the adopted values indicated in Table 5.1. Regarding the numerical vibration modes, there are detailed views of span 2, according to the experimental measurement points, and also views of the three analysed spans.

Vibration modes 1L and 2L mainly involve movements of the footway cantilevers, which, in turn, produce movements in the central zone of the upper slab of the deck due to structural compatibility. On the contrary, modes 3L, 4L and 5L are predominantly associated with bending movements of the central zone of the upper slab whose movements are transmitted to the cantilevers.

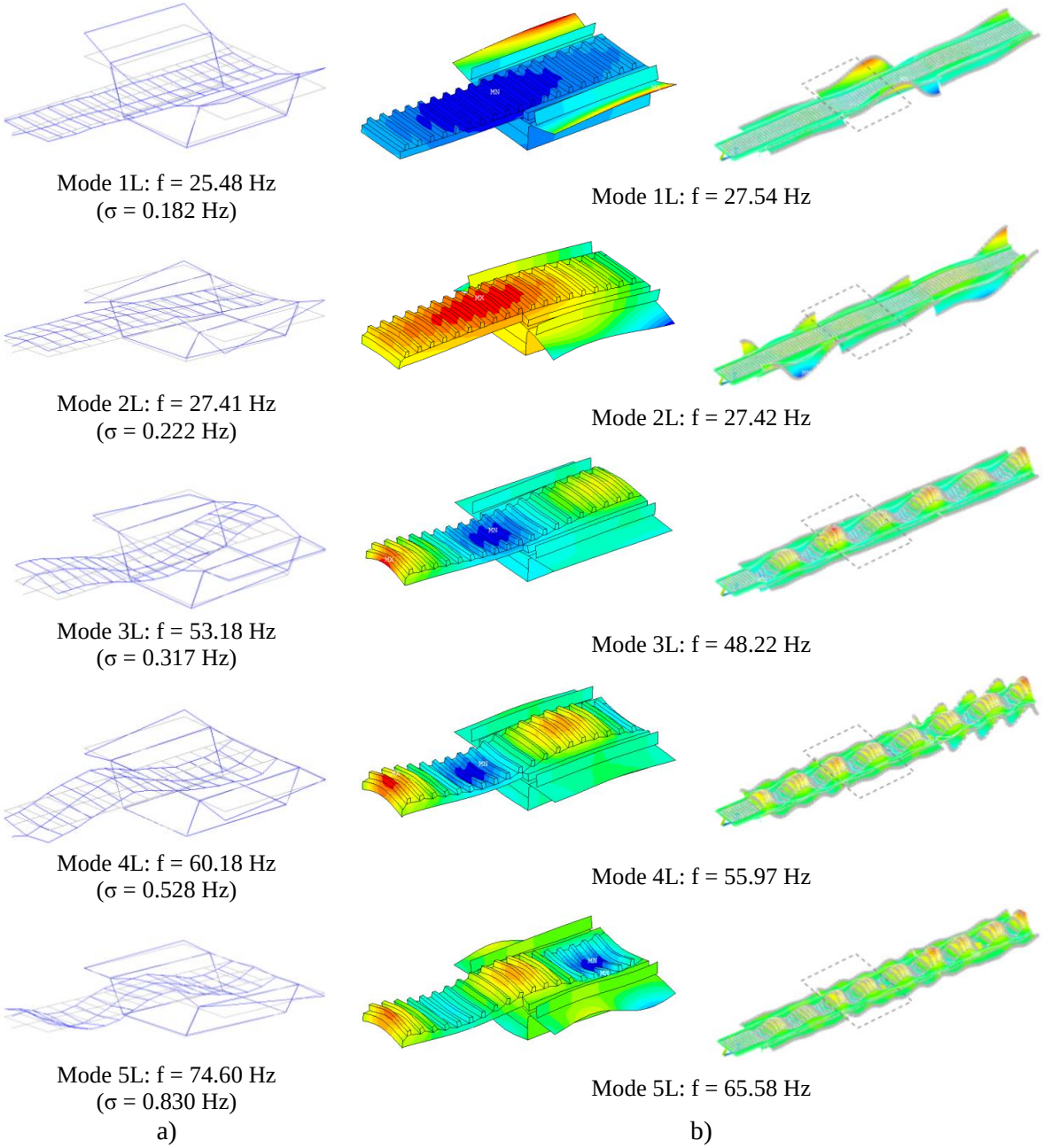

Figure 5.16 – Local vibration modes: a) experimental; b) numerical

It is important to note that the installation of the accelerometers in the sleepers has proved to be particularly efficient in the identification of local vibration modes of the upper slab. Due to the high level of confinement of the ballast layer, especially under the sleepers, and considering that vibration modes of the track have frequencies generally above 100 Hz (Man 2002), it was possible to clearly separate and identify the local vibration modes associated with the movements of the upper slab based on the measurement of the sleepers' vibrations.

Figure 5.17 shows the damping coefficient of each local vibration mode, estimated by the SSI-DATA method for all experimental setups. The mean values of the damping coefficients and the corresponding values of the standard deviation are presented in Table 5.3.

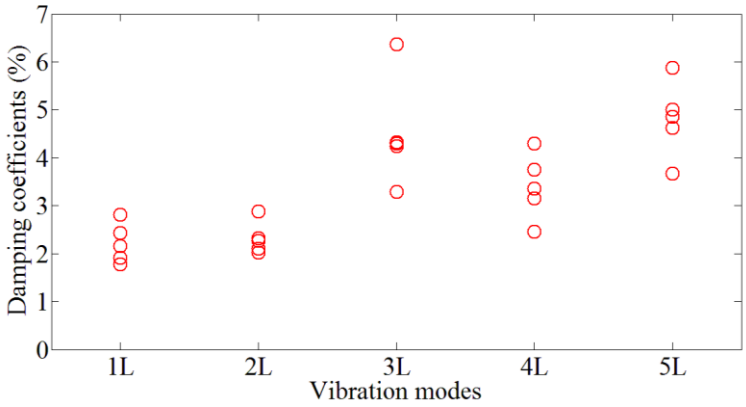

Figure 5.17 – Damping coefficients of the local vibration modes

Table 5.3 – Statistical properties of the damping coefficients of the local vibration modes

Vibration mode	Damping coefficient (%)	
	Mean value	Standard deviation
1L	2.16	0.396
2L	2.13	0.541
3L	4.47	0.961
4L	3.35	0.624
5L	4.81	0.712

The mean values of the damping coefficients for local vibration modes range between approximately 2.2 % and 4.8 %. By observing Figure 5.17 one can notice a little higher distribution of the results of vibration modes 3L, 4L and 5L, also seen from the standard deviation values presented in Table 5.3.

5.4.2 Calibration

The calibration of the numerical model of the viaduct was based on the results of the ambient vibration test, presented in the previous section, and involved the application of an iterative procedure based on an optimisation technique that is grounded on a genetic algorithm. This methodology is previously referred to in Chapter 4 and is described in detail by Ribeiro (2012). The calibration procedure is preceded by a discussion of the technique adopted for the

mode pairing between numerical and experimental vibration modes (section 5.4.2.1) and a sensitivity analysis to the parameters of the numerical model (section 5.4.2.2).

5.4.2.1 Mode pairing criteria

The mode pairing technique establishes the correspondence between each experimentally obtained mode and each numerically derived mode. In the present thesis this correspondence is performed by the MAC parameter, in global vibration modes and by EMAC parameter, in the case of local vibration modes.

Regarding the mode pairing for local vibration modes, Figure 5.18 presents the four *clusters* that were defined based on the positioning of the sensors in phase 2 of the ambient vibration test. In that phase only accelerations in the vertical direction were recorded, reason why these *clusters* include only the translational degrees-of-freedom in the vertical direction of the cantilevers, upper slab of the deck and precast U-shaped girder of span 2. The *cluster* denominated as other elements contains the remaining degrees-of-freedom of the structure.

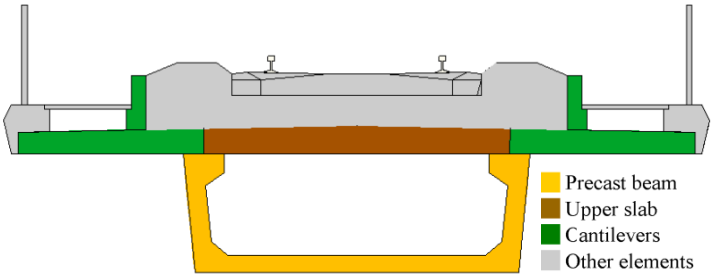

Figure 5.18 – Clusters used in the mode pairing process

Figure 5.19 shows the values of relative modal strain energy for the *clusters* considering 100 numerical vibration modes of the initial FE model. Global vibration modes are related to higher values of energy on the U-shaped girder's *cluster* while local vibration modes of span 2 are associated to higher values of energy on the upper slab's and cantilevers' *clusters*. Considerable values of energy of the *cluster* "Other elements" appear in almost all vibration modes, either global or local, due to the inclusion of all degrees-of-freedom related to spans 1 and 3 in this *cluster*.

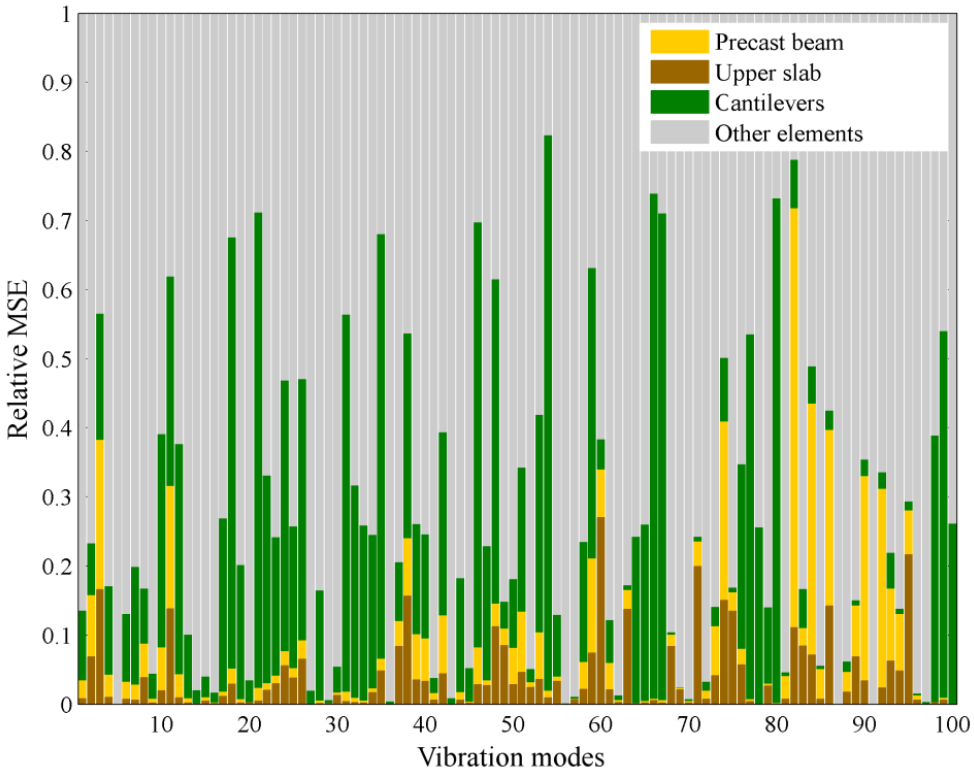

Figure 5.19 – Relative modal strain energy of each vibration mode based on the initial FE model

Figure 5.20 illustrates the MAC and EMAC correlation matrices between experimental and numerical vibration modes of the initial finite element model. For global vibration modes, only the MAC correlation matrix is presented.

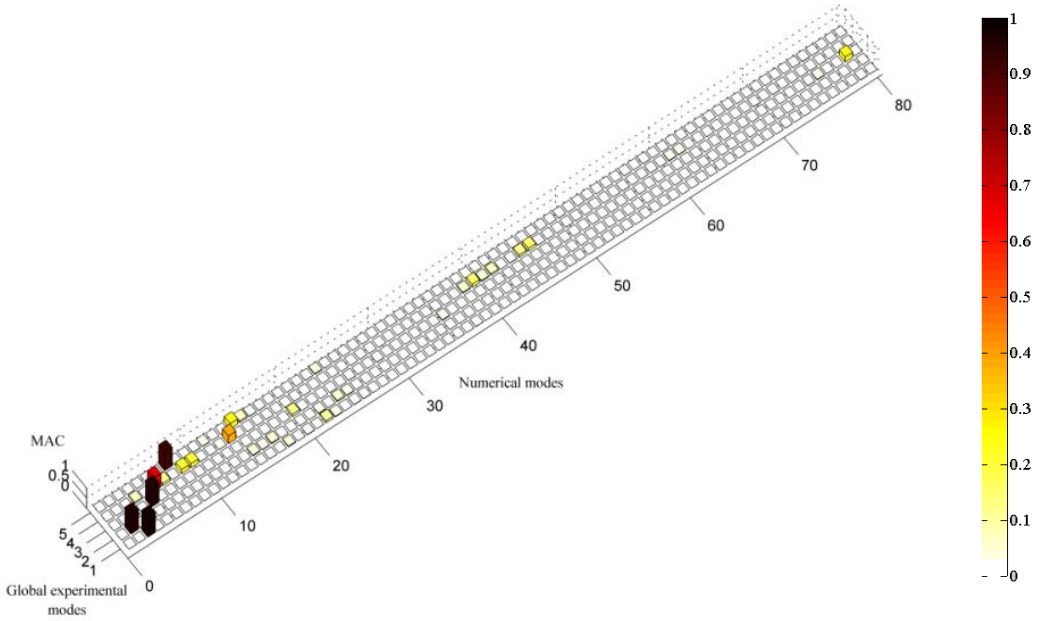

a)

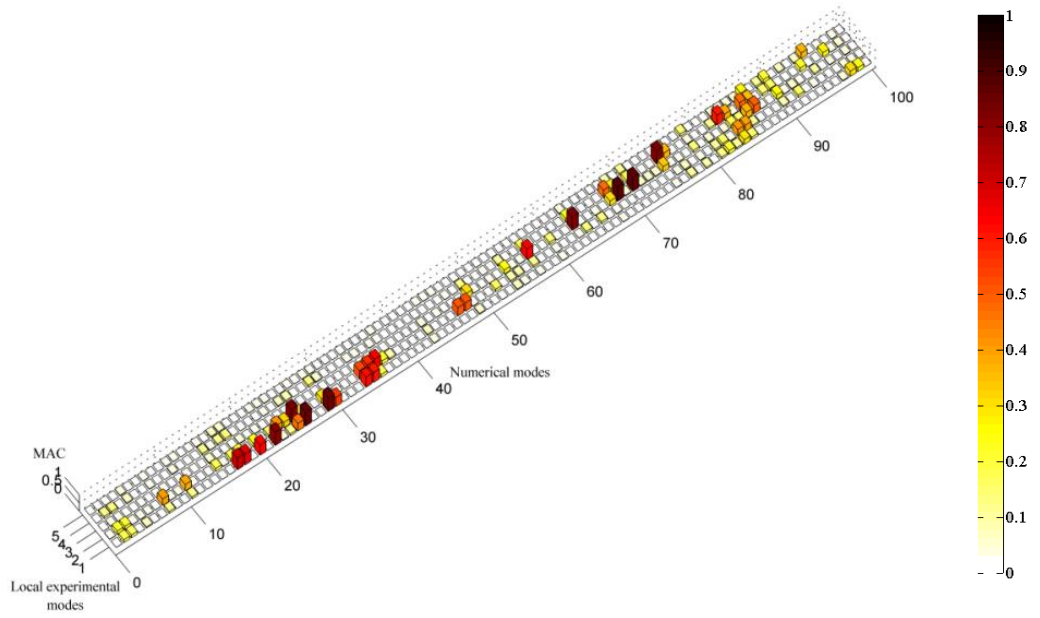

b)

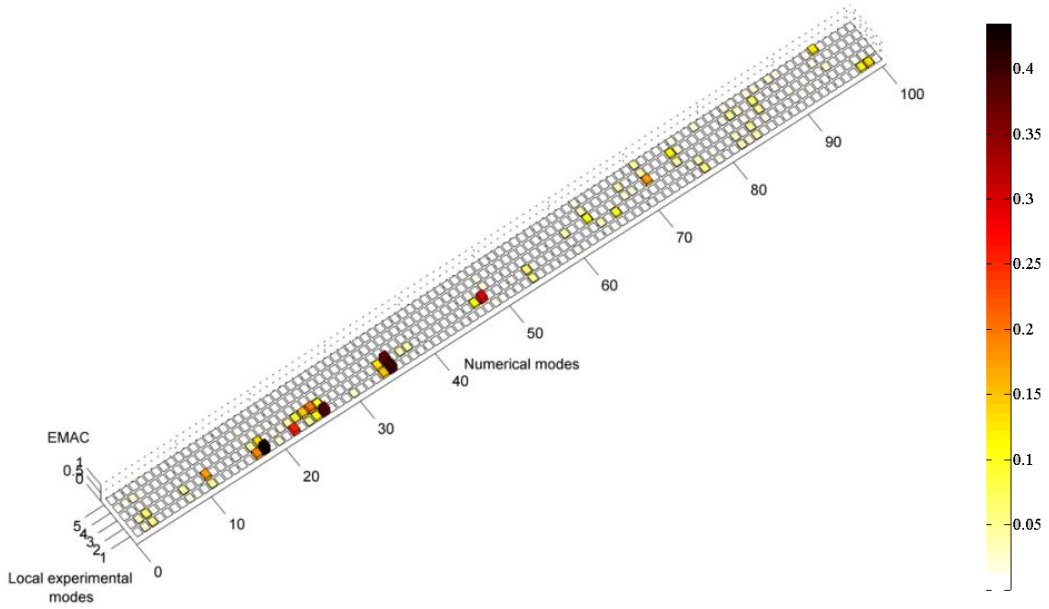

c)

Figure 5.20 – Correlation matrices between experimental and numerical modes: a) MAC for global vibration modes; b) MAC for local vibration modes and c) EMAC for local vibration modes

The application of the MAC criterion to global vibration modes of the structure allowed a stable pairing between experimental and numerical vibration modes to be achieved. However, the use of the MAC parameter does not guarantee a stable pairing in experimental and numerical local vibration modes, particularly in modes 1L, 2L and 3L, for which several numerical modes with high values of the MAC parameter arise. For example, it is possible to

note that the experimental mode 1L would be paired with the numerical mode 29 using the MAC parameter, which is characterized by the vibration of cantilevers in span 1 that, by compatibility, create small amplitude bending movements in cantilevers of span 2. Based on the EMAC parameter, experimental mode 1L is paired with numerical mode 18, this one involving only the vibration of the span 2 cantilevers.

The EMAC values for the local vibration modes 1L and 2L were obtained by weighting the MAC values using the modal strain energy of the *clusters* "upper slab" and "cantilevers". Due to the mode shape of the remaining local vibration modes, only the *cluster* "upper slab" was considered to obtain the EMAC values. To improve the efficiency of the pairing of modes 1L and 2L, in addition to the adoption of EMAC values, frequency limits were imposed to avoid pairing with higher order modes.

5.4.2.2 Sensitivity analysis

The sensitivity analysis allowed the selection of the parameters that most influence the frequencies and MAC values of the global and local vibration modes and, consequently, should be included in the subsequent optimisation phase. For the parameters previously indicated in Table 5.1, their statistical properties and lower/upper limits, which will later be taken into account during the calibration process, are presented in Table 5.4. Some references are also presented and, in some situations, an explanation of their limits of variation is discussed below.

Table 5.4 – Statistical properties of the numerical parameters

	Parameter	Designation	Statistical distribution		Limits (lower/upper)	Unit	References
			Type	Mean value/ standard deviation			
Deck	t_c	Thickness of the upper slab	normal	0.27 / 0.0056	0.26 / 0.28	m	(JCSS 2001, Henriques 1998)
	E_{c1}	Concrete elasticity modulus of the upper slab (span 1)	normal	35.4 / 4.3	28.4 / 42.4	GPa	(Henriques 1998, Mirza et al. 1979)
	E_{c2}	Concrete elasticity modulus of the upper slab (span 2)					
	E_{c3}	Concrete elasticity modulus of the upper slab (span 3)					
	E_c	Concrete elasticity modulus of the prefabricated beam	normal	40.9 / 4.9	32.9 / 49.0	GPa	
	ρ_c	Concrete density weight	normal	2446.5 / 122.3	2245.9 / 2647.1	kg/m^3	(IAPF 2010)
	k_v	Vertical bearing stiffness	uniform	5400 / 2020.7	1900 / 8900	MN/ m	-
	k_{h1}	Longitudinal bearing stiffness (span 1)	uniform	3.35 / 0.89	1.8 / 4.9	MN/ m	-
	k_{h2}	Longitudinal bearing stiffness (span 2)					
	k_{h3}	Longitudinal bearing stiffness (span 3)					
Track	t_{bal}	Thickness of the ballast layer	normal	0.25 / 0.013	0.23 / 0.27	m	(UIC 2008, Knothe and Wu 1998, Fortunato 2005)
	E_{bal}	Ballast elasticity modulus	uniform	140 / 34.6	80 / 200	MPa	
	ρ_{bal}	Ballast density weight	uniform	1875 / 129.9	1650 / 2100	kg/m^3	

Regarding the thickness of the RC upper slab, a coefficient of variation equal to 4 % was considered, taking into account some studies showing that a variation between 10 and 15 mm relatively to the nominal measure is considered acceptable.

Henriques (1998) and Wisniewski (2007) reported a strong correlation between the concrete elasticity modulus and its compressive strength, indicating values of the coefficient of variation of the concrete elasticity modulus equal to 8% in the case of the tangential elasticity modulus and 12% in the case of the secant modulus. Bearing this in mind, a value of 12 % was adopted.

Studies carried out by JCSS (2001) suggest that the concrete density weight follows a normal statistical distribution, with an average value of 2446.5 kg/m^3 and a coefficient of variation equal to 4 %, in the case of current concrete, and a coefficient equal to 3 % in the case of high strength concrete. The Spanish standard IAPF (2010) requires that the coefficient of variation of this parameter should not exceed 5 % in the case of concrete or composite steel-

concrete railway bridges. In the present thesis, a value of 5 % was adopted for the concrete density weight.

Regarding the bearing stiffness, the lower and upper limits, either in vertical and horizontal directions, were obtained based on the calculation of this parameter following the approach proposed by Manterola (see section 5.3.2.1.3) and considering shore hardness' values of the neoprene equal to 40 and 70, respectively.

As mentioned before, the adopted value for the thickness of the ballast layer is a result of measurements taken during the experimental tests. Since no significant differences were noticed from the measurements along the span, a coefficient of variation equal to 5 % was adopted for the statistical properties of this parameter. Concerning the ballast elasticity modulus, the lower and upper limits were defined following the guidelines suggested by UIC 719-R (2008) and Knothe and Wu (1998), respectively. In terms of the ballast density weight, the adopted values for lower and upper limits are based on the suggestions of Fortunato (2005) for dry and saturated material, respectively.

Figure 5.21 shows the results of a global sensitivity analysis through a Spearman correlation matrix (Brehm et al. 2010), excluding from graphical representation the correlation coefficients in the range [-0.25 0.25]. The analysis was conducted based on 800 samples generated by the Latin Hypercube method and only encompassed the global vibration modes 1G to 3G and local vibration modes 1L, 3L and 4L. The remaining modes were not considered since they present low values of the MAC parameter.

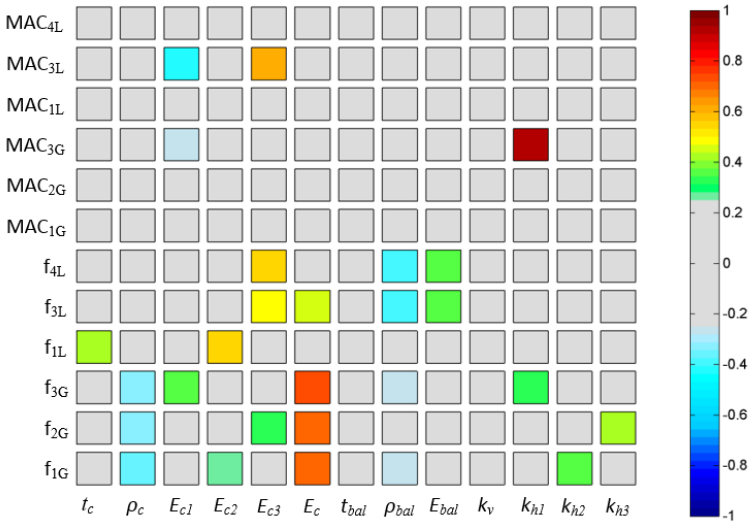

Figure 5.21 – Spearman correlation matrix

By observing the previous figure, it is found that both the concrete elasticity modulus of the precast beam and the concrete density weight have significant influence over the vibration frequencies of global modes. The same is true for the horizontal bearing stiffness's in relation to frequencies of the modes involving respective spans. In turn, the concrete elasticity modulus of the upper slab, in different spans, seems to have more influence over the frequencies and MAC values of local vibration modes. The vertical bearing stiffness and the depth of the ballast layer have minor influence over the modal responses and, therefore, were excluded from the optimisation phase.

5.4.2.3 Optimisation

The optimisation phase aimed to obtain the parameter values of the numerical model that minimise the differences between numerical and experimental modal responses. This process involved the definition of an objective function and the application of an optimisation technique based on a genetic algorithm.

The objective function (f) includes two terms, one related to the natural frequencies and the other related to the MAC values, comprising the global and local vibration modes:

$$\mathrm{f} = a \sum_{i=1}^{n\,modes} \frac{\left|f_i^{exp} - f_i^{num}\right|}{f_i^{exp}} + b \sum_{i=1}^{n\,modes} \left|\mathrm{MAC}\left(\boldsymbol{\phi}_i^{exp}, \boldsymbol{\phi}_i^{num}\right) - 1\right| \tag{5.8}$$

where f_i^{exp} and f_i^{num} are the experimental and numerical frequencies for mode i, $\boldsymbol{\phi}_i^{exp}$ and $\boldsymbol{\phi}_i^{num}$ are the vectors containing the experimental and numerical modal information regarding mode i, a and b are weighting factors of the objective function's terms, considered equal to 1.0 in this case, and *nmodes* is the total number of modes, equal to 6.

The optimisation of the model involved the use of 11 design variables and 12 modal responses (6 frequencies and 6 MAC values) regarding the global and local vibration modes of the structure. The genetic algorithm was based on an initial population consisting of 30 individuals and 150 generations, for a total of 4500 individuals. In this algorithm the number of elites, as well as the number of substitute individuals, was equal to 1. The crossing rate was equal to 50 % and the mutation rate was equal to 15 % with a standard deviation varying throughout the optimisation process and ranging between 0.10 and 0.01.

Table 5.5 shows the values of the numerical parameters, obtained from three independent optimisation runs (GA1 to GA3) based on different initial populations.

Table 5.5 – Optimal numerical parameters for the independent optimisation runs GA1 to GA3

Parameter	Adopted value	Optimal value			Unit
		GA1	GA2	GA3	
t_c	0.270	0.262	0.265	0.265	m
E_{c1}	35.40	30.29	30.07	31.50	GPa
E_{c2}	35.40	33.30	33.35	33.77	GPa
E_{c3}	35.40	34.60	35.10	34.50	GPa
E_c	40.94	47.10	48.08	47.90	GPa
ρ_c	2469.8	2605.1	2590.4	2628.5	Kg/m^3
E_{bal}	145.00	153.40	142.70	139.60	MPa
ρ_{bal}	2039.0	1964.5	1995.9	1960.5	Kg/m^3
K_{h1}	3.6	199	188	207	MN/m
K_{h2}	3.6	231	238	233	MN/m
K_{h3}	3.6	249	252	255	MN/m

The parameters that have more influence over modal responses, e.g., the concrete elasticity modulus of the precast beam and upper slab of the decks, the horizontal bearing stiffness and the concrete density, provide estimates with lower variability over the three runs. The parameters that have less influence in the modal responses, such as density and elasticity modulus of ballast tend to present greater variation for the different optimisation runs.

The upper variation limits of the horizontal bearing stiffness have been extended from 4.9 MN/m to 490 MN/m due to the systematic tendency of this parameters optimum solutions to reach the upper limit indicated in Table 5.4. This must be related to the fact that under ambient actions, the movements of the bearings are reduced, assuming a behaviour which is similar to that of fixed bearings.

Figure 5.22 shows the percentage results of the optimisation, in the form of ratios, between the values of numerical and experimental natural frequencies [Figure 5.22 a)], and the MAC values [Figure 5.22 b)], for runs GA1 to GA3.

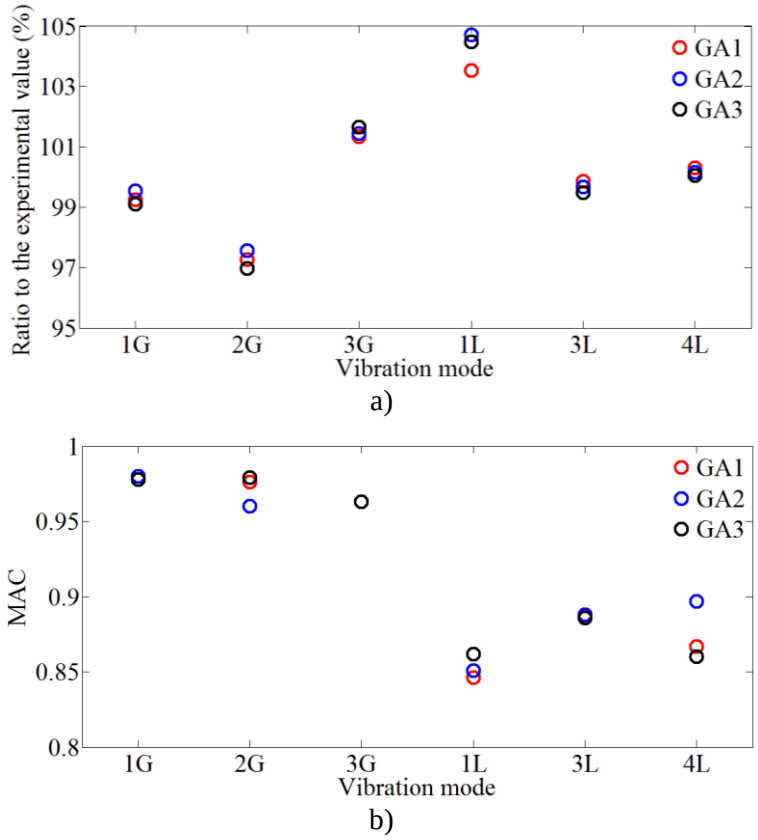

Figure 5.22 – Response values for independent optimisation runs GA1 to GA3: a) frequencies; b) MAC

The differences between experimental and numerical frequencies are always less than 5 % for all analysed modes. Regarding MAC parameter, the values obtained for global modes, situated above 0.95, are higher than the values obtained for local modes, situated between 0.85 and 0.90. In general, the results obtained from the different optimisation runs are very similar, demonstrating, once again, the robustness of the genetic algorithm.

The optimal set of parameters, used in the updated numerical model, consists of the parameters' values obtained from the GA2 optimisation run, which presents the lowest residual value of the objective function.

Figure 5.23 a) and b) presents the values of experimental and numerical frequencies and MAC values, respectively, before and after calibration. Despite the fact that the modes 4G, 5G, 2L and 5L were not considered in the optimisation, their frequencies' values and MAC parameters are also presented.

The average error in global modes frequencies decreased from 11.6 % before calibration to 6.5 % after calibration. The average value of the MAC parameter slightly increased from 0.899,

before calibration, to 0.902 after calibration. For local modes, the average error of the frequencies went from 7.3 %, before calibration, to 3.1 % after calibration, while the average value of the MAC parameter increased from 0.657, before calibration, to 0.760 after calibration.

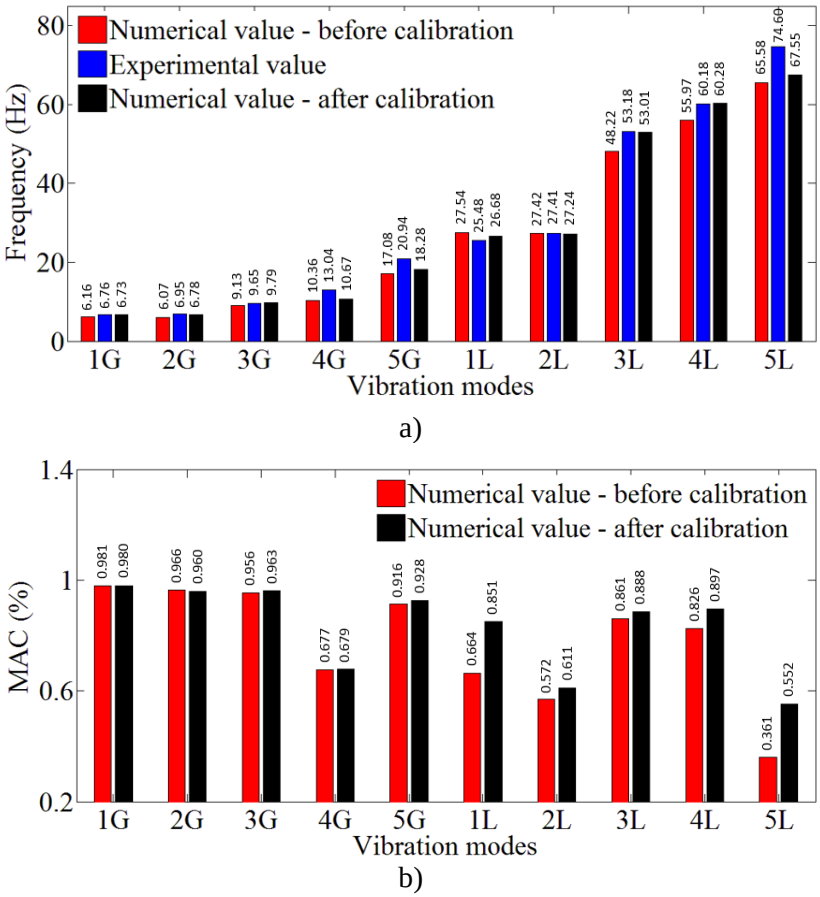

Figure 5.23 – Modal parameters' values before and after calibration: a) frequencies; b) MAC

Figure 5.24 presents a comparison between experimental and numerical modal configurations, before and after calibration. In order to allow a better understanding an undeformed configuration is shown. Modal configurations 4G, 5G, 2L and 5L, which were not considered in the calibration of the numerical model, are also presented. By observing this figure one can realise that there is a good agreement between numerical and experimental modal configurations, particularly in global vibration modes.

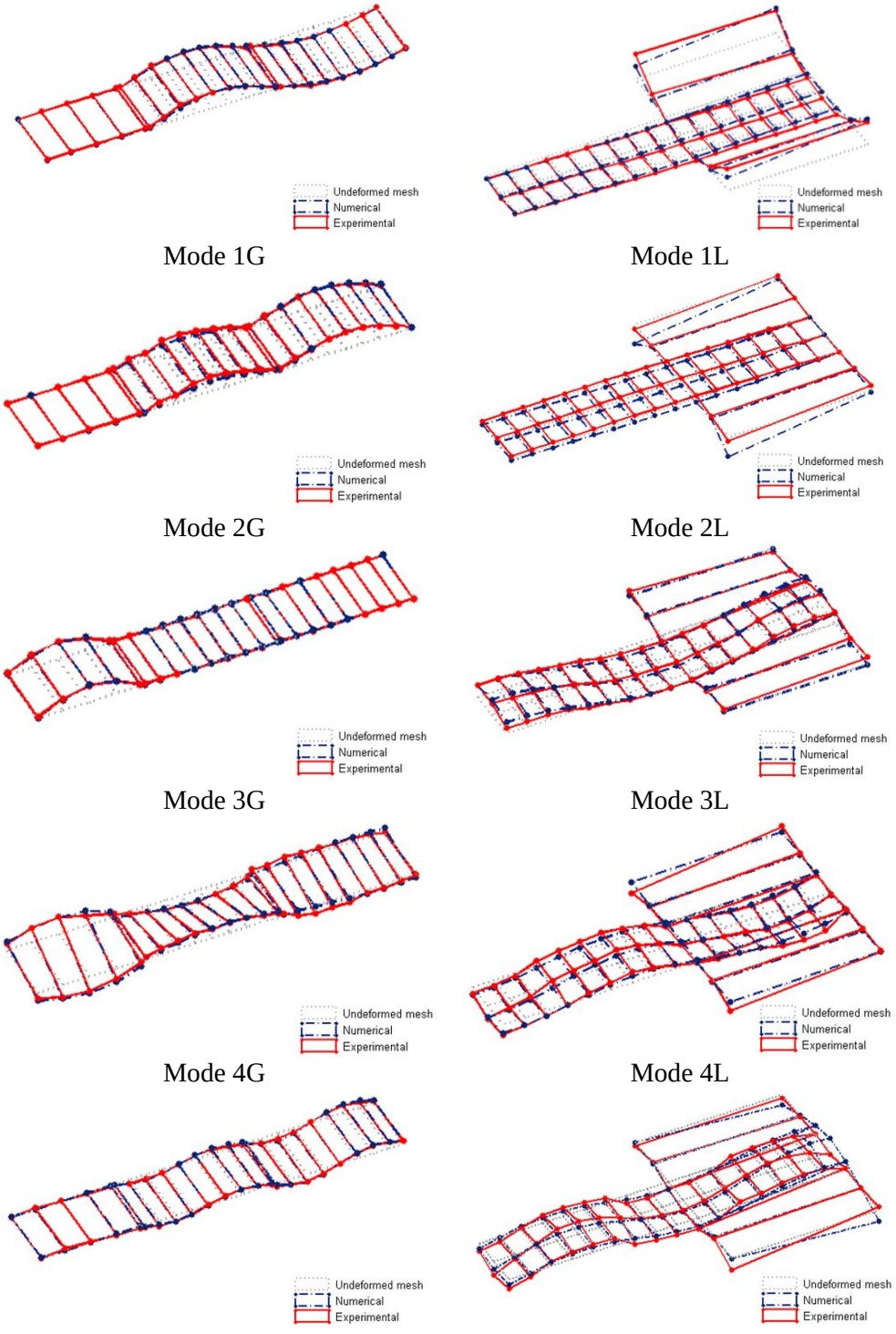

Figure 5.24 – Comparison between experimental and numerical modal configurations, after updating

5.5 Global dynamic behaviour of the structure under railway traffic

In this section the global dynamic behaviour of the Alverca viaduct is analysed, based on the comparison between experimental and numerical responses of the structure. The experimental responses were obtained through a dynamic test under real railway traffic. The numerical responses were determined taking into account the previously calibrated FE numerical model simulating the passage of the same real trains.

5.5.1 Dynamic test under railway traffic

In order to perform the experimental validation of the numerical model through the comparison between numerical and experimental dynamic responses, the latter were obtained in a dynamic test under railway traffic. For this purpose, only measurements of the dynamic response of span 2 were recorded, namely displacements, accelerations and deformations in the mid-span section of the lower deck slab and displacements at the supports' area. Vertical accelerations of the upper deck slab, in mid-span and quarter-span sections, were also measured but they will only be used further in section 5.6. Figure 5.25 shows the location of the sensors in the mid-span cross section of the deck.

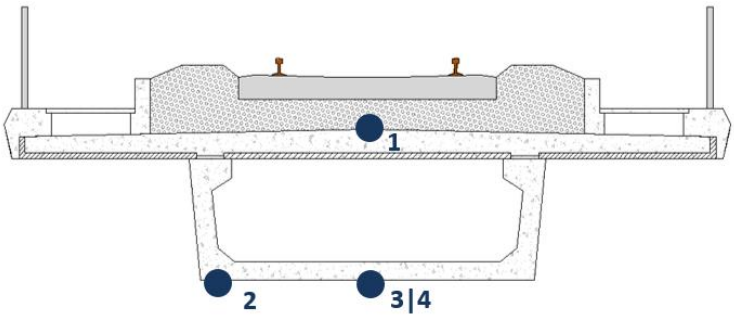

a)

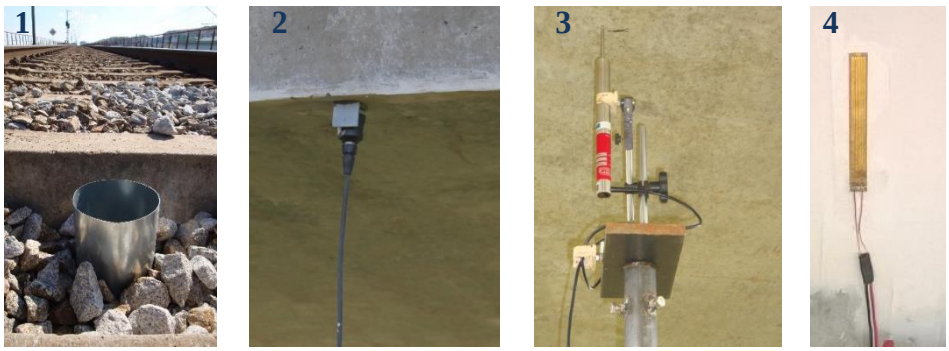

b) c) d)

Figure 5.25 – Dynamic test under railway traffic: a) location of the sensors in the mid-span cross section; b) accelerometers; c) LVDT; c) strain gage

The vertical acceleration was measured using a piezoelectric accelerometer model PCB 393A03 [Figure 5.25 b)]. The vertical displacement was measured by a Linear Variable Differential Transformer (LVDT), model RDP ACT1000A [Figure 5.25 c)]. The deformation of the lower slab of the deck in the longitudinal direction was measured by an electrical resistance strain gage, model Vishay N2A-06-20CBW-350, bonded to the concrete surface [Figure 5.25 d)] and installed as a quarter Wheatstone bridge. The data acquisition was performed using the cDAQ-9172 system from National Instruments (NI), equipped with Integrated Electronic Piezoelectric (IEPE) analogue input modules NI 9233 for accelerometers, NI 9239 for tension measures and NI 9237 for strain gages.

The dynamic response of the deck was measured for the passage of an Alfa Pendular (AP) train at 157 km/h and 185 km/h. Figure 5.26 a) depicts the loading scheme of the AP train. This conventional train has a total length of approximately 150 m and is composed of four motor vehicles (BAS, BBS, BBN and BAN) and two hauled vehicles (RNB and RNH), with axle loads varying between 128.8 kN and 136.6 kN. Figure 5.26 b) shows the dynamic signature of the train for a range of wavelengths from 4 m to 30 m. The dynamic signature that characterises the dynamic excitation of the train and depends on the axle loads and the distances between axles, is given by the following expression (ERRI D214/RP9 2001):

$$S_0(\lambda) = \underset{i=1,N-1}{MAX} \sqrt{\left[\sum_{k=0}^{i} P_K \cos\left(\frac{2\pi x_k}{\lambda}\right)\right]^2 + \left[\sum_{k=0}^{i} P_K \, sen\left(\frac{2\pi x_k}{\lambda}\right)\right]^2} \tag{5.9}$$

where i is the number of axles in the train, P_k is the static load per axle k, x_k is the distance between axle k and the first axle of the train and λ is the wavelength of excitation. The peak with the most dynamic aggressiveness of the train, with a wavelength of 25.9 m, is associated to the regular distance between groups of four axles, composed by the two axles of the rear bogie and the two axles of the front bogie of adjacent vehicles.

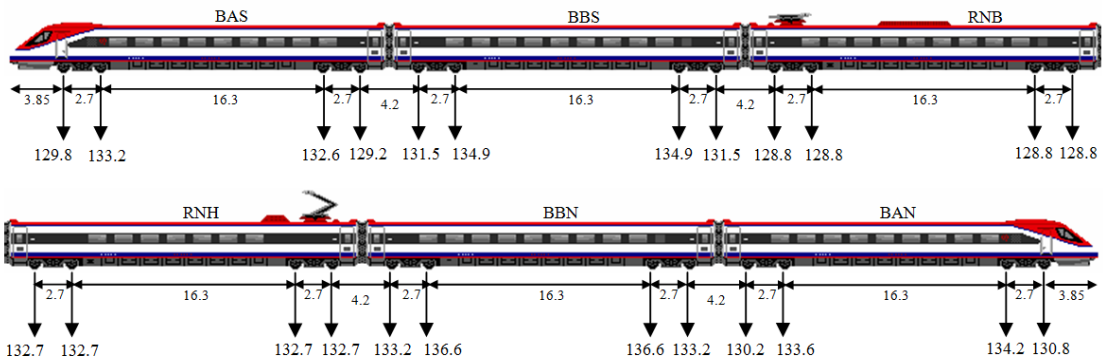

a)

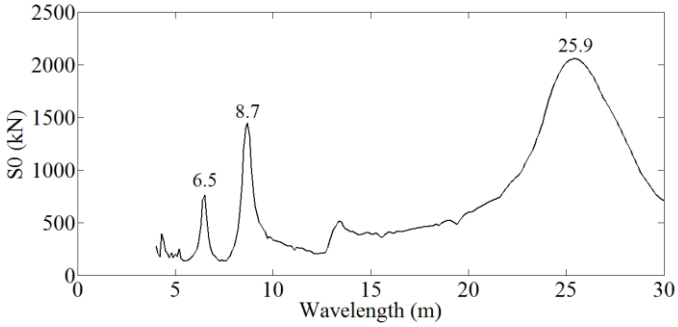

b)

Figure 5.26 – AP train: a) loading scheme; b) dynamic signature

Figure 5.27 a) presents the time records of vertical accelerations of the lower slab in the mid-span section, for two different AP train speeds. The experimental acceleration records were filtered by a Chebyshev (type II) low-pass digital filter of order 20, a cut-off frequency equal to 30 Hz and stopband attenuation equal to 45 dB. Figure 5.27 b) shows the auto-spectra in correspondence to the time records, as well as the dynamic signatures of the train for the corresponding speeds.

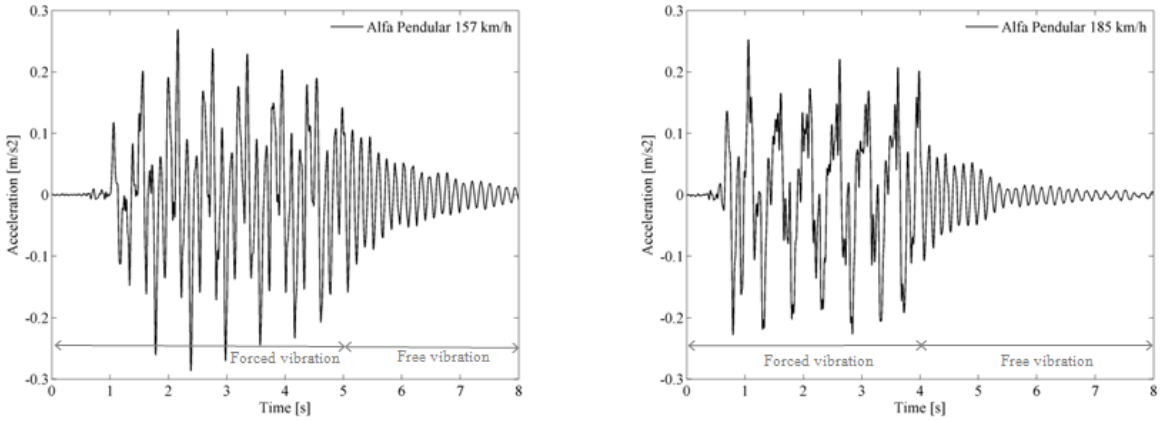

a)

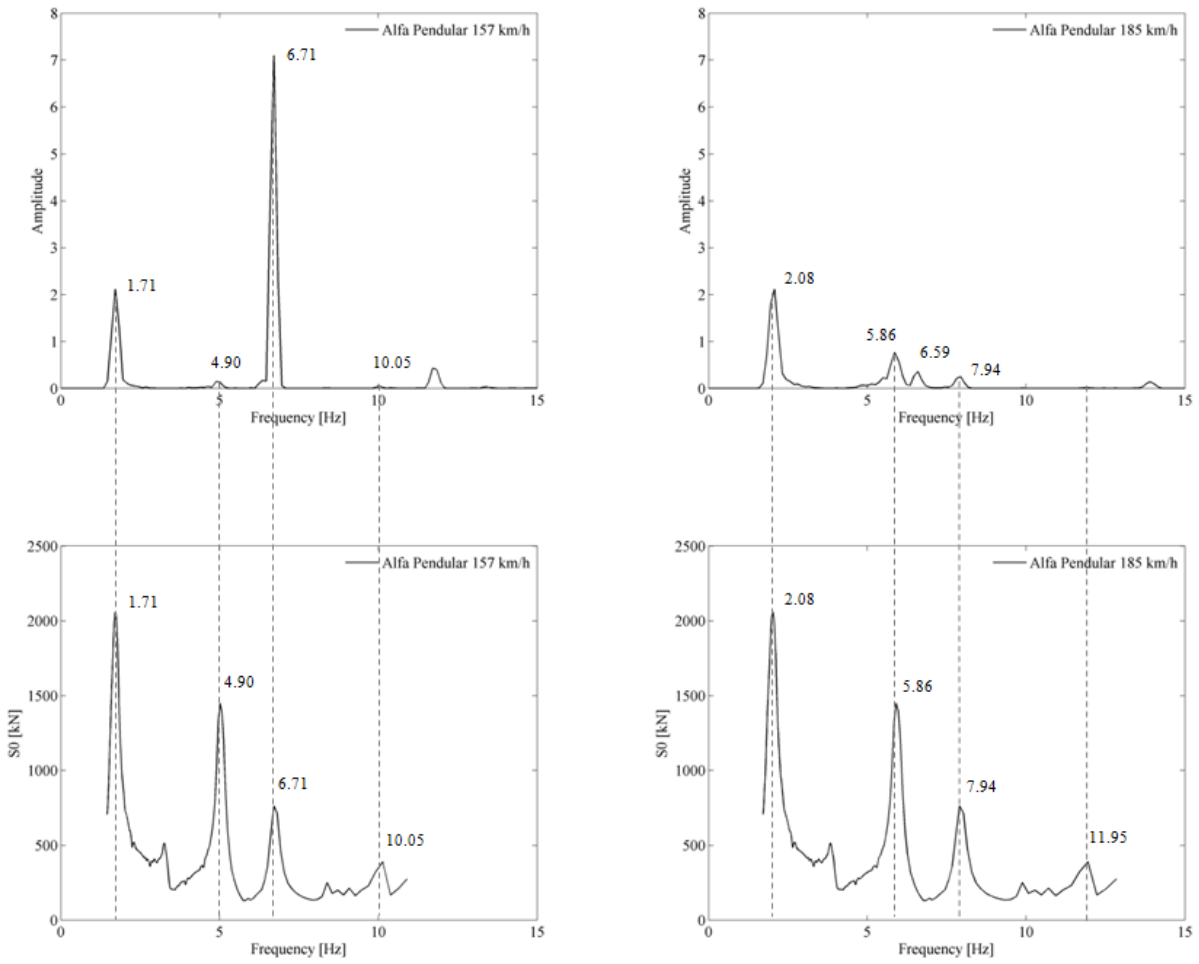

b)

Figure 5.27 – Acceleration in the mid-span section of the lower slab of the deck for the passage of AP train at 157 km/h and 185 km/h: a) time records; b) auto-spectra and dynamic signatures

By observing Figure 5.27 one can notice significant differences in the global dynamic response of the structure for both train speeds, particularly evident in terms of frequencies. The dynamic response is dominated by frequencies related to the train action, as noted by the perfect correspondence between the peaks in the graph of the train's dynamic signature and the peaks identified in the auto-spectra of acceleration records. For a speed of 157 km/h there is a frequency associated to the train action equal to 6.71 Hz that is very close to the frequency of vibration mode 1G, equal to 6.76 Hz, so the dynamic response is quite amplified and assumes a preponderant contribution towards the remaining frequencies. The same effect is not visible at the speed of 185 km/h due to the difference between natural frequencies of the structure and frequencies associated with the train's action.

This experimental test also allowed the identification of the damping coefficient for vibration mode 1G, the only one with significant contribution to the global dynamic response of the viaduct. It was obtained by the logarithmic decrement method (Paz 1980), using the time records corresponding to the free vibration responses, as indicated in Figure 5.27 a).

This method involves the application of a bandpass digital filter to the acceleration record, centred on the vibration mode's frequency, followed by the adjustment of an exponential function to the maximum values of the filtered record, using the following expression:

$$a = C \cdot e^{-\xi \omega t} \tag{5.10}$$

where C is a constant value, ξ is the damping coefficient and ω is the angular frequency related to the vibration mode. Figure 5.28 a) shows the filtered time records according to the free vibration response and Figure 5.28 b) shows the auto-spectra in correspondence with the time records, including the applied bandpass filters.

The records were filtered by a Chebyshev (type II) bandpass digital filter of order 9, a stopband attenuation equal to 45 dB and bandwidths of 5 Hz for the record at 157 km/h and 9 Hz for the record at 185 km/h. It can be observed, in Figure 5.28, that at the speed of 185 km/h it is not possible to isolate the contribution of the first vibration mode, precluding the determination of the damping coefficient at this speed.

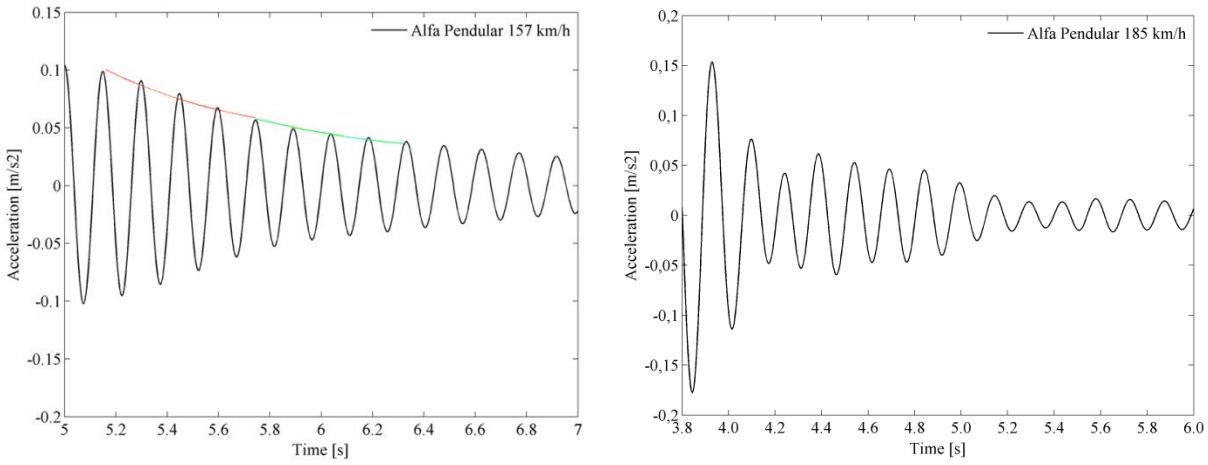

a)

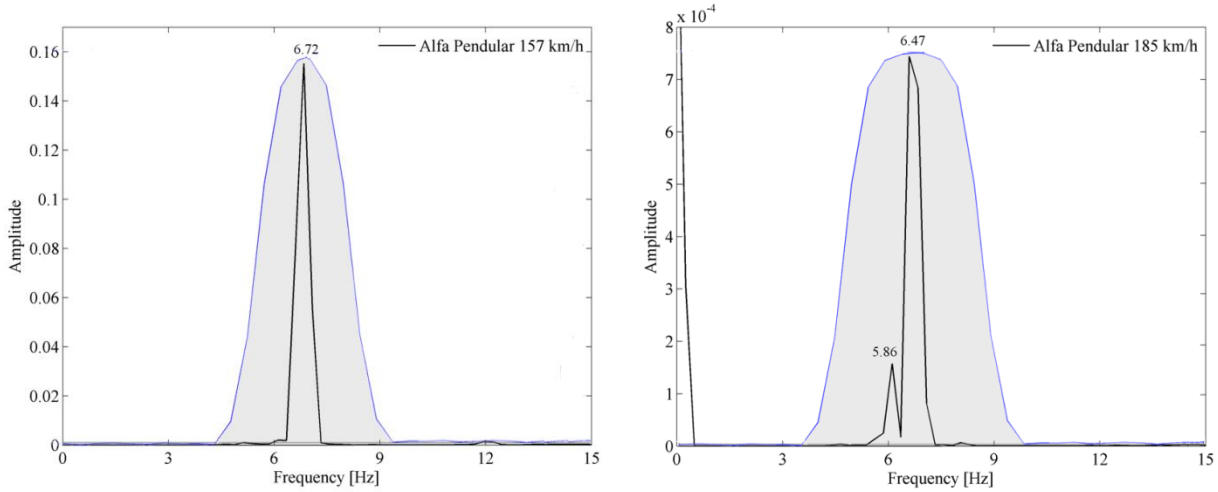

b)

Figure 5.28 – Free vibration of dynamic responses in terms of accelerations of the lower slab of the deck, for the passage of AP train: a) filtered time records; b) auto-spectra

Damping coefficient estimates were carried out for a speed of 157 km/h considering the decay of the initial part or the intermediate part of the free vibration response, using the red and green curves depicted in Figure 5.28 a), respectively. It was verified that the damping coefficient for the initial zone, equal to 2.31 %, is higher than the damping coefficient for the intermediate zone, equal to 1.62 %. This result confirms the damping coefficient's tendency to increase resulting from the increase of the vibration level, as reported by several authors. It is also noted that the damping coefficient in the intermediate zone, where the vibration amplitude assumes identical values to those registered under ambient actions, presents a value which is very similar to the mean value estimated by the ambient vibration test (equal to 1.63 %).

5.5.2 Experimental validation of the numerical model

The experimental validation of the numerical model allowed understanding of the global dynamic behaviour of the viaduct and was performed based on the results of the test under railway traffic. For this purpose, the train was considered as a set of moving loads, with wheel loads, on both rails, equal to half the value of the load per axle indicated in Figure 5.26.

The dynamic analyses were performed using the modal-superposition method, considering vibration modes with frequencies up to 30 Hz and an integration time increment equal to 0.002 s. The modal damping coefficients were considered equal to those obtained in the ambient vibration test. A value of 1 % of damping coefficient was considered for the

experimentally unidentified modes, following the guidelines of the standard EN1991-2 (CEN 2003).

In addition to the numerical model with the parameters calculated through the previously presented calibration procedure, here known as model M1, a new model, here known as model M2, was taken under consideration. The latter was obtained by reducing the longitudinal bearing stiffness of model M1, in order to achieve a mobility effect of the bearings closer to the one shown in the dynamic test under railway traffic. In order to minimise the differences between experimental and numerical responses, in terms of the longitudinal displacement of the mobile bearing, the longitudinal bearing stiffness (k_h) was manually reduced to 4.40 MN/m. This value is slightly higher than the one adopted in the initial numerical model, which was equal to 3.6 MN/m, but still within the initially estimated range [1.8; 4.9] MN/m (see Table 5.4).

Table 5.6 shows the vibration frequencies and MAC values of numerical models M1 and M2. As expected, due to the reduction in the structural stiffness, it is possible to see a decrease in the structure's vibration frequencies in model M2, especially for vibration modes 1G and 2G.

Table 5.6 – Vibration frequencies and MAC values obtained from numerical models M1 and M2

Mode	Frequency (Hz)		MAC (%)	
	M1	M2	M1	M2
1G	6.73	6.52	0.960	0.947
2G	6.78	6.49	0.980	0.979
3G	9.79	9.57	0.963	0.959
4G	10.67	10.64	0.679	0.864
5G	18.28	18.23	0.928	0.929
1L	26.68	26.52	0.851	0.837
2L	27.24	27.23	0.611	0.727
3L	53.01	53.01	0.888	0.888
4L	60.28	60.27	0.899	0.896
5L	67.55	67.54	0.552	0.551

Figure 5.29 shows the comparison between the experimental and numerical responses based on numerical models M1 and M2, in terms of displacements, accelerations and deformations in the mid-span section of the lower slab of the deck, during the passage of the AP train at a speed of 185 km/h. The responses regarding longitudinal displacements of the mobile bearing in span 2 are also presented, but in this case for a speed of 157 km/h. Due to a limitation in the maximum number of sensors used in the data acquisition during the experimental test under

railway traffic, the measurement of longitudinal displacements of the mobile bearing was only possible during a certain period of time, namely during the passage of the AP train at 157 km/h, reason why these results are only presented to this train speed. Responses were filtered by a Chebyshev (type II) low-pass digital filter of order 20, a cut-off frequency equal to 30 Hz and a stopband attenuation equal to 45 dB.

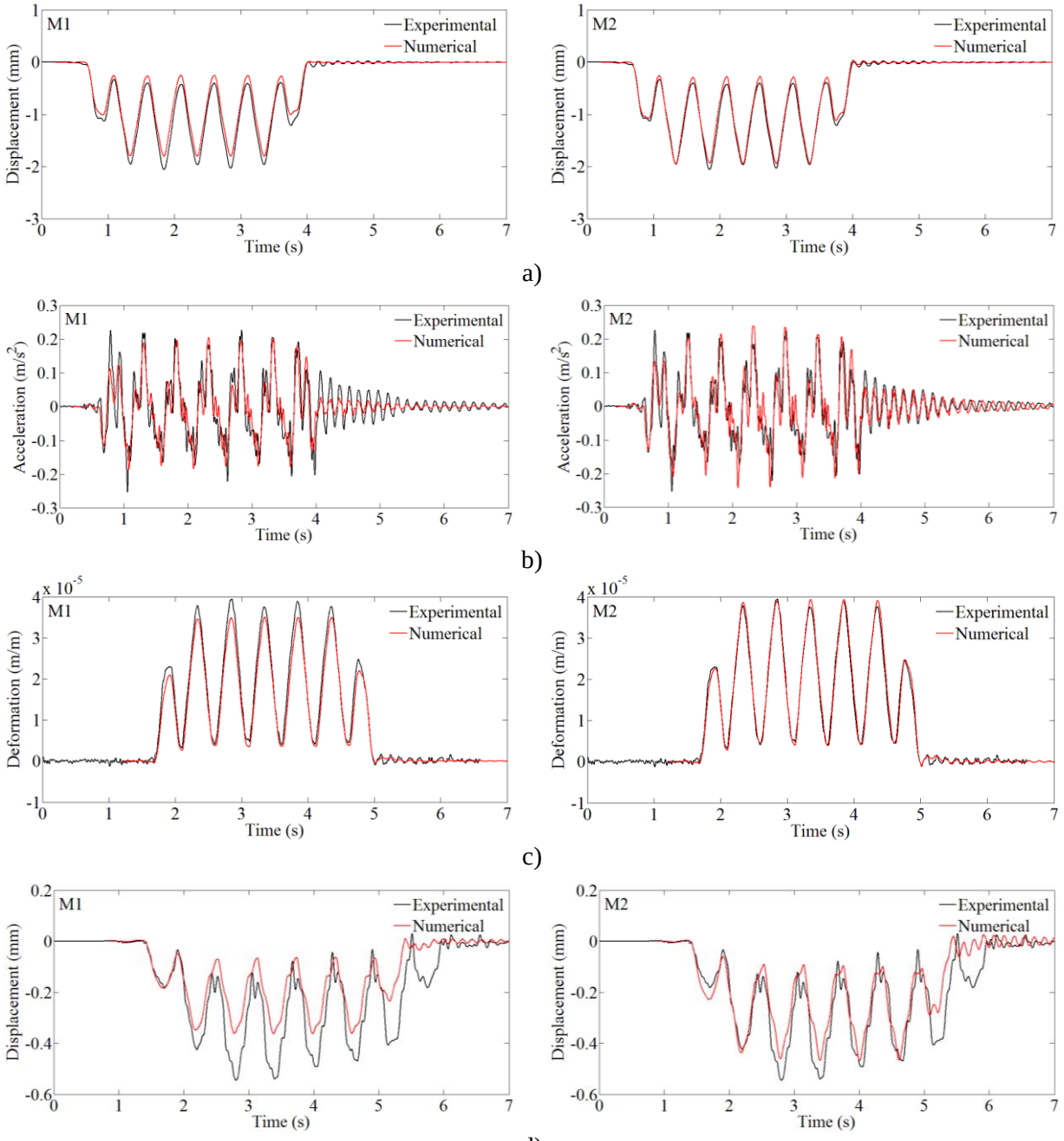

Figure 5.29 – Comparison between experimental and numerical responses according to models M1 and M2: a) vertical displacement; b) vertical acceleration; c) deformation of the mid-span section of the lower slab; d) longitudinal displacement of the mobile bearing of span 2

By observing the previous figure, it is easy to conclude that there is a better agreement between experimental and numerical results provided by the numerical model M2. This result seems to confirm the non-linear behaviour of the bearings that behave as fixed bearings under ambient actions and as mobile bearings under railway traffic.

Figure 5.30 a) shows the comparison between the acceleration records experimentally obtained and numerically calculated taking into account numerical model M2, in the mid-span section of the lower slab of span 2 during the passage of the AP train at 157 km/h and 185 km/h. Figure 5.30 b) shows the auto-spectra according to the time records. By observing this figure, a very good agreement between numerical and experimental results for both speeds of the AP train can be noted, thereby also validating the numerical model of the viaduct.

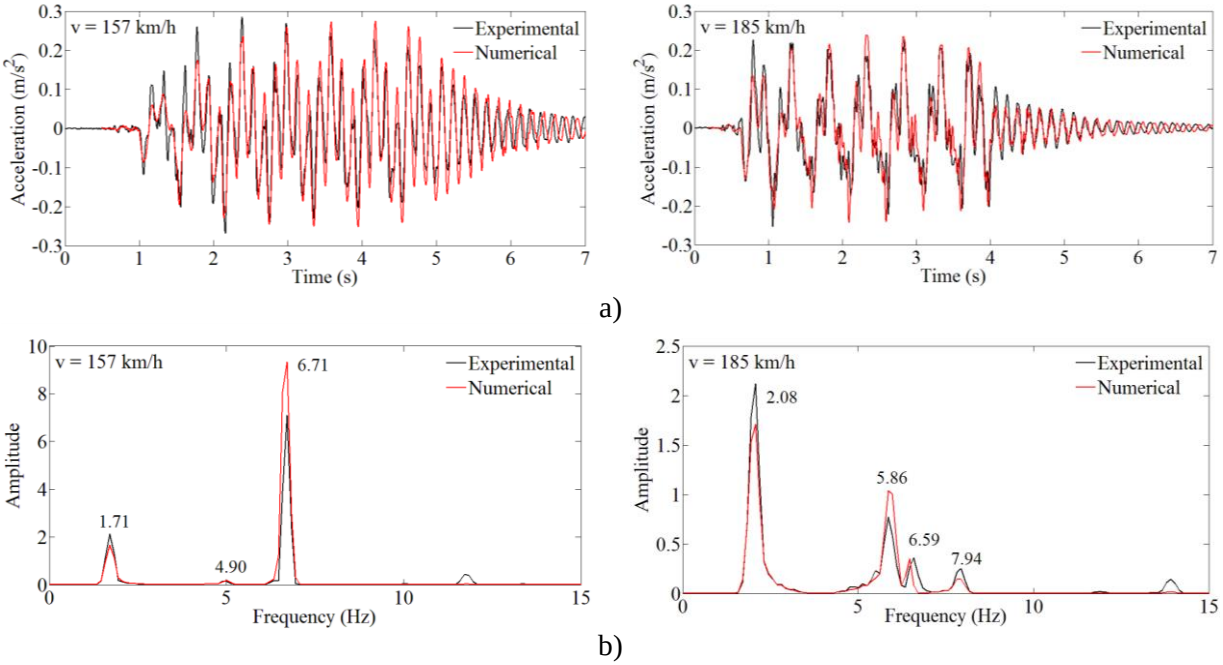

Figure 5.30 – Comparison between measured and calculated accelerations through numerical model M2 on the lower slab of the deck during the passage of the AP train at 157 km/h and 185 km/h: a) time records; b) auto-spectra

5.6 Local dynamic behaviour of the upper deck slab under railway traffic

In this section the local dynamic behaviour of the upper RC slab of the viaduct is analysed, taking into account the influence of the following parameters: train speed, track irregularities and modal damping coefficients. Since the fatigue damage in the transverse slab's reinforcing bars is strongly influenced by the time variation of bending moments, during the passage of the train, the influence of the aforementioned parameters is discussed in terms of transverse

bending moments of the upper deck slab. Before that, this influence is also evaluated in terms of vertical acceleration of the slab.

This section starts with the presentation of a new 3D numerical model that was developed and a static correction procedure that was implemented in the train-bridge interaction methodology, both performed in order to obtain more accurate results in the study of the local dynamic behaviour.

5.6.1 New FE numerical model

For evaluation of the local behaviour of the upper deck slab, a new FE model of the Alverca viaduct, here known as Model M3, was used. In order to perform a more detailed calculation of applied stresses and internal forces in the upper slab due to the passage of railway traffic, a finer discretisation was adopted in one of the structure's spans (the second span near the North abutment, the one where local vibration modes were experimentally determined, with a length of 21 m).

Since the focus of the analysis is, in particular, in the central region of the upper slab, the adjacent spans (spans 1 and 3) were not considered. An extension of the track, for 10 m each side of the span was adopted in the numerical model, in order to avoid an abrupt entrance of the train in the span under analysis. Figure 5.31 illustrates an overview of the numerical model with a detail of the track components.

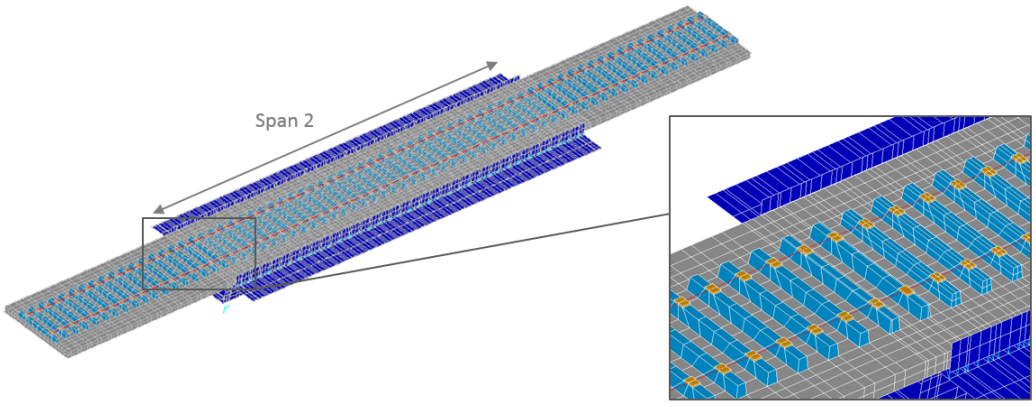

Figure 5.31 – 3D detailed FE model of span 2 of Alverca viaduct

A refined mesh was adopted for the upper RC slab, the ballast retaining walls, the ballast layer and the sleepers. Figure 5.32 a) shows a cross section of the span and Figure 5.32 b) and c) details of the discretisation adopted in the beam-slab connection area and in track components, respectively. This new numerical model of the viaduct, although representing only one span, includes 21911 nodes and 20336 elements.

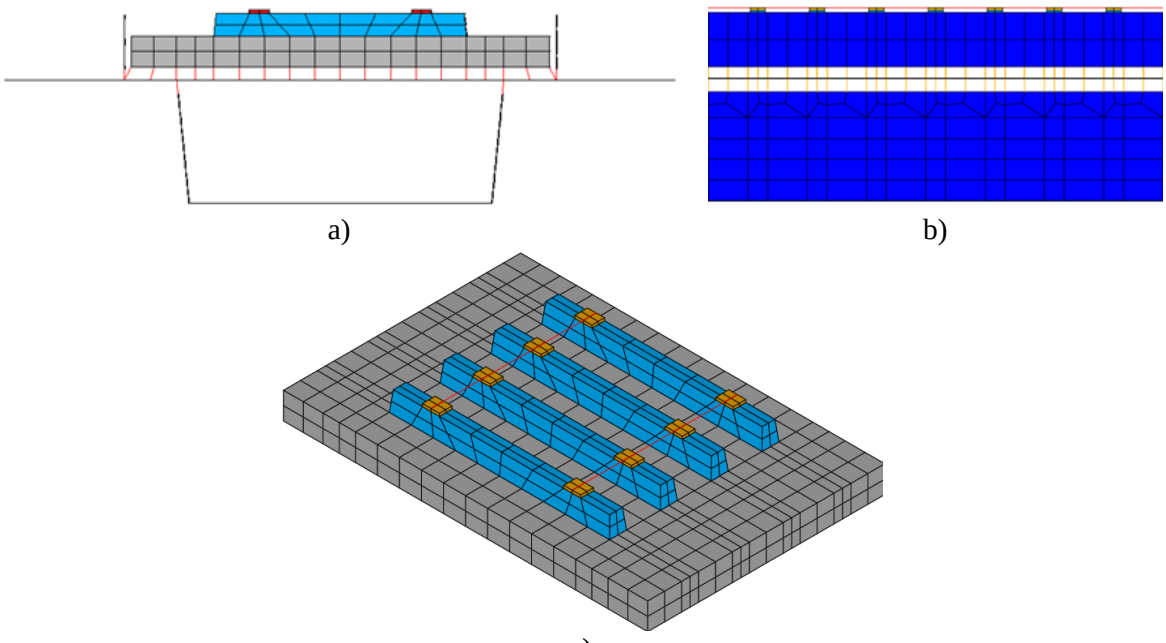

Figure 5.32 – Detailed views of new FE mesh adopted for span 2: a) cross section; b) lateral view of the beam-slab connection area; c) track components

Table 5.7 shows the vibration frequencies of numerical models M2 and M3. Vibration modes 2G and 3G do not appear in model M3 since they are related to vibration movements of the adjacent spans. As expected, due to the change in the structural stiffness, especially because of the absence of the connection to neighbouring spans in model M3, some differences are noted in the structure's vibration frequencies, particularly in the case of global vibration modes. Bearing in mind that model M3 is to be used for evaluation of the local behaviour of the upper slab, local vibration modes are more relevant than global ones. Table 5.7 confirms that the elimination of neighbouring spans has a minor influence on such local modes. Therefore, it can be concluded that model M3 is acceptable for the intended purpose.

Table 5.7 – Vibration frequencies obtained from numerical models M2 and M3

Vibration mode	Frequency (Hz)	
	M2	M3
1G	6.52	6.47
2G	6.49	-
3G	9.57	-
4G	10.64	8.9
5G	18.23	18.7
1L	26.52	26.32
2L	27.23	27.16
3L	53.01	52.19
4L	60.27	58.75
5L	67.54	65.57

The dynamic responses provided by models M2 and M3, during the passage of a railway train were also compared. For this purpose, Figure 5.33 shows the transverse bending moment in the upper deck slab, in the mid-span section, for both numerical models, for the passage of the AP train at a speed of 100 km/h. These dynamic analyses were performed in the same conditions indicated in section 5.5.2 but considering frequencies up to 60 Hz.

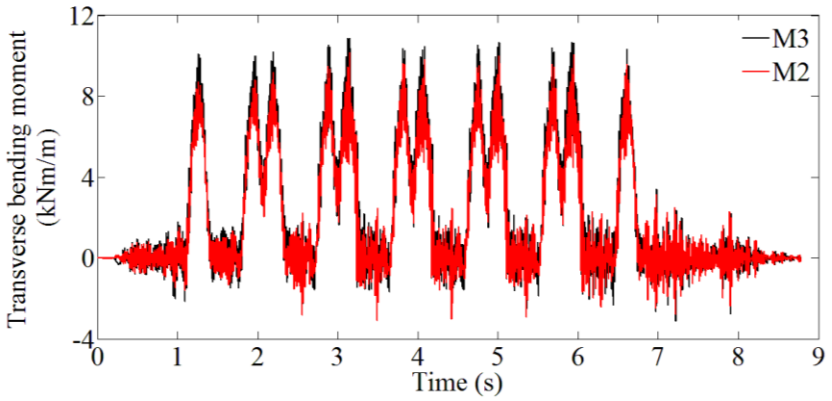

Figure 5.33 – Comparison between FE models M2 and M3 in terms of transverse bending moment in the RC upper deck slab for the passage of AP train at a speed of 100 km/h

By observing the previous figure one can notice only slight differences between these two numerical responses, with the maximum difference, equal to 1.37 kNm/m, occurring for the passage of the first group of axles of the AP train. Despite the small magnitude of this difference, model M3 is considered to be more adequate for the evaluation of local effects in the slab, because of its finer discretisation. The elimination of neighbouring spans in the model brings important advantages in terms of computational resources needed and calculation times.

5.6.2 Static correction procedure

As the structural response of reinforced concrete slabs in railway viaducts may be governed by local effects, detailed analysis procedures are required for a proper quantification of the stress records due to the passage of trains. Regarding the train loading, although in the previous sections of this Chapter a simple approach based on moving loads was used, in the following analyses a numerical methodology that considers the interaction between the bridge and the train is considered.

As shown before, in Chapter 2, it consists of an iterative procedure that in each time increment two subsystems are solved independently: the bridge subsystem is solved by the modal-superposition method and the train subsystem is solved using the Newmark's direct integration method. An improved formulation of the modal-superposition method is applied in the present thesis, in the analysis of the bridge subsystem. It combines the modal-superposition method with a static correction procedure, using the influence surface to obtain the static contribution of vibration modes of higher frequencies, which are not explicitly considered in the basic modal-superposition method. This methodology guarantees that the static component of the structural response is properly captured, and is correctly added to the dynamic component of the response associated to all the vibration modes considered in the analysis. This procedure is described in detail in section 2.2.5.

In order to validate the implemented static correction procedure and verify its relevance, either in analyses where the railway traffic is represented by moving loads or considering the train-bridge interaction, distinct analysis methodologies were considered. Table 5.8 presents the differences between each analysis considered in this section. It should be pointed out that, in the present section, track irregularities are not considered in TBI analyses.

The Newmark's direct integration method was considered as the reference methodology for calculation of the correct static structure response in analyses where the inertial forces (i.e., the dynamic enhancement of internal forces) are not considered. Regarding the dynamic analyses including dynamic effects, two hypotheses were considered for definition of modal damping ratios in the bridge subsystem: (*i*) Rayleigh damping, for analyses with Newmark's direct integration method and for the remaining analyses which are to be compared with the former; (*ii*) a constant modal damping ratio of 1% (consistent with the Eurocode recommendations)

when different analyses based on the modal-superposition method are to be compared to each other.

In all the analyses, the railway traffic consists of an AP train travelling at a speed of 100 km/h. All the analyses of the bridge subsystem based on the modal-superposition method are carried out considering all the structure's vibration modes with a frequency lower than 100 Hz (77 vibration modes).

Table 5.8 – Numerical analysis methodologies considered in the validation of the implemented static correction procedure

Analysis	Analysis of the bridge subsystem*	Train-Bridge interaction	Static correction	Damping coefficients	Inertial forces
A	M.S.	-	-	1%	✓
B	M.S.	-	✓	1%	✓
C	M.S.	✓	-	1%	✓
D	M.S.	✓	✓	1%	✓
E	D.I.	-	-	**	✓
F	D.I.	-	-	-	-
G	M.S.	-	-	**	✓
H	M.S.	-	✓	**	✓
I	M.S.	-	-	-	-
J	M.S.	-	✓	-	-

* M.S. stands for Modal-Superposition and D.I. stands for Newmark's Direct Integration methods

** Rayleigh damping matrix, setting the damping equal to 1% for vibration modes 1G and 4L

The results here shown correspond to the bending moment in the upper deck slab, in the transverse direction, in a position which corresponds to the mid-span, both in the longitudinal and in the transverse directions.

Figure 5.34 shows the comparison between analyses *F*, *I* and *J*, in order to verify if the static response is well characterized in analyses based on the basic modal-superposition method. All of these analyses were performed without considering dynamic effects and the static correction procedure was considered in analysis *J*. It can be seen that the basic modal-superposition method (analysis *I*) is not able to correctly reproduce the static response. A perfect agreement with the reference results provided by the Newmark's direct integration method (analysis *F*) was achieved when the static correction procedure was considered (analysis *J*), as can be seen by the overlap of both responses.

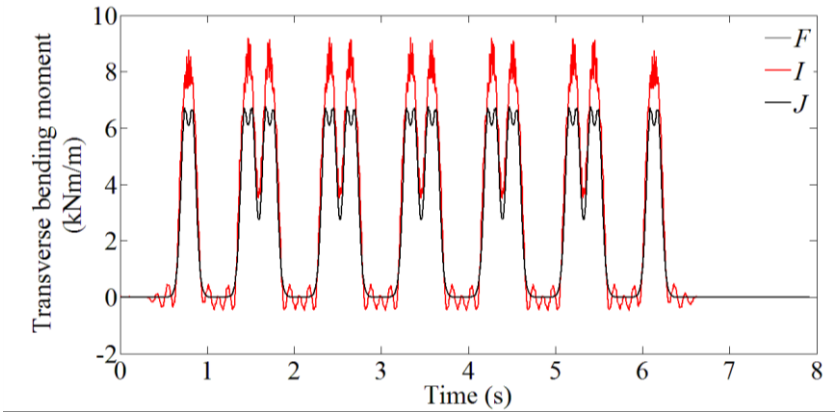

Figure 5.34 – Comparison of transverse bending moments from analyses *F*, *I* and *J*

Considering similar analyses to those shown in the previous figure but taking into account, now, the dynamic effects, Figure 5.35 a) illustrates a comparison of the results provided by analyses *E*, *G* and *H*. By comparing the results of analyses *E* and *G*, one can see that the basic modal-superposition method is not able to properly characterize the RC slab response, obtained through the direct integration method. If the static correction is considered (analysis *H*), the results of the improved modal-superposition method tend to approximate to those obtained through the reference analysis, as shown in the detailed view presented in Figure 5.35 b).

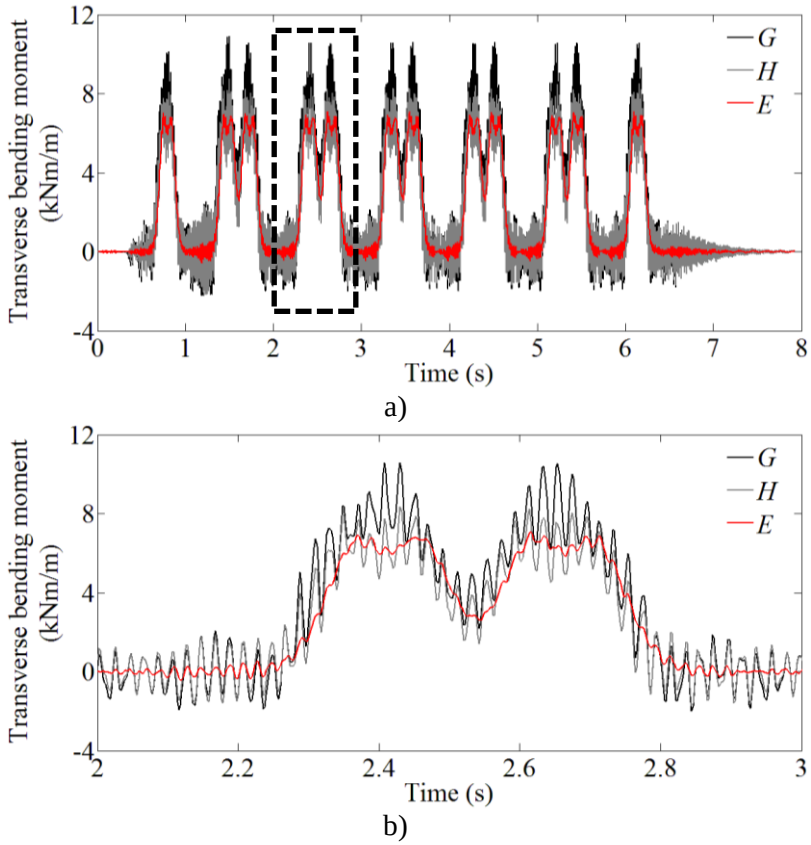

Figure 5.35 – Comparison of transverse bending moments from analyses *E*, *G* and *H*: a) total time interval; b) detailed results in the time interval 2-3 s

Figure 5.36 compares the results of analyses *A* and *B*, using the simple approach based on moving loads, and Figure 5.37 compares the results provided by analyses *C* and *D*, performed taking into account the interaction between train and bridge. All these analyses consider only the modal-superposition method and the static correction procedure was implemented in analyses *B* and *D*.

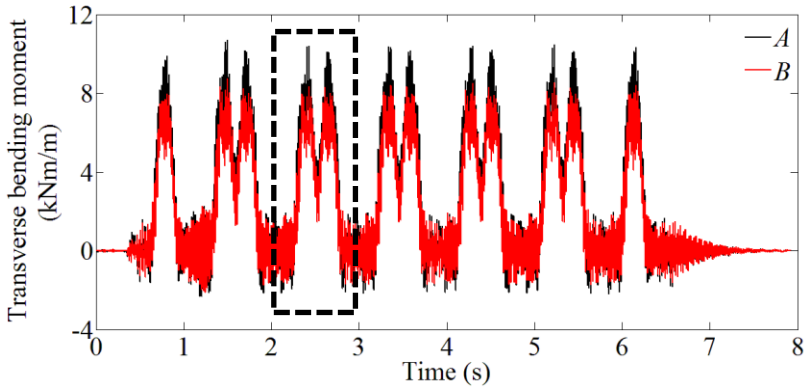

a)

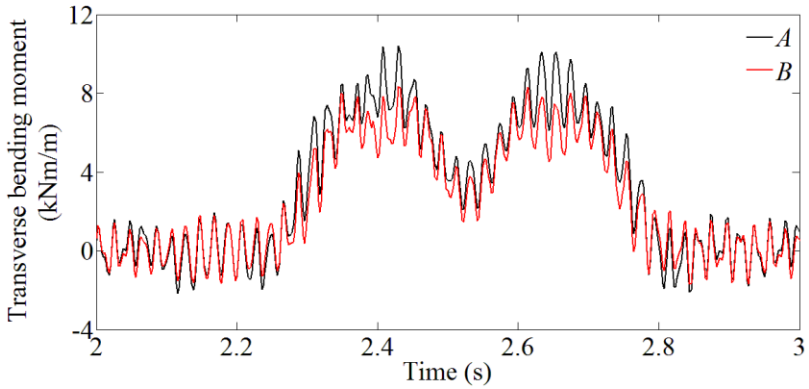

b)

Figure 5.36 – Comparison of transverse bending moments from analyses *A* and *B*: a) total time interval; b) detailed results in the time interval 2-3 s

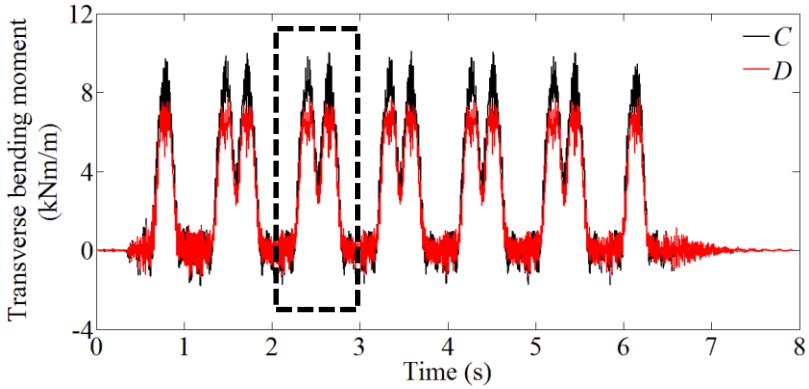

a)

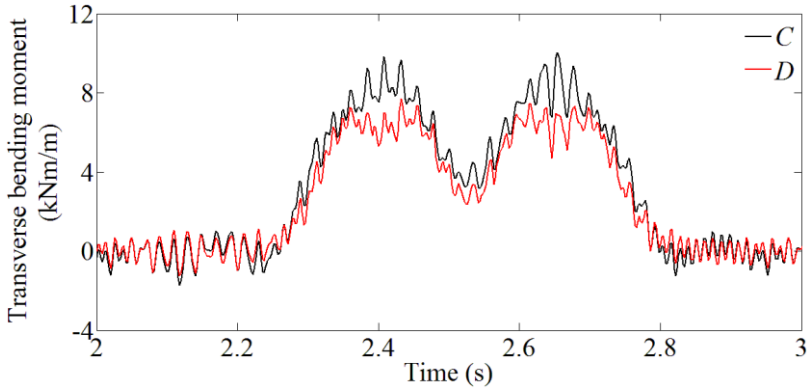

b)

Figure 5.37 – Comparison of transverse bending moments from analyses *C* and *D*: a) total time interval; b) detailed results in the time interval 2-3 s

By observing the results presented in these figures, one can realise that the maximum bending forces associated to the passage of each bogie would be overestimated if the static correction procedure was not considered. This fact is particularly important in the case of the more refined analyses considering the train-bridge interaction (see Figure 5.37).

The results presented in this section allowed validation of the implemented procedure for static correction, and revealed that this procedure should be considered in the calculation of local effects in railway deck slabs, when the modal-superposition method is used in the analysis of the bridge subsystem. In the fatigue analysis of the RC slab, the static correction should be considered, since fatigue damage is very sensitive to the calculated stress ranges due to passage of railway traffic.

5.6.3 Train-bridge interaction dynamic analysis

In order to evaluate the local dynamic behaviour of the RC upper deck slab, TBI numerical analyses were performed. In the present section, the influence of track irregularities and modal damping coefficients, in terms of vertical accelerations and transverse bending moments of the upper deck slab, during the passage of the AP train is discussed. The numerical models of the viaduct and the train, presented before in sections 5.6.1 and 2.2.2.3, respectively, were used in these analyses.

5.6.3.1 Influence of track irregularities

5.6.3.1.1 Irregularities profiles

The irregularities profiles used in the present section were measured by the Portuguese railway network management company. A total track length of 51 m was considered, including the 21 m long bridge span and extra 15 m for each side of that span. Figure 5.38 shows four irregularities profiles of the left rail obtained yearly from 2011 to 2014 (the irregularities profiles of the right rail are similar), considering the contribution of wavelengths (λ) in the ranges 1-25 m (D1) and 25-70 m (D2) [Figure 5.38 a)], and two rail corrugation profiles from 2012 and 2014, considering wavelengths below 1 m, [Figure 5.38 b) and c), respectively].

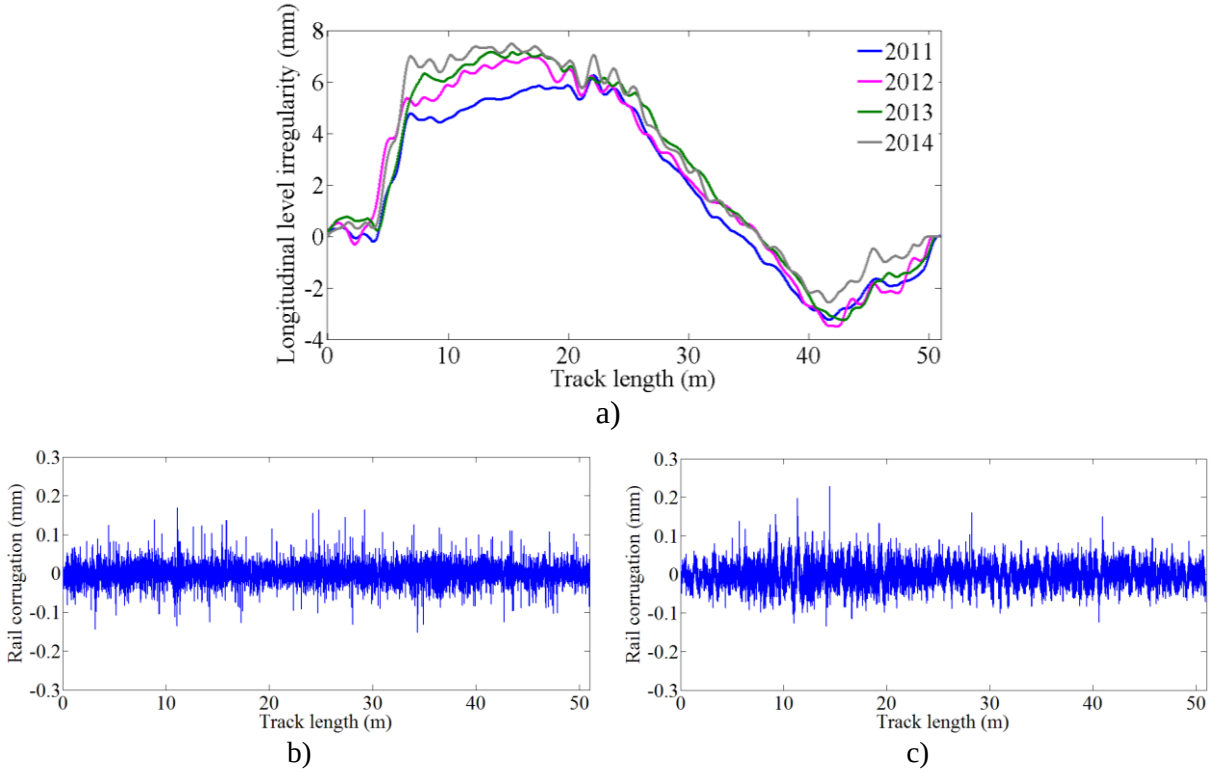

Figure 5.38 – Irregularities profiles of left rail: a) four profiles with wavelengths in range 1-70 m; rail corrugation from b) 2012 and c) 2014

The final irregularities profiles result from the sum of the contributions of wavelengths D1, D2 and rail corrugation. In order to ensure a correct representation of the main vibration modes of the structure and the excitation frequencies due to track irregularities, the irregularities profiles were filtered at a minimum wavelength of 0.55 m, taking into account the time increment considered (equal to 0.001 s) and the train frequent speed equal to 200 km/h.

The influence of different rail corrugation data in the final response of the structure was firstly evaluated by means of dynamic analyses considering the passage of the AP train at a speed of 185 km/h. For this purpose, the irregularities profile of wavelengths 1-70 m of 2011 was used, together with rail corrugation profiles, to obtain the final irregularities profile. Figure 5.39 shows the vertical acceleration time records of the upper slab in the mid-span section of the deck, considering the contribution of frequencies up to 20 Hz [Figure 5.39 a)] and up to 60 Hz [Figure 5.39 b) and detailed view in Figure 5.39 c)].

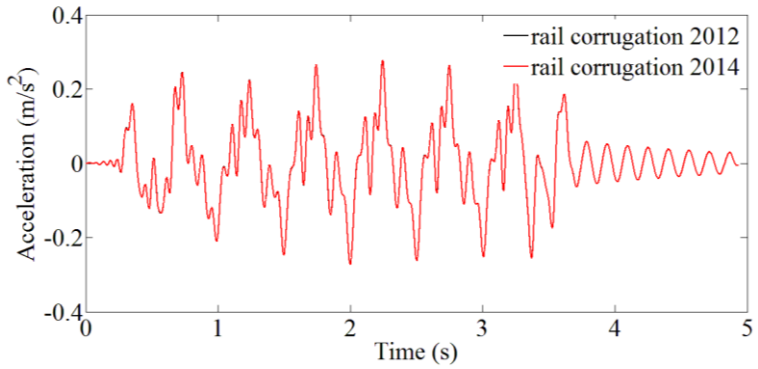

a)

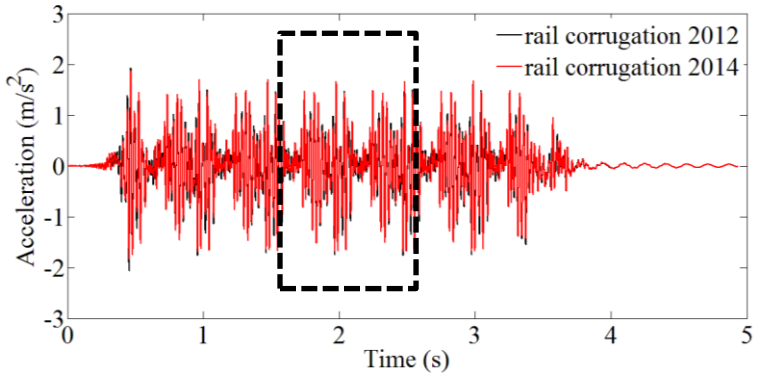

b)

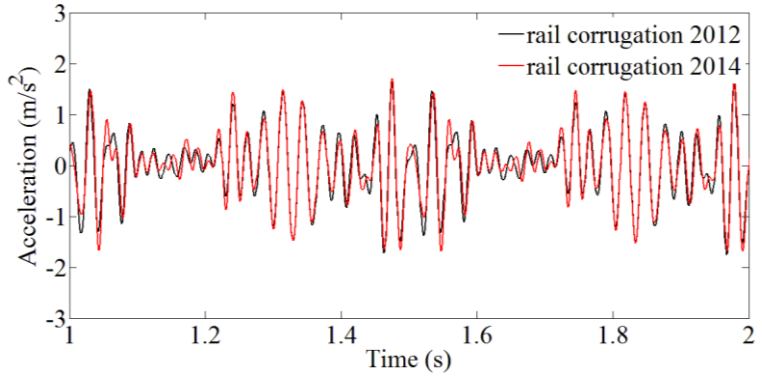

c)

Figure 5.39 – Vertical acceleration time records of the upper deck slab for different rail corrugation profiles, considering frequencies up to: a) 20 Hz; b) and c) 60 Hz

As can be seen by the results shown in the previous figure, especially in the detail presented in Figure 5.39 c), for the range of frequencies considered in the analysis, there are very small differences in the final dynamic response of the structure. This can be explained by the fact that for this train speed, irregularities with wavelengths below 1 m only affect excitation frequencies above approximately 52 Hz. For this reason, only one rail corrugation profile was taken into account in the following analyses, namely, the one measured in 2012.

Figure 5.40 presents the final four rail level profiles, distinguishing the contribution of wavelengths between 3 m and 70 m [Figure 5.40 a)] and lower than 3 m [Figure 5.40 b)]. Figure 5.41 shows the auto-spectra according to the space records presented only in Figure 5.40 b). The auto-spectra related to Figure 5.40 a) is not depicted since there are not enough cycles of higher wavelengths to be representative. By observing both figures, one can notice that the major differences are related to wavelengths lower than 3 m, especially between 1.25 and 3 m, with significant differences between profiles, both in terms of maximum amplitude and preponderant wavelengths. Concerning higher wavelengths, the differences are essentially in terms of maximum amplitude.

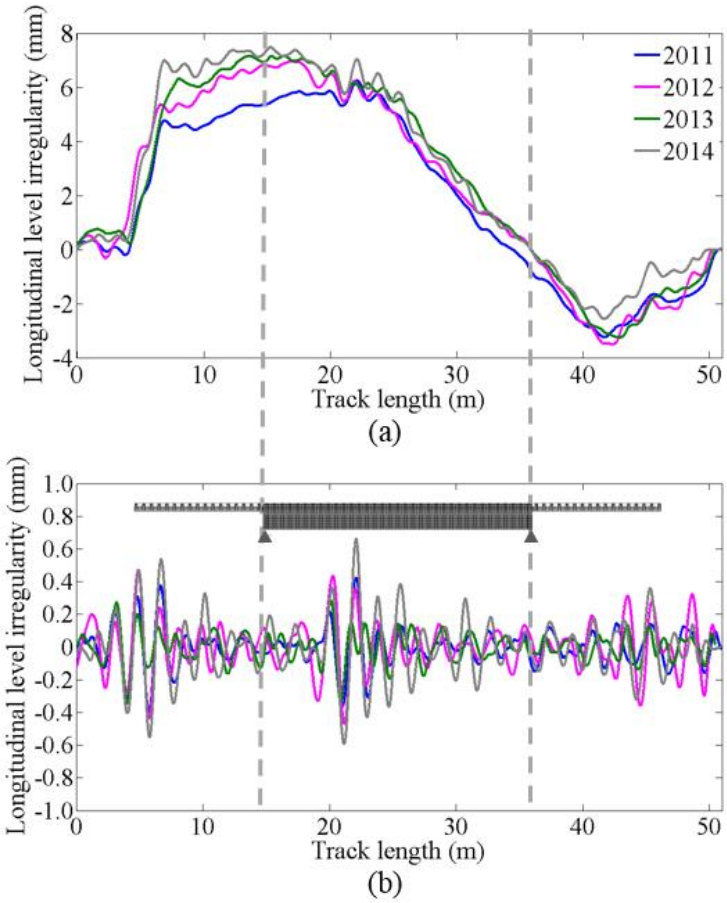

Figure 5.40 – Left rail level profiles with wavelengths: a) between 3 m and 70 m; b) lower than 3 m

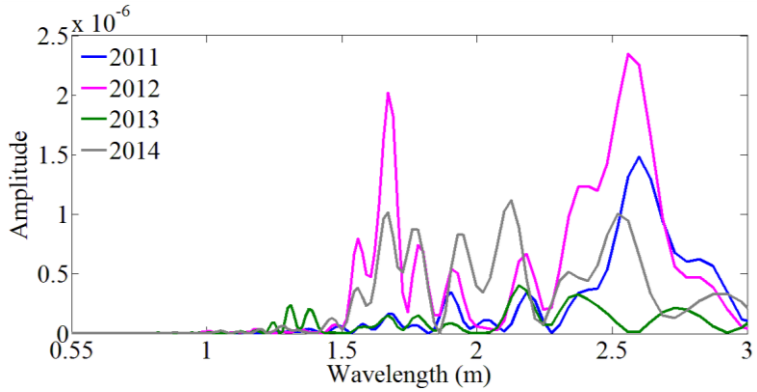

Figure 5.41 – Left rail irregularities auto-spectra considering wavelengths lower than 3 m

Figure 5.42 illustrates the Power Spectral Density (PSD) functions of the rail level profiles. In order to evaluate the severity of the irregularities, two of the most commonly used reference PSD functions in the railway infrastructure research field (Cantero et al. 2016, Fryba 1996, Rocha et al. 2014), provided by SNCF and FRA, are also depicted in Figure 5.42. It is possible to observe that the irregularities profiles are well located within the limits defined by classes 1 and 6 of FRA's PSD function, with exception of the wavelengths in the range 1.25-2.7 m.

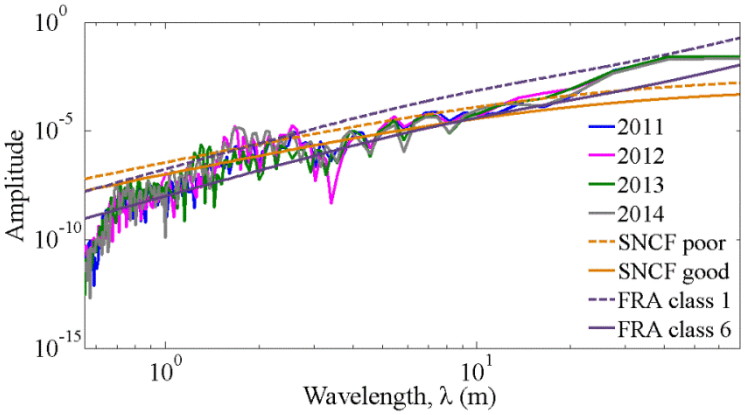

Figure 5.42 – PSD functions for left rail level profiles

5.6.3.1.2 Vertical acceleration

As presented before in section 5.5.1, during the dynamic test under railway traffic, vertical accelerations of the upper deck slab were also measured. In Figure 5.43 a) and Figure 5.44 a), a comparison between acceleration records experimentally obtained and numerically calculated through numerical model M3, in the mid-span section of the upper slab, for the passage of AP

train at a speed of 185 km/h, is presented. The acceleration records were filtered by a Chebyshev (type II) low-pass digital filter of order 11 and 20, for cut-off frequencies of 20 Hz (Figure 5.43) and 60 Hz (Figure 5.44), respectively, and stopband attenuation equal to 45 dB. Figure 5.43 b) and Figure 5.44 b) show the corresponding auto-spectra.

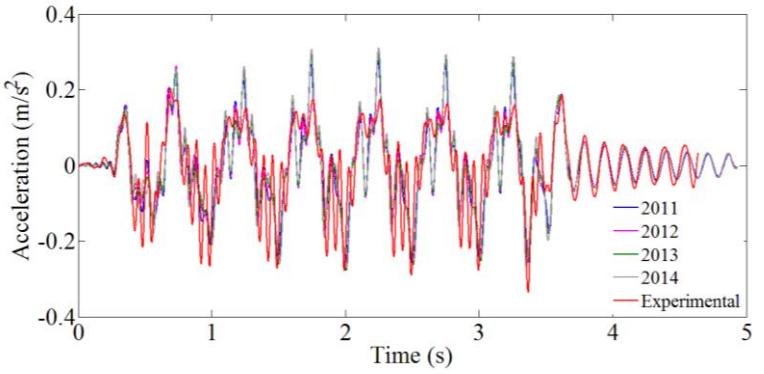

a)

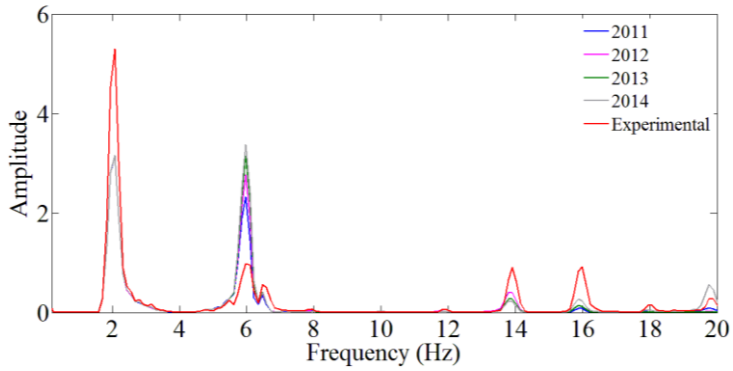

b)

Figure 5.43 – Comparison between measured and calculated accelerations on the upper slab for the passage of AP train at 185 km/h, considering frequencies up to 20 Hz: a) time records; b) auto-spectra

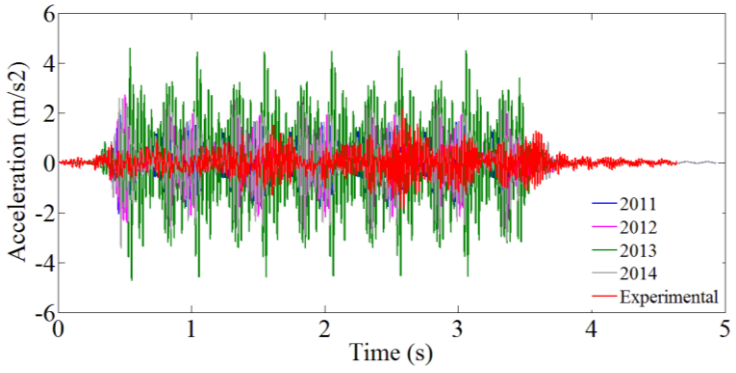

a)

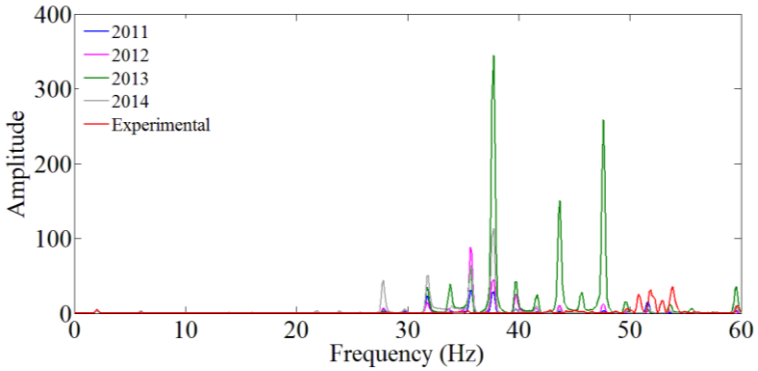

b)

Figure 5.44 – Comparison between measured and calculated accelerations on the upper slab for the passage of AP train at 185 km/h, considering frequencies up to 60 Hz: a) time records; b) auto-spectra

Concerning frequencies up to 20 Hz, a reasonable agreement can be noticed. However, by observing Figure 5.44 it is possible to see larger differences between both responses when higher frequencies are considered in the analyses. The excitation frequency, f, generated by irregularities of wavelength λ, when a bridge is crossed by a train with a speed v, is given by $f = v/\lambda$. Therefore, for the train speed of 185 km/h, the aforementioned wavelengths in the range 1-3 m correspond to excitation frequencies between approximately 17 Hz and 52 Hz, precisely those in which there is greater contribution of the slab's response.

For this train speed, the irregularities profile of 2013 is the one that leads to higher vertical acceleration values, as shown in Figure 5.44. In order to understand this considerable difference to the other irregularities profiles, taking into account the train speed and the preponderant range of frequencies, it is important to analyse the correspondent irregularities auto-spectra (Figure 5.45). Considering the contribution of wavelengths between 1.10 m and 1.45 m, it is possible to note a predominant contribution of the referred irregularities profile in this range of wavelengths, which for the train speed of 185 km/h led to excitation frequencies between approximately 36 Hz and 48 Hz. This aspect allows justification of either the higher amplitude seen at certain frequencies or the higher excitation frequencies, as observed in the auto-spectra, which does not happen when other irregularities profiles are considered.

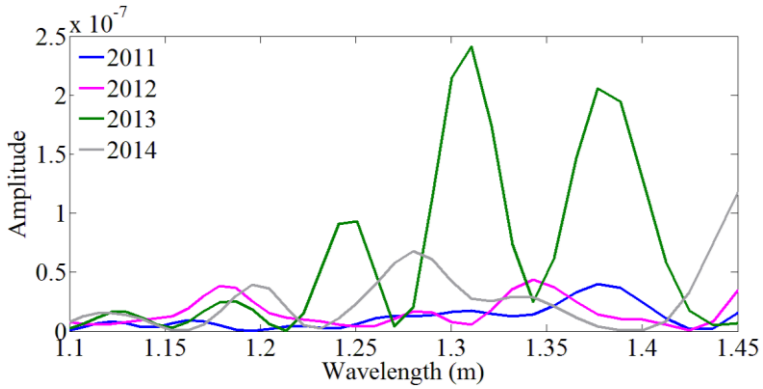

Figure 5.45 – Left rail irregularities auto-spectra of 2013 (1.10 m < λ < 1.45 m)

It should also be pointed out that the best agreement, when higher frequencies are considered in the analyses, occurs when the irregularities profile from 2011 is used, precisely the year in which the dynamic test under railway traffic was performed.

5.6.3.1.3 Transverse bending moments

Transverse bending moments were obtained for two different lines in the upper slab, namely the lines of maximum sagging and hogging transverse bending moments, indicated in Figure 5.46. The line of maximum sagging bending moments is the one which coincides with the cross-section's axis of symmetry. These lines are extended along a distance of 10.5 m in the centre of the deck, corresponding to a half of the girder length, not considering elements near the span's extremities. In a static analysis these values would be almost constant along each line. That does not occur in a dynamic calculation due to the influence of local vibration modes, which is the reason why the most unfavourable position is evaluated along those lines.

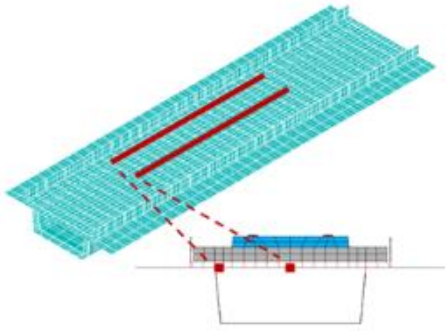

Figure 5.46 – Lines along which bending moments are calculated

Since the train speed is also a relevant parameter, an interval between 160 km/h and 240 km/h is considered in the following analyses, which corresponds to a variation of ± 20 % with respect to a frequent train speed of 200 km/h. All analyses were carried out using the TBI methodology, considering an integration time increment equal to 0.001 s. In the analysis of the bridge subsystem through the modal-superposition method, all the vibration modes with frequencies up to 60 Hz were considered. The static correction procedure was applied in order to take into account the static component of the contribution of higher order modes.

Figure 5.47 presents the envelope of transverse bending moments for different train speeds, *v*, and different track irregularities profiles. Each value shown in this figure corresponds to the maximum value obtained from the time records of each FE. Abscissa axis consists of the order number of each element, with increasing numbering from left to right according to Figure 5.46. It is possible to observe considerable differences in the results obtained taking into account different train speeds, especially for those higher than 200 km/h.

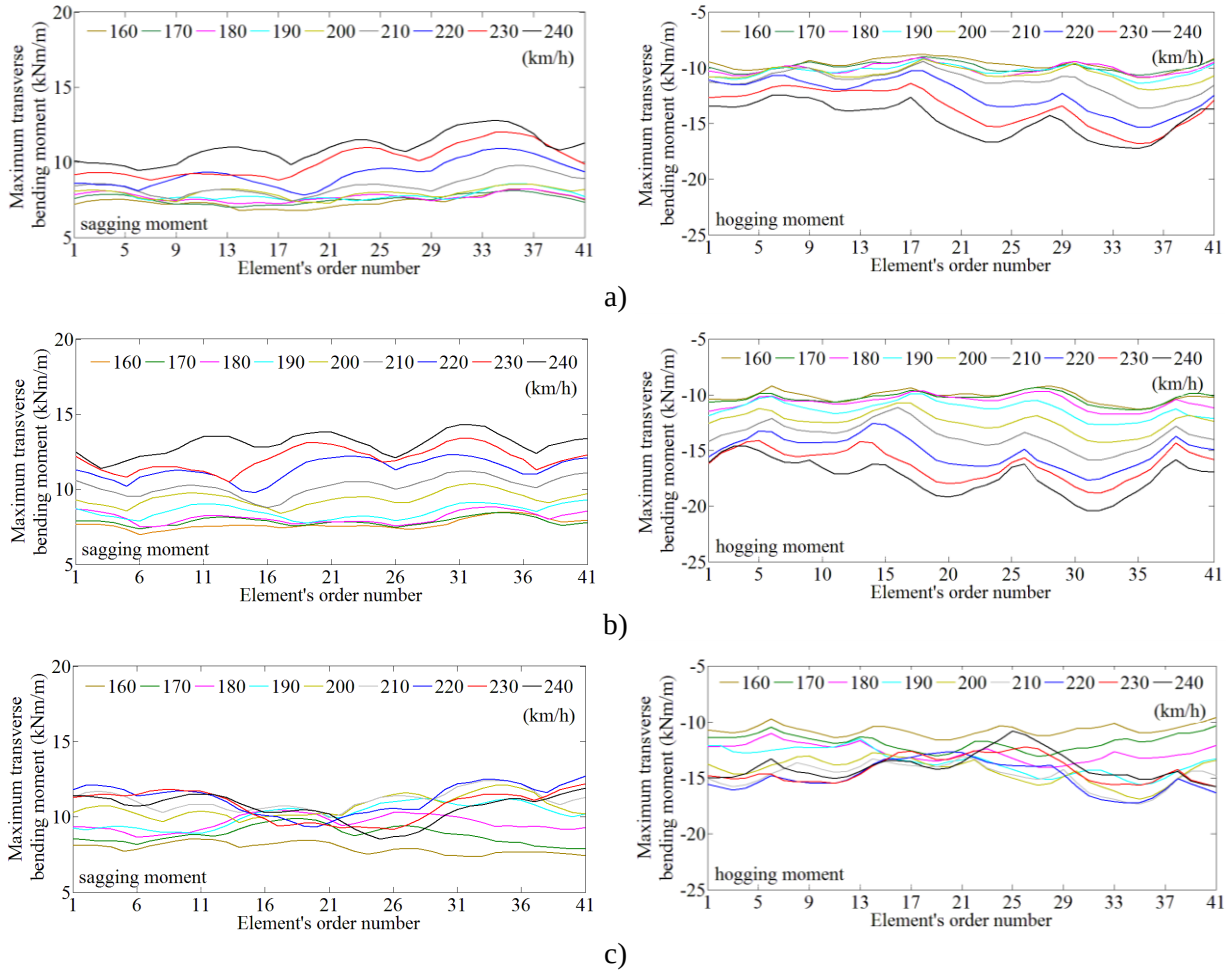

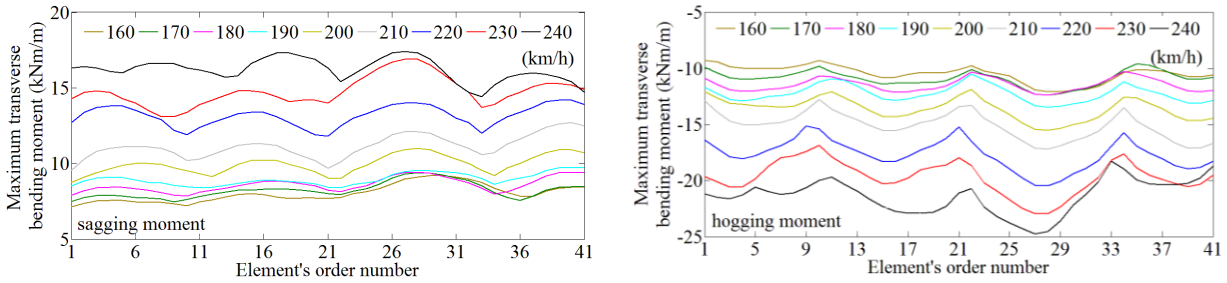

d)

Figure 5.47 – Envelope of transverse sagging (on the left side) and hogging (on the right side) bending moments as function of train speeds, considering different irregularities profiles: a) 2011; b) 2012; c) 2013; d) 2014

Figure 5.48 shows a different envelope, considering not only the most unfavourable instant of time, but also the most unfavourable position along the sagging and hogging bending moment lines. These results are depicted as a function of train speed. For this comparison, the results of TBI analyses without irregularities are also presented.

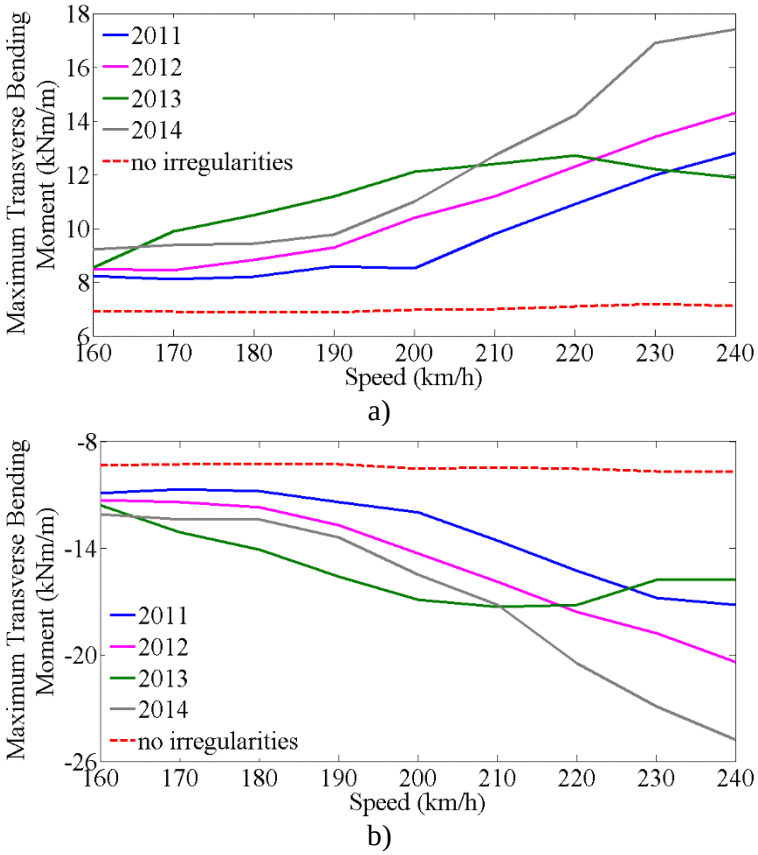

a)

b)

Figure 5.48 – Influence of track irregularities on the maximum transverse bending moment in the upper deck slab: a) sagging moment; b) hogging moment

It can be confirmed that the transverse bending moments are strongly affected by the irregularities profile, especially for speeds above 200 km/h. One can realise that train speed is also an important influencing parameter. Taking as an example the irregularities profile from 2014, it is possible to observe increases of 89 % and 105 % in the maximum sagging and hogging transverse bending moments, respectively, when the train speed increases from 160 km/h to 240 km/h.

Figure 5.49 exemplifies the bending moment time histories [Figure 5.49 a)] and correspondent auto-spectra [Figure 5.49 b)], for the location of maximum sagging moment at the mid-span cross-section, for a speed of 240 km/h. Irregularities profiles from 2013 and 2014 are used in this comparison.

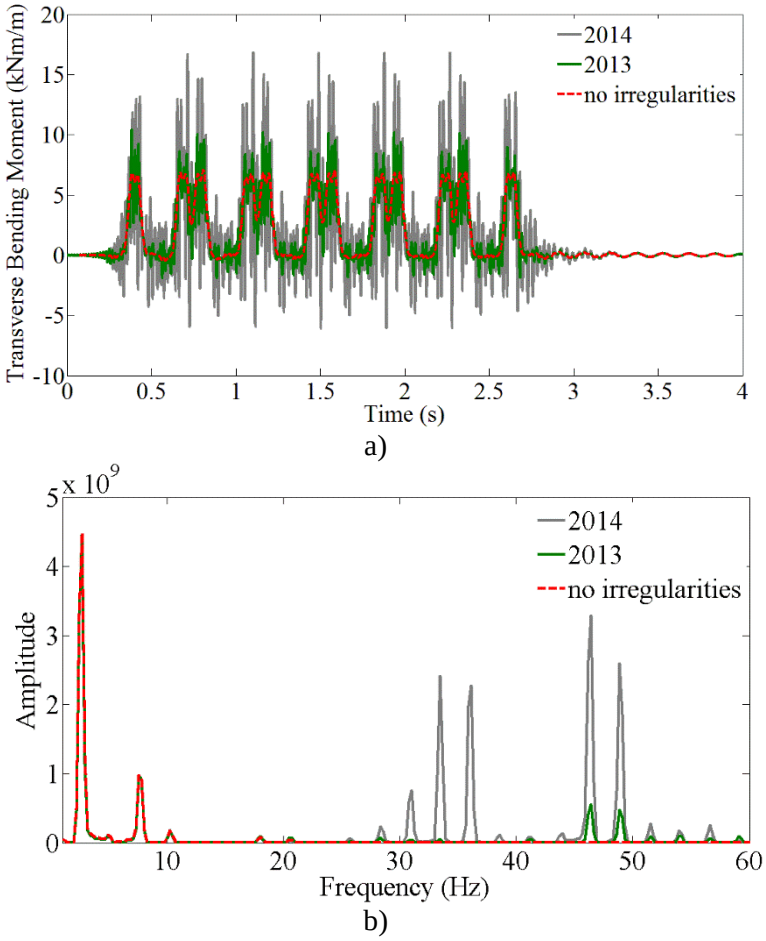

Figure 5.49 – Comparison of transverse bending moments, considering or not track irregularities: a) time responses; b) auto-spectra

By observing Figure 5.49, a considerable amplification of the bending moment can be noticed when irregularities profiles are considered, especially the one of 2014, resulting in much higher peak-values, due to the excitation induced mainly by irregularities of short

wavelength. The important aforementioned wavelengths in the range 1.25 m to 3.0 m (see Figure 5.41) correspond to excitation frequencies between 22.2 Hz and 53.3 Hz (when the train speed is 240 km/h). These values are close to the frequency of some vibration modes of the upper slab, being responsible for their excitation. By observing Figure 5.42, one can notice that irregularities profile of 2014 are generally below the limit provided by class 1 of FRA's PSD function with exception, precisely, of this wavelength range (1.25 m to 3.0 m). Therefore, the 2014 profile gives rise to a significant excitation of the slab's modes of vibration in the range 22 Hz to 53 Hz. Consequently, a considerable amplification of dynamic effects is observed [see Figure 5.49 b)] when these irregularities are considered in the analyses.

On the contrary, the irregularities profile of 2013 is less severe in the wavelength range 1.25 m to 3.0 m (see Figure 5.41). This fact justifies the lower amplification of dynamic effects when this profile is considered in analyses with trains travelling at high speed (see Figure 5.48) and, in particular, when the train speed is 240 km/h (results in Figure 5.49).

5.6.3.2 Influence of damping coefficients

5.6.3.2.1 Identification of modal damping coefficients of the upper slab

Global and local modal damping coefficients were identified, as shown previously in section 5.4.1, through ambient vibration tests. However, in order to identify modal damping coefficients of the RC deck slab, for vibration levels corresponding to the passage of trains, the results provided by two accelerometers installed in the upper slab during the dynamic test under railway traffic (see Figure 5.25) were used. They were located in a position which corresponds to the mid-span both in the longitudinal and in the transverse directions.

Acceleration records were obtained for the passage of the AP train at speeds of 157 km/h and 185 km/h and filtered by a Chebyshev (type II) low-pass digital filter of order 28, a stopband attenuation equal to 45 dB and a cut-off frequency equal to 100 Hz. The methodology adopted for the modal damping estimation comprises two phases: the first phase for detection of the train axle positions in each instant of time; the second phase for modal damping identification.

In phase 1, the experimental displacements of the upper slab were obtained by a double integration of the acceleration records. A Chebyshev (type II) high-pass digital filter, with cut-

off frequency of 0.8 Hz, was applied, in order to obtain only the dynamic component of displacements. Then, the experimental displacements were compared with the results calculated through the TBI methodology (for an AP train passage at the same speed).

Figure 5.50 shows the results of this first phase for the passage of AP train at 185 km/h in the mid-span section of the deck. The results obtained for the quarter-span section and for the passage of the AP at 157 km/h are very similar, the reason why only the following example is presented in this section to describe this methodology. On the one hand, this comparison provided an additional validation of the numerical model, because a very good agreement was obtained between measurements and calculations [see Figure 5.50 b)]. On the other hand, the comparison confirmed the precise instant of passage of each axle over each bridge position. The AP train picture in Figure 5.50 b) illustrates the instant of time when each axle crosses the mid-span cross section.

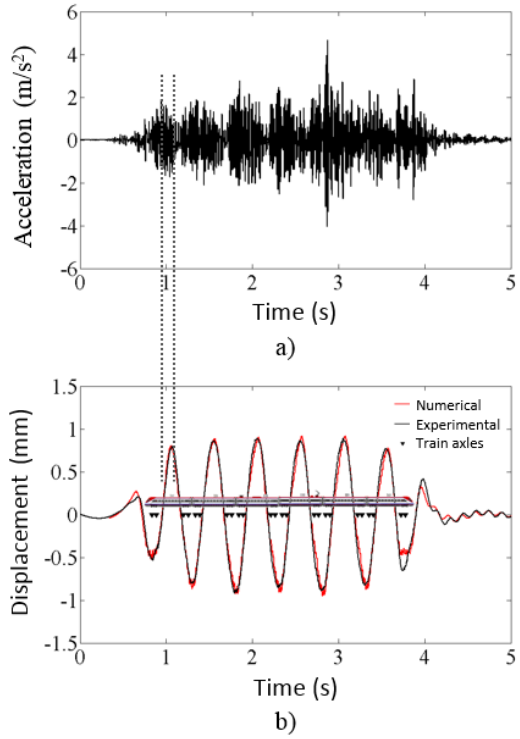

Figure 5.50 – Results for the mid-span section, for the passage of the AP train at 185 km/h: a) measured vertical acceleration; b) vertical displacement and train picture showing the instant of time when each axle crosses that cross section

In phase 2, the damping identification is performed for local vibration modes, which are excited by the passage of each train's axles group. The acceleration record for a time interval after the passage of the axles group is considered for this purpose. One of these time intervals is

marked in Figure 5.50 with dotted lines. For each time interval an auto-spectra of accelerations is determined, which allows identification of the frequencies with significant contribution to the response. These frequencies are essentially related with local vibration modes. Then, a band-pass digital filter, centred on the vibration mode's frequency, is applied to the acceleration record. After that, an exponential function is adjusted to the maximum values of the filtered response, in order to obtain the damping coefficient of each vibration mode according to the logarithmic decrement method (Paz 1980).

To exemplify this procedure, Figure 5.51 a) shows the auto-spectra for the time interval marked in Figure 5.50. The shaded region in Figure 5.51 a) represents the applied band-pass filter. The respective mode shape is also presented. Figure 5.51 b) shows the filtered acceleration time record, in correspondence with the vibration mode with frequency equal to 74.60 Hz (see also Figure 5.16), which led to a damping coefficient estimate equal to 5.97 %.

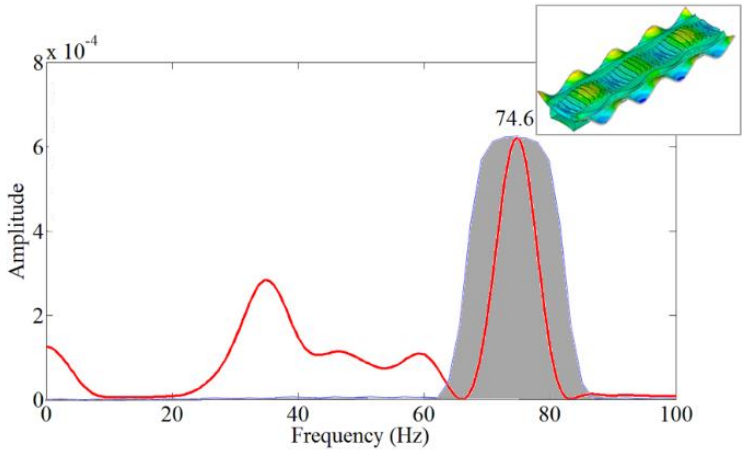

a)

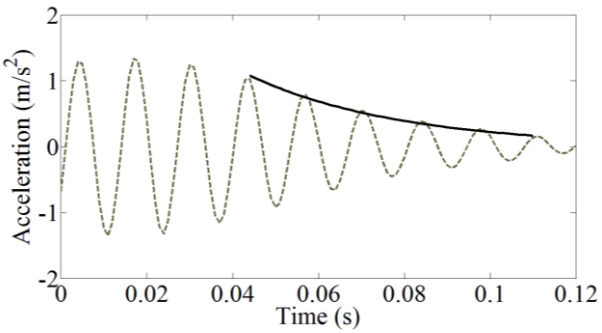

b)

Figure 5.51 – Damping estimation of a local vibration mode: a) auto-spectra; b) filtered response

This procedure was applied for each passage of the axles group, in mid-span and quarter-span sections, for the passage of AP train at speeds of 157 km/h and 185 km/h. Due to

difficulties in applying either the band-pass filter (for example due to the proximity of other natural frequencies) or the logarithmic decrement method (for example due to the quality of the records), not all time intervals after the passage of a train's axles group allowed estimation of the damping coefficient.

Figure 5.52 shows the 12 estimates obtained for the upper slab's local damping coefficients as a function of the natural frequency of the respective local vibration mode. Due to the mode shape similarity of all identified vibration modes, with bending movements of the central zone of the upper slab, the results of the damping coefficients were grouped, leading to a mean value equal to 5.02 % and a standard deviation equal to 0.94 %.

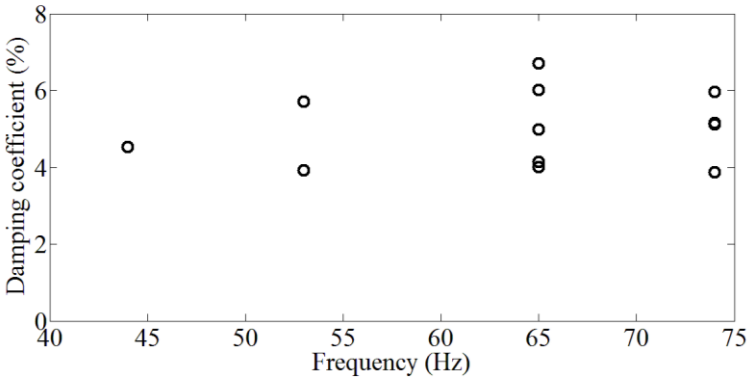

Figure 5.52 – Damping estimates of upper slab's local vibration modes

5.6.3.2.2 Vertical acceleration

In order to understand the effect of the modal damping coefficient in the dynamic response of the structure, especially in the local behaviour of the RC upper deck slab, two scenarios were considered for the adopted damping values: a value of 1 % for all vibration modes (as suggested by the EN 1991-2 guidelines); or the values identified from experimental tests. In the latter scenario, the modal damping coefficients for global vibration modes took the values identified in ambient vibration tests [see

Table 5.2] and the damping coefficients of local vibration modes, whose identification is shown in the present section, were taken equal to 5.02 %. For the remaining unidentified vibration modes a damping coefficient equal to 1 % was assumed.

In Figure 5.53 a) and Figure 5.54 a) a comparison between acceleration records experimentally obtained and numerically calculated in the mid-span section of the upper slab, for the passage of AP train at a speed of 185 km/h, is presented. The acceleration records were filtered by a Chebyshev (type II) low-pass digital filter of order 11 and 20 for cut-off frequencies of 20 Hz (Figure 5.53) and 60 Hz (Figure 5.54), respectively, and stopband attenuation equal to 45 dB. Figure 5.53 b) and Figure 5.54 b) show the corresponding auto-spectra. For this purpose, the irregularities profile of 2013, the most unfavourable one for this train speed (see Figure 5.44), is taken into account in TBI analyses.

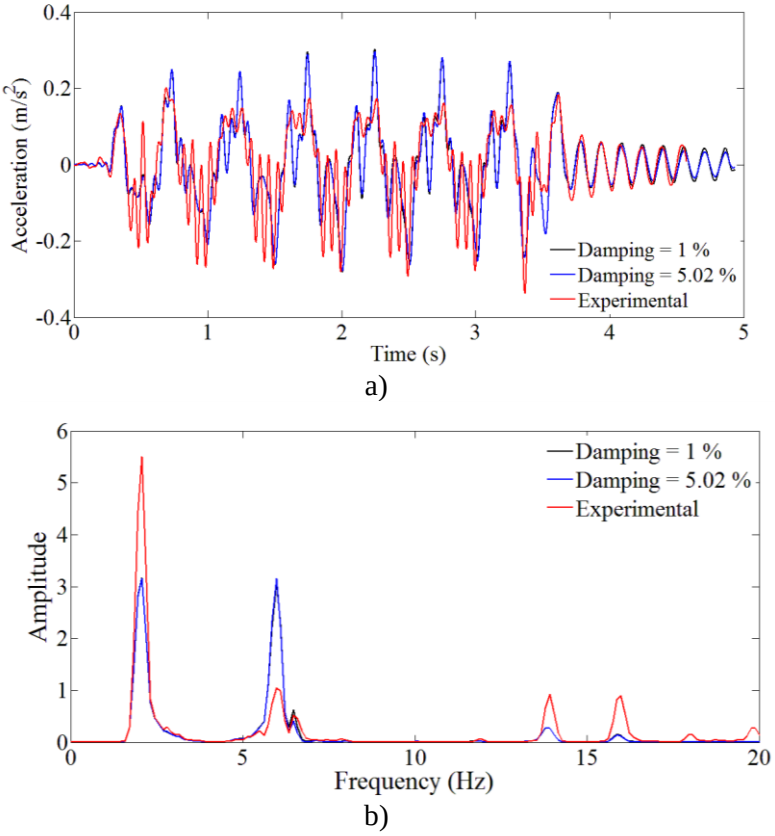

Figure 5.53 – Comparison between measured and calculated accelerations on the upper slab for the passage of AP train at 185 km/h, considering frequencies up to 20 Hz: a) time records; b) auto-spectra

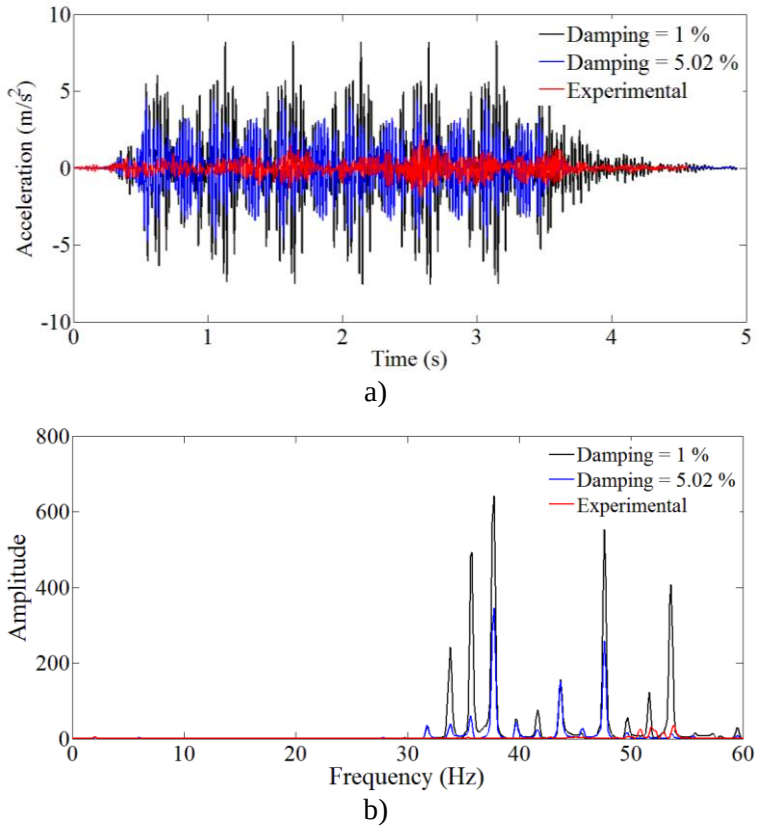

Figure 5.54 – Comparison between measured and calculated accelerations on the upper slab for the passage of AP train at 185 km/h, considering frequencies up to 60 Hz: a) time records; b) auto-spectra

By observing Figure 5.53, for a maximum frequency of 20 Hz, one can notice a negligible difference in the slab's dynamic response when the two damping scenarios are considered. This is due to the fact that, in this range of frequencies, the dynamic response is essentially dominated by frequencies related to the train action and by the frequency of the first global vibration mode of the bridge. However, observing the Figure 5.54, important amplifications can be seen in the response associated to some local vibration modes, with frequencies in the range between 30 and 60 Hz, when a value of 1 % is adopted as damping coefficient.

Regarding the comparison with experimental results, it should be pointed out that, in order to obtain the maximum differences when two different damping scenarios are considered, the irregularities profile of 2013 was adopted (the most unfavourable one for this train speed). As previously discussed (see section 5.6.3.1.2), the main contribution to the calculated slab's dynamic response comes from vibration modes in the range of frequencies between 30 and 60 Hz, where the main differences to the experimental response can be observed.

As shown before, the irregularities profile from 2011 (year in which the dynamic test under railway traffic was performed), is the one that leads to minor differences between numerical and experimental responses. In order to understand the effect of the damping coefficient when this irregularities profile is used in numerical analyses, Figure 5.55 shows the comparison of vertical accelerations at the mid-span section of the slab for the passage of the AP at 185 km/h for a maximum frequency of 60 Hz. As can be seen, although there are differences in the range of frequencies with major contribution to the response, a much better agreement between numerical and experimental results was achieved when both this irregularities profile and the most realistic damping scenario were adopted. It can also be observed that, in this particular case, the effect of the use of a normative value equal to 1 % is not too preponderant as in the case shown in Figure 5.54, leading only to a small amplification of the dynamic response [see Figure 5.55 a)].

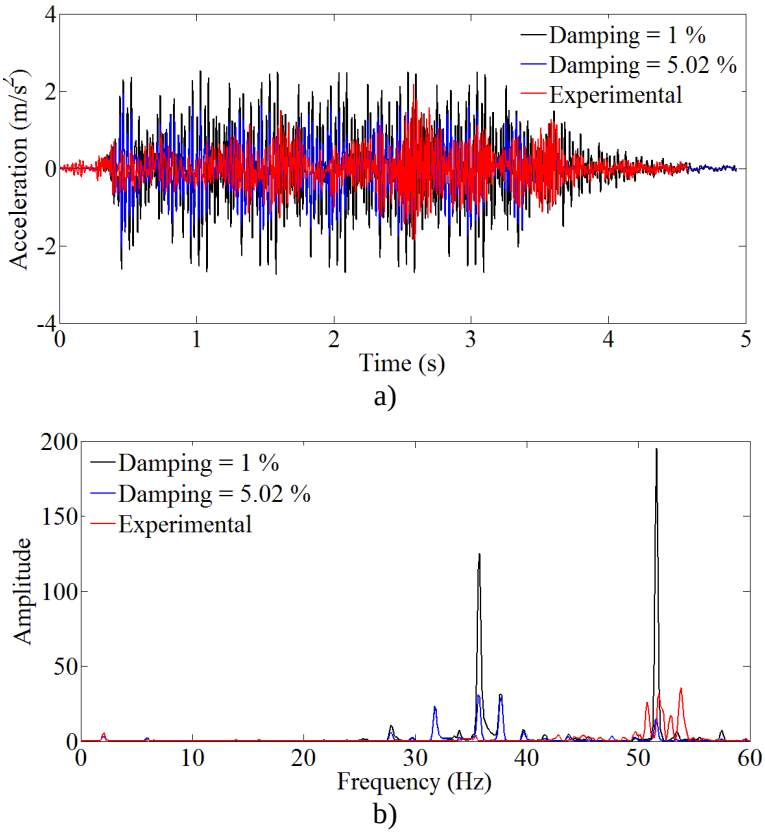

Figure 5.55 – Comparison between measured and calculated accelerations on the upper slab for the passage of AP train at 185 km/h and using the irregularities profile from 2011, considering frequencies up to 60 Hz: a) time records; b) auto-spectra

5.6.3.2.3 Transverse bending moments

Concerning the assessment of the effects of different damping coefficients in transverse bending moments of the upper slab, the same aforementioned two scenarios for the adopted damping values were considered.

Figure 5.56 shows the envelopes of transverse bending moments, considering the most unfavourable instant of time and the most unfavourable position along the sagging [Figure 5.56 a)] and hogging [Figure 5.56 b)] bending moment lines depicted in Figure 5.46, for both scenarios and for different train speeds, considering frequencies up to 60Hz. The irregularities profile of 2014, the most unfavourable one for higher train speeds, is taken into account in both TBI analyses.

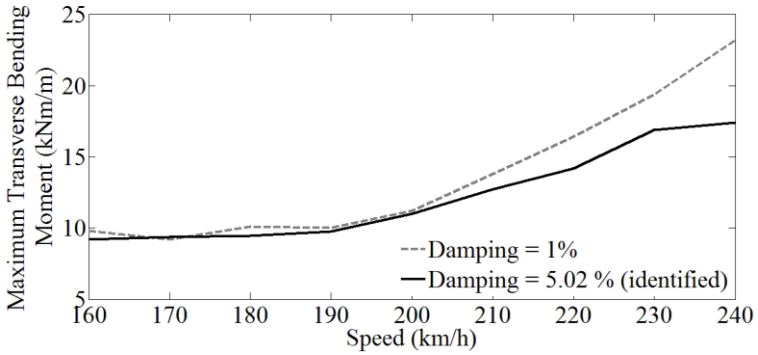

a)

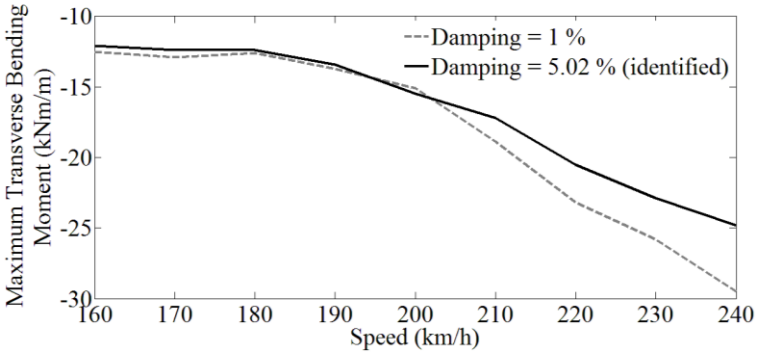

b)

Figure 5.56 – Influence of damping on the maximum transverse bending moment, considering the irregularities profile of 2014: a) sagging moment; b) hogging moment

Figure 5.57 shows the bending moment time histories [Figure 5.57 a)] and corresponding auto-spectra [Figure 5.57 b)] for the passage of AP train at a speed of 240 km/h, considering different damping coefficients.

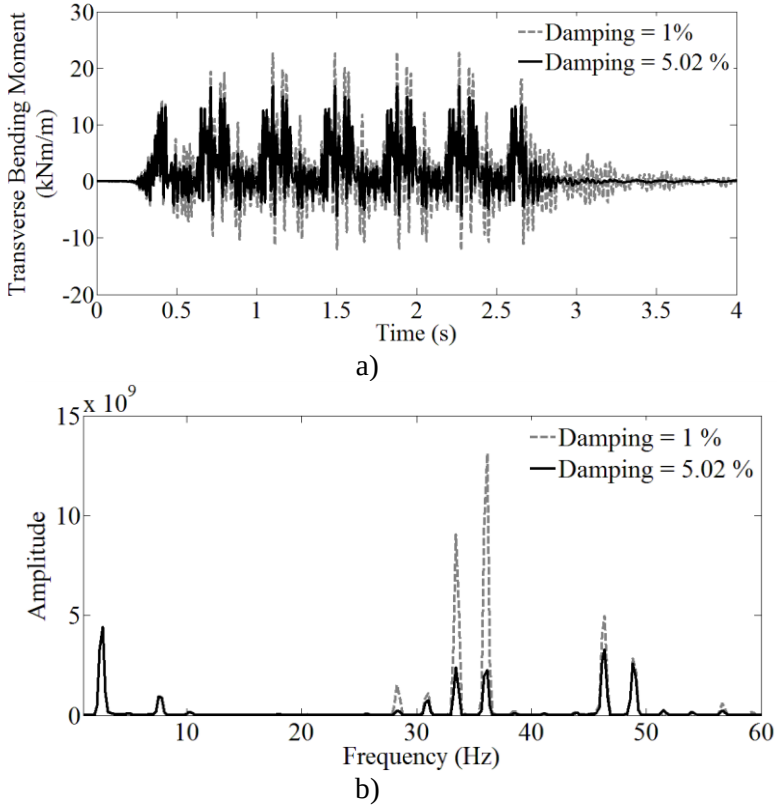

Figure 5.57 – Comparison of transverse bending moments considering different damping coefficients, for the irregularities profile of 2014: a) time histories; b) auto-spectra

By observing Figure 5.56 and Figure 5.57, a clear increase of the bending moment can be noticed when a value of 1 % is adopted as damping coefficient for all vibration modes, by comparison with the results achieved when experimentally identified values are considered. The use of this standard damping coefficient led to increases of 33 % and 19 % in the maximum values of sagging and hogging transverse bending moments, respectively. This is due to higher vibration amplitude in local vibration modes of the deck slab, with frequencies in a range between 25 Hz and 50 Hz, as shown in Figure 5.57 b).

5.6.4 Dynamic coefficients

In the present section the dynamic factors φ' (dynamic amplification factor) and φ'' (amplification factor to account for the existence of track irregularities and vehicle imperfections) are calculated and compared with the ones suggested by the EN 1991-2 guidelines. These dynamic factors were obtained based on the results of transverse sagging and hogging bending moments in the upper slab, previously presented, considering the most

unfavourable instant of time and the most unfavourable position along the lines depicted in Figure 5.46.

The maximum values were obtained from four types of numerical analyses: static (A); moving loads (B); TBI without irregularities (C); and TBI with irregularities (D). Concerning the track irregularities, the aforementioned four levelling profiles, from 2011 to 2014, were taken into account. In terms of modal damping coefficients, the two scenarios presented in section 5.6.3.2.2 were also considered as well as the normative value equal to 1%. It is important to note once again that the latter value is not the more realistic one but it is the Eurocode's recommendation for this type of structure. For that reason, the dynamic amplification, obtained when this value is considered, is also compared with the results when a more realistic scenario is adopted. AP train speeds between 160 km/h and 240 km/h were adopted in the analyses, which correspond to a variation of ± 20 % with respect to a frequent train speed of 200 km/h. All analyses were carried out using an integration time increment equal to 0.001 s. In the analysis of the bridge subsystem through to the modal-superposition method, all the vibration modes with frequencies up to 60 Hz were considered. The static correction procedure was applied in order to take into account the static component of the contribution of higher order modes.

According to Equation 2.15, φ' can be calculated through the following expression:

$$M_A \cdot (1 + \varphi') = M_{B/C} \leftrightarrow \varphi' = \frac{M_{B/C}}{M_A} - 1 \tag{5.11}$$

where M_A is the bending moment obtained by static analysis and $M_{B/C}$ is either the bending moment obtained from moving loads analysis or TBI analysis, without irregularities, respectively.

The amplification factor φ'' can be calculated through the following expressions:

$$M_A \cdot (1 + \varphi' + \varphi'') = M_D \leftrightarrow \varphi'' = \frac{M_D - M_C}{M_A} \tag{5.12}$$

with

$$\varphi' = \frac{M_C}{M_A} - 1 \tag{5.13}$$

where M_D is the bending moment obtained through TBI dynamic analyses considering the effect of track irregularities.

Table 5.9 summarises the maximum transverse bending moments obtained through each analysis. As previously mentioned, the damping scenario involving normative values (1 %) was only evaluated taking into account the irregularities profile of 2014, the most unfavourable one for higher train speeds.

Table 5.9 – Maximum transverse bending moments for two scenarios of modal damping

		Maximum transverse bending moment (kNm/m)						
Damping scenario	Moment line	M_A	M_B	M_C	$M_{D\ 2011}$	$M_{D\ 2012}$	$M_{D\ 2013}$	$M_{D\ 2014}$
Identified (5.02 %)	Sagging	6.63	7.06	7.20	12.79	14.32	12.67	17.41
	Hogging	-8.70	-9.55	-9.72	-17.23	-20.42	-17.33	-24.76
Normative (1 %)	Sagging	6.63	7.26	7.39	-	-	-	23.16
	Hogging	-8.70	-9.93	-9.87	-	-	-	-29.53

Table 5.10 presents the values of dynamic amplification factor obtained taking into the account the analyses *B* and *C*, through the application of Equation (5.11). The values suggested by the guidelines of the standard EN1991-2, obtained from annex C and D, are also presented.

Table 5.10 – Calculated values of the amplification factor φ'

Bending moment	EN1991-2 (Annex C)	EN1991-2 (Annex D)	φ' [Equation (5.11); analysis B]		φ' [Equation (5.11); analysis C]	
	φ'	$0.5 \times \varphi'$	Damping=5.02%	Damping=1%	Damping=5.02%	Damping=1%
Sagging	0.125	0.26	0.065	0.095	0.087	0.116
Hogging			0.098	0.141	0.117	0.134

Concerning the guidelines presented in annexes C and D of the standard EN1991-2, the values presented in Table 5.10 were calculated through the application of Equations 2.18 and 3.14, respectively. For this purpose, the maximum permitted vehicle speed was considered equal to 200 km/h and the first natural bending frequency of the upper slab equal to 24.72 Hz. The determinant length was adopted equal to 10.098 m, considering a concrete deck slab with ballast bed and 3.366 m span between webs of the U-shaped girder, in the transverse direction (according to Table 6.2 of EN1991-2).

These dynamic analyses allowed the calculation of more realistic dynamic factors because numerical models of the bridge and the train, calibrated based on experimental results, were used. By observing Table 5.10 one can notice some differences between the numerically calculated and suggested values, even if in the latter case some parameters of the structure, such as the transverse span of the upper slab and its first natural frequency, have been used. With exception of the values obtained for the hogging bending moment, using modal damping coefficients equal to 1 %, the values of φ' obtained using either the moving loads or TBI analyses, are lower than those suggested by EN1991-2. The dynamic amplifications proposed by this code are therefore on the safe side, in this case.

Table 5.11 presents the values of the amplification factor obtained taking into account the TBI analyses, considering the influence of track irregularities, through the application of Equation (5.12). The values suggested by the guidelines of the standard EN1991-2 obtained from annex C, considering different track maintenance levels, and from annex D are also presented. By observing the following results, one can see that the normative value suggested by Annex C, considering a careful level of track maintenance, would not be on the safe side to evaluate the effect of dynamic analyses. A similar conclusion can be drawn for the value suggested by Annex D, used in fatigue analyses, where the difference for the calculated factors is even higher.

Table 5.11 – Calculated values of the dynamic amplification factor φ''

Bending moment	EN1991-2 (Annex C)		EN1991-2 (Annex D)	φ'' [Equation (5.12)]				
				Damping = 5.02 %				Damping = 1 %
	Standard (φ'')	*Careful* ($0.5 \times \varphi''$)	$0.25 \times \varphi''$	2011	2012	2013	2014	2014
Sagging	1.024	0.512	0.127	0.843	1.074	0.824	1.540	2.379
Hogging				0.862	1.229	0.873	1.727	2.259

5.7 Fatigue analysis of the upper deck slab

The fatigue analysis of the upper deck slab was performed in terms of the assessment of the fatigue damage in its transverse reinforcement bars, calculated based on the linear damage accumulation method, taking into account the results of TBI dynamic analyses previously

presented in section 5.6.3. For this purpose, internal forces (transverse bending moments and axial forces) were obtained for the lines presented in Figure 5.46.

Once the time history of internal forces has been calculated, the history record of stresses in the transverse steel reinforcement can be obtained. Although advanced models are available for the calculation of steel stresses in cracked RC members subjected to cyclic loading, a simplified procedure was used in this work. The steel stress at each instant of time, $\sigma_s(t)$, is given by:

$$\sigma_s(t) = \left(\frac{N(t)}{2} + \frac{M(t)}{z}\right) \cdot \frac{1}{A_s} \tag{5.14}$$

where $M(t)$ is the transverse bending moment, $N(t)$ is the transverse axial force, z is the internal lever arm and A_s is the cross-sectional area of transverse reinforcement.

Figure 5.58 shows a 1 m wide portion of the cross section of the upper deck slab with a layout of the reinforcement presented in the transverse direction. The total reinforcement area is equal to 19.2 cm^2/m and 14.0 cm^2/m for bottom and top reinforcements, respectively. Two layers of reinforcement exist at the bottom level because one of those layers is embedded in the precast plank. The internal lever arm is taken as 0.195 m and 0.165 m in the sagging and hogging moment lines, respectively.

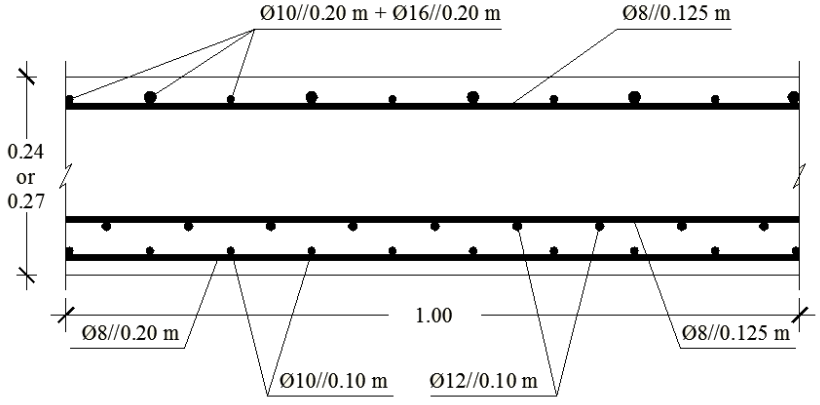

Figure 5.58 – Transverse cross section of the upper deck slab and reinforcement layout

The counting of stress cycles was carried out using the rainflow method. The result can be represented through a histogram that expresses the number of applied cycles for each stress range. The fatigue damage caused by the passage of a train was calculated according to the Palmgren-Miner linear damage accumulation rule (Miner 1945), using Equation 3.6, and the S-

N curve of the material. Figure 5.59 shows the S-N curve proposed by the EN 1992-1-1 (CEN 2004) for reinforcing straight bars, used in the present thesis, which allows to obtain the number of resistant cycles for each stress range. The stress range values given by the curve in Figure 5.59 are design values (characteristic values divided by a partial safety factor of 1.15).

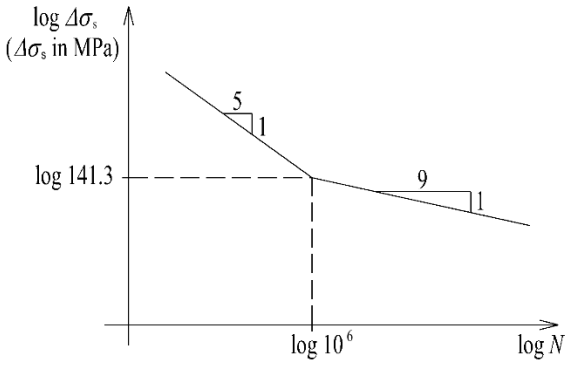

Figure 5.59 – S-N curve to define the design value of the number of resisting load cycles (adapted from EN 1992-1-1)

To illustrate the procedure for calculation of the fatigue damage, Figure 5.60 a) exemplifies the time variation of steel stresses in the bottom reinforcement [given by Equation (5.14)], at the location of maximum sagging moment at the mid-span cross-section, during the passage of one AP train, at a speed of 240 km/h. The irregularities profile considered in this analysis is the one of 2014 and the damping coefficient was taken as 5.02 % (identified value). The time variation of transverse bending moments for this analysis is shown in Figure 5.49 a).

Figure 5.60 b) demonstrates the results of the cycle counting procedure, using the rainflow method, organized in a histogram with 20 categories (i.e., intervals of stress ranges). The number of resistant load cycles for each of the 20 categories (intervals) is given by the S-N curve presented in Figure 5.59, considering the maximum stress range $\Delta\sigma_s$ in the interval. By applying the Equation 3.6 the fatigue damage result, D, is equal to 3.93×10^{-9}.

Naturally, this calculation result depends on the adopted number of categories and the obtained fatigue damage value, D, increases as the number of categories decreases. In order to avoid this source of uncertainty, the damage value can be quantified considering the individual stress ranges determined with the rainflow method (n_i is, in this case, equal to either 1 or 0.5). For the stress history given by Figure 5.60 a), the total number of stress ranges was i = 182, and the resulting fatigue damage was D = 2.97×10-9. This was the procedure employed in the remaining fatigue analyses shown in the present thesis.

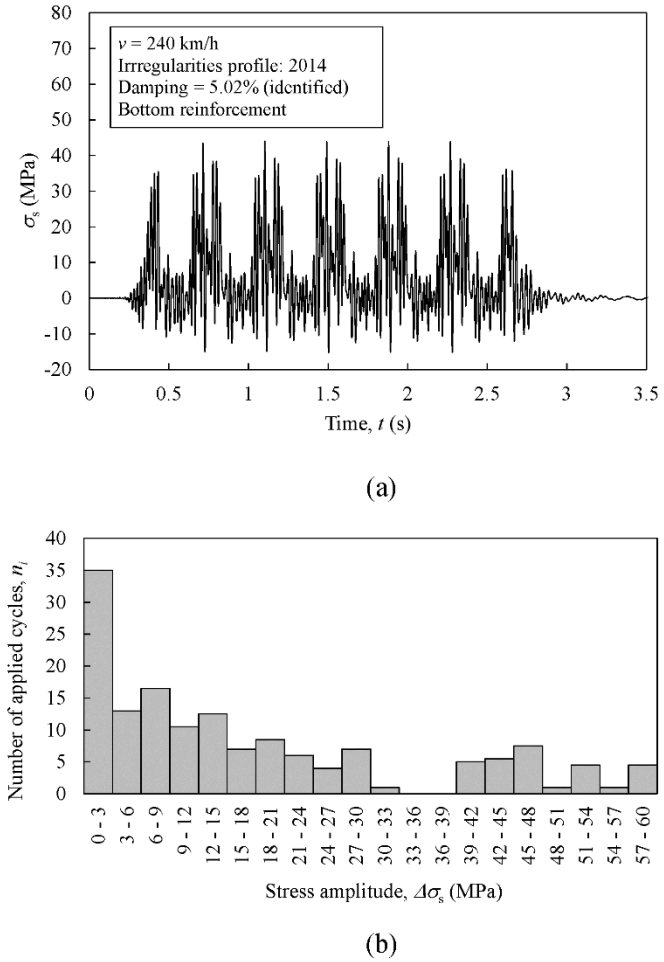

Figure 5.60 – Calculation of fatigue damage at the mid-span cross-section: a) time variation of stresses at the bottom reinforcement; b) corresponding histogram of stress ranges, calculated according to the rainflow method

The influence of different irregularities profiles and different modal damping coefficients in the fatigue damage of the transverse reinforcement of the upper deck slab was evaluated. Figure 5.61 presents the envelope of fatigue damage for different train speeds, *v*, and different track irregularities profiles, along the sagging and hogging moment lines. Abscissa axis consists of the order number of each element, with increasing numbering from left to right according to Figure 5.46. In these calculations, the aforementioned cross-sectional area of transverse reinforcement (according to Figure 5.58) was considered. It is possible to observe considerable differences in the results obtained taking into account different train speeds, especially for those higher than 200 km/h.

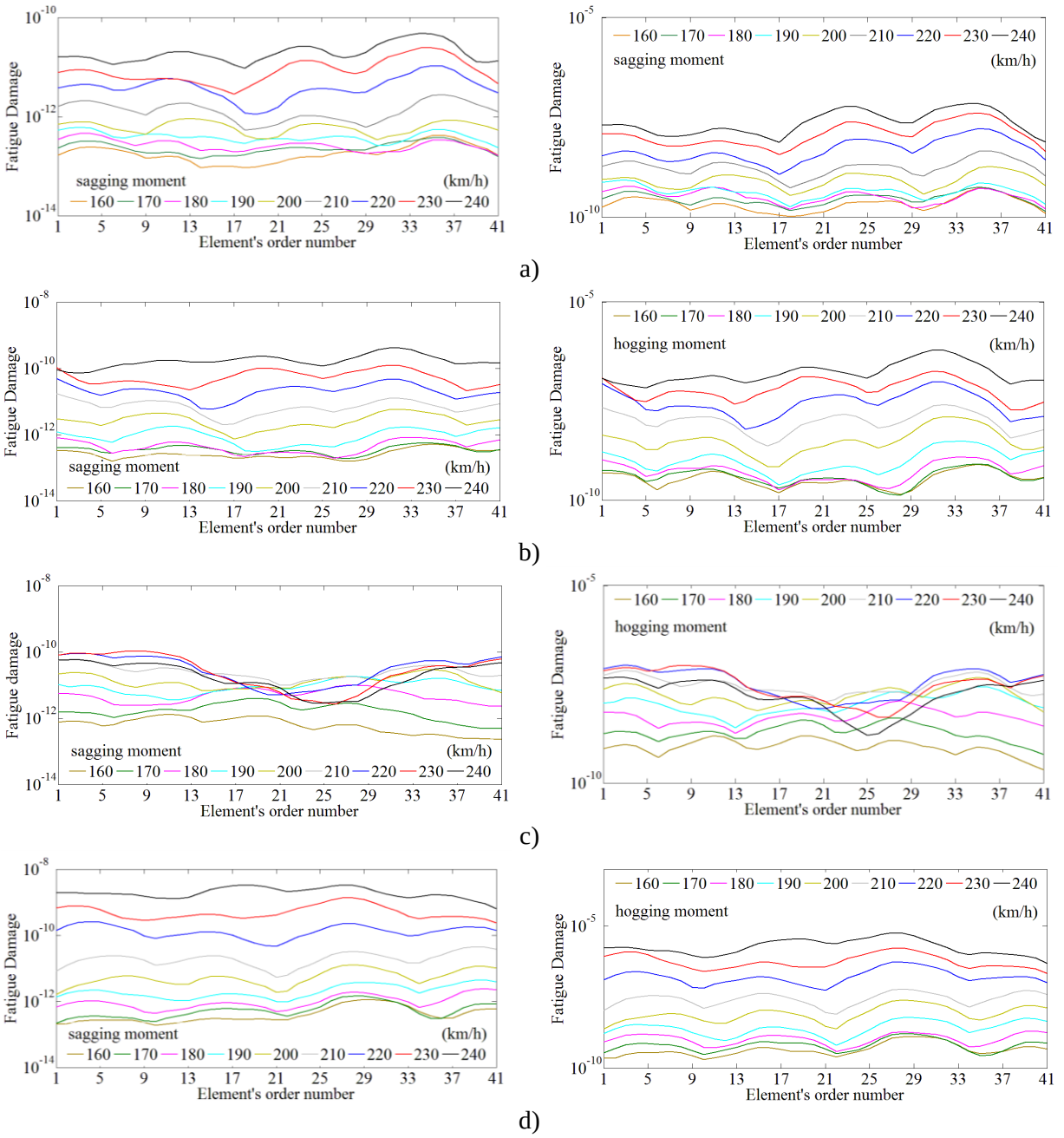

Figure 5.61 – Envelope of transverse sagging and hogging bending moments as function of train speeds, considering different irregularities profiles: a) 2011; b) 2012; c) 2013; d) 2014

Figure 5.62 displays another envelope of fatigue damage, considering now the most unfavourable position along the sagging and hogging bending moment lines. For this reason, the word "maximum" is used in the ordinate axis. The fatigue damage in the bottom and top transverse reinforcement was calculated for the passage of a single AP train, considering different train speeds and different track irregularities profiles as well. For this comparison, the results obtained without considering irregularities are also presented.

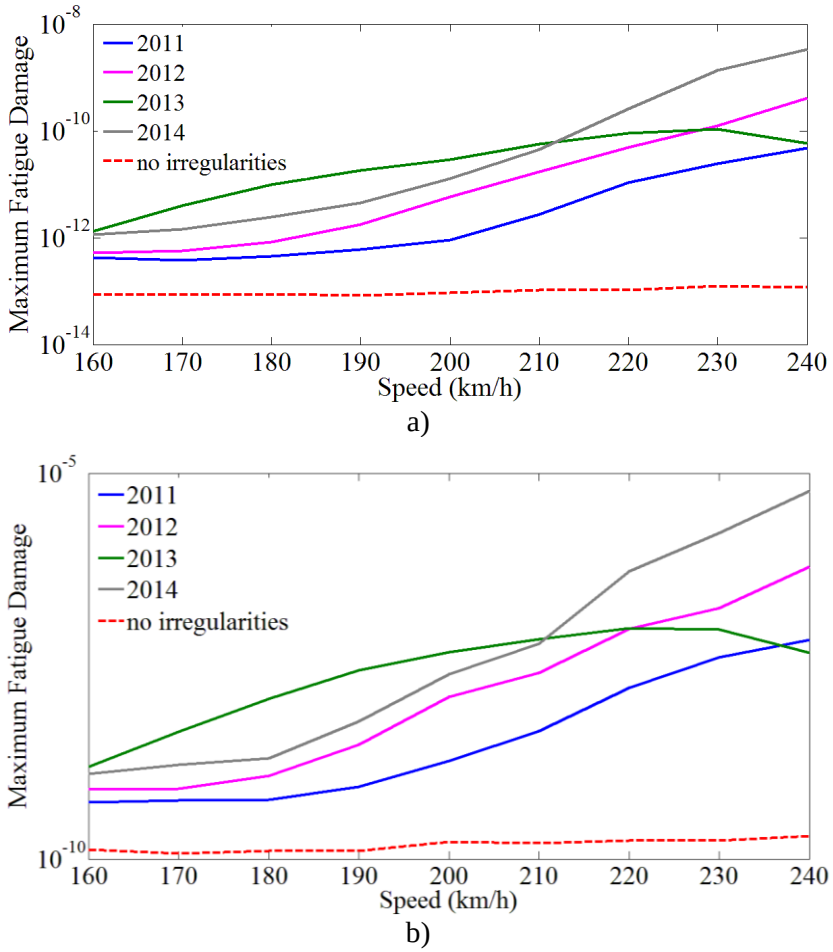

Figure 5.62 – Influence of track irregularities in the maximum fatigue damage, for the passage of one AP train, in: a) bottom reinforcement; b) top reinforcement

By observing Figure 5.62 one can confirm that track irregularities are responsible for a very significant increase of the calculated fatigue damage, in comparison with the results for a track without irregularities. Following a similar trend to that previously observed in the bending moment results, the train speed is also an important influencing parameter. Taking as an example the irregularities profile from 2014, the fatigue damage increases approximately 5×10^3 times when the train speed increases from 160 km/h to 240 km/h.

As previously concluded, in terms of dynamic behaviour of the upper slab, higher frequencies are not less critical than the lower frequencies, since they are associated with smaller wavelengths and with a more localised phenomenon. In order to understand the evolution of the fatigue damage with the maximum frequency threshold adopted in the dynamic results, Figure 5.63 shows the results of the fatigue damage calculated in the most unfavourable position along the sagging and hogging bending moment lines for the passage of one AP train at 220 km/h. For this purpose, successive Chebyshev (type II) low-pass digital filter were

previously applied to the bending moments and axial force records, with cut-off frequencies spaced from 5 Hz. Important increases in the fatigue damage of the slab can be seen up to a frequency of approximately 60 Hz, both for the bottom and top reinforcement, which are associated with the contribution of several local vibration modes of the slab in this range of frequencies. These results revealed the importance of adopt a higher frequency threshold when studying a localised phenomenon, reason why this maximum frequency is adopted in the present thesis.

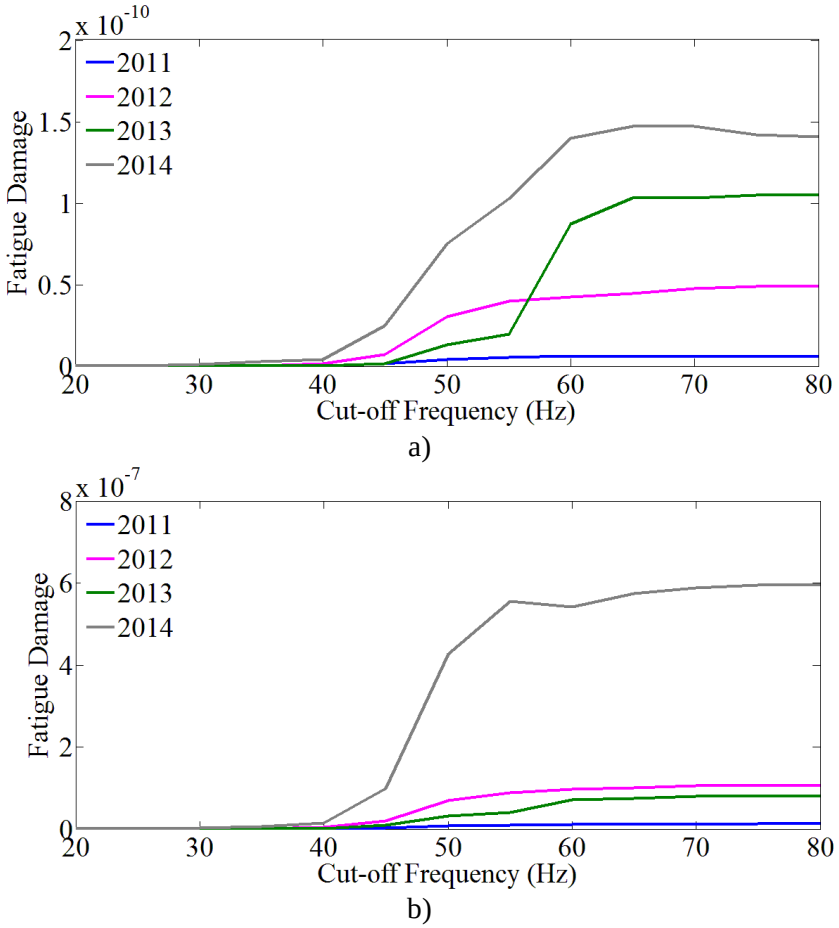

Figure 5.63 – Influence of the cut-off frequency in the fatigue damage, for the passage of one AP train at 220 km/h, in: a) bottom reinforcement; b) top reinforcement

Figure 5.64 shows the results of analyses that were performed in order to evaluate the effect of different damping coefficients in the fatigue damage. The two scenarios of adopted damping values, presented in section 5.6.3.2.2, and the irregularities profile of 2014 (the most unfavourable one for higher train speeds) were considered. By observing this figure, it is possible to conclude that the damping effect is not so significant. The highest difference shown in Figure 16(b) occurs for the train speed of 220 km/h. In this case the fatigue damage

decreases 10 times when the experimentally identified damping coefficients are considered rather than the value of 1%.

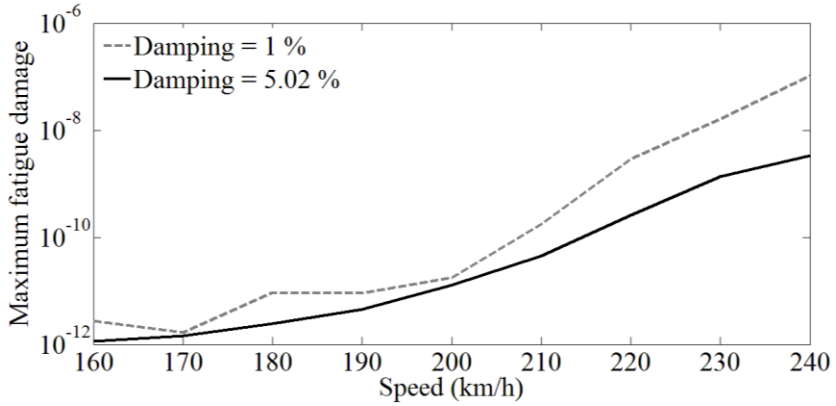

a)

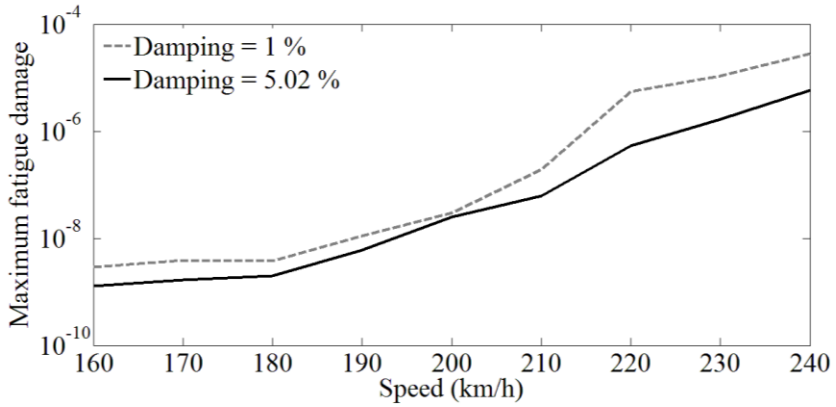

b)

Figure 5.64 – Influence of damping coefficient in the maximum fatigue damage, for the passage of one AP train, in: a) bottom reinforcement; b) top reinforcement

The consequences of the various influencing parameters, in terms of fatigue damage, can be understood in a clearer way by quantifying the area of transverse reinforcement required to prevent a fatigue failure of the reinforcement. For this purpose, the required area of reinforcement was determined so that the fatigue damage *D*, during 100 years, is equal to 1. Table 5.12 shows the results for the various scenarios addressed before, in terms of track irregularities and damping coefficients. The traffic volume corresponds to 30 AP trains per day. The results presented in Table 5.12 correspond to the most unfavourable train speed in the interval 160 km/h – 240 km/h, and to the most critical position along the lines indicated in Figure 5.46. The area of reinforcement actually existing in this structure is also presented in this table.

Table 5.12 – Area of transverse reinforcement required to prevent fatigue failure, for different scenarios of track irregularities and structural damping, and area provided in the existing structure

Type of result	Irregularities profile	Damping	Area of reinforcement (cm^2/m)	
			Sagging	Hogging
Calculated area	no irregularities	identified	3.32	5.49
	2011		6.42	10.52
	2012		8.15	13.41
	2013		7.03	10.88
	2014		10.30	17.20
		1 %	15.09	21.93
Area provided in the existing structure	--	--	19.2	14.0

It is important to note that, in each of the calculation scenarios whose results are shown in Table 5.12, it was assumed that the track irregularities remain unchanged throughout time. This hypothetical assumption was adopted with the purpose of showing the impact of different irregularities profiles. These results confirm that track irregularities play a paramount role in the definition of fatigue requirements for transverse reinforcement of bridge deck slabs. For the structure under analysis, the required area of reinforcement for the most unfavourable scenario of track irregularities is 3.13 times higher than the value for a perfect track without irregularities. On the other hand, Table 5.12 also confirms that the use of realistic estimates for the damping coefficients is very important for an accurate fatigue assessment. The cross-sectional area of reinforcement calculated with a damping coefficient of 1 % is in this case 1.47 times higher than the one for the identified damping values.

By comparing the area of reinforcement obtained through the calculations presented in this work with that really existing in the structure, one can see that, particularly in the sagging moment line, it is enough to ensure that, for this traffic scenario, fatigue damage will not occur throughout the fatigue life of the bridge. However, in the hogging moment line, it is possible to observe that, for one related with the irregularities profile (2014), the required area of reinforcement to prevent fatigue failure is higher than what is present in reality. This does not mean that the structure is unsafe, because a scenario with constant irregularities throughout

time is not realistic. The fatigue damage for the irregularities profiles measured in the remaining years is notably smaller.

Another important aspect to analyse is whether it is feasible to perform the fatigue safety assessment, in terms of the transverse reinforcement of the upper deck slab, based on the multiplication of the static effects (A) by the dynamic amplification factor $(1 + \varphi' + \varphi'')$ rather than using an evaluation based on dynamic analyses (D). For this purpose, the required area of reinforcement was determined again so that the fatigue damage *D*, during 100 years, is equal to 1. Table 5.13 shows the results for both analyses taking into account the most unfavourable train speed and to the most critical position along the lines indicated in Figure 5.46, considering a traffic volume of 30 AP trains per day. The dynamic amplification factors φ' (see Table 5.10) were considered equal to 0.087 and 0.117 for sagging and hogging moments, respectively, and the φ'' (see Table 5.11) were considered equal to 1.540 and 1.727 for sagging and hogging moments, respectively.

Table 5.13 – Area of transverse reinforcement required to prevent fatigue failure using different analysis approaches

	Required area of reinforcement (cm^2/m)	
Bending moment lines	$A \times (1 + \varphi' + \varphi'')$	D
Sagging	7.78	10.30
Hogging	13.63	17.20

By observing the results one can realise that there is a considerable difference in the values obtained by these two analyses, either for the sagging or hogging bending moment lines, with the dynamic analysis leading to higher values of reinforcement area. That is, a simpler analysis approach (considering a static analysis multiplied by a dynamic coefficient) leads to a fatigue damage calculation which is not on the safe side, even if there is no uncertainty related to the quantification of the dynamic coefficient. This is because the dynamic coefficient affects proportionally the internal forces (calculated through the static analysis) in all time steps. This simplification leads to a time variation of internal forces which is different from the actual one (quantified with greater accuracy through a dynamic analysis). These results show the inability of using the dynamic amplification factor, multiplied by the static effects of the train, to assess the fatigue safety of the upper deck slab of the Alverca viaduct.

5.8 Concluding remarks

In this Chapter, the numerical and experimental methodologies presented in the previous chapters were applied in the study of the dynamic behaviour and fatigue phenomenon of a real railway bridge. The assessment of the performance of the upper RC slab of the single-cell box girder deck of the Alverca railway viaduct led to a few very interesting conclusions.

First of all, the fact that the existence of local vibration modes of the upper slab with natural frequencies up to 60 Hz revealed a preponderant contribution to its local dynamic behaviour, showing a considerable increase in the maximum amplitude of its response, both in terms of vertical accelerations and transverse bending moments. Furthermore, the presence of these local vibration modes of higher frequencies, usually associated with smaller wavelengths and with a more localised phenomenon, when excited by the passage of regularly spaced axles of a train at a certain speed contributes to a high number of loading cycles of this structural element. Some parameters such as train speed, track irregularities and damping coefficients have proved to lead to considerably different vertical accelerations and bending moments in the deck slab, which is related to the way how the local vibration modes are particularly excited. It is worth mentioning that there is a great different in the calculation results when the irregularities are not considered in TBI dynamic analyses, since the excitation of local vibration modes does not occur in that case.

Secondly, as consequence of that mentioned above, since the fatigue damage in the transverse slab's reinforcing bars is strongly influenced by the time variation of bending moments, during the passage of a train, a strong influence of the aforementioned parameters is also noticed in the fatigue damage and in the transverse reinforcement area needed to prevent fatigue failure. Specifically, in this case study, track irregularities gave rise to an increase of 213 % in terms of reinforcement area required for fatigue safety, by comparison when they are not considered in the analyses, and different damping scenarios led to differences of 46.5 % in that required area. Important increases in the fatigue damage of the slab are seen, up to a frequency of approximately 60 Hz, both for the bottom and top reinforcement, which are related with the contribution of several local vibration modes of the slab in this range of frequencies. These results reveal the importance of adopting a higher frequency threshold when

studying a localised phenomenon, which is the reason why this maximum frequency was adopted in the present thesis.

It should also be pointed out that the experimental identification of the modal parameters of the structure, especially those related to the upper slab of the viaduct, has proved to play an important role in the understanding of the real performance of the upper slab of the deck. Its inclusion in the calibration of the FE numerical model allowed more realistic results to be obtained: on one hand, by means of the updating of numerical parameters directly related to the study of the local dynamic behaviour of the slab, such as the thickness of the upper slab, the elasticity modulus of concrete and ballast and the ballast density weight; and on the other hand leading to more accurate dynamic responses obtained when subjected to the passage of railway traffic, allowing to minimise the differences between numerical and experimental results. Bearing this in mind, the adopted analysis methodology (based on the use of experimental measurements, advanced calibrated numerical models, TBI analyses, measured track irregularities and identified damping coefficients) appears to have the potential to be used in the detailed study of the dynamic behaviour and fatigue assessment of existing structures. This also demonstrated that the application of this methodology might contribute to the improvement of current design guidelines.

Chapter 6

Case study II: Access viaduct to Alcácer do Sal bridge

6.1 Introduction

In this chapter, the local dynamic behaviour and fatigue assessment of a RC slab, used in another typical structural solution widely used in the construction of bridges and viaducts in railway lines, is presented and discussed. The case study is the north access viaduct to Alcácer do Sal bridge, part of a new railway variant located in the Southern Line of the Portuguese railway network, which is composed of a composite steel-concrete solution with two steel I-girders connected by an upper RC slab.

For that purpose, a 3D FE numerical model is developed and calibrated based on the experimental identification of the modal parameters of the slab. Once again, the calibration of the numerical model is performed by applying an iterative methodology based on a genetic algorithm. The validation of the numerical model is carried out through the comparison between numerical and experimental responses, in terms of displacements, accelerations and deformations measured in several locations of the viaduct, for the passage of AP trains with different running speeds. It should be pointed out that, in this case, the validation takes into account the experimental responses directly measured in the slab instead of other elements where the global response could be determinant.

The effects of the train speed, track irregularities, damping coefficients and different cut-off frequencies on the dynamic behaviour of the upper deck slab are discussed, when subjected to the passage of trains at speeds up to 260 km/h. The results of different train-bridge interaction dynamic analyses are the basis for the assessment of the fatigue damage in the transverse reinforcement bars of the deck slab. The fatigue damage is calculated based on the linear damage accumulation rule, considering the transverse bending moments and axial forces obtained for two different positions in the slab (positions of maximum sagging and hogging transverse bending moments).

6.2 Description of the access viaduct to Alcácer do Sal bridge

The Alcácer do Sal bridge is part of a new railway variant located in the Southern Line of the Portuguese railway network, which establishes the rail connection between Lisbon and Algarve. Figure 6.1 depicts a map of the Portuguese railway network (Portugal 2017), highlighting the location of the Alcácer do Sal bridge and showing a generic aerial view. This variant allows, at the moment, the circulation of passenger trains with speeds up to 220 km/h and freight trains with maximum axle load of 25 t. The bridge, presented in Figure 6.2, has a total length of 2735 m, divided into three parts: the north access viaduct with 1115 m (34.75 m + 6 × 37.5 m + 45.0 m + 17 × 45.0 m + 45.0 m), the main bridge with three spans of 160 m each and the south access viaduct with 1140 m (45.0 m + 16 × 45.0 m + 37.5 m + 9 × 37.5 m).

Figure 6.1 – Location of the Alcácer do Sal bridge in the Portuguese railway network (Portugal 2017)

Figure 6.2 – Overview of Alcácer do Sal bridge and access viaducts (REFER 2010)

The main bridge (bowstring structural solution) has three continuous spans. Most of the spans of access viaducts are also continuous. However, due to constraints related to the track-bridge interaction problem, some neutral sections (simply supported spans) were created, in order to limit the continuous maximum length to about 750/800 m. In these sections, rail expansion devices were also installed.

These particular spans have no continuity with the adjacent spans, either by the structure, due to the presence of structural joints, or by the railway track, due to existence of rail expansion devices. In this thesis, the study focuses on one of those simply supported spans of the north access viaduct, with a total length of 45.0 m, located approximately at 260 m from the North abutment. Figure 6.3 illustrates the elevation of the north access viaduct [Figure 6.3 a)], in which this span is highlighted, and its respective cross section [Figure 6.3 b)].

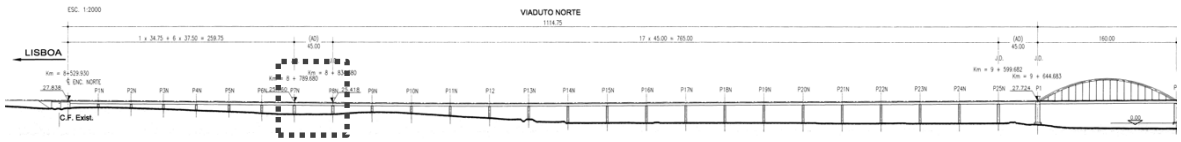

a)

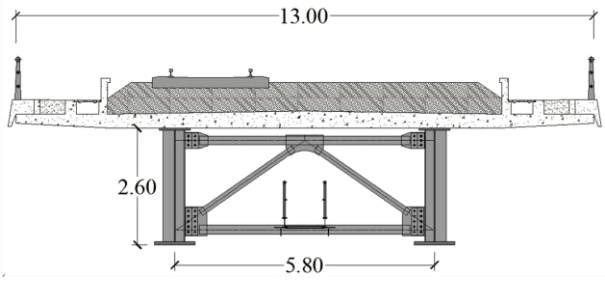

b)

Figure 6.3 –Alcácer do Sal bridge: a) elevation view of the north access viaduct; b) cross section

The access viaduct consists of a composite steel-concrete structural solution with two steel I-girders which support an upper RC slab. Figure 6.4 presents a global view of the north access viaduct.

Figure 6.4 – Global view of the north access viaduct to Alcácer do Sal bridge (Geoview 2017)

The steel I-girders are spaced 5.80 m apart and have a constant height equal to 2.60 m. The top and bottom flanges are 0.70 m and 1.0 m wide, respectively, with variable thickness along the span: varying from 4.0 cm to 8.0 cm (top flange) and from 5.0 cm to 12.0 cm (bottom flange) in the bearing zones and in the central zone, respectively. The webs also present variable thickness along the span, varying from 2.5 cm to 1.6 cm, in the bearing zones and in the central zone, respectively. The webs stiffeners are composed by ½ IPE 400 steel profiles, welded to the webs, and are spaced 1.7 m and 3.5 m apart, in the bearing zones and in the central zone, respectively.

There are diaphragms between the girders, spaced 7.5 m apart, formed by circular hollow sections: upper and lower beams with diameter of 193.7 mm and thicknesses of 12 mm and 8 mm, respectively, and diagonals with diameter of 139.7 mm and thickness of 8 mm. The horizontal bracing system, located approximately 0.35 m above the girder bottom flanges, is composed by ½ HEA 400 steel profiles. Figure 6.5 shows the metallic elements referred above.

Figure 6.5 – Structural metallic elements of the viaduct (REFER 2010)

The RC slab has a total width of 13 m with variable thickness: 0.20 m in the extremity of the cantilevers, 0.35 m in the girder-slab connection sections and 0.38 m at mid-span section between girders. The ballast retaining walls are 0.5 m deep, with a thickness equal to 0.20 m. The footways, edge beams and catenary bearings are all laid over the slab, as well as the waterproofing cap.

The deck girders are directly supported in the piers by means of pot bearings, two on each pier, longitudinally aligned with the main girders. In the south side both supports are fixed and in the north side horizontal movements are allowed: longitudinal displacements are allowed in both supports while transverse displacements are allowed only in one of them. Figure 6.6 shows a schematic representation of the bearings system [Figure 6.6 a)] and an example of two bearings over a pier [Figure 6.6 b)].

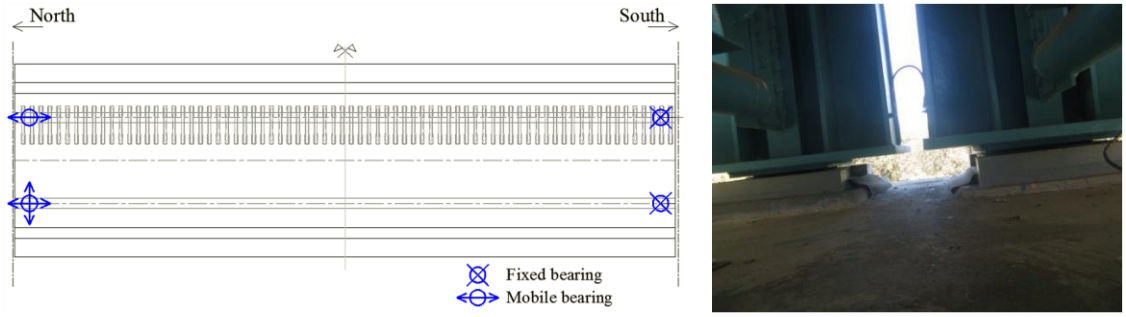

a) b)

Figure 6.6 – Bearings system: a) schematic representation; b) generic view of the bearings

Concerning the track, although the bridge was designed for the operation of two railway lines, only one is currently in full operation. The track consists of continuously welded UIC60 rails spaced 1.688 m apart, elastomeric rubber pads, monoblock prestressed concrete sleepers and a 40 cm ballast layer.

As mentioned before, the simply supported span, studied in this thesis, was adopted to deal with the track-bridge interaction phenomena, containing the rail expansion devices near the structural joints of the deck. In order to provide greater stability to the track in these transitional zones, T16 monoblock sleepers were used, larger than the type DW commonly used, some of them connected by two U-shaped steel profiles. Figure 6.7 shows an overview of the railway track over the referred span, showing the transition to the continuous deck.

Figure 6.7 – Overview of the railway track

6.3 Bridge FE numerical model

In this section, the numerical model of the simply supported span of the north access viaduct to Alcácer do Sal bridge is presented and the geometrical and mechanical properties of its main

structural elements are characterized. Particular aspects concerning the modelling of the railway track are also discussed.

6.3.1 Description

A 3D numerical model of the north access viaduct to Alcácer do Sal bridge was developed in ANSYS software (ANSYS 2007). Figure 6.8 shows an overview of the numerical model.

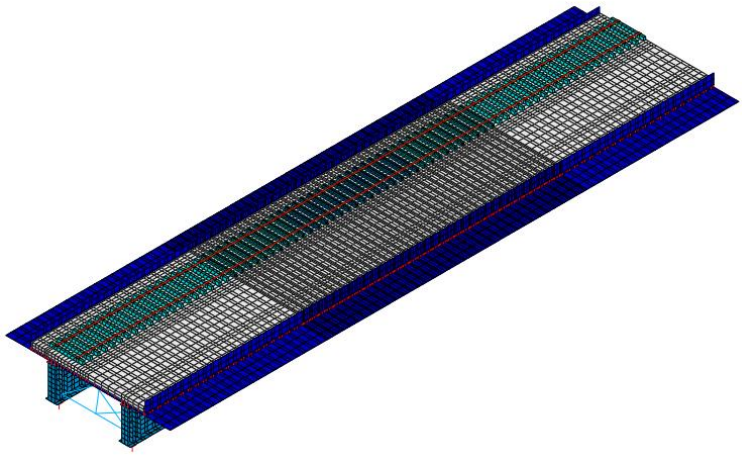

Figure 6.8 – Global view of the 3D numerical model of the viaduct

The girders, the slab, the ballast retaining walls and the stiffeners were modelled by shell FEs, while solid FEs were used to simulate sleepers, rail pads and the ballast layer. Beam FEs were adopted to discretize the diaphragms, bracings and rails, all of them positioned at their centre of gravity. The compatibility of displacements and rotations between the nodes of the girders and the nodes of the slab, as well as the compatibility of displacements between the nodes of the deck slab and the lower nodes of the ballast layer, were accomplished by rigid FEs [Figure 6.9 b)]. Each support was regarded as a single point and modelled by a spring element. Non-structural elements such as handrails, edge beams and the inspection footway were considered as additional masses, applied to the nodes of the FE mesh according to the real location of those elements.

The numerical model of the viaduct includes only one span because, as mentioned before, there is no continuity to the neighbouring spans, either by the structure (discontinuity of the structure and ballast layer assured by structural joints) or by the railway (due to existence of rail expansion devices). Furthermore, bearing this in mind, an additional extension of the railway

track was not considered in this modelling, unlike the modelling developed in the case study of the Alverca viaduct (see Chapter 5).

A more refined mesh was adopted for the central part (mid-span region of the span) of the upper RC slab, ballast retaining walls, ballast layer and sleepers. This is due to the fact that the study focuses on the central zone of the upper RC slab. Besides that, transversely, a more refined mesh is used in the region of the single track that is in service, which corresponds to the loaded region. The numerical model of the viaduct includes 40829 nodes and 39504 elements, with a total of 142487 degrees-of-freedom. Figure 6.9 a) shows a cross section of the structure and Figure 6.9 b) and c) depict details of the discretization adopted in the girder-slab connection area and in track components, respectively.

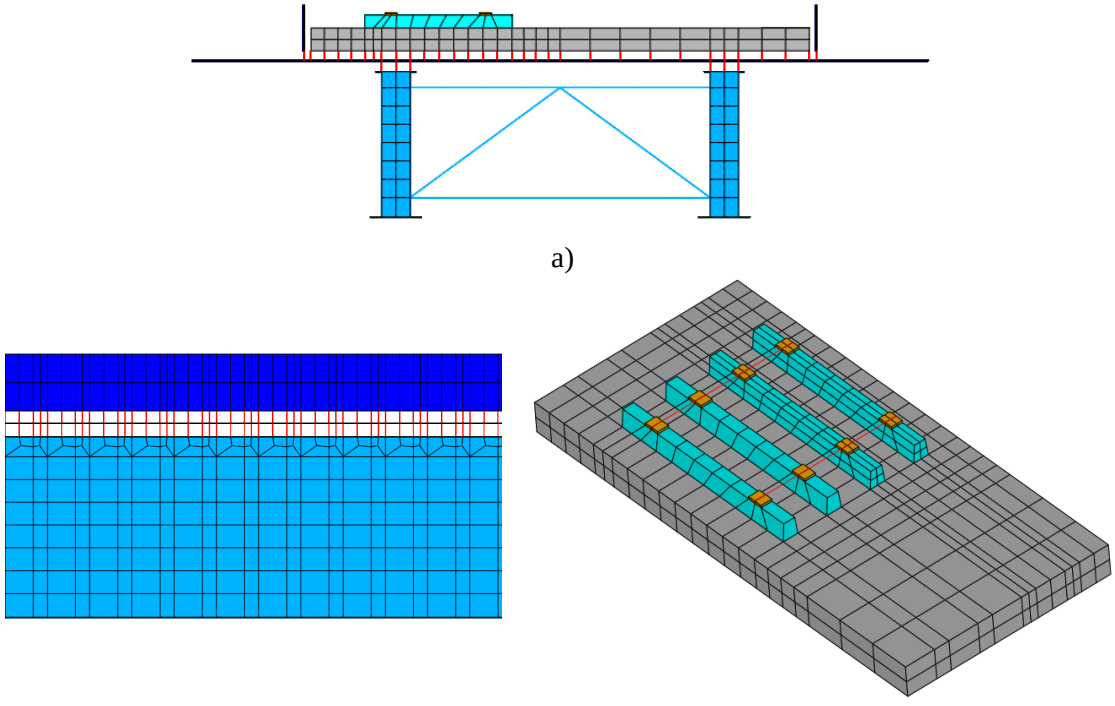

a)

b) c)

Figure 6.9 – Detailed views of the adopted FE mesh: a) cross section; b) girder-slab connection area; c) track components

6.3.2 Geometrical and mechanical properties

The main geometrical and mechanical parameters considered in the FE model for the various structural components are presented in Table 6.1, basically divided in deck and track parameters. Most of these parameters were defined based on the information provided by design drawings or quality control documents. Others, such as the ballast layer's thickness,

were obtained from local measurements. Detailed explanation about some of these parameters is presented below.

Table 6.1 – Geometrical and mechanical parameters of the numerical model

	Parameter	Description	Adopted value	Unit
Deck	t_c	Thickness of the RC slab (cantilevers / central zone)	0.257 / 0.362	m
	E_c	Concrete elasticity modulus	42.6	GPa
	ρ_c	Concrete density	2548.4	kg/m^3
	ν_c	Concrete Poisson's ratio	0.2	-
	E_s	Steel elasticity modulus	200	GPa
	ρ_s	Steel density	7850	kg/m^3
	ν_s	Steel Poisson's ratio	0.3	-
	A_{diap} / I_{diap}	Area / Inertia of diaphragms	68.5 / 2840	cm^2 / cm^4
	A_{brac} / I_{brac}	Area / Inertia of bracings	76.4 / 1890	cm^2 / cm^4
	k_v	Vertical bearing stiffness	556.6	MN/m
	k_h	Longitudinal bearing stiffness	5566	MN/m
Track	t_{bal}	Thickness of the ballast	0.40	m
	h_{bal}	Additional height of the ballast	0.17	m
	E_{bal}	Ballast elasticity modulus	145	MPa
	ρ_{bal}	Ballast density	2039	kg/m^3
	ν_{bal}	Ballast Poisson's ratio	0.15	-
	E_{pad}	Rail pad elasticity modulus	500	MPa
	k_{pad}	Vertical rail pads stiffness	500	kN/mm
	A_{rail} / I_{rail}	Area / Inertia of the rail UIC 60	76.7 / 3038	cm^2 / cm^4
	$E_{sleeper}$	Concrete (sleeper) elasticity modulus (type DW / T16)	36.0 / 38.2	GPa
	$\rho_{sleeper}$	Concrete (sleeper) density (type DW / T16)	3010 / 3899	kg/m^3
	$\nu_{sleeper}$	Concrete (sleeper) Poisson's ratio	0.2	-

6.3.2.1 Deck

6.3.2.1.1 RC slab

Concerning the thickness of the slab, although it is variable, a constant value was adopted in order to simplify its modelling: 0.257 m in the cantilevers zones and 0.362 m in the central zone between steel I-girders.

The concrete elasticity modulus was indirectly estimated based on the results of compressive tests performed on 28-day concrete specimens. These tests led to a mean value of the concrete compressive strength, f_{cm}, equal to 67.2 MPa. Taking into account Equation 5.1, in order to consider the age of the concrete at the date of the experimental tests (≈ 6 years), a value for the concrete compressive strength equal to 80.2 MPa was obtained (cement CEM II A/L 42.5R was considered). By applying Equations 5.2 and 5.3, a corrected elasticity modulus equal to 41.0 GPa was achieved.

Furthermore, in order to take into account the presence of reinforcement, the elasticity modulus of the concrete homogenised section (E_{hm}) was calculated based on the concrete elasticity modulus (E_{cm}) and steel elasticity modulus (E_{sm}), using the following equation:

$$E_{hm} = \frac{1}{100}[E_{cm}(100 - \rho_s) + E_{sm}p_s] \tag{6.1}$$

where ρ_s is the percentage of reinforcement, taken for this purpose as 1 %. A homogenised concrete elasticity modulus equal to 42.6 GPa was obtained.

Following the guidelines of standards EN1991-1-1 (CEN 2002) and EN1992-1-1 (CEN 2004), the concrete density weight and concrete Poisson's ratio were adopted equal to 2548 kg/m^3 (25 kN/m^3) and 0.20, respectively.

6.3.2.1.2 Steel elements

Concerning the steel elements, Table 6.2 presents the geometrical parameters of diaphragms, bracings, stiffeners and reinforcing elements along the span. For the web's stiffeners, an equivalent rectangular section, 0.25 m wide and 0.024 m thick, was adopted in the model in order to keep the same bending inertia of the real element (composed by ½ IPE 400 steel profile and considering a web's effective width equal to 0.50 m). An identical procedure was adopted in the modelling of reinforcing elements near the bearing zones, using FEs with a width of 0.50 m and a thickness of 0.025 m. The mass and inertia of the steel plates, used in the connections between different steel elements, were not considered in this model.

Table 6.2 – Geometrical parameters of the steel elements

Steel element	Cross section	Geometrical properties
Diaphragms	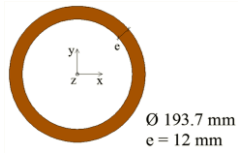	$A = 0.00685\ m^2$ $I_x = 0.284 \times 10^{-4}\ m^4$ $I_y = 0.284 \times 10^{-4}\ m^4$ $I_z = 0.567 \times 10^{-4}\ m^4$
	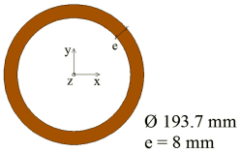	$A = 0.00467\ m^2$ $I_x = 0.202 \times 10^{-4}\ m^4$ $I_y = 0.202 \times 10^{-4}\ m^4$ $I_z = 0.402 \times 10^{-4}\ m^4$
	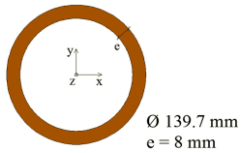	$A = 0.00331\ m^2$ $I_x = 0.072 \times 10^{-4}\ m^4$ $I_y = 0.072 \times 10^{-4}\ m^4$ $I_z = 0.144 \times 10^{-4}\ m^4$
Bracings	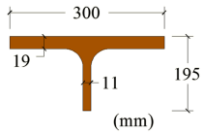	$A = 0.00764\ m^2$ $I_x = 0.189 \times 10^{-4}\ m^4$ $I_y = 0.428 \times 10^{-4}\ m^4$ $I_z = 0.776 \times 10^{-6}\ m^4$
Stiffeners	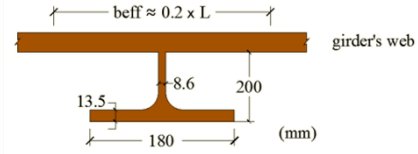	$A = 0.014\ m^2$ $I_x = 0.90 \times 10^{-4}\ m^4$

6.3.2.1.3 Bearings

The viaduct girders are directly supported in the piers by means of pot bearings, manufactured by ALGA. The model PN7500-1500-1500 was used for the fixed bearings. The models PNU7500/120-3000 and PNM7500/120/20 were used for the mobile bearings: the first allowing displacements only in the longitudinal direction and the latter allowing displacements in longitudinal and transverse directions. Figure 6.10 shows the design drawings of the PNM7500/120/20 bearing.

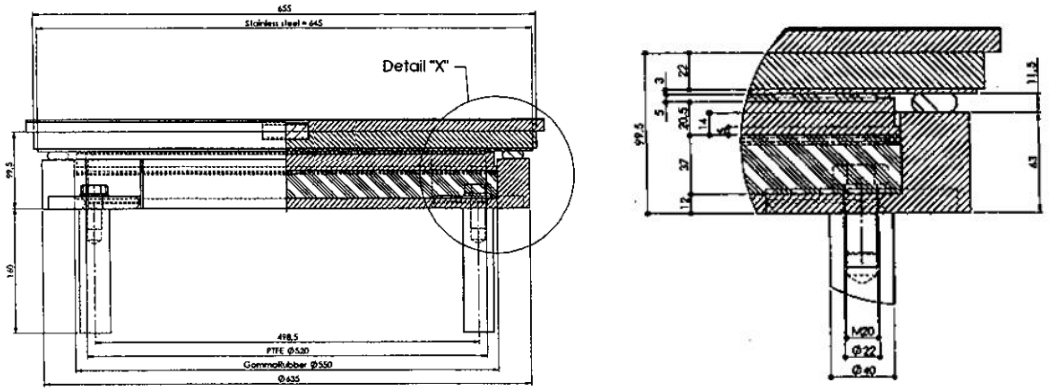

a) b)

Figure 6.10 – Design drawings of PNM7500/120/20 bearing: a) elevation view; b) detailed view

Due to the lack of information in the project documentation about the vertical bearings stiffness, a similar approach to the one followed by Ribeiro et al. (2012) was adopted in order to evaluate this parameter. Thus, a specific FE model of the mobile bearing was developed, based on the geometrical data specified in the design drawings, including the metallic pot, the elastomeric rubber pad, the piston, the Teflon layer and the upper metallic plate. All these elements were modelled in axisymmetric conditions, with exception of the interfaces between rubber-steel and Teflon-steel that were modelled by Coulomb friction elements with a resistance dependent of the normal load on sliding surface. Figure 6.11 illustrates a detailed view of the bearing's numerical model.

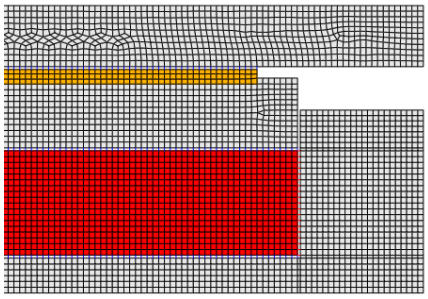

Figure 6.11 – Detailed view of the FE numerical model of the mobile bearing

The elasticity modulus for neoprene (E_{neop}) and Teflon (E_{Tef}) were considered equal to 10 MPa (Toolbox 2011) and 650 MPa (Fluorseals 2006), respectively. The Poisson's ratios of neoprene (ν_{neop}) and Teflon (ν_{Tef}) were taken equal to 0.48 (Rinde 1970) and 0.46 (Rae and Dattelbaum 2004), respectively. Values equal to 0.10 (Toolbox 2011) and 0.07 (Fluorseals

2006) were adopted to the friction coefficients in the neoprene-steel (μ_{neop}) and Teflon-steel (μ_{Tef}) connections, respectively.

The vertical bearing stiffness, k_v, was calculated as the quotient between the vertical load applied in the upper metallic plate, corresponding to a unit uniformly distributed load, and the average displacement of the plate. A value equal to 556.6 MN/m was achieved and adopted for all bearings in the numerical model.

Concerning the horizontal bearing stiffness, the results obtained from the calibration of the FE numerical model of Alverca viaduct (see Chapter 5) showed a systematic tendency for this parameter to present higher values comparatively to the values of the vertical stiffness, due to the fact that under ambient actions their movements are typically reduced and with tendency to act as fixed supports. Due to the lack of information about this parameter in the project documentation, a value of the horizontal bearings stiffness 10 times higher than the value considered to the vertical stiffness was adopted.

6.3.2.2 Railway track

Regarding the ballast properties, it should be pointed out that the adopted values, presented in Table 6.1, for the thickness and additional height of the ballast layer were obtained from several measurements performed in the structure during the experimental tests. In this model, a layer of constant thickness, equal to 0.40 m measured between the slab and the base of the sleepers, was adopted. The ballast between successive sleepers as well as the additional height laterally to these, with a height equal to 0.17 m, was considered as additional mass, using mass point elements concentrated at the nodes of the FEs of the upper face of the ballast layer. This FE model did not consider the explicit modelling of the additional ballast since it did not significantly influence the longitudinal stiffness of the track and, consequently, the composite effect between the deck and the track (ERRI 1997).

The adopted value for the ballast elasticity modulus comes from an experimental calibration of a railway track FE numerical model performed by Ribeiro (2012), studying also a bridge in the Portuguese railway network and using a similar modelling technique. The initial value for ballast density weight was adopted following the guidelines of standard EN1991-1-1.

The rail pads were modelled considering plan dimensions of 0.15×0.20 m^2, a thickness of 0.03 m and a modulus of elasticity equal to 500 MPa, leading to a vertical stiffness equal to

500 kN/mm. Due to the lack of information regarding the rail pads, these dimensions were adopted in order to get a vertical stiffness similar to that used by Ribeiro (2012) for a rail pad model Vossloh ZW687.

The geometrical and mechanical properties of the UIC60 rail were adopted following the guidelines of the standards EN 13674-1:2003 and UIC 861-3. The steel elasticity modulus and density weight were taken equal to 200 GPa and 7850 kg/m^3, respectively.

Concerning the concrete sleepers, as mentioned before, two different types of sleepers exist in the viaduct. For both of them, an approximate geometry to the type DW one was considered, with a length of 2.60 m and a trapezoidal cross section with the greater base equal to 0.20 m, the smaller base equal to 0.15 m and a height of 0.23 m. The density of these elements was corrected to take into account the change of geometry and the presence of reinforcements, resulting in values of 3010 kg/m^3 and 3899 kg/m^3 for types DW and T16, respectively. The concrete elasticity modulus and the Poisson's ratio were taken equal to 36 GPa (concrete strength class C45/55) and 0.2, respectively, for the sleeper type DW. For the sleeper type T16, in order to keep the real bending stiffness of the real element (around the horizontal barycentric axis, since the difference of dimensions in the sleeper's cross section is more evident), its concrete elasticity modulus was corrected, resulting in a value equal to 38.16 GPa.

6.4 Calibration of the numerical model

The calibration of the FE numerical model of the viaduct was performed based on the results of ambient vibration tests, described in the present section, which allowed the identification of modal parameters of the structure. The calibration process involved the pairing between numerical and experimental vibration modes, a sensitivity analysis and an optimisation process, both presented in this chapter.

6.4.1 Identification of modal parameters

Ambient vibration tests allowed the experimental identification of the modal parameters of the viaduct, namely its natural frequencies, mode shapes and damping coefficients. Specifically, this test enabled the identification of: global modal parameters (G), which involve

joined modal deflections of the girders and the RC slab; and local modal parameters (L), associated with local vibrations of the slab. Due to the low acceleration levels of the deck under ambient conditions, since railway traffic is not considered as an ambient action (as explained in Chapter 5), a forced excitation (Figure 6.12) of the structure was once again materialised by a group of people jumping randomly over the viaduct.

Figure 6.12 – External forced excitation applied during ambient vibration tests

A technique based on fixed reference points and mobile measuring points was implemented, involving 26 highly sensitive piezoelectric accelerometers model PCB 393B12. The data acquisition was performed using the cDAQ-9172 system from National Instruments (NI), equipped with Integrated Electronic Piezoelectric (IEPE) analogue input modules (NI 9234). The time series were acquired in periods of 6 min with a sampling frequency of 2048 Hz, which was then decimated to a frequency of 256 Hz.

The purpose of the dynamic test was the identification of the modal parameters related to vertical bending and torsion movements of the deck. For that reason, most of the accelerometers were installed in the vertical direction. However, there are also some transverse vibration modes that by structural compatibility present small scale movements in the vertical direction, showing a similar configuration with the vertical bending modes. Bearing this in mind, some accelerometers were also installed in the transverse direction in order to adequately distinguish the vertical from the transverse vibration modes of the deck.

Figure 6.13 shows the plan location of the measurement points, complemented with a detailed cross-section view, used for the identification of the modal parameters of the deck. Figure 6.13 a) presents the single setup used for the identification of global modal parameters,

which involved the use of 22 measurement points, distributed along the span and in the closest alignments of the main girders, and positioned in the vertical and transverse directions. Figure 6.13 b) presents the setup used for the identification of local modal parameters, which involved a total of 99 measurement points, all located in one half of the span and envisaging the measurement of accelerations only in the vertical direction. In the latter figure, the fixed reference locations are identified in black colour.

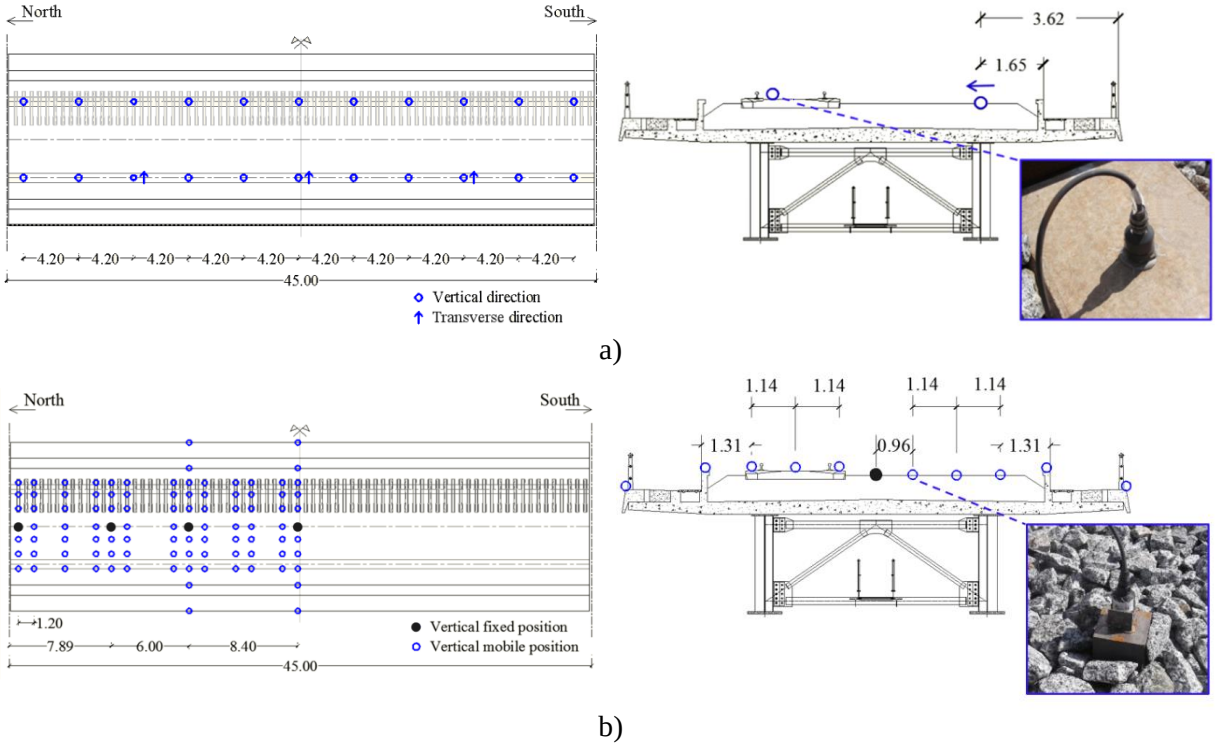

Figure 6.13 – Measurement points for the identification of modal parameters: a) global and b) local setups

The difficulties to access the bottom surface of the deck slab and the steel girders in safe conditions led to constraints in the positioning of the accelerometers. Consequently, all accelerometers were installed on the railway track and footway. In particular, the accelerometers were placed on the sleepers, through metallic plates bonded to the concrete surface, and directly in the ballast, through steel cubes, with dimensions $8 \times 8 \times 8\ cm^3$, previously installed within the ballast layer. In the setup for the identification of local modal parameters, some accelerometers were also placed on the ballast retaining walls and in the extremity of the footway cantilevers.

In this case, the modal parameters were estimated using the EFDD method available in the ARTeMIS software (ARTeMIS 2009). Figure 6.14 shows the curves of the average normalised

singular values of the spectral density matrices for the setup used to identify the global parameters [Figure 6.14 a)] and for all the experimental setups used to identify the local parameters of RC slab [Figure 6.14 b)].

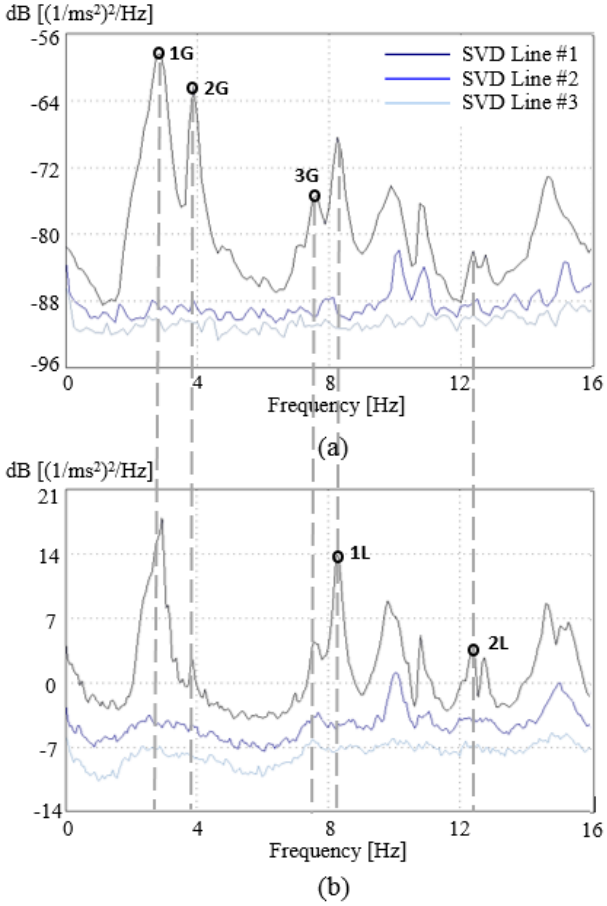

Figure 6.14 – EFDD method – average normalised singular values of the spectral density matrices: a) global and b) local

The peaks marked in each figure correspond to global (1G to 3G) and local (1L and 2L) vibration modes, respectively. The presence of other peaks, particularly in the frequency range between 9 Hz and 12 Hz, is related to vibration modes essentially involving movements in the transverse direction.

Figure 6.15 presents the identified mode shapes with the corresponding value of the natural frequency (f). The same figure also presents the numerical vibration modes obtained from a preliminary modal analysis of the numerical model, before calibration, considering the adopted values indicated in Table 6.1. For local vibration modes, there are detailed views of the half span where the accelerometers were installed, and also a global view of the span.

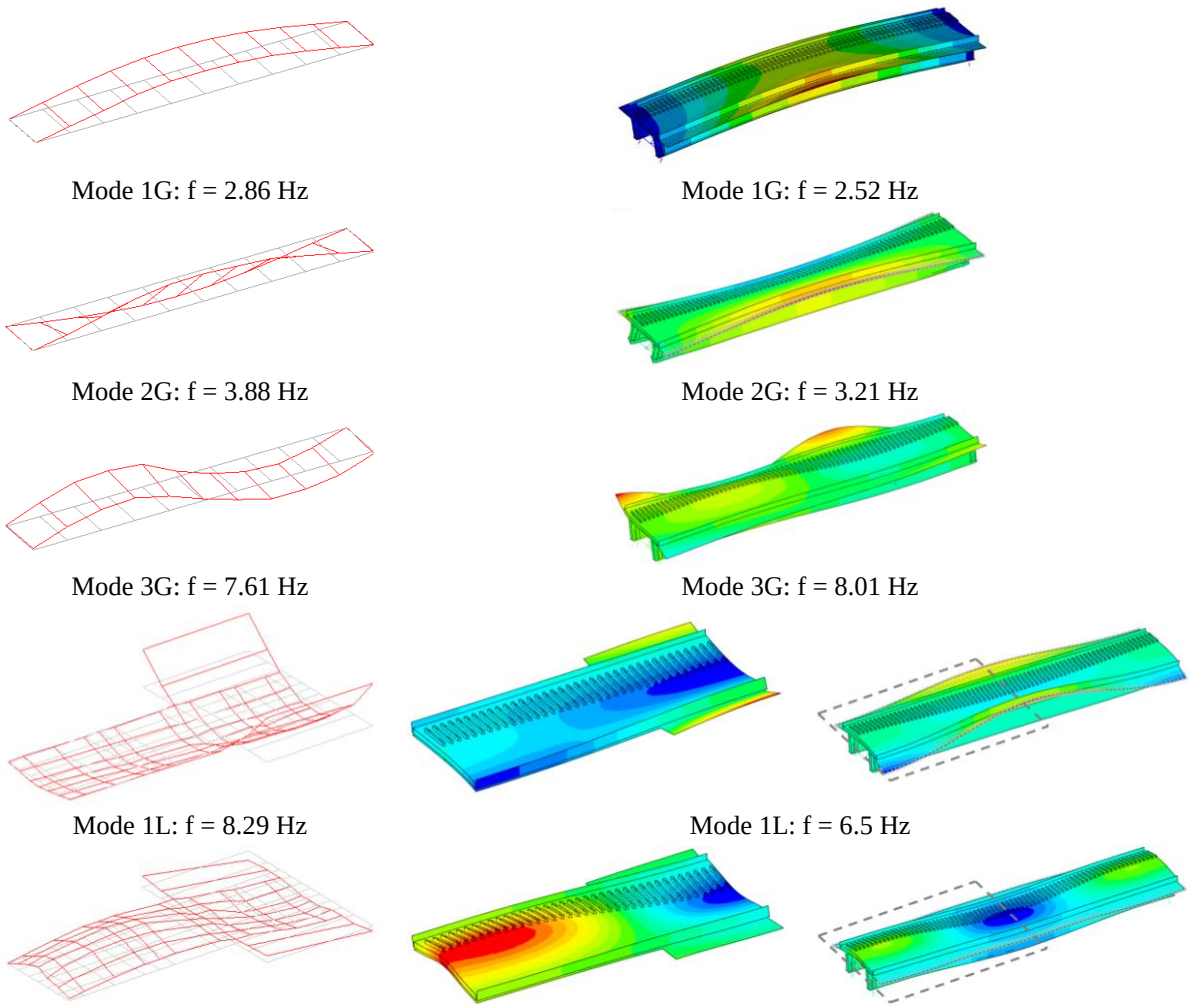

Figure 6.15 – Global (G) and local (L) vibration modes: a) experimental; b) numerical

Vibration modes 1G and 3G correspond to the bending movements of the entire span while vibration mode 2G is related to its torsion. Vibration mode 1L involves large movements of the footway cantilevers, which, in turn, produce movements in the central zone of the slab due to structural compatibility. Mode 2L is predominantly associated to bending movements of the central (i.e. between girders) zone of the upper slab.

It is important to note that the installation of accelerometers in the sleepers and in heavy steel cubes as well, placed within the ballast layer, has proved again to be particularly efficient in the identification of vibration modes of the slab, as shown in Chapter 5 for the case of the Alverca viaduct. In the Alcácer viaduct, this approach also allowed the identification of global

vibration modes since the accelerometers were placed near the longitudinal alignment of the girders.

Table 6.3 shows the mean values of the damping coefficients for all vibration modes and the corresponding values of the standard deviation. The latter are only presented for the local vibration modes, which were obtained from several experimental setups rather than the ones related to global vibration modes that were obtained resorting to only one measurement setup. Since the vibration modes are mainly associated with vertical movements of the deck, only the experimental results recorded in the vertical direction were used for this estimation. Figure 6.16 illustrates the variation of the modal damping coefficient of each local vibration mode, obtained for each experimental *setup*.

Table 6.3 – Statistical properties of the damping coefficients of the global vibration modes

Vibration mode	Damping coefficient (%)	
	Mean value	Standard deviation
1G	2.82	-
2G	2.28	-
3G	2.40	-
1L	1.19	0.690
2L	1.33	0.469

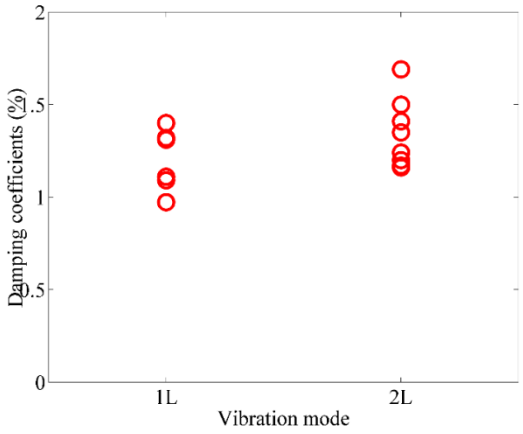

Figure 6.16 – Damping coefficients of the local vibration modes

6.4.2 Calibration

The calibration of the viaduct FE model was based on the results of the ambient vibration tests, presented in the previous section, and involved the application of the same iterative

procedure referred in Chapter 4 and used in Chapter 5. The optimisation process (section 6.4.2.3) was preceded by the mode pairing between numerical and experimental vibration modes (section 6.4.2.1) and a sensitivity analysis to the parameters of the numerical model (section 6.4.2.2).

6.4.2.1 Mode pairing criteria

The mode pairing technique establishes the correspondence between each experimentally obtained mode and one numerically derived mode. In the present case study this correspondence is performed by using the EMAC parameter, for global and local vibration modes. In this specific case, the MAC criterion did not allow a stable and evident pairing between experimental and numerical vibration modes as demonstrated by the correlation matrices shown in Figure 6.17. As noted, higher MAC coefficients were obtained in the correlation between several numerical modes and the same experimental vibration mode.

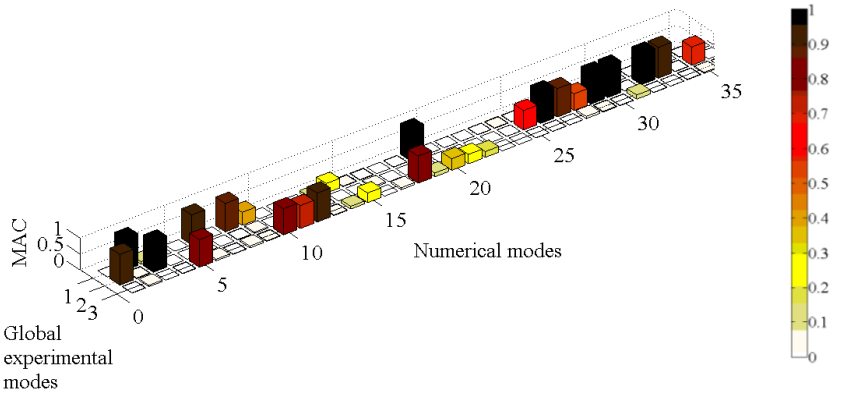

a)

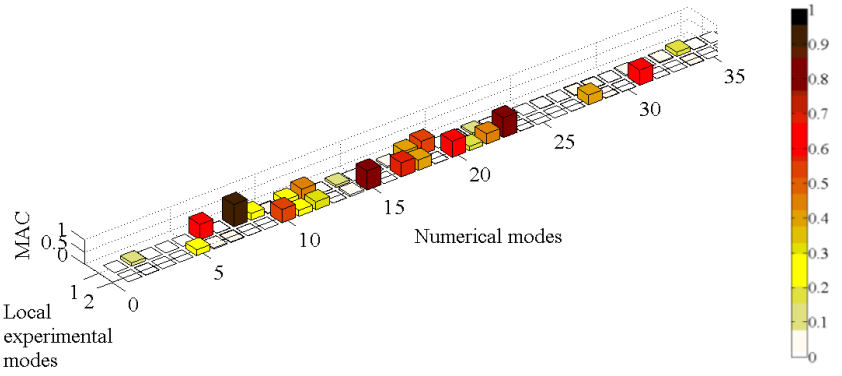

b)

Figure 6.17 – MAC correlation matrices between experimental and numerical modes: a) global; b) local

Regarding the EMAC criterion for the mode pairing, Figure 6.18 presents the four *clusters* that were defined based on the positioning of the sensors in the experimental test. Only accelerations in the vertical direction were recorded, reason why these *clusters* include only the translational DOFs in the vertical direction of the cantilevers, inner slab and steel I-girders. The *cluster* denominated as other elements contains the remaining DOFs of the structure.

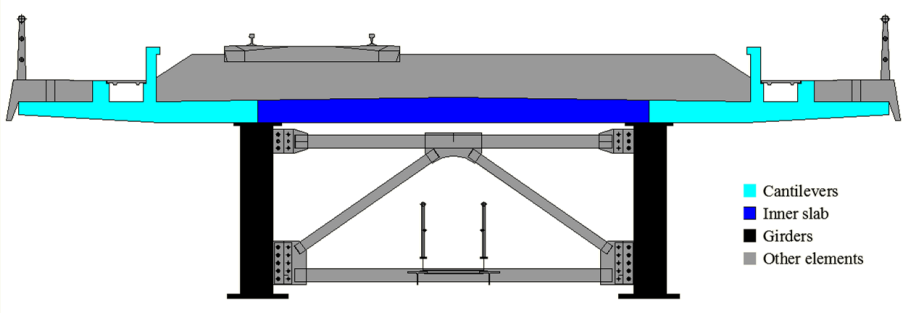

Figure 6.18 – Clusters used in the mode pairing process

Figure 6.19 shows the values of the relative modal strain energy for the referred *clusters*, considering 35 numerical vibration modes of the initial FE model (natural frequencies up to ≈ 15 Hz). Global vibration modes are related to higher energy values on the main girder's *cluster* while local vibration modes are associated to higher energy values on the inner slab's and cantilevers' *clusters*. Considerable values of energy of the *cluster* "Other elements" appear above the fourteenth vibration mode, which are related to local vibration modes of the metallic structure of the deck.

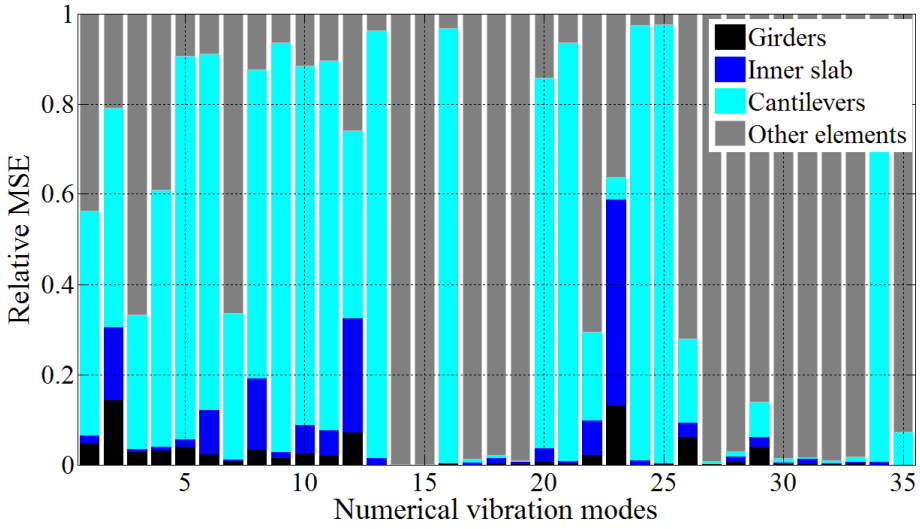

Figure 6.19 – Relative modal strain energy of each vibration mode based on the initial FE model

Figure 6.20 illustrates the EMAC correlation matrices between experimental and numerical vibration modes of the initial finite element model. In opposition to the results presented in Figure 6.17, by observing this figure one can notice that the EMAC criterion provides a stable and separate pairing between each experimental and numerical vibration mode. The EMAC values for the global vibration modes were obtained by weighing the MAC values with the modal strain energy of the main girders' *cluster*, since the accelerometers were installed specifically to identify movements of these structural elements. In the case of local vibration modes, the MAC values were weighted with the modal strain energy related to the inner slab's and cantilevers' *clusters*. To improve the efficiency of the pairing of modes 1L and 2L in addition to the adoption of EMAC values, frequency limits were imposed to avoid pairing with other vibration modes.

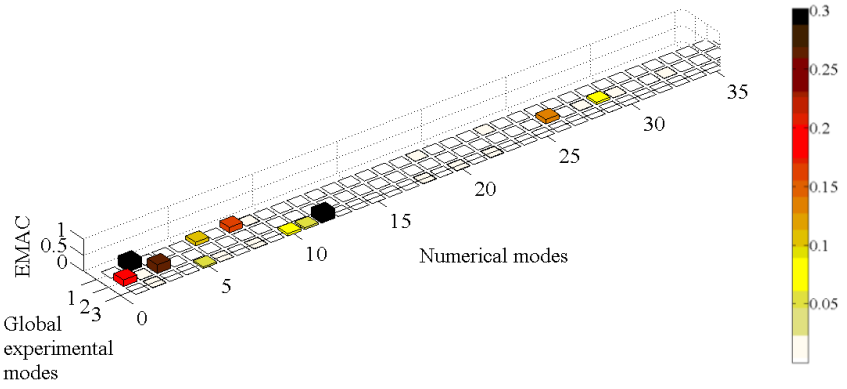

a)

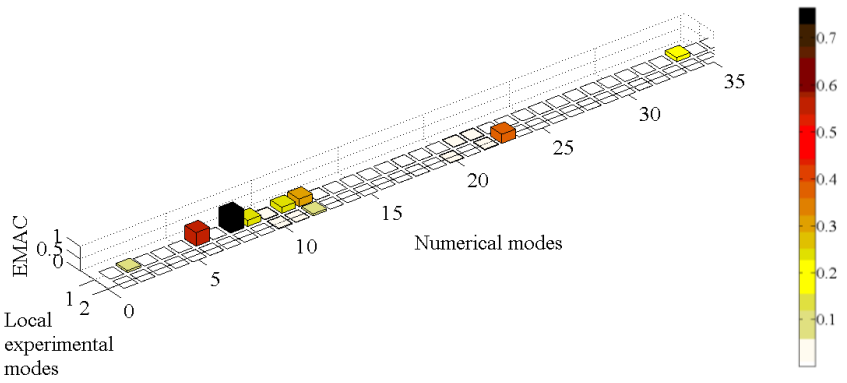

b)

Figure 6.20 – EMAC correlation matrices between experimental and numerical modes: a) global; b) local

6.4.2.2 Sensitivity analysis

The sensitivity analysis allowed the selection of the parameters that most influence the frequencies and MAC values of the global and local vibration modes and, consequently, should be included in the subsequent optimisation phase. For the variable parameters among the ones previously indicated in Table 6.1, their statistical properties and the lower/upper limits (which will later be taken into account during the optimisation process) are presented in Table 6.4. The bibliographic references which support the adopted values are shown in the same table. Additional explanations about the adopted limits of variation are shown below.

Table 6.4 – Statistical properties of the numerical parameters

	Parameter	Designation	Statistical distribution		Limits (lower/upper)	Unit	References
			Type	Mean value/ standard deviation			
Deck	t_c	Thickness of the RC slab (central zone)	normal	0.362 / 0.0362	0.308 / 0.416	m	(JCSS 2001, Henriques 1998, Wisniewski 2007)
	E_c	Concrete elasticity modulus	normal	42.6 / 4.26	35.6 / 49.6	GPa	(Henriques 1998, Mirza et al. 1979)
	ρ_c	Concrete density weight	normal	2446.5 / 97.86	2285.5 / 2607.5	kg/m^3	
	E_s	Steel elasticity modulus	normal	200 / 8.0	187 / 213	GPa	(Hess et al. 2002)
	ρ_s	Steel density weight	normal	7850 / 314	7334 / 8367	kg/m^3	
	k_v	Vertical bearing stiffness	log-normal	5766 / 6403	100 / 3500	MN/m	-
	k_h	Longitudinal bearing stiffness	uniform	- / -	0 / 15000	MN/m	-
Track	t_{bal}	Thickness of the ballast layer	normal	0.40 / 0.02	0.37 / 0.43	m	-
	h_{bal}	Additional height of the ballast	uniform	0.17 / 0.03	0.12 / 0.22	M	-
	E_{bal}	Ballast elasticity modulus	uniform	140 / 34.6	80 / 200	MPa	(UIC 2008, Knothe and Wu 1998)
	ρ_{bal}	Ballast density weight	uniform	1875 / 129.9	1650 / 2100	kg/m^3	(Fortunato 2005)

Regarding the thickness of the RC upper slab, a coefficient of variation equal to 4 % was adopted, following the suggestions of Wisniewski (2007) for cast in-situ RC slabs, which may be modelled considering a normal distribution with a standard deviation varying between 10 and 15 mm. This corresponds to the coefficient of variation initially adopted, however, a higher value was after considered (equal to 10 %) in order to correct the stiffness of the initial FE model, since in the first optimisation analyses the thickness of the slab tended always to assume the lower limit initially defined.

According to the suggestions referred in section 5.4.2.2, values of 10 % and 4 % were adopted for the coefficients of variation of concrete elasticity modulus and density weight, respectively.

Based on results of experimental tests performed on about 600 steel specimens, Hess et al. (2002) concluded that the steel elasticity modulus follows a normal distribution with mean value in the range 202-215 GPa and a coefficient of variation in the range 0.5-6 %. Bearing this in mind, a value of 4 % was adopted for the coefficient of variation of both the steel elasticity modulus and density weight.

Regarding the vertical bearing stiffness, a specific study was carried out in order to characterize the statistical distribution of this parameter using a methodology based on the Latin Hypercube method, similar to that followed by Ribeiro (2012), and using the numerical model aforementioned in section 6.3.2.1.3. The uniform distributions of the parameters used in the numerical model are characterised in Table 6.5.

Table 6.5 – Statistical properties of the parameters of the bearing's FE model

Parameter	Description	Statistical properties		Unit
		Type	Limits (lower/upper)	
E_{neop}	Neoprene elasticity modulus	Uniform	10 / 100	MPa
ν_{neop}	Neoprene Poisson's ratio		0.47 / 0.4999	-
μ_{neop}	Neoprene-steel friction coefficient		0.005 / 0.20	-
E_{Tef}	Teflon elasticity modulus		600 / 700	MPa
ν_{Tef}	Teflon Poisson's ratio		0.44 / 0.47	-
μ_{Tef}	Teflon-steel friction coefficient		0.06 / 0.10	-

Figure 6.21 shows the vertical bearing stiffness distribution obtained on the basis of 750 samples, which showed to be particularly sensitive to variations of the neoprene elasticity modulus and respective Poisson's ratio. The sample distribution was adjusted based on a log-normal probability density function with a mean value of 5766 MN/m and a standard deviation of 6403 MN/m.

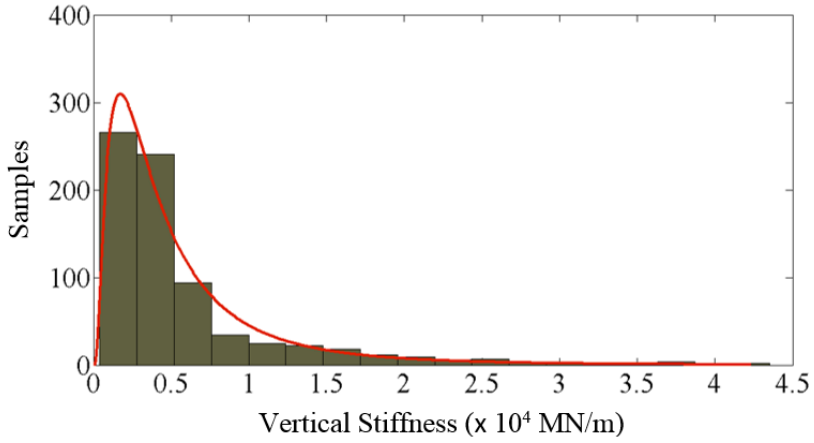

Figure 6.21 – Adjustment of a log-normal probability distribution function to the FE model results for the vertical bearing stiffness

Concerning the horizontal bearing stiffness, the results presented in Chapter 5 showed a systematic tendency for this parameter to present higher values comparatively to the values of the vertical stiffness, due to the fact that under ambient actions their movements are typically reduced and with tendency to act as fixed supports. Bearing this in mind, in terms of parameter's limits, the assumed lower and upper values correspond to situations where the bearing is unconstrained (0 MN/m) and fully constrained (15000 MN/m), respectively. In the latter case, the horizontal stiffness value corresponds approximately to the bending stiffness, in the longitudinal direction, of a group of viaduct's piers fully constrained at their base.

Figure 6.22 depicts the results of a global sensitivity analysis through a Spearman correlation matrix (Brehm et al. 2010). The correlation coefficients located in the range [-0.25; 0.25] were excluded from the graphical representation. By observing the Spearman matrix, one can realize that only three parameters have a preponderant influence in natural frequencies and MAC coefficients, namely, the RC slab thickness, the vertical bearing stiffness and the horizontal stiffness of the guided bearings. The remaining numerical parameters have minor influence over the modal responses and therefore were excluded from the optimization phase.

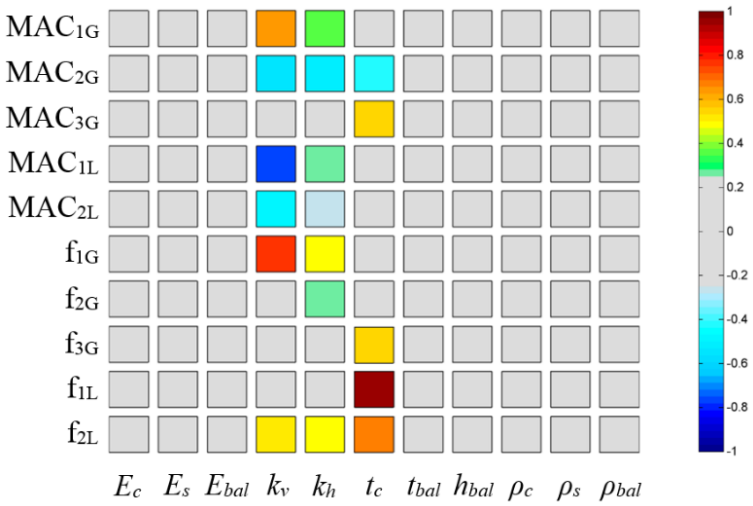

Figure 6.22 – Spearman correlation matrix

6.4.2.3 Optimisation

The optimisation was carried out in order to obtain the optimum values, for the three parameters identified in the sensitivity analysis, which minimise the differences between numerical and experimental modal responses. This phase involved the definition of an objective function, which is equal to that presented in Equation 5.8, and the application of an optimisation technique based on a genetic algorithm.

The optimisation of the model involved the use of 3 design variables (the 3 parameters of the numerical model) and 10 modal responses (5 frequencies and 5 MAC values) regarding the global and local vibration modes of the structure. The genetic algorithm was based on an initial population, consisting of 30 individuals and 150 generations, in a total of 4500 individuals. Table 6.6 shows the values of the numerical parameters, obtained from three independent optimisation runs (GA1 to GA3) based on different initial populations.

Table 6.6 – Optimal numerical parameters for the independent optimisation runs GA1 to GA3

Parameter	Optimal value			Unit
	GA 1	GA 2	GA 3	
t_c	0.400	0.405	0.405	m
k_v	474.5	493.5	490.6	MN/m
k_h	8199	7177	6488	MN/m

The parameters that demonstrated to have more influence over the modal responses, in particular, the thickness of the RC slab and the vertical bearing stiffness provide estimates with lower variability. Furthermore, the horizontal stiffness of the mobile bearings, which have less influence on the modal responses, tend to present higher variations for the different optimisation runs. The optimal set of parameters used in the updated numerical model concerns to the parameters' values obtained from the GA3 optimization run, which presented the lowest residual of the objective function.

Figure 6.23 presents a comparison in terms of frequencies [Figure 6.23 a)] and MAC parameters [Figure 6.23 b)], before and after calibration. The natural frequencies obtained experimentally are also shown in the figure. The average error of the frequencies of global modes decreased from 10.8 % before calibration to 7.6 % after calibration. For local modes, it varied from 12.0 % to 7.7 %, before and after calibration, respectively. The average value of the MAC coefficients increased from 0.908 to 0.929 for global modes and from 0.853 to 0.869 for local modes, before and after calibration, respectively.

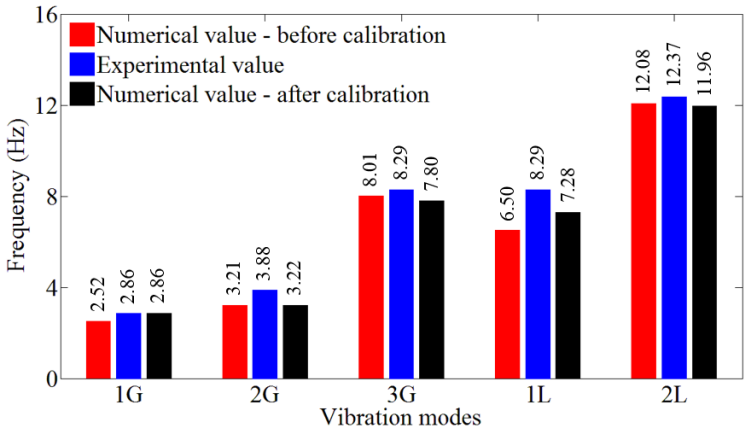

a)

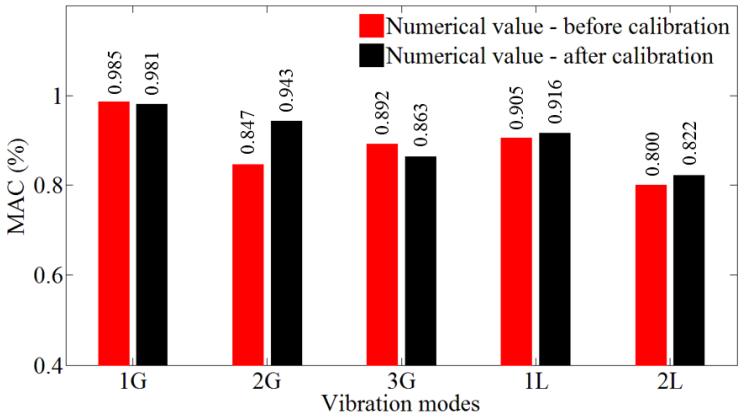

b)

Figure 6.23 – Modal parameters' values before and after calibration: a) frequencies and b) MAC

Figure 6.24 presents a comparison between experimental and numerical modal configurations, before and after calibration. There is a good match between the numerical and experimental mode shapes, particularly in global vibration modes.

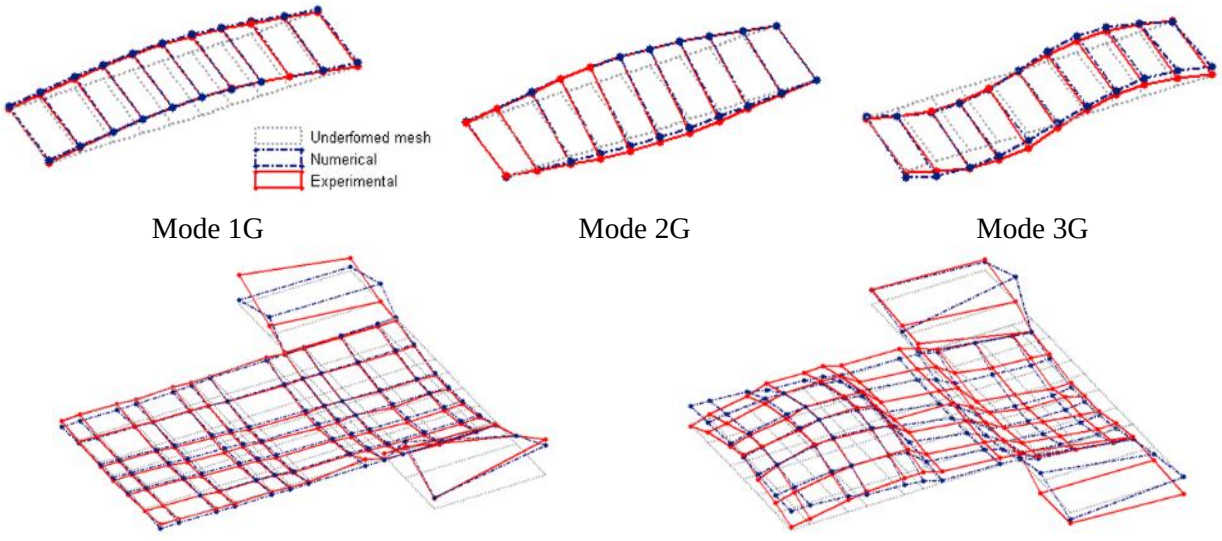

Mode 1G Mode 2G Mode 3G

Mode 1L Mode 2L

Figure 6.24 – Comparison between experimental and calibrated numerical mode shapes

6.5 Experimental validation of the numerical model

6.5.1 Dynamic test under railway traffic

6.5.1.1 Description

A dynamic test under railway traffic allowed the measurement of the dynamic response in terms of displacements, deformations and accelerations at several locations of the RC slab for the passage of the AP train at a speed of 220 km/h. Figure 6.25 shows a schematic representation of the location of the sensors in a lateral view of approximately half-span and in the cross-section of the deck.

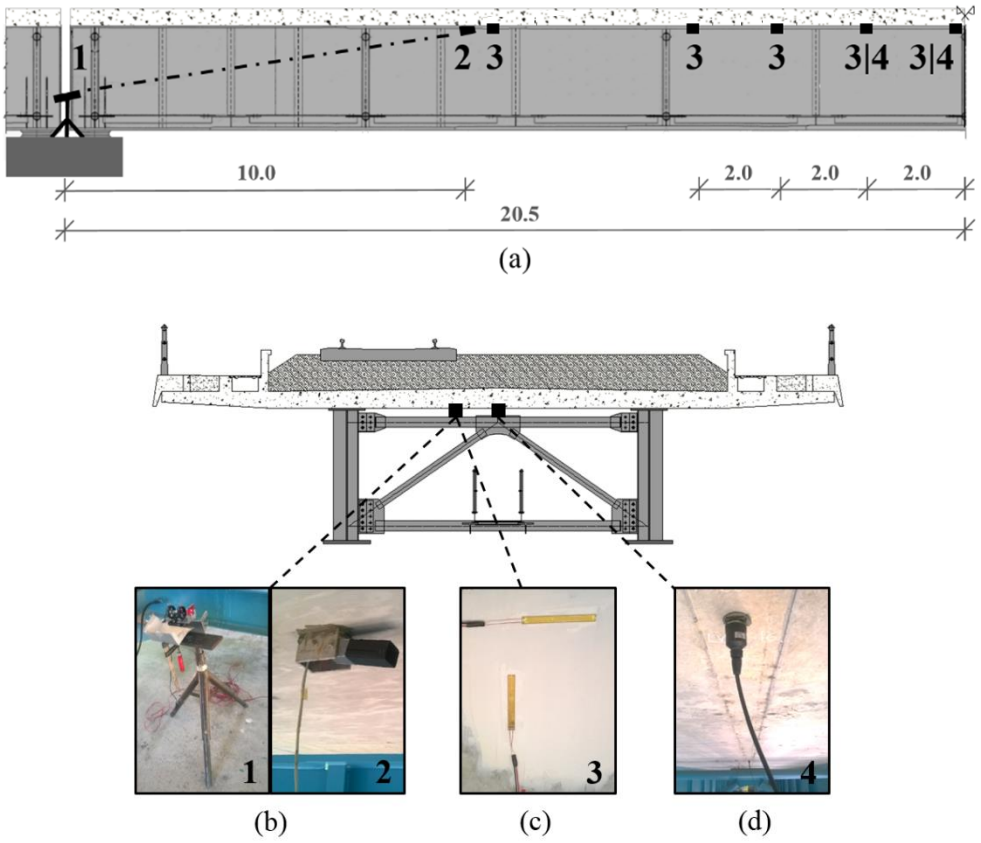

Figure 6.25 – Location of the sensors to measure the RC slab dynamic response under railway traffic: (a) lateral view; (b) displacements, (c) deformations and (d) accelerations in the cross-section

The vertical displacement was measured by a system based on a diode laser module installed in the top of the southern pier [Figure 6.25 (b1)] and a *Position Sensitive Detector* (PSD) attached to a support fixed on the slab [Figure 6.25 (b2)], approximately at 10 m away from the

pier, as schematically shown in Figure 6.25 (a). More details about this system can be found in Pinto et al. (2009).

The deformations were measured by electrical resistance strain gages, model Vishay N2A-06-20CBW-350, bonded to the concrete surface at the mid-span section and mounted as 1/4 Wheatstone bridge in the longitudinal and transverse directions [Figure 6.25 (c)]. Figure 6.26 shows the location of the strain gages throughout the span. The vertical acceleration was measured using a piezoelectric accelerometer, PCB model 393A03 [Figure 6.25 (d)], positioned at the mid-span section of the deck. The data acquisition was performed using the cDAQ-9172 system from NI, equipped with IEPE analog input modules NI 9234 for accelerometers, NI 9239 for the laser system and NI 9237 for strain gages. The data were acquired at a sampling rate of 2048 Hz and then decimated to 1024 Hz.

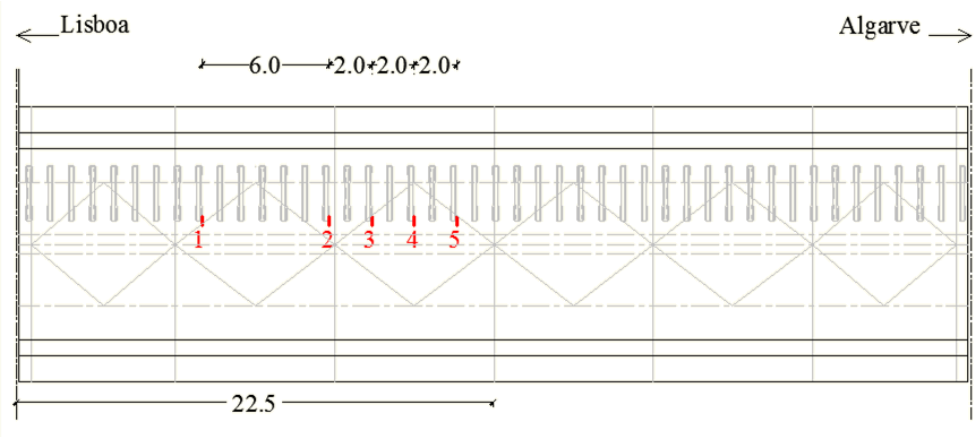

Figure 6.26 – Plan view with the location of the strain gages throughout the span

6.5.1.2 Modal damping estimation

Measuring the slab's acceleration responses allowed the estimation of modal damping coefficients, following the same 2-phase methodology presented in section 5.6.3.2.1. Two distinct positions of the slab´s central alignment were also considered: at the mid-span section and at 2 m apart the mid-span section, according to the details of Figure 6.25 (a). The acceleration records were filtered by a Chebyshev (type II) low-pass digital filter of order 20, a stopband attenuation equal to 45 dB and a cut-off frequency equal to 60 Hz.

In phase 1 (that involves the detection of the train axles position in each instant of time) a double integration of the acceleration records was performed in order to obtain the displacements of the deck slab. Then, a Chebyshev (type II) high-pass digital filter, with cut-off

frequency of 1.3 Hz, allowing to remove the quasi-static component of the response, was applied, in order to obtain only the dynamic component of displacements.

Figure 6.27 illustrates, as example, the acceleration record obtained for the passage of the AP train at 220 km/h at the mid-span section [Figure 6.27 (a)] and the correspondent dynamic displacement record [Figure 6.27 (b)]. The latter allowed determining the precise instant of time when each train axle crosses a certain bridge position, through the comparison between experimental and numerical displacement records. Such instants of time are shown, in Figure 6.27 (b), by means of a train image. Each train axle is drawn in a positon corresponding to the instant of time when it crosses the mid-span section of the deck.

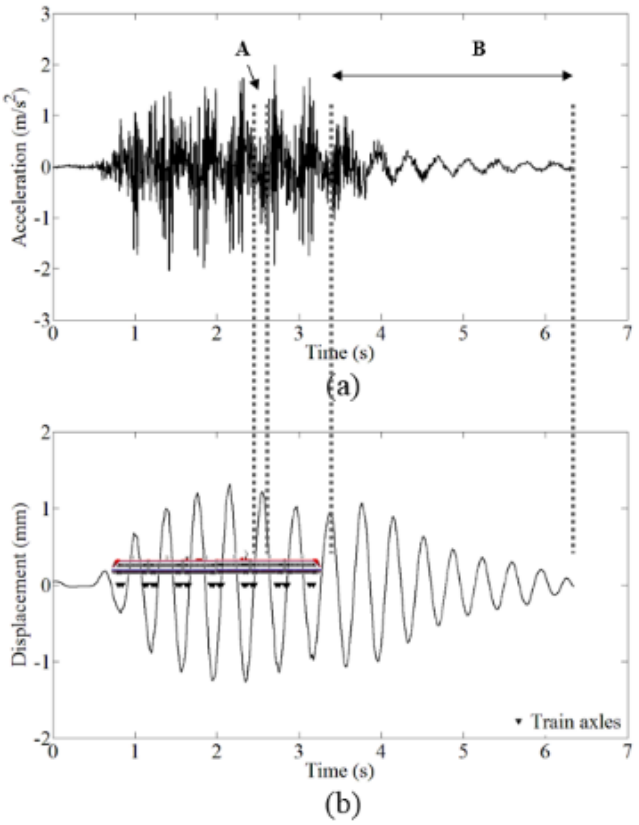

Figure 6.27 – Dynamic results at mid-span section for the passage of the AP train at 220 km/h: (a) vertical acceleration; (b) vertical dynamic displacement

In phase 2, the damping identification is performed for local vibration modes, based on the accelerations measured after the passage of each axles group in a section, and for global vibration modes, based on the free-vibration time interval after the last train's axle group leaves the bridge. Figure 6.27 identifies these two specific time intervals, marked with dotted lines:

one considering the vibration period between the passage of two consecutive axles groups (A) and the other related to the free-vibration time interval after the passage of the train (B).

Based on the partial acceleration records, for the time intervals A and B, auto-spectra were determined in order to identify the significant natural frequencies that take part in each response. Then, a band-pass digital filter, centred on a natural frequency of the structure, associated with a local or global vibration mode, was applied to the acceleration record. After that, an exponential decay function was adjusted to the local maximum values of the filtered response, in order to obtain the damping coefficient of each vibration mode by application of the logarithmic decrement method.

To exemplify this procedure, Figure 6.28 a) and b) shows the auto-spectra of the accelerations records for the time intervals A and B marked in Figure 6.27, respectively. The shaded regions in Figure 6.28 represent the applied band-pass filters in each situation. The acceleration time histories presented in each figure show the filtered responses with the isolated contribute of the vibration modes with frequencies equal to 44 Hz (local mode) and 2.86 Hz (global mode), which led to damping coefficient estimates equal to 3.98 % and 3.81 %, respectively. The configurations of both local and global vibration modes are also presented in Figure 6.28 a) and b), respectively. Even though the local vibration mode of the slab with a frequency equal to 44 Hz was not experimentally identified, probably due to the characteristics of the forced external excitation used in the dynamic test, it should be refereed that under traffic actions it has an important contribute to the overall dynamic response of the slab.

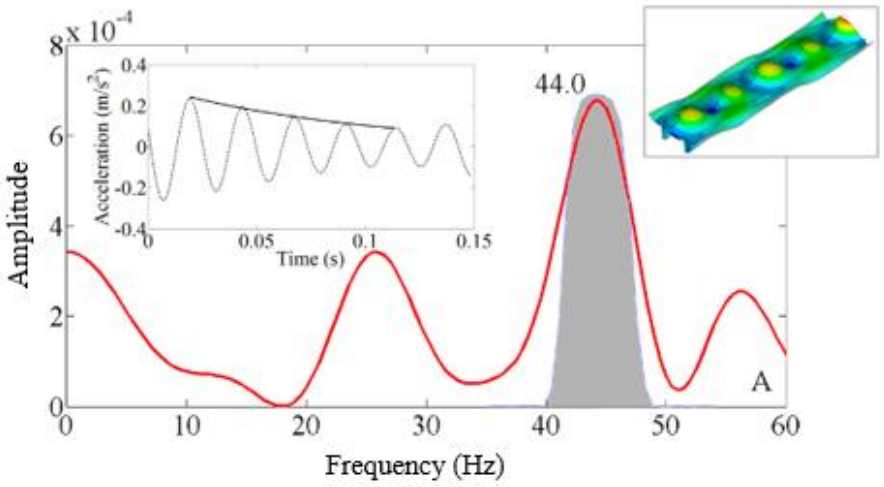

a)

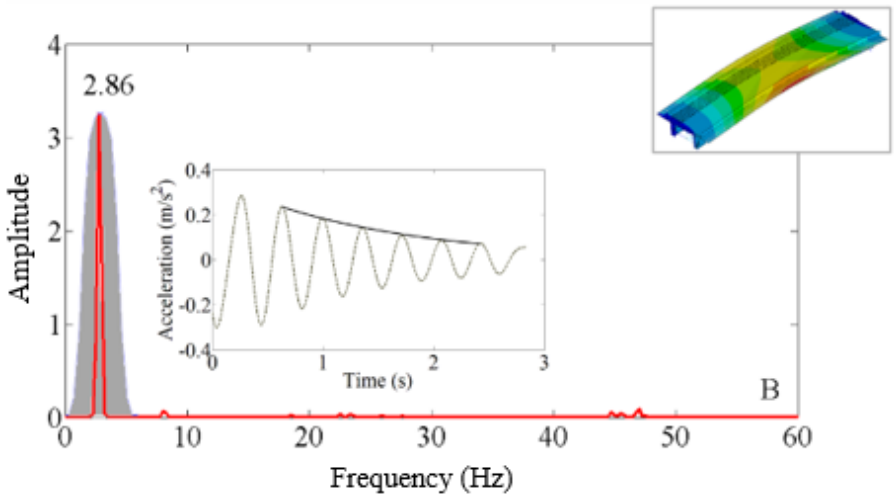

b)

Figure 6.28 – Auto-spectra and filtered acceleration records: a) local and b) global (1G) vibration modes

This procedure was applied for the passage of each of the axles groups existing by train, in two sections of the viaduct, and considering the passage of two AP trains at the speed of 220 km/h, giving rise to 12 estimates of the damping coefficient for local vibration modes. Due to the mode shape similarity of all local vibration modes of interest, particularly with bending movements at the central zone of the deck slab, the results of the damping coefficients were grouped, leading to a mean value equal to 5.08 % and a standard deviation equal to 1.53 %.

Concerning the damping coefficients associated with global mode 1G, 4 estimates were obtained, in correspondence with the two instrumented sections of the viaduct and for the passage of two AP trains, leading to a mean value equal to 3.71 % and a standard deviation equal to 0.08 %.

6.5.2 Validation

The validation of the bridge's numerical model was made by comparing the results of numerical simulations, considering train-bridge dynamic interaction, and the results from the dynamic test under railway traffic.

The FE model calibration was based on the results of the ambient vibration tests. However, the vibration levels reached in that test are much lower than the vibration levels under railway traffic. Following the same approach explained in Chapter 5, in order to achieve a better

similarity with the observed structure behaviour (measured results), some modifications were done initially in the calibrated FE model and in the modal damping coefficients, particularly: i) a correction in the value of the longitudinal stiffness of the guided supports, in order to take into account the nonlinear behaviour of the supports under traffic actions; ii) a modification of the modal damping coefficients values, from those obtained in the ambient vibration test to those identified in the dynamic test under railway traffic, in order to reproduce the increase of damping with the increase of vibration under traffic actions (a detailed description of the adopted values is given in the following sub-sections).

Furthermore, the effect of other parameters in the comparison between numerical and experimental responses, such as the train speed, the cut-off frequency values, the track irregularities and the damping coefficient of higher-order local vibration modes, was analysed.

6.5.2.1 Train-Bridge Interaction dynamic analysis

The numerical dynamic analysis considered the interaction between the train and the bridge and included the measured track irregularities. A 3D numerical model of the AP train was used. The model was presented in Chapter 2 and previously applied in the calculations shown in Chapter 5.

The track irregularities were obtained based on records provided by the track inspection vehicle EM 120 from REFER. Figure 6.29 illustrates the longitudinal levelling profiles of the left and right rail, in a track section with 45.0 m corresponding to the length of the simply supported span under study. The adopted irregularities consider the contribution of wavelengths in the ranges 1-70 m and wavelengths below 1 m, taken from the rail corrugation profile also provided. In order to ensure a correct representation of the main vibration modes of the structure and the excitation frequencies due to track irregularities, the irregularities profiles were filtered at a minimum wavelength of 0.55 m, taking into account the time increment considered equal to 0.001 s and the train frequent speed equal to 220 km/h.

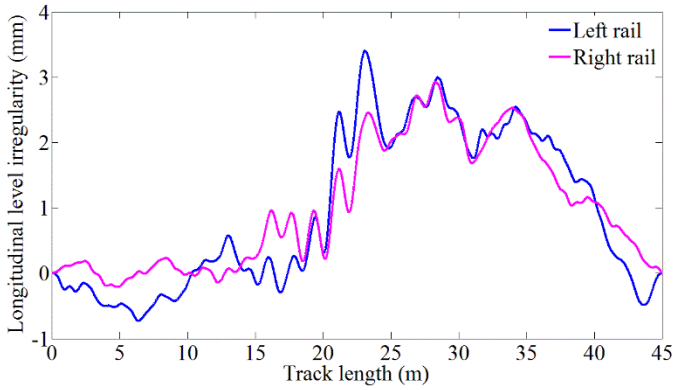

Figure 6.29 – Left and right rails' longitudinal levelling profiles

Bearing in mind the frequencies values related both to the train action and the vibration modes experimentally identified, generically with frequencies up to 15 Hz, this threshold was considered in a first validation of the FE model, evaluating the influence of the longitudinal bearing stiffness and local modal damping coefficients in the dynamic response. Afterwards, the influence of different cut-off frequencies in the response, namely up to 20 Hz, 30 Hz and 60 Hz, the influence of the train speed and the effect of different irregularities profiles were analysed.

The integration time increment was equal to 0.001 s. The modal damping coefficients were defined, in a first approximation, based on the results of the ambient vibration tests: the global and local identified vibration modes took the values presented in Table 6.3; for the remaining global and slab's local vibration modes, the adopted modal damping coefficients were the average of the values experimentally identified (2.5 % for global modes and 1.3% for local ones). A value of 0.5 % was adopted for the remaining vibration modes (local vibration modes of the steel structure), following the guidelines of the EN1991-2 (2003) standard for this type of structure. In order to avoid using a high number of vibration modes to solve the bridge subsystem's dynamic equations, the static correction procedure presented in section 5.6.2 was implemented.

6.5.2.2 Influence of the longitudinal bearing stiffness

According to the results presented in Chapter 5, the existence of a nonlinear behaviour of the supports in the longitudinal direction under traffic actions was proved once again. Typically,

guided or mobile bearings tend to work as fixed bearings under ambient actions and as mobile bearings under railway traffic actions.

A modified numerical model of the bridge, denominated as Model 2, was obtained from the updated numerical model, denominated as Model 1, by a successive reduction of the longitudinal stiffness of the supports, originally at 6488 MN/m, until reaching a value of 1180 MN/m, which guarantees the best agreement in terms of the slab's vertical displacement. Table 6.7 shows the vibration frequencies and MAC values of numerical Models 1 and 2. In a general way, there is a decrease in the structure's vibration frequencies, when Model 2 is considered, especially for vibration mode 1G.

Table 6.7 – Vibration frequencies and MAC values obtained from numerical Models 1 and 2

Vibration mode	Frequency (Hz)		MAC (%)	
	Model 1	Model 2	Model 1	Model 2
1G	2.86	2.63	0.981	0.980
2G	3.22	3.21	0.943	0.966
3G	7.81	7.74	0.863	0.923
1L	7.28	7.26	0.916	0.905
2L	11.96	11.96	0.822	0.746

Figure 6.30 shows a comparison between the experimental and numerical responses based on Models 1 and 2, for the passage of an AP train at a speed of 220 km/h. The displacements records were obtained in a section 10 m away from the support and the deformations and accelerations records were obtained near the mid-span section (position of the strain gage 5 depicted in Figure 6.26). A better agreement can be clearly observed when the numerical Model 2 is used, thereby confirming the relevance of the nonlinear behaviour of the guided supports in the longitudinal direction.

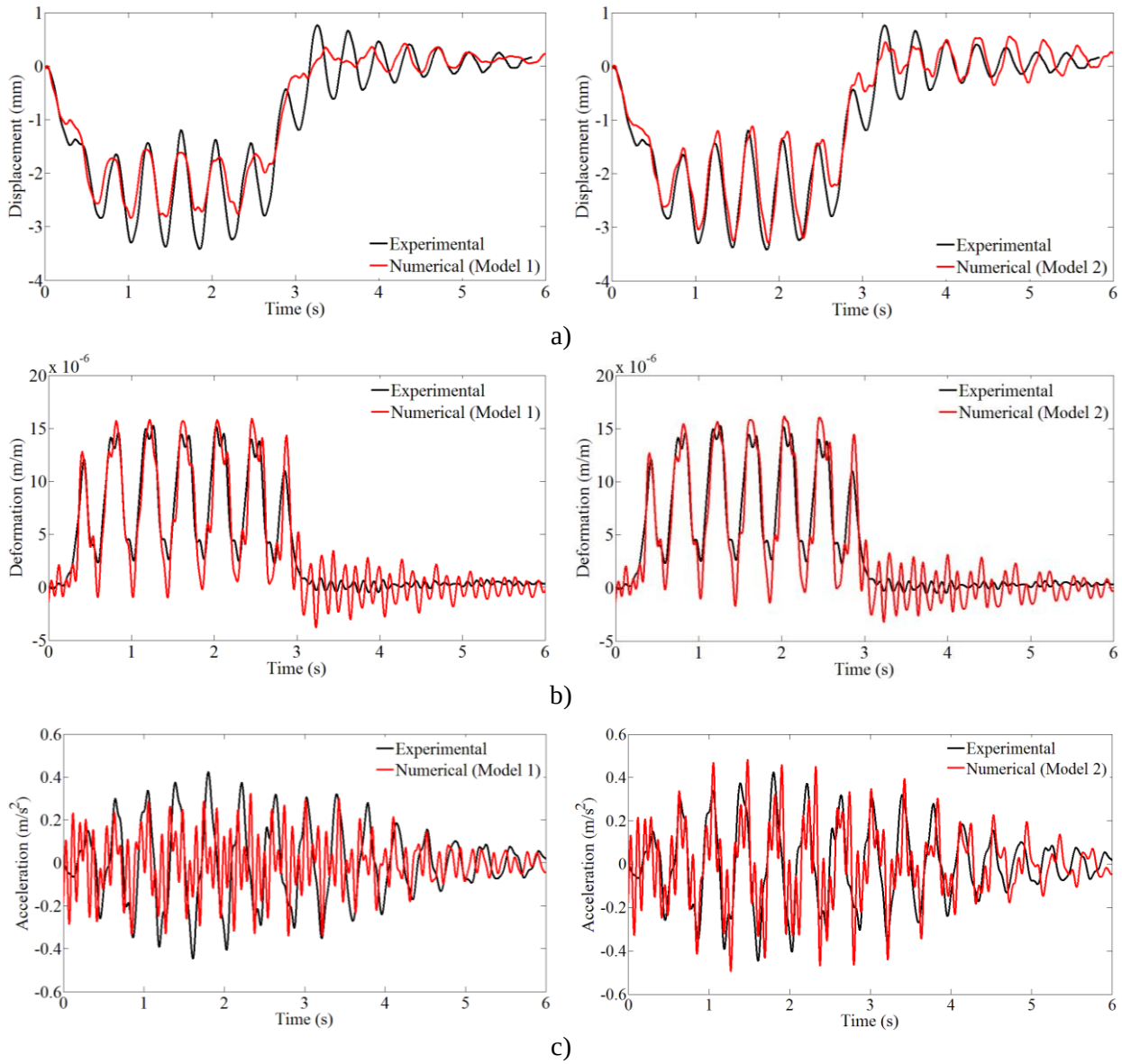

Figure 6.30 – Comparison between experimental and numerical RC slab dynamic responses according to Models 1 and 2: a) vertical displacement; b) transverse deformation; c) vertical acceleration

Figure 6.31 shows the auto-spectra in correspondence to the time history records of accelerations presented in Figure 6.30 c). By observing this figure, one can notice that the experimental response is dominated by a frequency equal to 2.63 Hz, which corresponds to the vibration mode 1G. Only by correcting the horizontal stiffness of the guided supports in Model 2, a better match between the numerical and experimental frequency of the global vibration mode 1G was achieved. Numerical frequencies equal to 7.30 Hz and 11.90 Hz, corresponding to local vibration modes 1L and 2L respectively, remain unchanged in both numerical models because the change in the horizontal stiffness of the supports presents low

correlations with the local modal parameters of the RC slab, as stated in the sensitivity analysis results (see Figure 6.22). The considerably higher amplitudes in the numerical auto-spectra, comparatively to experimental ones, may probably suggest the need to adjust the adopted modal damping coefficients values.

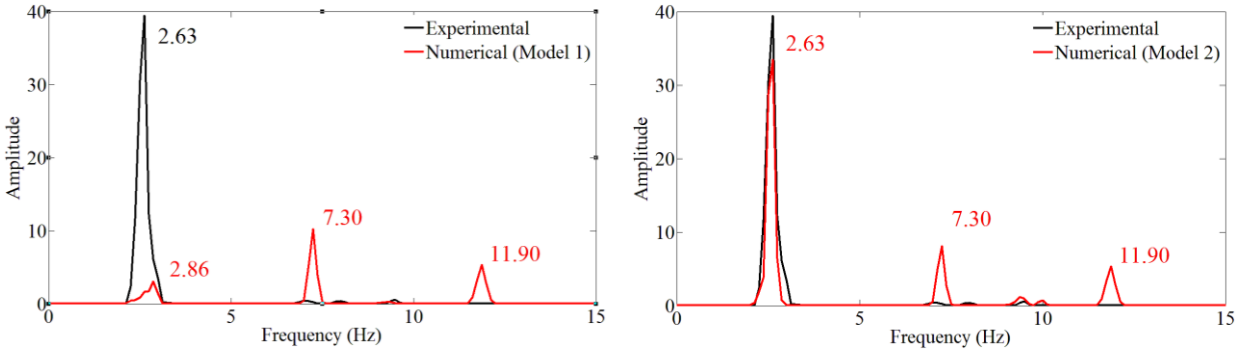

Figure 6.31 – Comparison between experimental and numerical auto-spectra regarding the acceleration records: a) Model 1; b) Model 2

Figure 6.32 shows the dynamic signature of the AP train for the speed of 220 km/h, obtained by applying Equation 5.9 (ERRI D214/RP9 2001). The frequency value of 2.63 Hz, related to the vibration mode 1G, is very close to the frequency of 2.4 Hz, associated with the regularly spaced groups of axles with a distance of 25.9 m and, therefore, the dynamic response associated to the vibration model 1G is significantly amplified and assumes a preponderant contribution towards the remaining frequencies.

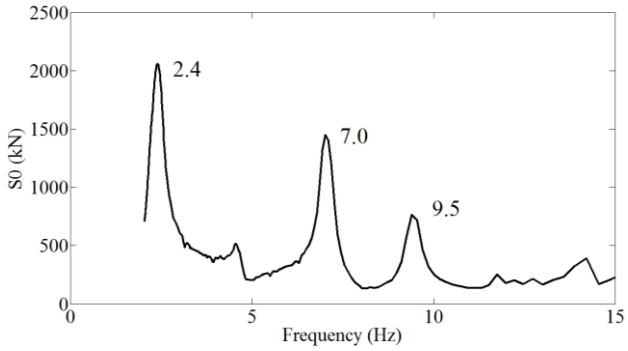

Figure 6.32 – Dynamic signature of the AP train at a speed of 220 km/h

6.5.2.3 Influence of damping coefficients for local vibration modes

Figure 6.33 presents the comparison between the experimental and numerical responses based on Model 2, in terms of displacements, deformations and accelerations, obtained in the

aforementioned sections of the deck slab for the passage of AP train at a speed of 220 km/h, and considering a distinct scenario in terms of damping coefficient values.

The adopted modal damping coefficients were the following: 3.71 % and 5.08 % for all global and slab's local vibration modes, respectively, according to the estimation from the dynamic test under railway traffic; a value of 0.5 % for the remaining vibration modes (local vibration modes of the steel structure), following the guidelines of the EN1991-2 (2003) standard for this type of structure.

Figure 6.33 confirms a very good agreement between numerical and experimental results for the passage of AP train, thereby proving the importance of the damping coefficients for a better correlation between experimental and numerical records.

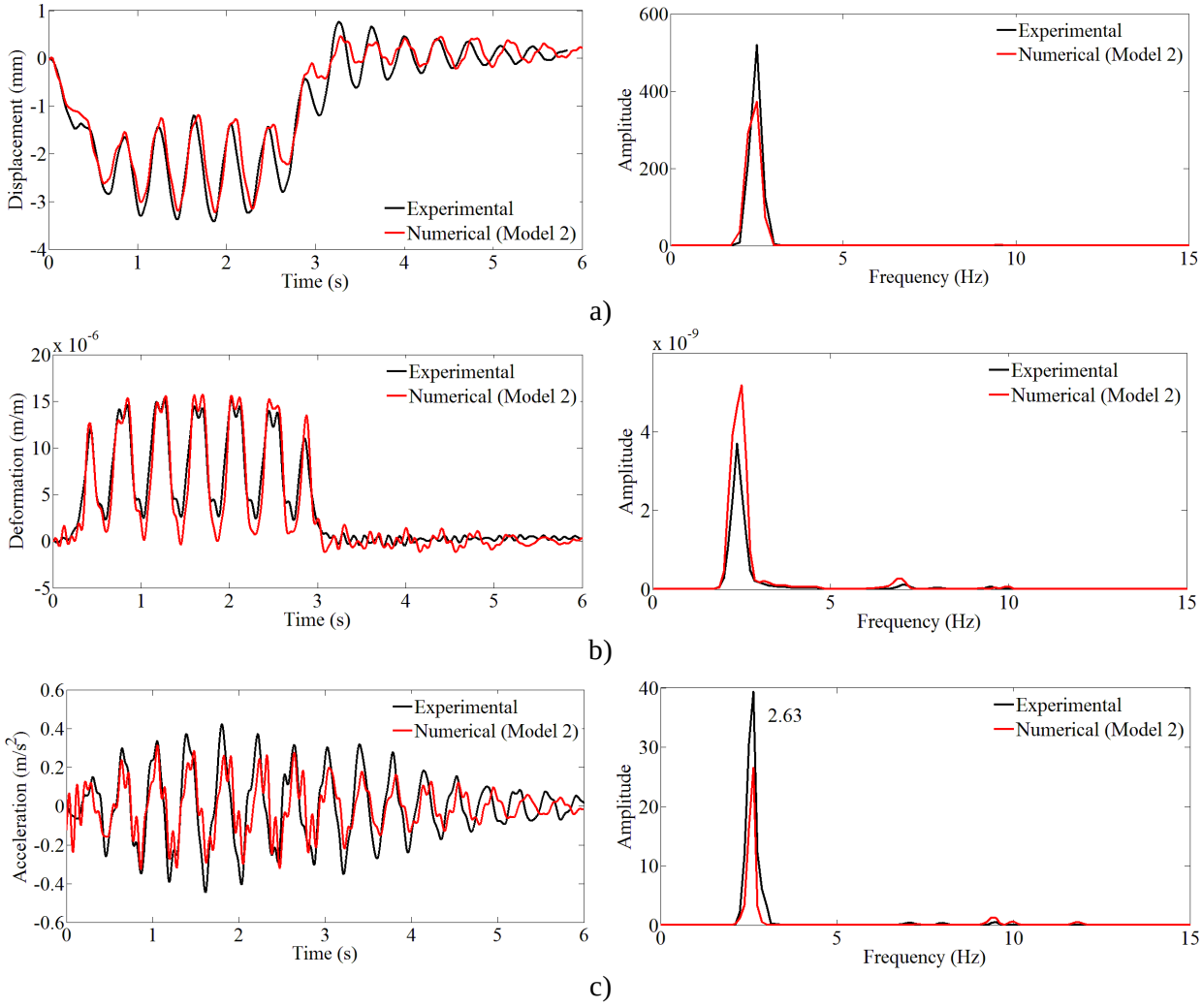

Figure 6.33 – Comparison between measured and calculated (Model 2) responses in terms of time records and auto-spectra: a) vertical displacement; b) transverse deformation; c) vertical acceleration

6.5.2.4 Influence of the cut-off frequency

As shown in the previous sub-sections, a good agreement was achieved when numerical and experimental dynamic responses were compared, considering frequencies up to 15 Hz. This threshold allowed ensuring that both the global dynamic behaviour of the structure and, at least, part of the local dynamic behaviour of the RC slab was being well characterised. However, in order to evaluate the suitability of the FE model to obtain a proper dynamic response in higher frequencies, new thresholds are now considered, namely up to 20 Hz, 30 Hz and 60 Hz.

It is worth mentioning that this validated model will be used, in this work, to calculate the efforts in the deck slab, which will be, in turn, used to calculate the fatigue damage. It is known the importance of considering all the frequencies that contribute to the structural response when the aim is to quantify efforts in the slab, reason why the comparison between numerical and experimental results for cut-off frequency values above 15Hz should be properly evaluated.

The damping scenario adopted in the previous section (3.71 % and 5.08 % for all global and slab's local vibration modes, respectively, and 0.5 % for the remaining vibration modes related to the steel structure) was considered.

Figure 6.34 shows the displacement records, considering cut-off frequencies equal to 20, 30 and 60 Hz, obtained by the application of Chebyshev (type II) low-pass digital filters of order 11, 13 and 20, respectively, and stopband attenuation equal to 45 dB. The time history records correspond to the figures presented on the left-hand side while the respective auto-spectra are presented in the right-hand side.

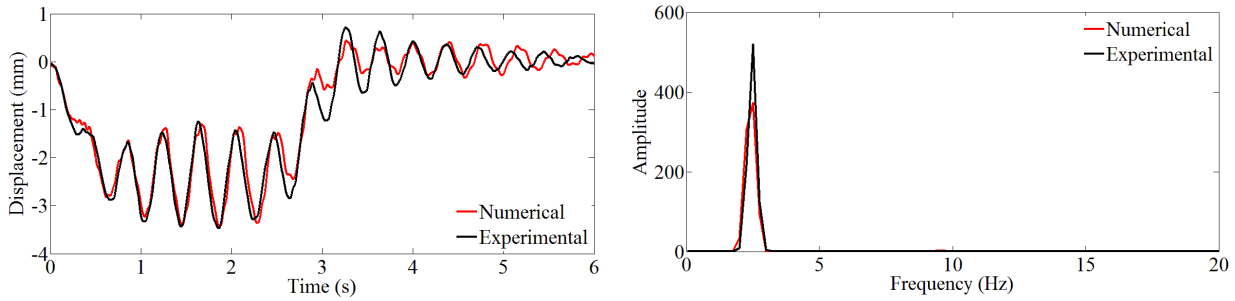

a)

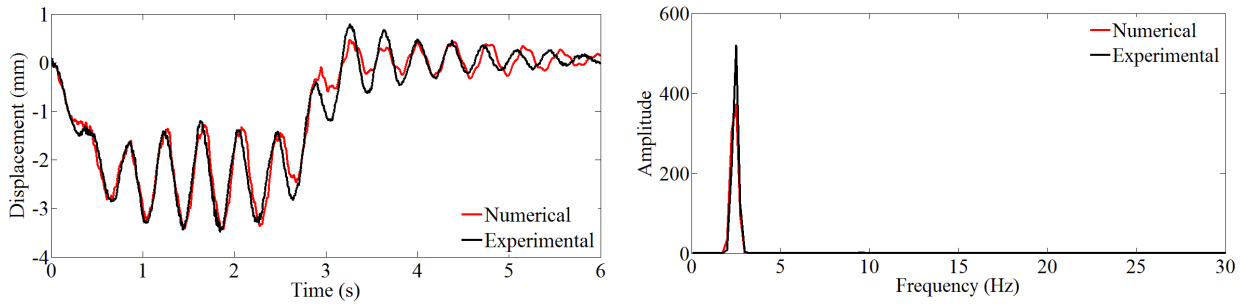

b)

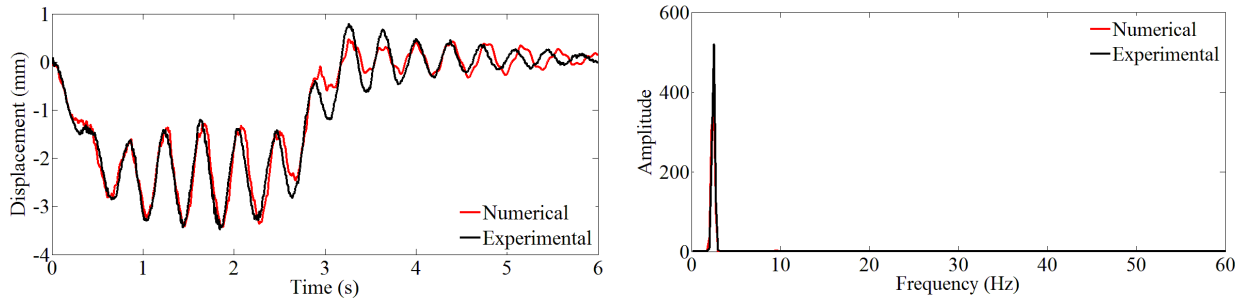

c)

Figure 6.34 – Comparison between measured and calculated displacement records in terms of time records and auto-spectra, for different cut-off frequencies: a) 20 Hz; b) 30 Hz; c) 60 Hz

As one can see in the previous figure, there is a very good agreement between numerical and experimental responses regardless the cut-off frequency values. As mentioned before, the displacement response is dominated by lower frequencies and, for that reason, there are no significant differences in the results, either numerical or experimental, when different frequency thresholds are used (i.e. the results are almost coincident).

Figure 6.35 and Figure 6.36 show the deformation and acceleration records, respectively, obtained through the application of the same cut-off frequencies and digital filters referred in the previous figure.

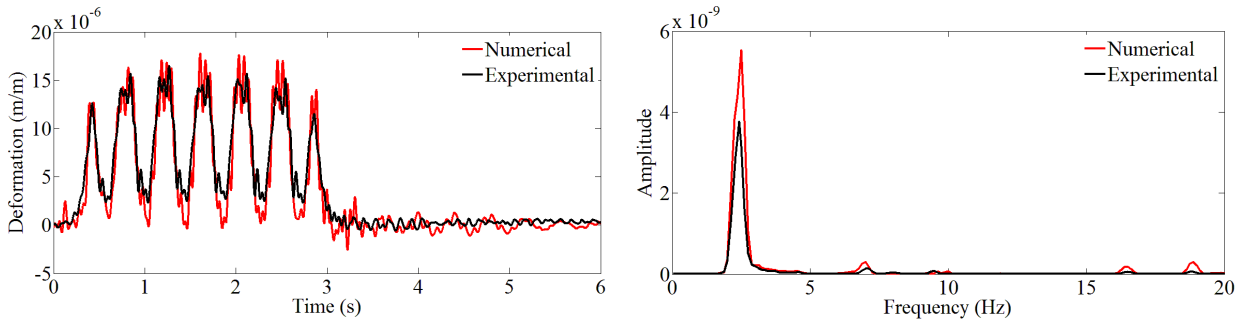

a)

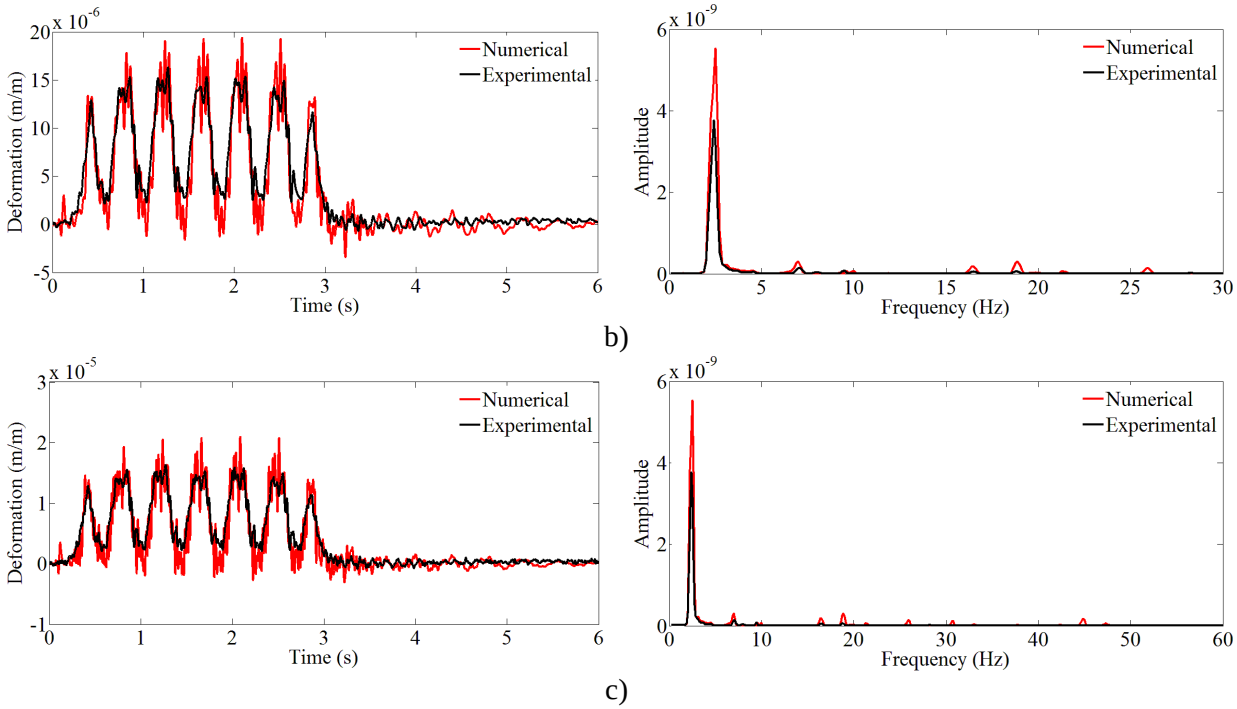

Figure 6.35 – Comparison between measured and calculated deformation records in terms of time records and auto-spectra, for different cut-off frequencies: a) 20 Hz; b) 30 Hz; c) 60 Hz

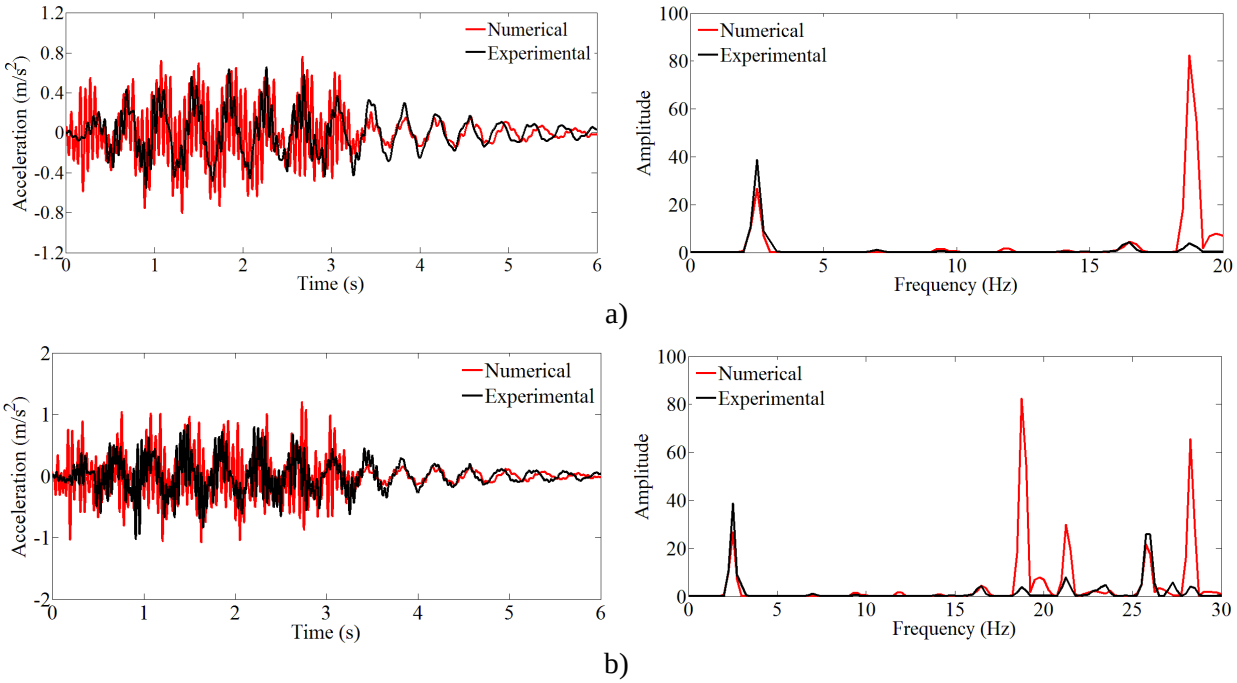

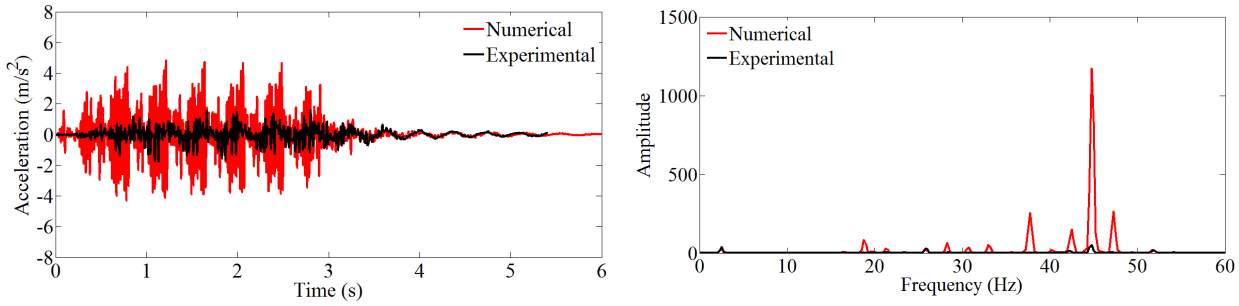

c)

Figure 6.36 – Comparison between measured and calculated acceleration records in terms of time records and auto-spectra, for different cut-off frequencies: a) 20 Hz; b) 30 Hz; c) 60 Hz

By observing Figure 6.35 and Figure 6.36, one can notice that significant differences are obtained between numerical and experimental responses when frequencies higher than 15 Hz are considered in the responses. One conclusion that comes from these results, either in terms of deformations and accelerations, is that the dynamic responses obtained by the FE model are being overestimated when higher frequencies values are taken into account.

A comparison between numerical and experimental deformations, obtained in the locations 1 to 4 depicted in Figure 6.26, was also carried on. Cut-off frequencies equal to 15 Hz, 20 Hz and 60 Hz were also adopted. These results are presented in the Annex A.

By observing these results, one can notice that the numerical responses tend to be similar in different locations, throughout the span, either in terms of general behaviour or maximum amplitude. However, depending on the range of frequencies considered, some important differences can be detected and have to be discussed.

On the one side, it is important to discuss the deformations obtained for a cut-off frequency of 15Hz. In the calculated results, the maximum deformation exhibits very small variation throughout the various monitored positions, which is approximately equal to 16×10^{-6}. However, in the measured results, one can see important differences throughout those positions. The maximum experimental deformation varies between $\approx10\times10^{-6}$ and $\approx20\times10^{-6}$.

Some reasons can be pointed out to justify such differences. One of them is related to the values of thickness and elasticity modulus of the slab used in the calculations. The values for those parameters come from the calibration phase of the FE model (performed to achieve the best comparison between numerical and experimental frequencies and vibration modes) and are slightly different from the original ones. The thickness and elasticity modulus values quantified

through this procedure are global, averaged, values, which are not accurate values for the calculation of local deformations. This fact justifies some discrepancies with respect to the experimental results.

Another reason might be related to the cracking on concrete. A visual survey was carried out to identify the presence of cracks in the lower surface of the slab, in the region where the deformations were measured. Figure 6.37 shows the location of the strain gages and the location of the identified cracks. In the top end of each crack is shown its width and in the bottom end is shown the distance between successive cracks (all dimensions in mm). The strain gauges were installed at a minimum distance of 10 cm from visible cracks. Nevertheless, the observed crack pattern (cracks perpendicular to the girder axes) might influence the strains in the monitored positions. Besides that visible cracks, some micro cracks, which are not visible to the naked eye, may exist in the monitored region.

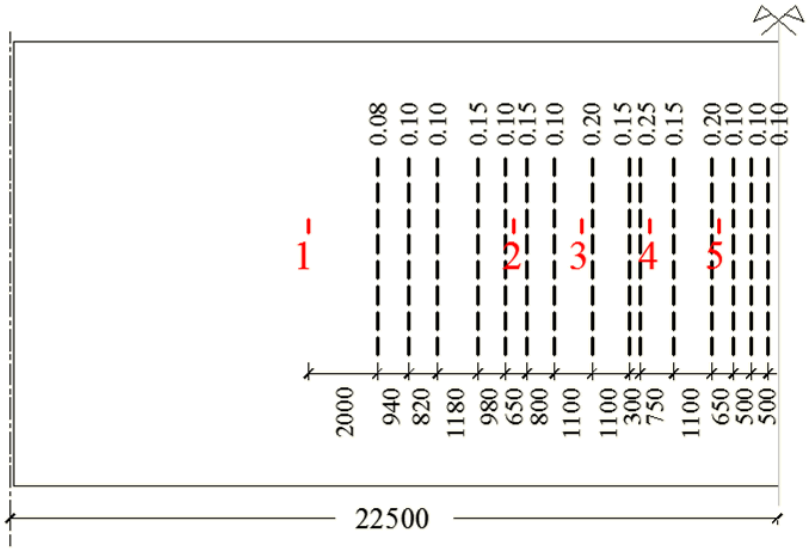

Figure 6.37 – Schematic representation of the visually identified cracks at the bottom of the RC slab (all dimensions in mm)

The measurement uncertainty associated to the deformation measurement process (based on electrical resistance strain gages bonded to the concrete surface) is also a source of differences between measurements and calculations.

Furthermore, although the modelling strategy is detailed, both in terms of structure discretisation and modelling of the train action, there are simplifications and assumptions that

are necessarily adopted. These simplifications also contribute to the existence of differences between experimental and numerical results.

On the other side, it is important to discuss the contribution of frequencies higher than 15Hz. For the purpose of this thesis, this discussion is even more important than the variability throughout the various measurement positions.

By observing only the experimental results in Annex A, one can see that frequencies higher than 15 Hz do not present a significant contribute to the dynamic responses. So, as previously discussed, these results have proved once again that numerical responses are being overestimated when frequencies above 15 Hz are used. Even for the results obtained in location 1, the fact that the experimental deformation is greater than the calculated one is due to the contribution of frequencies up to this threshold (higher frequencies only show a slight influence). Nevertheless, it is possible to see that, above 15Hz, there are slight contributions of frequencies approximately equal to 17Hz and 19Hz. This is practically visible at all measurement points and for both the experimental and numerical records. However, the numerical model overestimates the contribution of these frequencies when compared to the experimental records.

In order to understand the differences between measurements and calculations for frequencies higher than 15 Hz, additional analyses were made to investigate the influence of: minor variations in the train speed; variations in the track irregularities profile; the damping coefficients associated to local vibration modes (especially those with frequencies higher than 15Hz).

6.5.2.5 Influence of the train speed

Some uncertainties can occur in the measurement of the train speed during experimental tests, which might be related either to human or instruments errors when taking the readings. Small variations in the train speed might have an important influence in the structure's dynamic response. In fact, such variations might be sufficient to prevent resonance with a certain structure's vibration mode.

In order to assess whether these variations are able to explain some of the differences between calculations and measurements (especially for frequencies higher than 15Hz), numerical analyses considering both a reduction and an increase of 2 and 4 km/h, from the base

train speed equal to 220 km/h, were carried out. Special attention was given to the frequency with a peak value around 18.5 Hz (previously seen in Figure 6.35 and Figure 6.36). The damping scenario adopted in the analyses presented in section 6.5.2.4 was also adopted in this survey.

Figure 6.38 shows the deformation and acceleration records, respectively, considering a cut-off frequency equal to 20 Hz, when a reduction in the train speed was adopted. The time history records correspond to the figures presented on the left-hand side while the respective auto-spectra are presented in the right-hand side. Figure 6.39 shows identical results when an increasing train speed is considered.

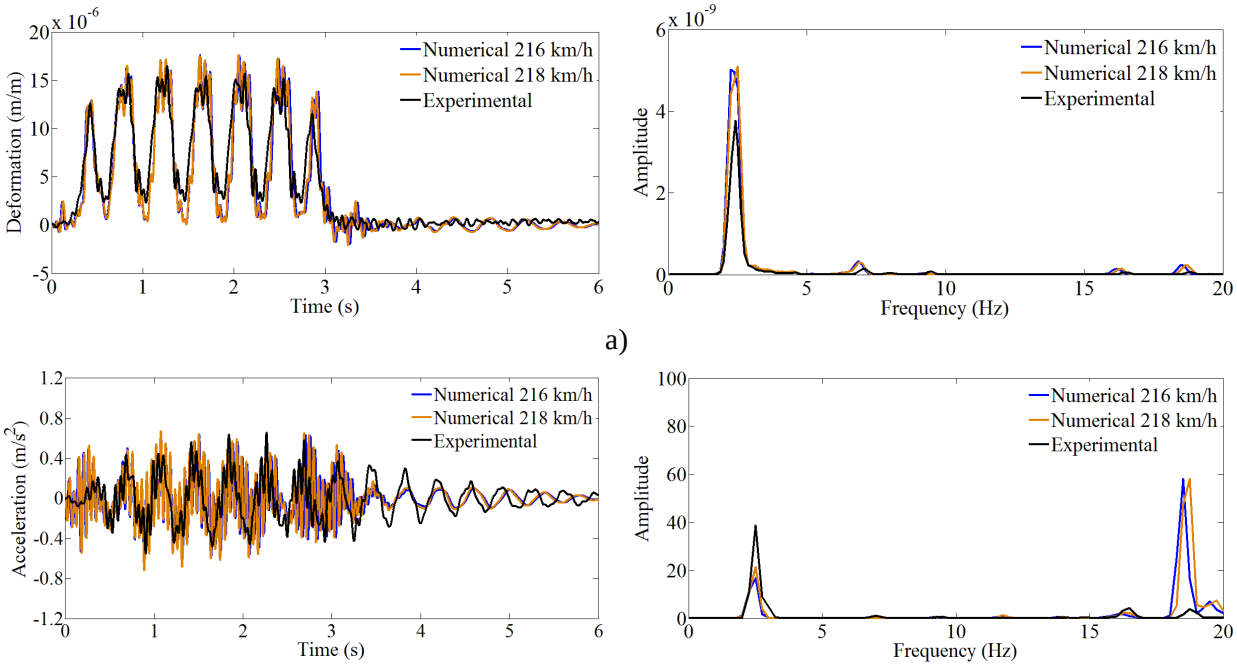

Figure 6.38 – Comparison between measured and calculated results when a decrease in the train speed is adopted in the numerical analyses: a) deformation and b) acceleration records

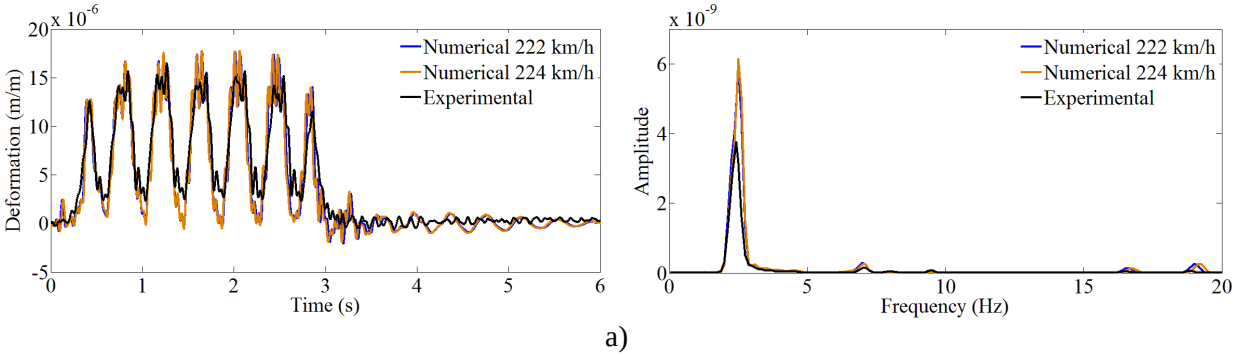

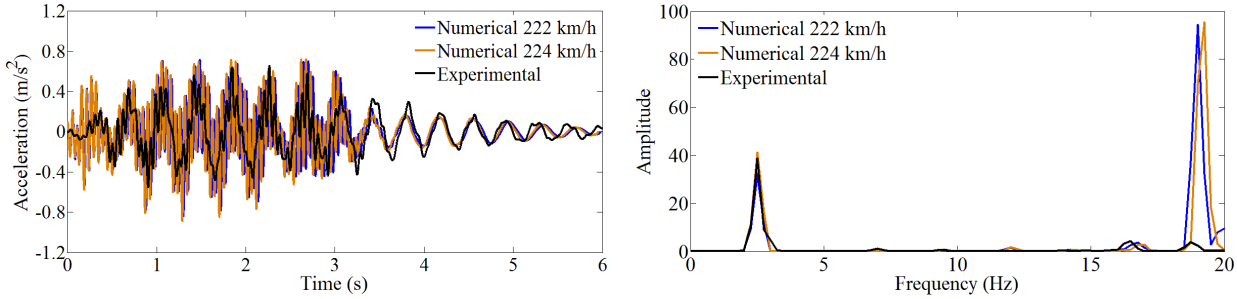

b)

Figure 6.39 – Comparison between measured and calculated results when an increase in the train speed is adopted in the numerical analyses: a) deformation and b) acceleration records

By observing the above figures, some changes can be noticed in the numerical responses when different train speeds are used, particularly visible in the auto-spectra. Reducing the train speed led to a reduction in the amplitude of the frequency initially around 18.5 Hz, but also to a shift in the frequency value, which is not enough to get a better approximation between numerical and experimental results. Furthermore, keep reducing the train speed would give rise to substantial differences in the time history records. The opposite effect happens when an increasing train speed is adopted.

6.5.2.6 Influence of track irregularities

The effect of track irregularities is discussed in the present section. Initially, the results considering or not the track irregularities are shown. The irregularities profile shown in Figure 6.29 and the damping scenario adopted in the analyses presented in section 6.5.2.4 were adopted in this evaluation. Figure 6.40 to Figure 6.42 show the displacement, deformation and acceleration records, respectively, for cut-off frequencies of 15, 20 and 60 Hz. The low-pass digital filters described in section 6.5.2.4 are also used in the post processing of these results.

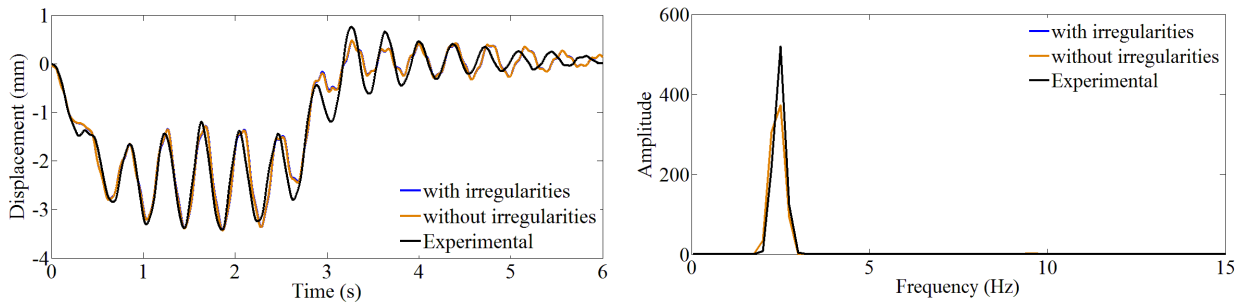

a)

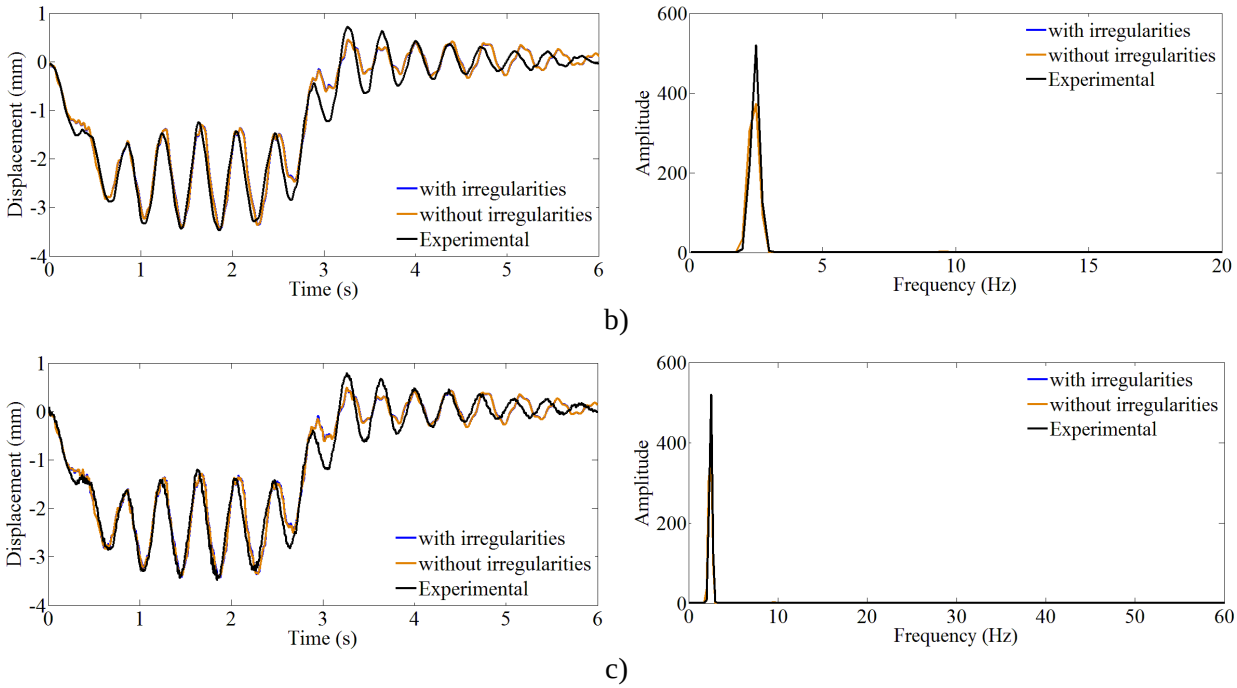

Figure 6.40 – Measured and calculated displacement records, considering or not the track irregularities effects, for different cut-off frequencies: a) 15 Hz; b) 20 Hz; c) 60 Hz

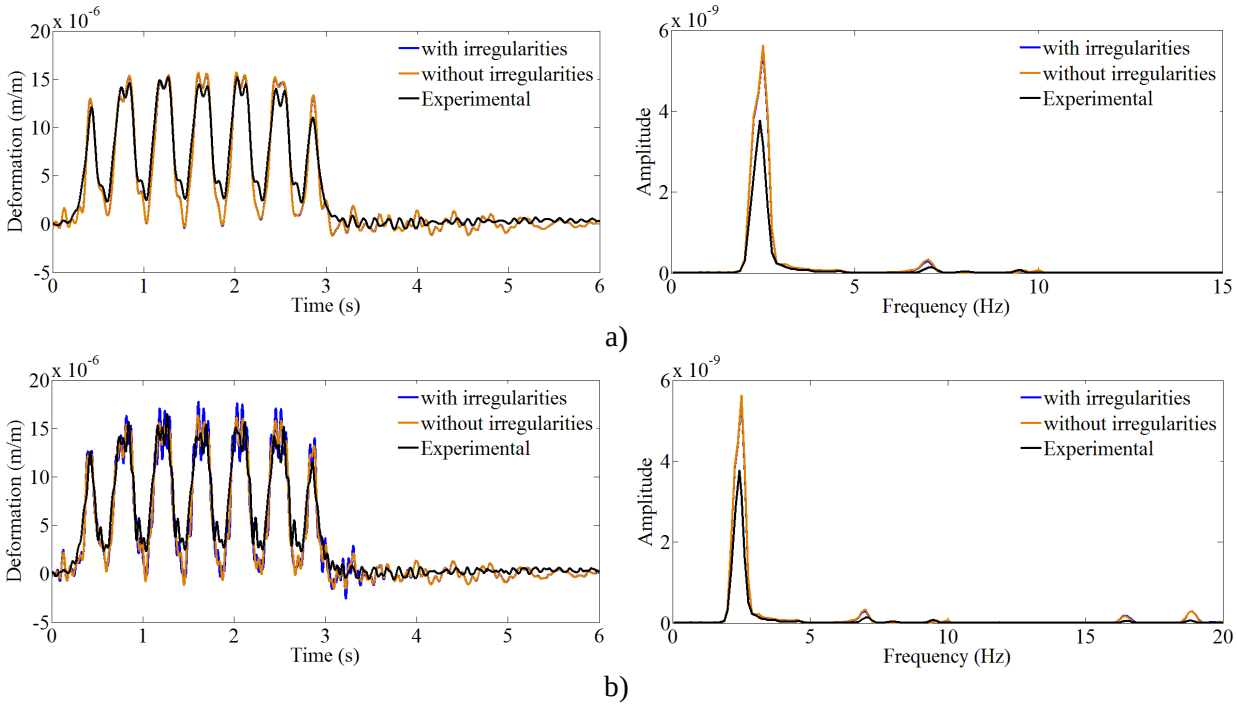

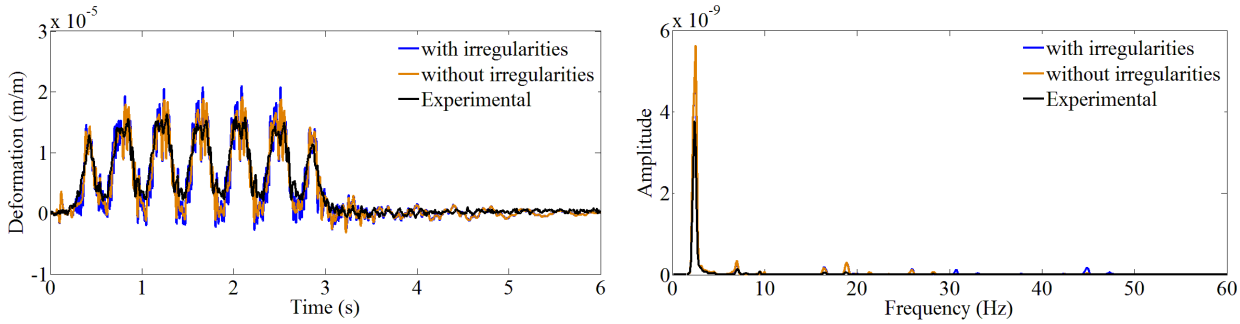

c)

Figure 6.41 – Measured and calculated deformation records, considering or not the track irregularities effects, for different cut-off frequencies: a) 15 Hz; b) 20 Hz; c) 60 Hz

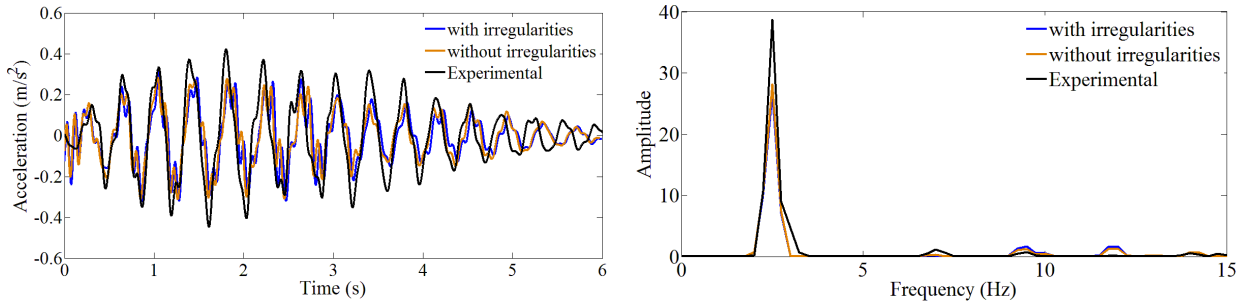

a)

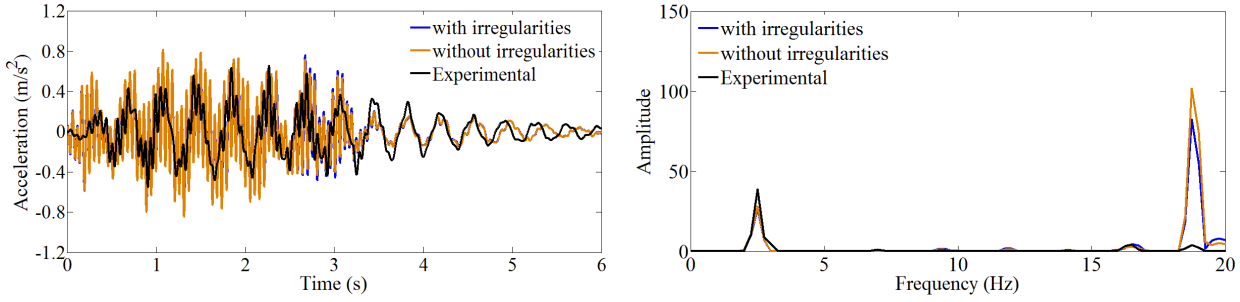

b)

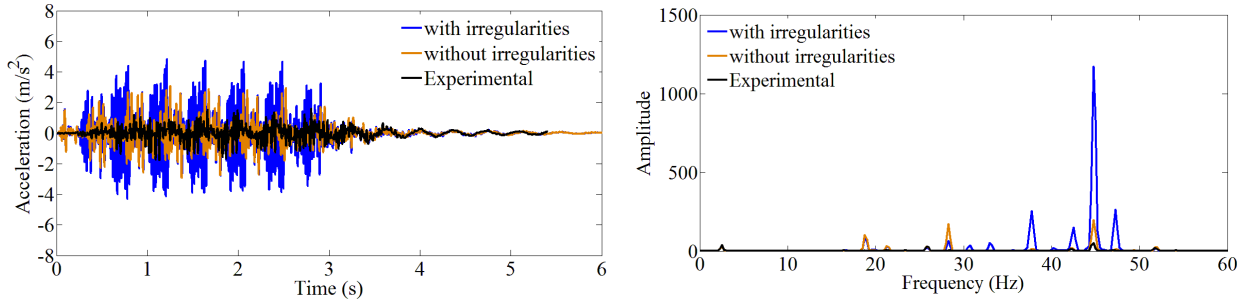

c)

Figure 6.42 – Measured and calculated acceleration records, considering or not the track irregularities effects, for different cut-off frequencies: a) 15 Hz; b) 20 Hz; c) 60 Hz

As observed in the above figures, a better approximation between numerical and experimental results can be achieved when the track irregularities are not considered in the

analyses, although only slight differences occur up to a frequency equal to 20 Hz. When a cut-off frequency equal to 60 Hz is considered, higher differences can be noticed, which are particularly visible in the acceleration records. However, as mentioned before, the dynamic responses obtained by the FE model are being overestimated when higher frequencies values are taken into account in the analyses.

Then, it becomes relevant to evaluate the effect of different track irregularities profiles in the numerical results. Unlike the case presented in the previous chapter, for this case study only one irregularities profile was provided by the Portuguese railway network management company, which is presented in Figure 6.29, for both left and right rails. As previously mentioned, the irregularities presented in that figure consider the contribution of wavelengths in the ranges 1-25 m and 25-70 m (measured in 2016) and wavelengths below than 1 m, taken from the only rail corrugation profile also provided (measured in 2014).

Since considerable discrepancies were found related to the coordinates of the profile's reference point (the location in the irregularities corresponding to the beginning of the viaduct's span), the space variability of the irregularities profile is considered in this section. For this purpose, three irregularities profiles are used in the numerical analyses: i) the initial one, depicted in Figure 6.29; ii) an alternative profile based on the translation of i) 10 m before; iii) another profile based on the translation of i) 10 m ahead. Figure 6.43 shows these three irregularities profiles for left [Figure 6.43 a)] and right [Figure 6.43 b)] rails.

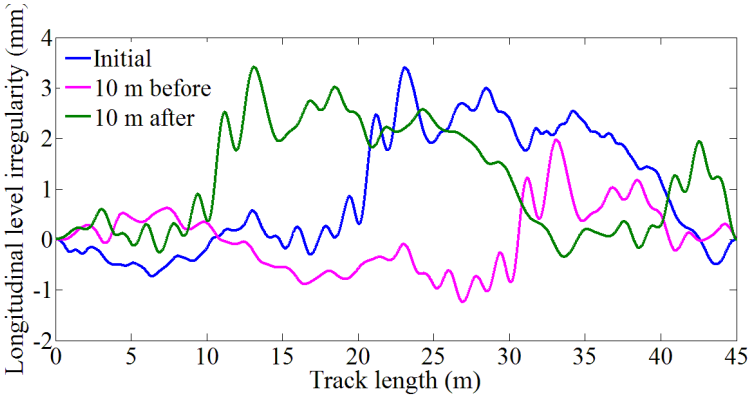

a)

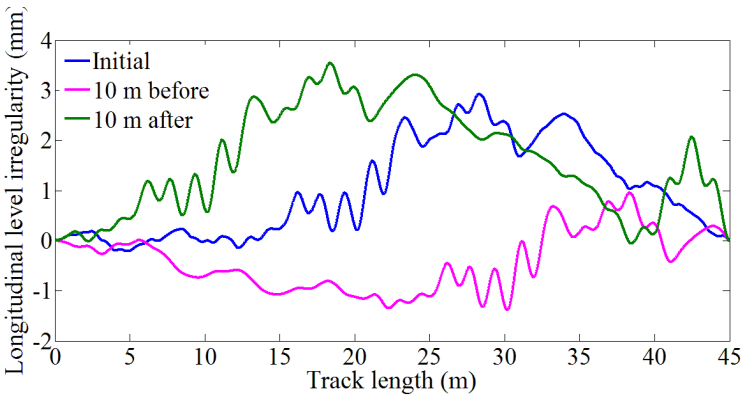

b)

Figure 6.43 – Irregularities profiles considering space variability: a) left rail; b) right rail

Figure 6.44 presents the contribution of wavelengths lower than 3 m, obtained from the above irregularities profiles, and Figure 6.45 the respective auto-spectra, both for left and right rails. The auto-spectra related to wavelengths higher than 3 m is not depicted since there are not enough cycles of higher wavelengths to be representative. By observing both figures, one can notice that the major differences are related to wavelengths between 1.5 and 3 m, with some differences between profiles, both in terms of maximum amplitude and preponderant wavelengths.

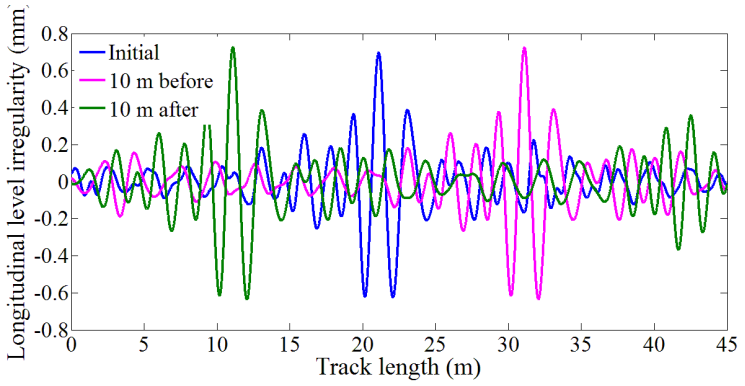

a)

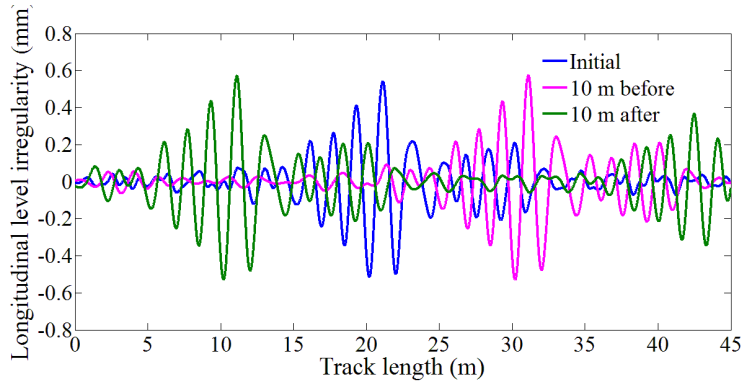

b)

Figure 6.44 – Left rail level profiles with wavelengths: a) between 3 m and 70 m; b) lower than 3 m

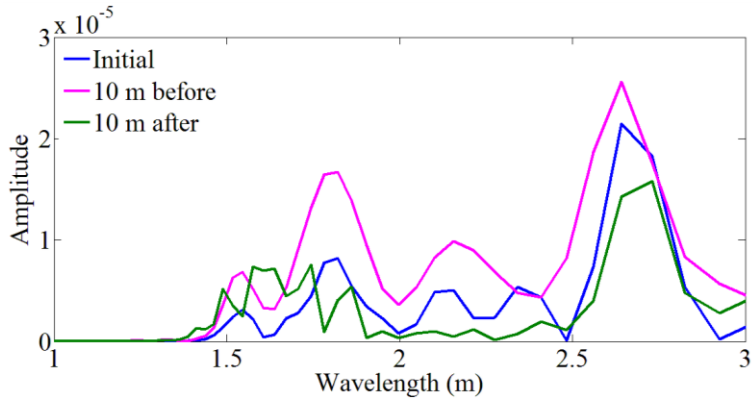

a)

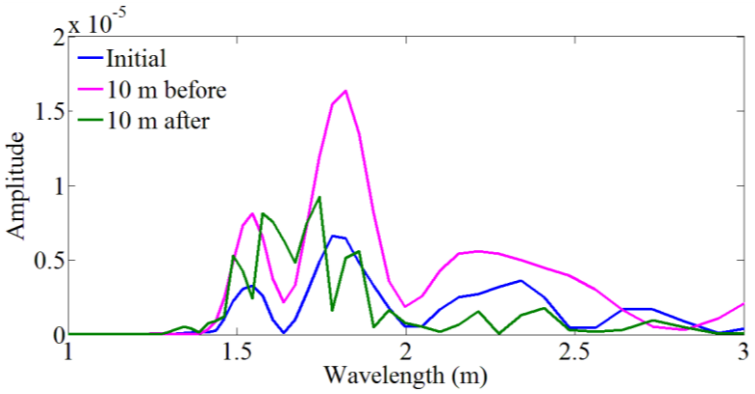

b)

Figure 6.45 – Rail irregularities auto-spectra considering wavelengths lower than 3 m:
a) left rail; b) right rail

Figure 6.46 illustrates the Power Spectral Density (PSD) functions of the rail level profiles. In order to evaluate the severity of the irregularities, two of the most commonly used reference PSD functions in the railway infrastructure research field (Cantero et al. 2016, Fryba 1996, Rocha et al. 2014), provided by SNCF and FRA, are also depicted in Figure 6.46. It is possible to observe that the irregularities profiles are well located within the limits defined by classes 1 and 6 of FRA's PSD function, with exception of the wavelengths in the range 1.4-2.8 m.

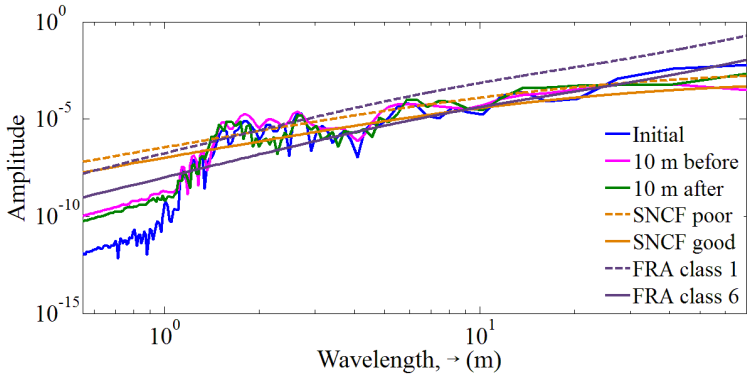

a)

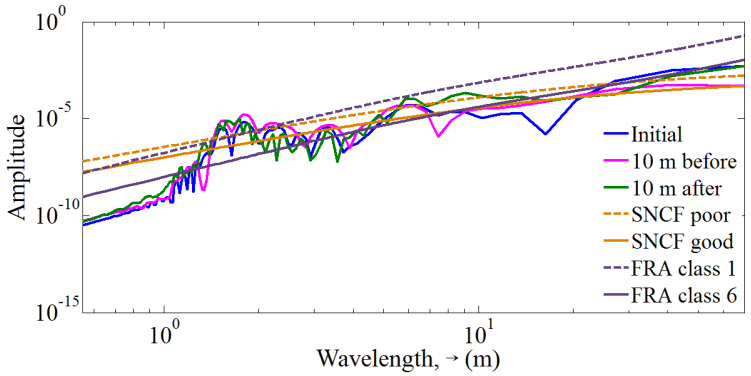

b)

Figure 6.46 – PSD functions rail level profiles: a) left rail; b) right rail

Since the vertical displacements of the slab did not reveal to be sensible to the effect of track irregularities (as seen in Figure 6.40), only the deformation and acceleration results are analysed. Figure 6.47 shows a comparison between the experimental and numerical deformations, for the passage of AP train at a speed of 220 km/h, considering cut-off frequencies of 15, 20 and 60 Hz. The time history records correspond to the figures presented on the left-hand side while the respective auto-spectra are presented in the right-hand side. Identical results are presented in Figure 6.48 in terms of acceleration records.

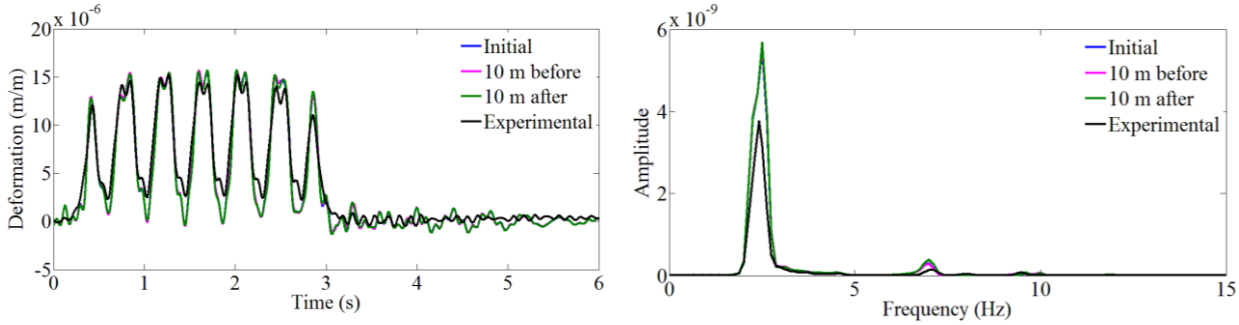

a)

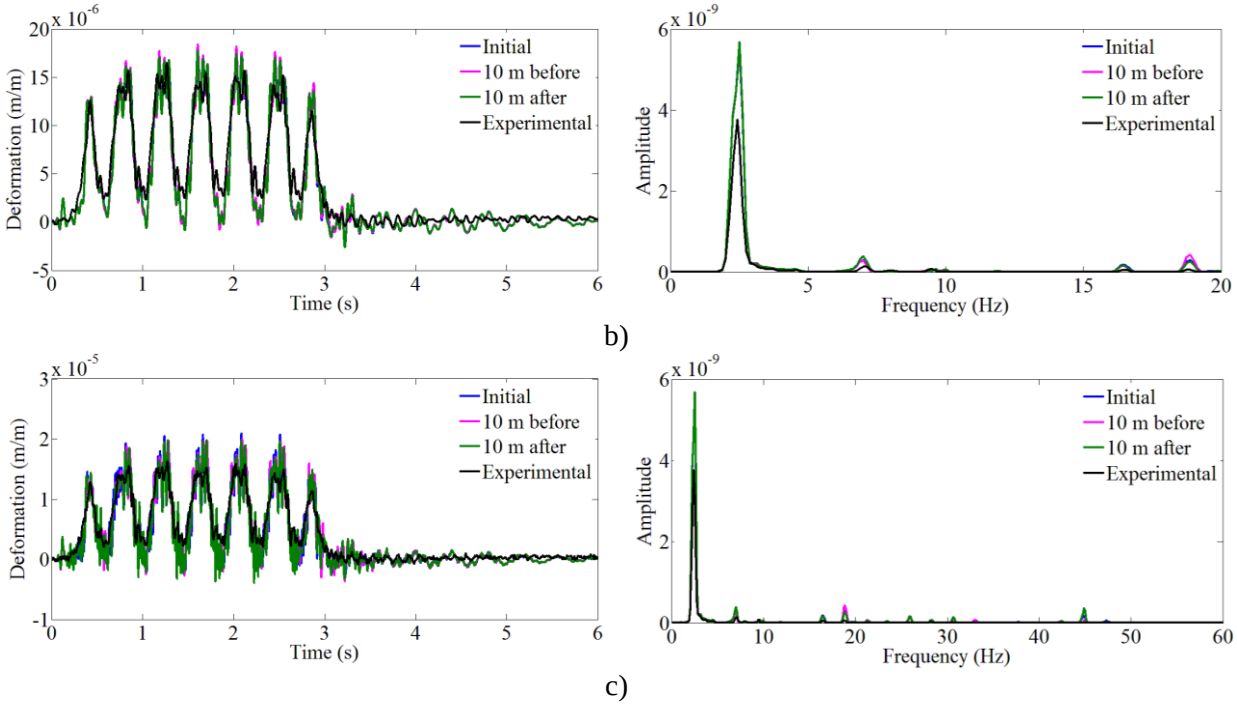

Figure 6.47 – Measured and calculated deformation records, considering different track irregularities profiles, for different cut-off frequencies: a) 15 Hz; b) 20 Hz; c) 60 Hz

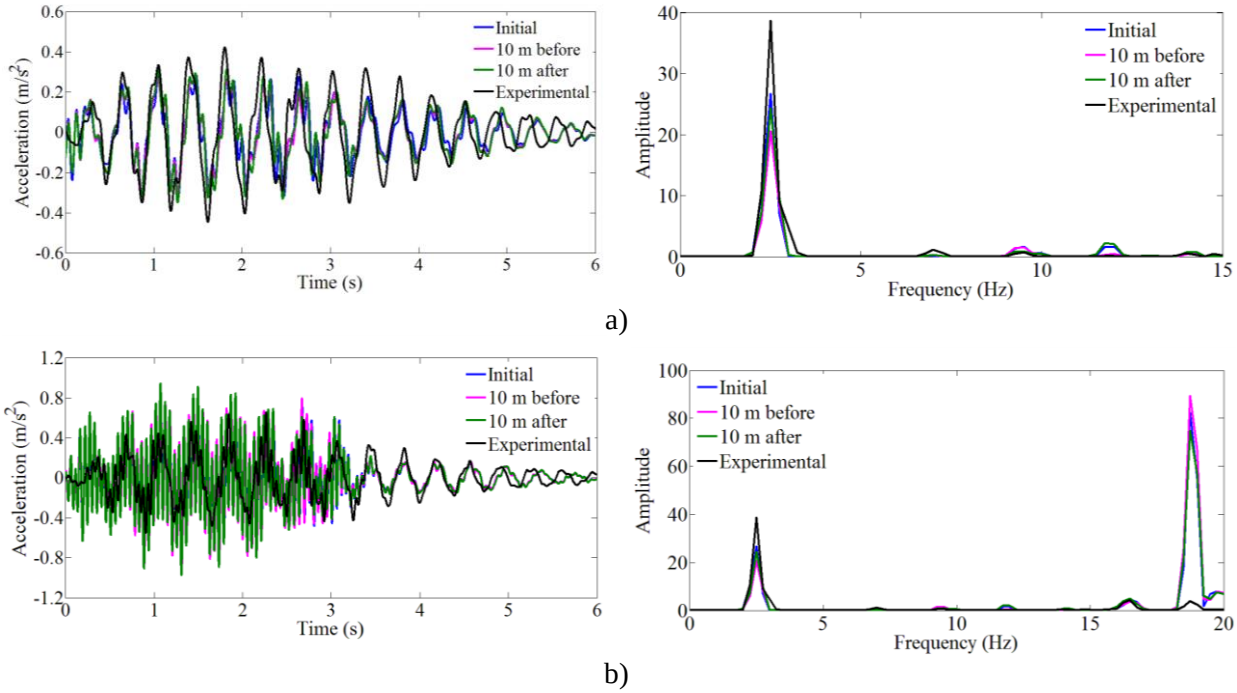

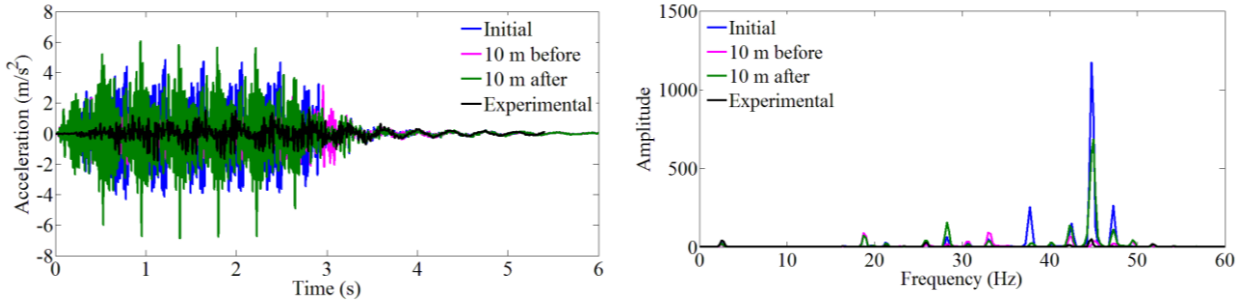

c)

Figure 6.48 – Measured and calculated acceleration records, considering different track irregularities profiles, for different cut-off frequencies: a) 15 Hz; b) 20 Hz; c) 60 Hz

As mentioned before, a very good agreement between numerical and experimental dynamic responses was achieved, both in terms of deformations and accelerations of the RC slab, when frequencies up to 15 Hz were considered. One can realise that the space variability taken into account in the track irregularities profiles only leads to slight differences in the numerical responses, particularly noticeable in the accelerations results.

It is possible to see once again how the dynamic responses obtained by the FE model are overestimated when higher frequencies values are taken into account, particularly visible to frequencies up to 60 Hz. In the analyses considering frequencies up to 20 Hz, one can realise that the frequency with a peak value around 18.5 Hz keeps roughly unchanged, being excited in a similar way by different track irregularities profiles.

Some differences can also be observed in the numerical results when distinct track irregularities profiles are used. In order to see this localised behaviour, Figure 6.49 shows a detailed view, in the time interval 1-2 s, of the time-history records of deformations and accelerations presented before (up to 60 Hz). These discrepancies, especially noticeable in the accelerations records, might be related with the way how these different profiles contribute to the excitation of some local vibration modes of the RC deck slab.

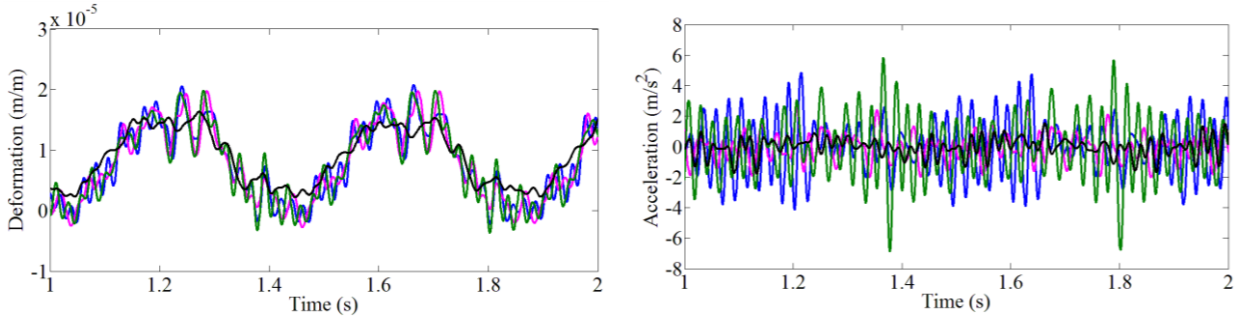

a) b)

Figure 6.49 – Detailed view in the time interval 1-2 s of the dynamic responses, considering frequencies up to 60 Hz: a) transverse deformation; b) vertical acceleration

6.5.2.7 Influence of damping coefficients for local vibration modes of the steel structure

It has been possible to figure out a considerable excitation that occurs in some frequencies, especially for values higher than 15 Hz. In this range of frequencies there are some local vibration modes of the metallic structure. The damping coefficient attributed to those modes, in the analyses presented before, was 0.5 % (the value recommended by the Eurocode 1 for metallic structures). The adoption of such a low damping coefficient is, therefore, not based on any experimental information gathered on this structure.

These so called "local vibration modes of the steel structure" involve also small movements of other structural components, namely the RC slab. Consequently, they play a role in the calculated dynamic response of the RC slab. The real damping coefficient for those vibration modes can be higher than 0.5%.

In order to understand the effects of the damping attributed to these vibration modes, a new analysis was carried out adopting a damping coefficient equal to 5.08 % (value previously identified in section 6.5.1.2 for slab's local vibration modes) to all vibration modes with frequency above 15 Hz.

Figure 6.50 and Figure 6.51 show a comparison between the experimental and numerical responses, in terms of deformations and accelerations, respectively, considering cut-off frequencies up to 15 Hz, 20 Hz and 60 Hz. Once again, the time history records correspond to the figures presented on the left-hand side while the respective auto-spectra are presented in the right-hand side. Bearing in mind that the results showed in the previous section, since the space variability taken into account in the track irregularities profiles did not lead to substantial differences in the numerical responses, only the initial irregularities profile was used in this section.

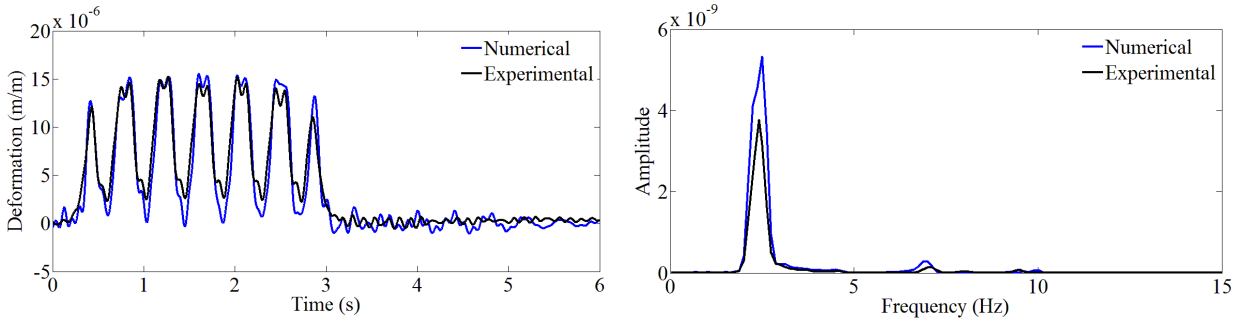

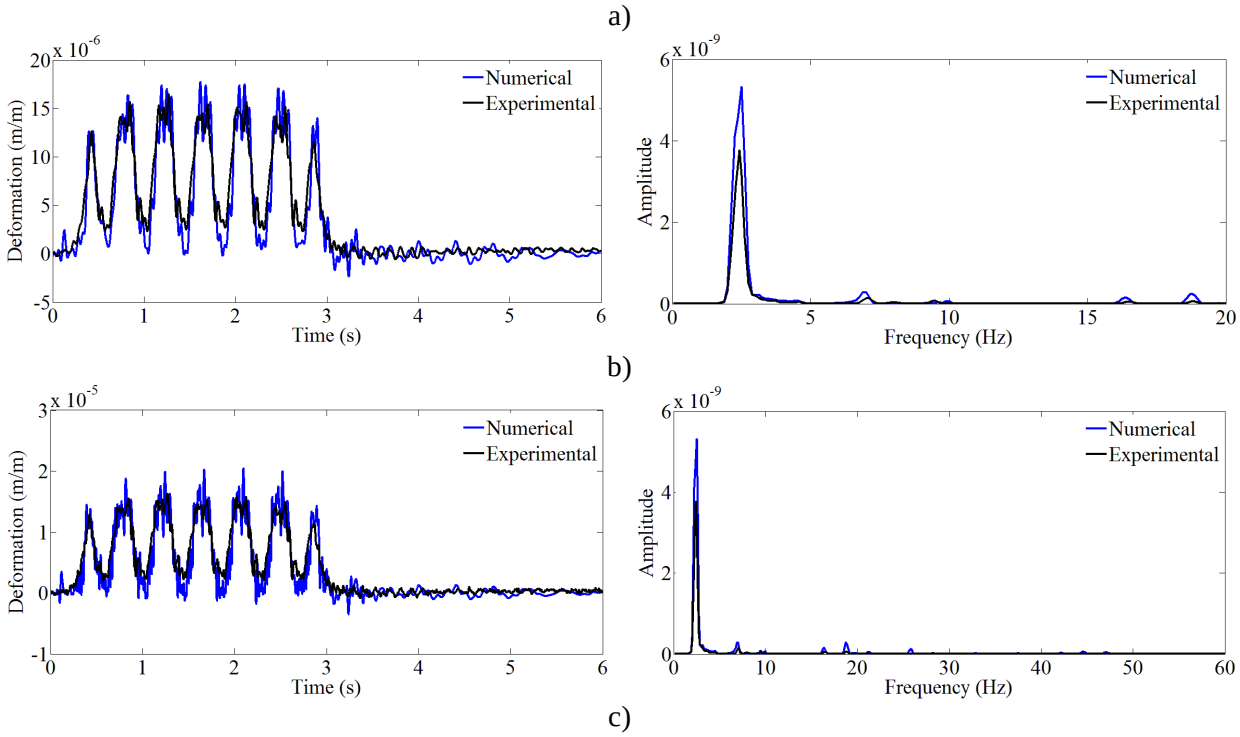

Figure 6.50 – Measured and calculated deformation records, adopting higher damping coefficients for vibration modes of the metallic structure, for different cut-off frequencies: a) 15 Hz; b) 20 Hz; c) 60 Hz

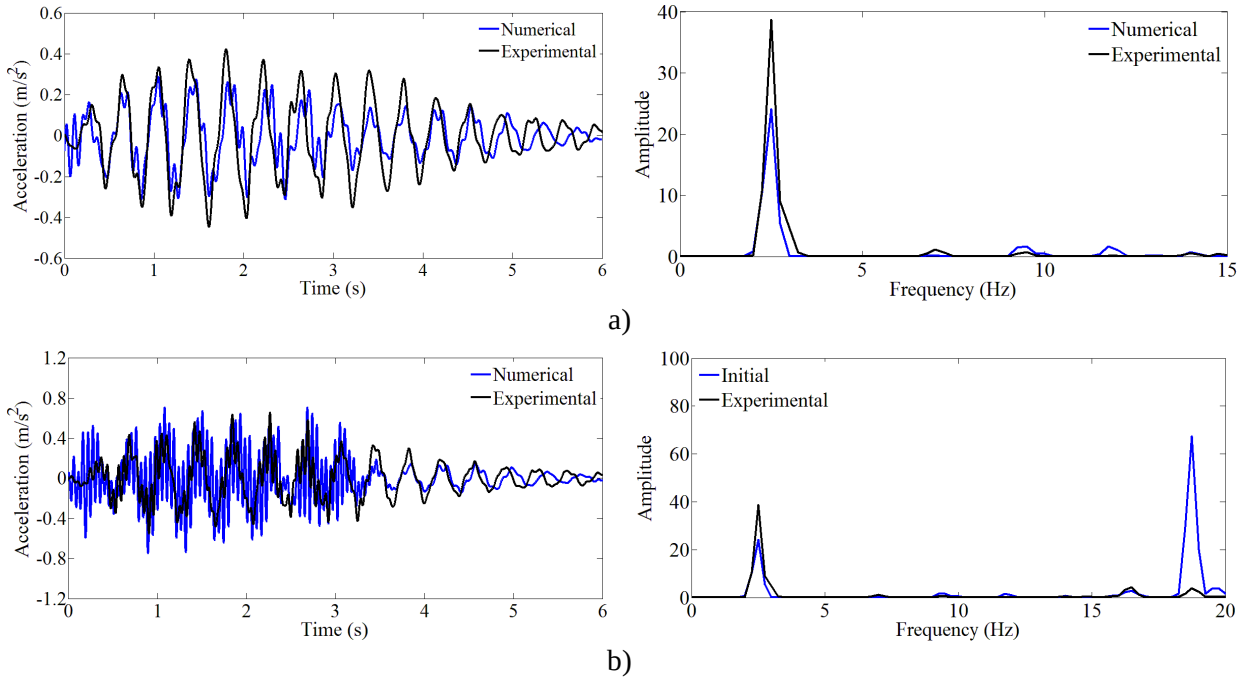

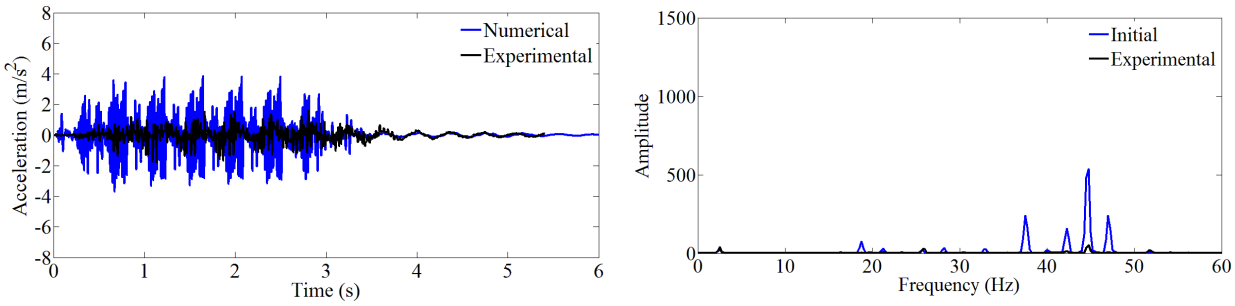

c)

Figure 6.51 – Measured and calculated acceleration records, adopting higher damping coefficients for vibration modes of the metallic structure, for different cut-off frequencies: a) 15 Hz; b) 20 Hz; c) 60 Hz

By comparison with the results shown in section 6.5.2.4, one can observe that resorting to this damping coefficients scenario, a better approximation between numerical and experimental results was achieved. However, some discrepancies still remain. Since the responses in terms of deformations are dominated essentially by low-value frequencies, only slight changes are observed. The main differences occur in terms of accelerations when frequencies up to 60 Hz are considered, in which a clear decrease in the amplitude associated with some vibration modes can be observed.

6.5.2.8 Influence of damping coefficients for higher-order local vibration modes

As shown in the previous section, even adopting an approach based on higher damping coefficients for the "local vibration modes of the metallic structure", some differences between measured and calculated responses still remain. These differences occur essentially for frequencies above approximately 17.5 Hz.

Bearing this in mind, a new damping scenario was adopted: 3.71 % for global vibration modes, 5.08 % for all local vibration modes up to a frequency equal to 17.5 Hz and 10 % for all the remaining vibration modes. It should be pointed out the works carried on by the ERRI's D214 (RP3) expert committee, in which the damping coefficient of the first vibration mode of several structures was identified, based on experimental tests, reached considerable higher values. For that reason, a damping coefficient equal to 10 % is not unrealistic for higher-order local vibration modes.

Since the displacements records have been affected only by lower frequency values, in which the damping coefficients were not changed, only results in terms of deformations and

accelerations are depicted in the present section. Once again, only the initial track irregularities profile was adopted in the numerical analyses.

Figure 6.52 and Figure 6.53 show a comparison between measured and calculated deformation and acceleration records, respectively, for cut-off frequencies equal to 15, 20, 30 and 60 Hz. The numerical results obtained using this new damping scenario are also compared with the ones presented before in sections 6.5.2.3 and 6.5.2.4, depicted in figures as using a base damping scenario. The low-pass digital filters described in section 6.5.2.4 are also used in the post processing of these results. The time history records correspond to the figures presented on the left-hand side while the respective auto-spectra are presented in the right-hand side.

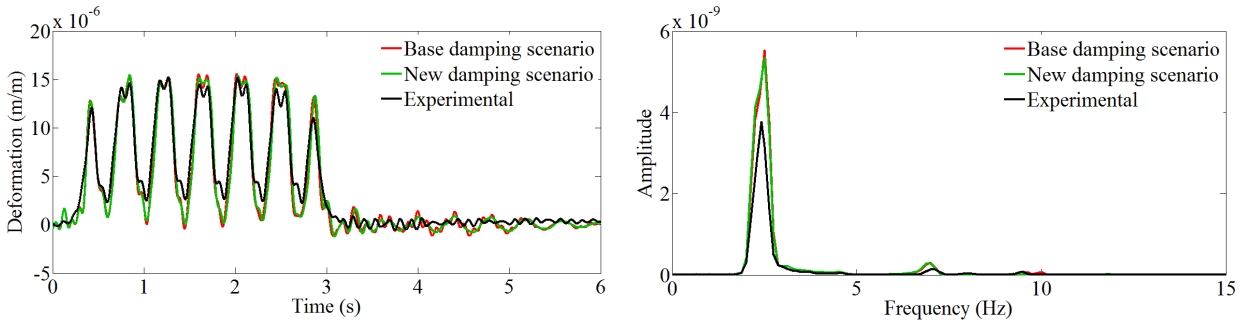

a)

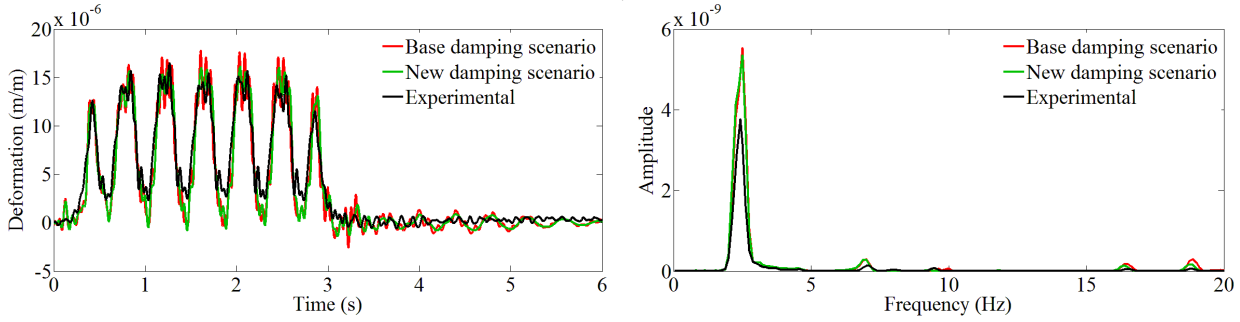

b)

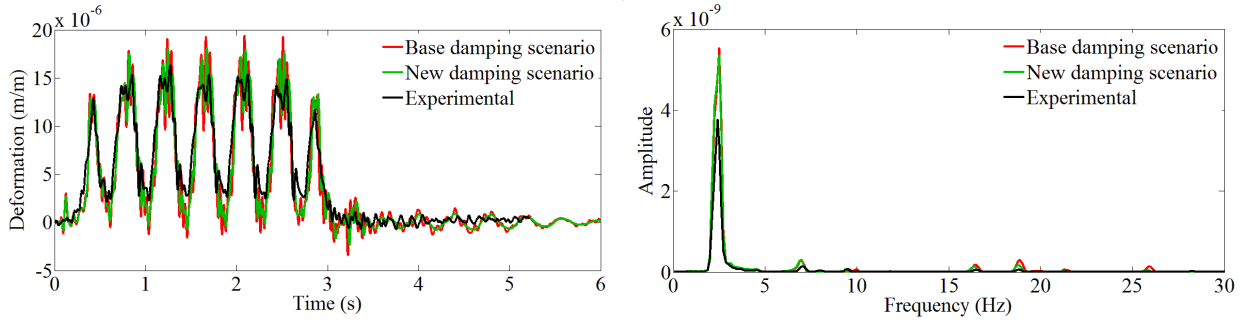

c)

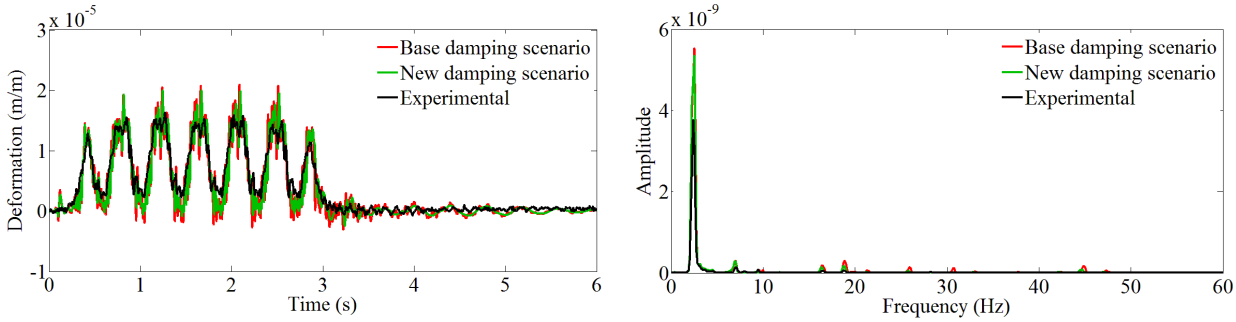

d)

Figure 6.52 – Measured and calculated deformation records, adopting a new damping scenario, for different cut-off frequencies: a) 15 Hz; b) 20 Hz; c) 30 Hz; d) 60 Hz

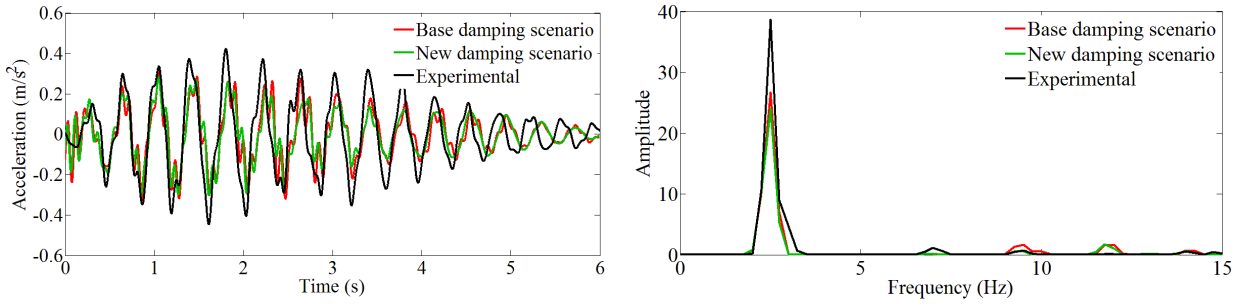

a)

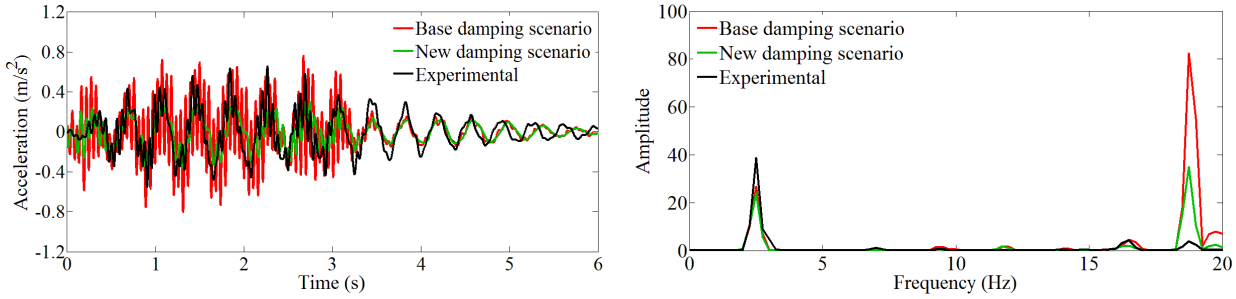

b)

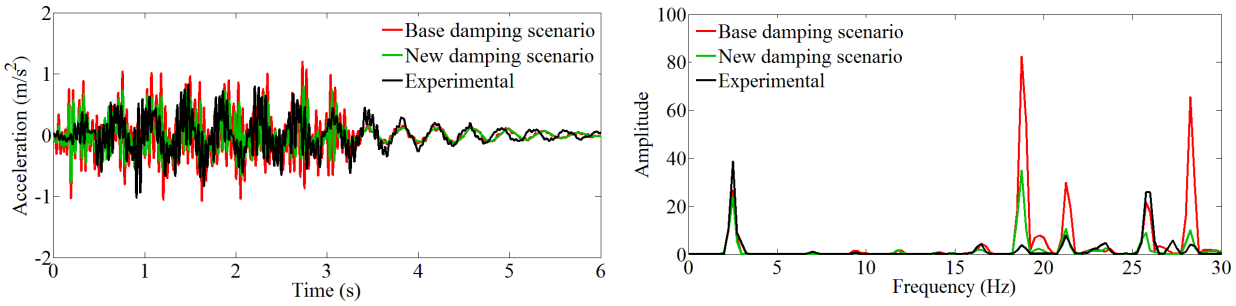

c)

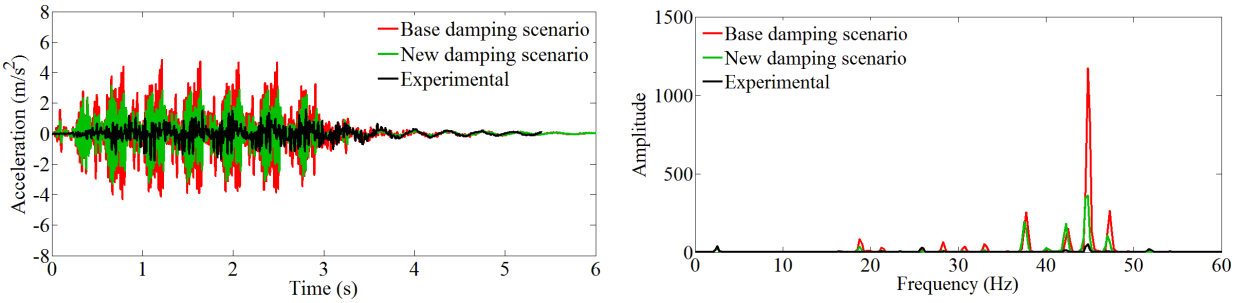

d)

Figure 6.53 – Measured and calculated acceleration records, adopting a new damping scenario, for different cut-off frequencies: a) 15 Hz; b) 20 Hz; c) 30 Hz; d) 60 Hz

Based on the results shown in the above figures, one can realise a better agreement that can be achieved between numerical and experimental results when this new damping scenario is adopted. This is particularly visible in both the deformation and acceleration records, considering frequencies up to 20 Hz, mainly due to the reduction of the amplitude value related to the vibration mode with frequency around 18.5 Hz. Once again, it is possible to observe that, even adopting this higher damping scenario, the numerical responses are being overestimated when frequencies above 20 Hz are considered.

As a final remark to this part of the work, dedicated to the validation of the numerical modelling approach, it is worth pointing out that the parametric analyses conducted so far did not allow getting a satisfactory agreement between measurements and calculations for frequencies higher than 20Hz. This fact does not impair the relevance of this work.

In fact, the measured deformations, in the various monitored positions, show that frequencies higher than 20Hz have a negligible contribution to the amplitude of the deformation cycles in the slab (caused by the train passage). This is *per se* an important information for anyone interested in calculating internal efforts due to railway traffic in this type of structure. Experimental data regarding the transverse dynamic behaviour of railway bridge deck slabs supported by longitudinal girders is, still today, scarce.

On the other hand, the extensive parametric analyses conducted in this validation stage demonstrated that the adopted numerical modelling approach, with a cut-off frequency equal to 20 Hz, provides a good agreement with the experimental results. It can, therefore, be used in the calculation of internal forces and fatigue damage in the RC slab.

Based on these parametric analyses and comparison with experimental results, it was also possible to conclude that the contribution of frequencies higher than 20Hz provided by this modelling approach should not be considered in the calculation of this RC slab response.

6.6 Calculation of internal efforts and fatigue damage in the deck slab

The main objective of the present section is the evaluation of the fatigue damage in the slab's transverse reinforcing bars. Since the fatigue damage is strongly influenced by the time variation of bending moments, during the passage of the train, its behaviour throughout the span is first discussed. The evaluation of this parameter, which cannot be experimentally measured, is relevant both to a structural analysis and to better understand the local behaviour of the RC slab. Dynamic coefficients, calculated based on the results of these transverse bending moments, are also presented.

For that purpose, numerical analyses were performed, using the FE Model 2 aforementioned. All numeric analyses were carried out using the TBI methodology, considering an integration time increment equal to 0.001 s. According to the conclusions addressed in the previous section, only frequencies up to 20 Hz and the initial irregularities profile were considered. As verified in Chapter 5, the damping coefficient equal to 1% has not revealed suitable for these analyses, reason why only the realistic damping scenario mentioned in section 6.5.2.8 was adopted. The static correction procedure was applied in order to take into account the static component of the contribution of higher order modes. Regarding the train speed, an interval between 180 km/h and 260 km/h is considered, which corresponds to a variation of ≈ 20 % with respect to a frequent train speed of 220 km/h.

6.6.1 Transverse bending moments

Transverse bending moments were obtained for two different lines in the upper slab, namely the lines of maximum sagging and hogging transverse bending moments, indicated in Figure 6.54. The line of maximum sagging bending moments is the one which coincides with the cross-section's axis of symmetry. These lines are extended along a distance of 22.5 m in the centre of the deck, corresponding to a half of the girder length, without elements near of span's extremities. As explained in Chapter 5, in a static analysis these values would be almost

constant along each line but that might not occur in a dynamic calculation due to the influence of local vibration modes, reason why the most unfavourable position is evaluated along those lines.

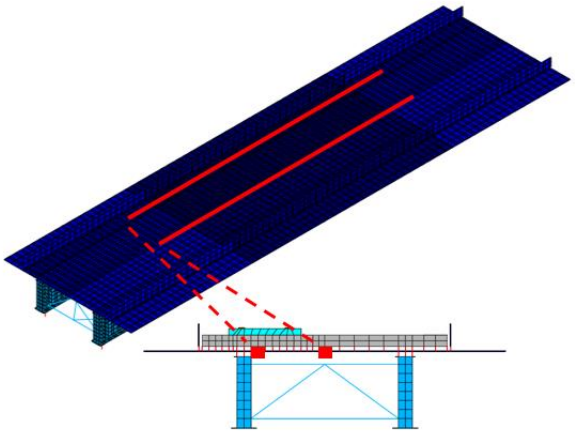

Figure 6.54 – Lines along which bending moments are calculated

Figure 6.55 shows the envelopes considering both the most unfavourable instant of time and position along the sagging and hogging bending moment lines, depicted as a function of the train speed. For this comparison, the results of TBI analyses without irregularities are also presented.

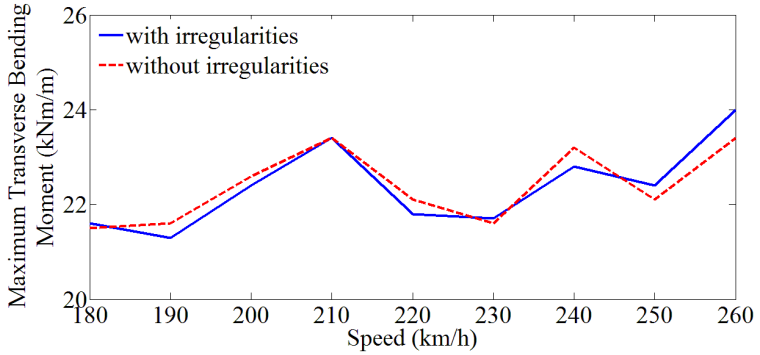

a)

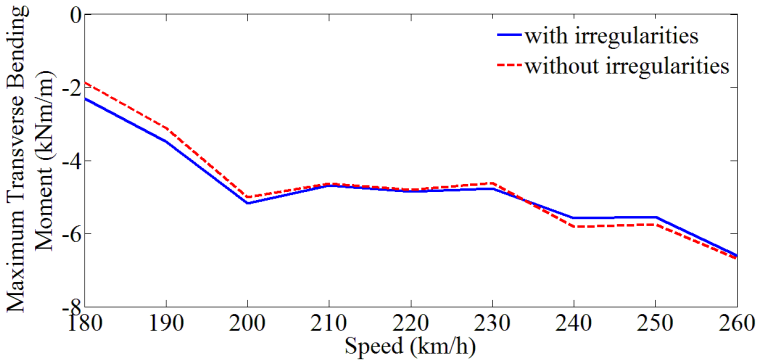

b)

Figure 6.55 – Influence of track irregularities on the maximum transverse bending moment in the deck slab: a) sagging moment; b) hogging moment

By observing the results presented in Figure 6.55 one can notice that only a slight difference occurs when track irregularities are considered in dynamic analyses. It should be pointed out that only frequencies up to 20 Hz were considered in the analyses, which take into account essentially vibration modes with higher wavelengths. This might be the reason why the dynamic response associated with these vibration modes has not been excited by the usually small irregularities wavelengths.

The train speed is also an important influencing parameter as it is possible to observe an increase of approximately 258 % in the maximum hogging transverse bending moment when the train speed increases from 180 km/h to 260 km/h.

Figure 6.56 exemplifies the bending moment time histories [Figure 6.56 a)] and correspondent auto-spectra [Figure 6.56 b)], for the location of maximum sagging moment at the mid-span cross-section, for a speed of 260 km/h. These results allow observing the negligible difference between responses considering or not the effect of track irregularities.

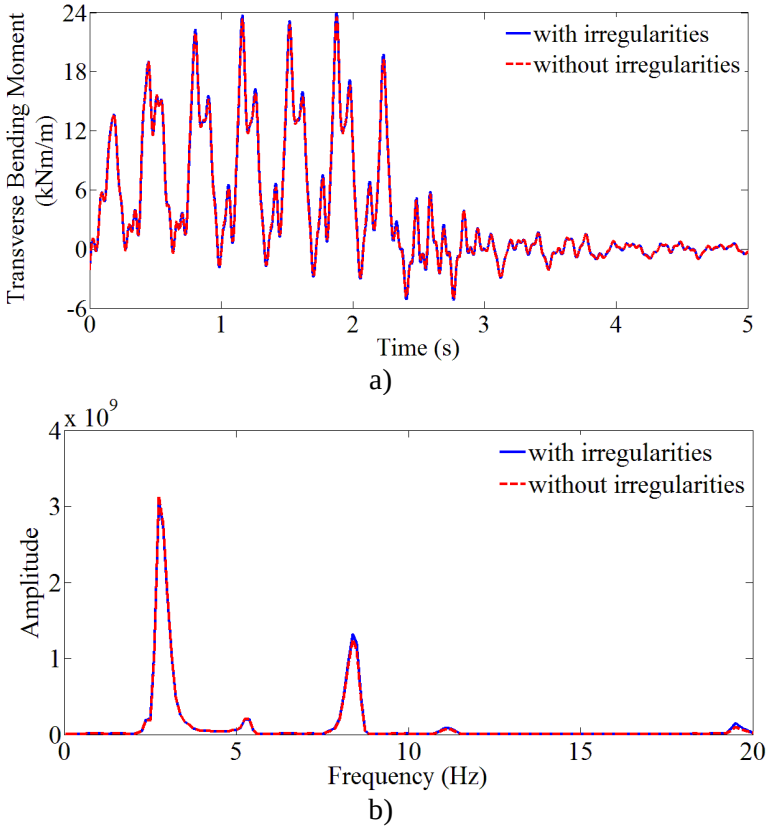

Figure 6.56 – Comparison of transverse bending moments, considering or not track irregularities, for a train speed of 260 km/h: a) time responses; b) auto-spectra

6.6.2 Dynamic coefficients

In the present section the dynamic amplification factors φ' and φ'' are calculated and compared with the ones suggested by the EN 1991-2 guidelines. These dynamic factors were obtained based on the results of transverse sagging and hogging bending moments in the deck slab, previously presented, considering the most unfavourable instant of time and the most unfavourable position along the lines depicted in Figure 6.54.

The procedure presented in section 5.6.4, based on Equations 5.15 to 5.17, was used in these calculations. As already mentioned, in this section only the initial track irregularities profile and the modal damping scenario mentioned in section 6.5.2.8 were considered. Table 6.8 summarises the maximum transverse bending moments obtained through each analysis.

Table 6.8 – Maximum transverse bending moments

	Maximum transverse bending moment (kNm/m)			
Moment line	M_A	M_B	M_C	$M_{D\ Initial}$
Sagging	16.45	23.79	23.43	24.00
Hogging	-4.85	-7.36	-6.69	-6.61

Table 6.9 presents the values of the dynamic amplification factor obtained based on the results of analyses *B* and *C*, through the application of Equation (5.15). The values suggested by the guidelines of the standard EN1991-2, obtained from annexes C and D, are also presented.

Table 6.9 – Calculated values of the amplification factor φ'

Bending moment	EN1991-2 (Annex C) φ'	EN1991-2 (Annex D) $0.5 \times \varphi'$	φ' [Equation (5.15)] (analysis B)	φ' [Equation (5.15)] (analysis C)
Sagging	0.318	0.299	0.446	0.424
Hogging			0.519	0.379

Concerning the guidelines presented in annexes C and D of the standard EN1991-2, the values presented in Table 6.9 were calculated through the application of Equations 2.18 and 3.14, respectively. For this purpose, the maximum permitted vehicle speed was taken equal to

220 km/h and the first natural bending frequency of the slab equal to 6.50 Hz. The determinant length is 17.40 m, considering a concrete deck slab with ballast bed and 5.80 m span between the two main girders, in the transverse direction (according to Table 6.2 of EN1991-2).

These dynamic analyses allowed the calculation of more realistic dynamic factors because numerical models of the bridge and the train, calibrated based on experimental results, were used. By observing Table 6.9 one can notice some differences between the numerically calculated values and code proposals. As can be seen, all the calculated values are higher than those suggested by EN1991-2, which means that, for this structure, the dynamic amplifications proposed by this code are not in the safe side.

Table 6.10 presents the values of the amplification factor φ'', obtained taking into account the TBI analyses considering the influence of track irregularities, through the application of Equation (5.16). The values suggested by the annex C of EN1991-2, considering different track maintenance levels, and by annex D, are also presented.

Table 6.10 – Calculated values of the dynamic amplification factor φ''

Bending moment	EN1991-2 (Annex C)		EN1991-2 (Annex D)	φ'' [Equation (5.16)]
	Standard (φ'')	*Careful* ($0.5 \times \varphi''$)	$0.25 \times \varphi''$	
Sagging	0.163	0.082	0.136	0.034
Hogging				0

By observing these results, one can see that the calculated dynamic amplification factor is generally lower than the suggested ones, even lower than the one indicated when a careful level of track maintenance is considered. It is worth mentioning that the amplification factor φ'' for the hogging moment position appears equal to zero because the calculations with irregularities led to a marginally lower value than the envelope result for the calculations without irregularities.

6.6.3 Fatigue damage

The fatigue analysis of the RC deck slab was performed focusing on the fatigue damage in its transverse reinforcement bars. It was calculated through the linear damage accumulation

method, taking into account the results of TBI dynamic analyses previously presented and following the same procedure described in section 5.7.

Figure 6.57 shows a 1 m wide element of the deck slab's cross section, including the reinforcement layout. The reinforcement area in the transverse direction is equal to 11.3 cm^2/m (Ø12//0.15m + Ø12//0.30m) either for bottom or top reinforcements. The lever arm, in the transverse direction, was taken as 0.334 m for both sagging and hogging moment lines.

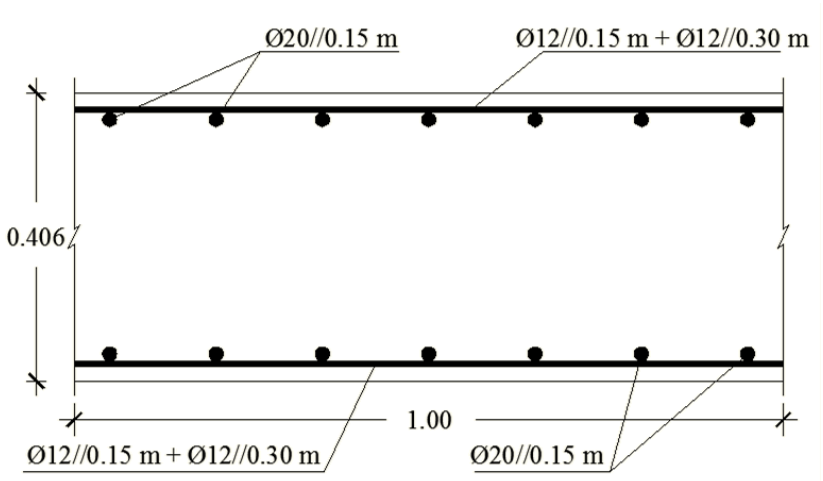

Figure 6.57 – Transverse cross section of the upper deck slab and reinforcement layout

The fatigue damage was determined for the most unfavourable position along the sagging and hogging bending moment lines depicted in Figure 6.54. It should be pointed out that the designation "sagging" and "hogging" was adopted according the results of the dynamic bending moments obtained taking into account only the effect due to the live load, i.e. the passage of AP trains, as previously presented in section 6.6.1. However, in this structure, the sum of dead and live load effects leads to hogging transverse bending moments in all the RC slab. Despite this, for a better understanding, the designation "sagging" will be kept for the results obtained along the line shown in Figure 6.54.

Figure 6.58 shows the envelopes of concrete stresses (in the transverse direction) at the upper and lower slab surfaces, considering the total effects from dead and live loads, along both sagging and hogging moment lines depicted in Figure 6.54. As can be seen, the upper surface is always in tension (positive stress values) while the lower surface is always in compression (negative stress values).

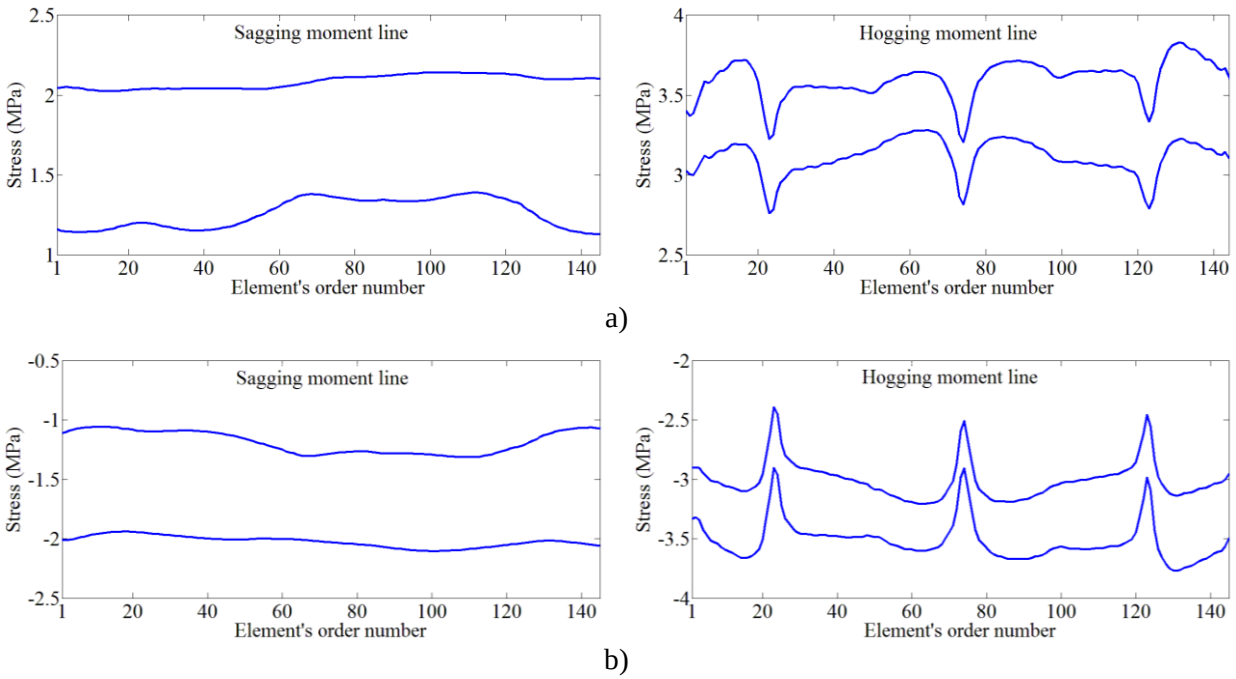

Figure 6.58 – Stress in the RC slab along both sagging and hogging moment lines for the passage of one AP train at 260 km/h: a) upper slab surface, b) lower slab surface

Bearing in mind the previous results, the fatigue damage in the top transverse reinforcement was calculated, in both sagging and hogging moment lines, for the passage of a single AP train. Figure 6.59 displays an envelope of fatigue damage, for the most unfavourable position along those lines, considering or not the effect of track irregularities.

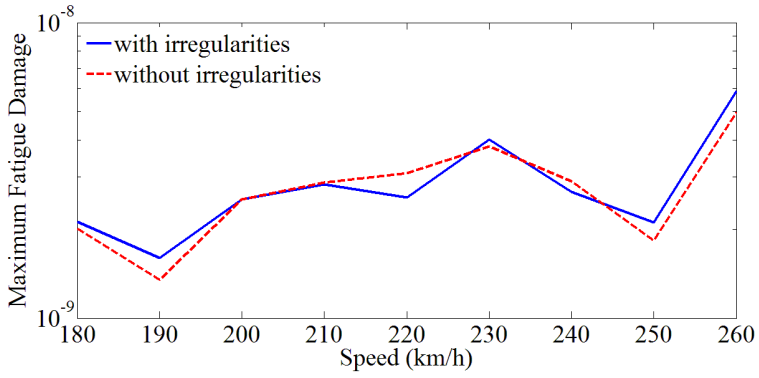

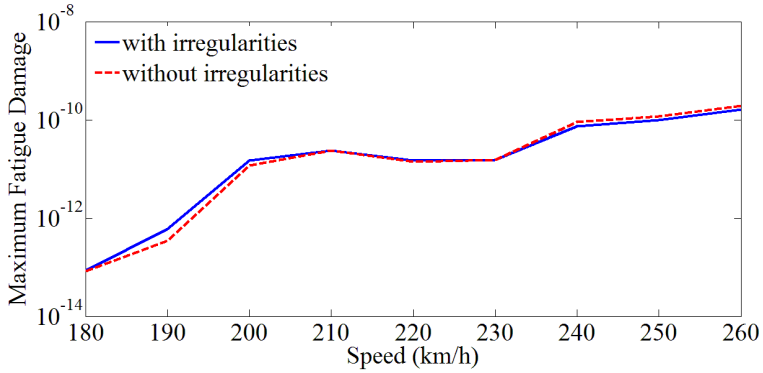

b)

Figure 6.59 – Influence of track irregularities in the maximum fatigue damage of the top reinforcement, for the passage of one AP train, in: a) sagging and b) hogging moment lines

By observing Figure 6.59 one can confirm that track irregularities are responsible by small differences in the calculated fatigue damage, in comparison with the results for a track without irregularities. However, the train speed is an important influencing parameter, with the fatigue damage increasing approximately 2×10^3 times when the train speed increases from 180 km/h to 260 km/h.

Once again, the area of transverse reinforcement required to prevent a fatigue failure of the reinforcement, was quantified. The required area of reinforcement was determined so that the fatigue damage *D*, during 100 years, is equal to 1. Table 6.11 shows the results for both the sagging and hogging moment positions (only the initial irregularities profile was taken into account). The traffic volume corresponds to 30 AP trains per day. The results here presented correspond to the most unfavourable train speed in the interval 180 km/h – 260 km/h and to the most critical position along the lines indicated in Figure 6.54. The area of reinforcement actually existing in this structure is also presented in this table.

Table 6.11 – Area of transverse reinforcement required to prevent fatigue failure, considering or not the influence of track irregularities, and area provided in the existing structure

Type of result	Area of reinforcement (cm^2/m)	
	Sagging	Hogging
Calculated area	6.45	4.33
Area provided in the existing structure	11.3	11.3

By comparing the area of reinforcement obtained through the calculations presented in this work with that really existing in the structure, one can see that, it is quite enough to ensure that, for this traffic scenario, fatigue damage in the transverse reinforcement of the RC slab will not occur throughout the fatigue life of the bridge.

6.7 Concluding remarks

In this Chapter, following a similar approach to the one explained in Chapter 5, the study of the dynamic behaviour and fatigue phenomenon of the RC slab of the access viaduct to Alcácer do Sal bridge is presented, where very interesting conclusions could be drawn.

As also previously verified, the experimental identification of the modal parameters, with particular attention to those related to local vibration modes of the slab, revealed to be an important step to the calibration of the numerical model. A preliminary sensitivity analysis showed a strong influence of the slab's thickness over modal parameters related to local vibration modes in which the slab behaviour is more prominent. Its inclusion on the calibration of the FE numerical model led to an increase in MAC coefficients, generically higher of 0.90, and a reduction in the average error between experimental and numerical frequencies to values approximately equal to 7.7 %, either for global and local vibration modes. One considerable difference for the previous case study was the possibility of measure directly the slab's dynamic response, when subjected to the passage of AP trains, enabling a direct numerical validation of this structural element through the comparison between numerical and experimental responses.

The influence of other parameters, such as longitudinal stiffness of the bearings, irregularities profiles, cut-off frequency values and damping coefficients, was studied in order to get a better agreement between numerical and experimental dynamic responses. Once again was confirmed the relevance of the nonlinear behaviour of the guided supports in the longitudinal direction, since better results were obtained after its correction. It was found that the space variability taken into account in the track irregularities profiles only led to non-significant differences in the numerical responses, particularly noticeable in the accelerations results. Regarding the cut-off frequencies, a good agreement between numerical and experimental dynamic responses was achieved, both in terms of displacements, deformations

and accelerations of the RC slab, when frequencies up to 20 Hz were considered. Particularly in terms of deformations, the numerical model was validated based on experimental results measured in several locations, showing generically that this modelling strategy overestimate the dynamic responses when higher frequencies are considered.

The effect of train speed and track irregularities in the dynamic behaviour and fatigue damage of the RC slab was analysed. In this case study, since only frequencies up to 20 Hz were considered, just a slight difference occurred when track irregularities were considered in dynamic analyses. However, the train speed revealed to be an important influencing parameter, since differences of 14 % and 258 % were observed in the maximum sagging and hogging transverse bending moments, respectively, when the train speed increases from 180 km/h to 260 km/h.

Regarding the fatigue damage, in this case study, it was calculated only for the top transverse reinforcement, in both sagging and hogging moment lines. This was due to the fact that, considering the sum of the effects of dead and live loads, the upper slab surface is always in tension while the bottom surface is always in compression, leading to the occurrence of fatigue only in the top reinforcement. The influence of track irregularities seems to be negligible in terms of fatigue damage of the RC slab. This was also noted in terms of the area of transverse reinforcement required to prevent fatigue failure. By comparing the area of reinforcement obtained through the calculations presented in this work with that really existing in the structure, it was possible to conclude that, for the traffic scenario adopted, fatigue damage in the transverse reinforcement of the RC slab will not occur throughout the fatigue life of the bridge.

Chapter 7

Conclusions and future research

7.1 Conclusions

This thesis is focused on the evaluation of the local behaviour of the upper RC slab of railway viaducts with longitudinal girders. The work aims at giving a contribution to understand the real performance of this structural element when subjected to cyclic loading due to the passage of railway traffic at different speeds. Particular attention was given to the development and validation of numerical models for calculation of internal efforts in the RC slab caused by the passage of real trains. Getting a realistic estimate of these internal efforts is a paramount step for carrying out a fatigue assessment of the structure. Throughout the thesis, the influence of some relevant parameters is analysed and discussed. These parameters are: the modal damping ratios; the stiffness of the bearings; the track irregularities; the train speed; the cut-off frequency considered in the analysis of each response variable. The relevance of additional geometric and physical parameters was also analysed in the process of calibration of numerical models.

Two different railway viaducts, with distinct structural solutions, were considered in this thesis: in one of the viaducts, the upper RC slab is connected to a precast, prestressed concrete, U-shaped girder; in the other one, the slab is connected to steel I-shaped girders. Extensive experimental works were performed on those viaducts in order to get experimental data for: i) the calibration of numerical models, based on experimentally identified frequencies and

vibration modes; ii) validation of the numerical models, based on the measured structural response during the passage of real trains.

The first part of the present work (Chapters 2, 3 and 4) presents a revision of the state of the art concerning the main numerical and experimental tools and methodologies used in the present thesis to study the dynamic behaviour of reinforced concrete slabs.

Chapter 2 describes the most common approaches that are used in the numerical evaluation of bridges' dynamic responses, showing the main advantages and drawbacks of each methodology, in terms of the balance between accuracy and computational costs. Particular attention was given to the train-bridge interaction method, which was used in the present work to perform numerical dynamic analyses. A description of the static correction procedure, implemented to take into account the static contribution of higher-frequency vibration modes (usually not explicitly considered in analyses according to the basic modal-superposition method), is addressed. Some of the recommendations defined in the European standards, in order to guarantee both the structural and operational safety of railway bridges in high-speed railway lines, are also presented. A review of some of the most up to date studies and recommendations about this topic allowed the discussion about current recommendations, especially regarding the vertical bridge deck acceleration limits.

A brief presentation of the fatigue behaviour of reinforcing steel, concrete and reinforced concrete structures is carried out in Chapter 3. Two procedures for fatigue analysis of railway bridge decks are shown: the damage equivalent stress method and the damage accumulation method. The limitations and field of application of each approach are identified. The various steps involved in the application of the damage accumulation method (the one used in the present work) are described.

Chapter 4 addresses the calibration of numerical models based on the comparison between numerical and experimental responses. Given the great importance of knowing the real response of structures, the first part of this chapter presents an overview of some experimental techniques widely used to obtain the dynamic response of bridges. Concerning the identification of modal parameters of the structures, two widely used techniques are discussed: the EFFD and SSI methods. Some examples of their application were shown. Furthermore, some of the most up to date studies related to the measurement of the dynamic response of structures under railway traffic were shown. In the final part of the chapter, the calibration methodology employed in this thesis is described. It is an iterative methodology, based on an

optimisation algorithm. Its main steps are: the sensitivity analysis; the vibration modes' pairing; the optimisation phase.

The two real railway bridges, which were considered in this thesis, are presented in Chapters 5 and 6. These structures, with typical solutions widely employed in the construction of railway bridges and viaducts, are: i) the Alverca railway viaduct, composed by a U-shaped precast and prestressed concrete girder and an upper slender reinforced concrete slab, forming a single-cell box girder; ii) the access viaduct to Alcácer do Sal bridge, a steel-concrete composite structure, composed by two I-shaped steel plate girders connected on the top by a reinforced concrete slab.

Extensive experimental work as well as detailed parametric analyses were carried out for both case studies, in order to assess the local dynamic behaviour and fatigue damage of their reinforced concrete slabs. The specific conclusions reached for each case study are presented in the following sections.

7.1.1 Alverca railway viaduct

A 3D numerical model of three simply supported adjacent spans was developed. In order to reproduce the longitudinal continuity established by the railway track along successive spans, a detailed modelling of track components was implemented. A preliminary numerical modal analysis allowed identifying different types of vibration modes, namely, global vibration modes related do movements of all structure and local vibration modes mainly related to movements of the upper deck slab.

In order to calibrate the numerical model, an ambient vibration test was performed, considering two distinct phases: the first allowed the identification of global vibration modes of the structure and the second one the identification of vibration modes of the upper deck slab. For the global identification, the installation of accelerometers in the ballast retaining walls rather than directly in the girder has proved to be particularly efficient. The installation of accelerometers, in the longitudinal direction, near the bearings also has proved to have a huge contribution to evaluate the coupling effect between adjacent spans provided by the track. Relating to the identification of local vibration modes, the installation of the accelerometers in the sleepers has also proved to be particularly efficient. Due to the high level of confinement of the ballast layer, especially under the sleepers, and attending that vibration modes of the track

have frequencies generally above 100 Hz, it was possible to clearly separate and identify the local vibration modes associated to the movements of the upper slab based on the measurement of sleepers' vibrations. The identification of the modal parameters (natural frequencies, mode shapes and damping coefficients), related to 10 vibration modes, was successfully performed by applying a stochastic subspace identification method.

The calibration of the FE numerical model of the viaduct was performed based on the results of both phases of the ambient vibration tests. The calibration process involved three steps: sensitivity analysis; modes' pairing; and optimisation.

The sensitivity analysis showed that some parameters of the numerical model, such as the elasticity modulus of concrete and ballast and the ballast density weight, influenced in a significant manner the modal parameters associated to the vibration of the upper slab. A considerable number of numerical parameters was used in the optimisation process due to two aspects: the fact that the deck's components (prefabricated U-shaped girder and upper slab) present distinct characteristics; the inclusion of the track in the numerical model.

The pairing between the numerical and the experimental vibration modes was only possible using a recent technique based on the EMAC parameter, which involves the creation of clusters of the numerical model and the calculation of modal strain energies associated to these clusters.

The optimisation of the numerical model using a genetic algorithm proved to be a robust process and allowed obtaining differences, between numerical and experimental frequencies, below 5 % for all vibration modes, and MAC coefficients above 0.95, for the global modes, and between 0.85 and 0.90, for the local modes.

The validation of the numerical model was based on the results of a dynamic test under railway traffic that allowed the measurement of displacements, accelerations and deformations in the mid-span section of the lower deck slab and displacements at the bearings' area, for the passage of AP trains at speeds of 157 km/h and 185 km/h. The comparison between numerical and experimental responses showed that the calibrated numerical model did not properly reflect the bearings' mobility effect, due to their non-linear behaviour, which differs whether they are solicited by ambient actions or by railway traffic. By changing the longitudinal stiffness in the numerical model it was possible to obtain a very good agreement between the experimental and numerical records for the passage of the AP train.

In order to properly evaluate the fatigue behaviour of the upper slab of the deck, a new FE model was developed, taking into account only one of the structure's spans and adopting a more refined discretisation of the slab and track components. For that purpose, train-bridge interaction (TBI) analyses were carried out in order to assess the dynamic behaviour of the upper slab when subjected to the passage of trains at speeds up to 240 km/h.

Since the presence of vibration modes of the upper slab with high frequencies was noticed, a static correction procedure was first implemented in TBI analyses to take into account the static contribution of higher-frequency vibration modes (usually not explicitly considered in analyses according to the basic modal-superposition method). The results provided by this methodology were compared with the ones obtained by Newmark's direct integration method and revealed that this procedure should be considered in the calculation of local effects in railway deck slabs.

The study carried out aimed to investigate the effects of track irregularities, damping coefficients and train speeds on the fatigue behaviour of the upper RC deck slab, based on its dynamic behaviour when subjected to the passage of trains at speeds up to 240 km/h. For a realistic assessment of the fatigue strength of transverse reinforcing bars, detailed calculations of the time histories of bending moments in the slab are needed. For this purpose, TBI analyses were carried out using the FE models previously calibrated based on experimental dynamic tests. It was shown that:

- Different track irregularities gave rise to considerably different vertical accelerations and bending moments in the deck slab. This fact is related to the way how the predominant wavelengths, in each irregularities profile, contribute to the excitation of local vibration modes of the upper deck slab. In this specific case, for the range of train speeds considered, the wavelengths in the range between 1.0 m to 3.0 m revealed to be preponderant, corresponding to excitation frequencies approximately between 18 Hz and 55 Hz, which values are close to the frequency of some vibration modes of the upper slab, being responsible for their excitation.
- Furthermore, a great different in the calculation results could be noticed when the irregularities were not considered in TBI dynamic analyses. This is because the excitation of local vibration modes of the upper slab, with higher frequency values, does not occur in that case.

- A procedure, based on the application of the logarithmic decrement method to the slab's acceleration records (measured during the passage of real trains), was used to identify the damping coefficients of local vibration modes of the upper deck slab. The acceleration record for the time interval after the passage of each axles group was considered for this purpose, which allowed identifying the frequencies with significant contribution to the response that are essentially related with local vibration modes. A mean value equal to 5.02 % was achieved, which is considerably higher than those values obtained during the ambient vibration tests and that were used in the initial validation of the numerical model.

- Significant differences in dynamic responses were observed, for train speeds higher than 200 km/h, when calculations based on the experimentally identified damping coefficients are compared with calculations using smaller damping coefficients (suggested by guidelines for the design of new structures). Increases of 33 % and 19 % were obtained in the maximum values of sagging and hogging transverse bending moments, respectively, once again due to higher vibration amplitudes in local vibration modes of the deck slab.

- Dynamic amplification factors, φ' and φ'', were obtained based on the results of sagging and hogging transverse bending moments in the upper slab provided by TBI analyses. These dynamic analyses allowed the calculation of more realistic dynamic factors because numerical models of the bridge and the train, calibrated based on experimental results, were used. By comparison between the calculated and suggested dynamic factors, it was possible to note that the normative values suggested by Annexes C and D of EN 1991-2 for dynamic and fatigue analyses, respectively, are not always on the safe side to evaluate the local behaviour of the upper RC slab of the bridge.

- The influence of track irregularities and damping was also shown for the fatigue damage due to the passage of a single train, and for the area of transverse reinforcement needed to prevent fatigue failure. It was shown that both influencing parameters are very important for the study of the fatigue behaviour of railway bridge deck slabs. Track irregularities gave rise to an increase of 213 % in terms of area of reinforcement required for fatigue safety. Different damping scenarios led to differences of 46.5 % in that required area.

- The train speed also revealed to be an important influencing parameter in the fatigue damage, where an increase of approximately 5×10^3 times was reported when the train speed increases from 160 km/h to 240 km/h (maximum value obtained using the irregularities profile of 2014).
- In this study, the structure response was calculated considering frequencies up to 60 Hz. It was expected beforehand that high frequencies have an important role because of the very small transverse span of this viaduct. It was concluded that important increases in the fatigue damage of the slab occur as the cut-off frequency is increased up to 60 Hz, both for the bottom and top reinforcement. These increases are associated with the contribution of several local vibration modes of the slab in this range of frequencies. These results suggest that it is very important to adopt a high frequency threshold when studying localised phenomenon. However, in this structure it was not possible to measure strains in the RC slab between supports in the girder webs. Measuring such strains would be very important for the validation of the calculated internal efforts.

  In the second case study of this thesis (the access viaduct to the Alcácer do Sal bridge) it was possible to measure such strains.

7.1.2 Access viaduct to the Alcácer do Sal bridge

The behaviour of the neutral span of this viaduct was simulated using a 3D numerical model. This is a simply supported span, without continuity to the neighbourhood spans, either provided by the structure (structural joints introduce a discontinuity of the structure and ballast layer) or by the rails (due to existence of rail expansion devices).

Experimental tests were performed to allow the identification of both global modal parameters of the structure and local modal parameters of the RC deck slab. During the ambient vibration tests, accelerometers were installed in the sleepers as well as in heavy steel cubes, the latter placed within the ballast layer. This approach was due to the difficult access to the main girders and the RC slab, either by the bottom or top side. This solution has proved once again to be particularly efficient in the identification of vibration modes of the slab as well as the identification of global vibration modes since, in the latter case, the accelerometers were placed

near the longitudinal alignment of the girders, which are responsible for the main global movements of the deck.

The experimental identification of the aforementioned modal parameters revealed to be an important step to the calibration of the numerical model. A preliminary sensitivity analysis showed a strong influence of the slab's thickness over modal parameters related to local vibration modes in which the slab behaviour is more prominent. The optimisation phase of the model, using a genetic algorithm, involved the use of 3 design variables (the 3 parameters of the numerical model) and 10 modal responses (5 frequencies and 5 MAC values) regarding the global and local vibration modes of the structure. It led to an increase in MAC coefficients, generically higher of 0.90, and a reduction in the average error between experimental and numerical frequencies to values approximately equal to 7.7 %, either for global and local vibration modes.

Measurements of the slab's dynamic response, when subjected to the passage of AP trains at speeds of 220 km/h, enabled a direct numerical validation of this structural element. The comparison between numerical and experimental responses, considering initially frequencies up to 15 Hz, showed a very good agreement, only possible by changing the longitudinal stiffness of mobile bearings (which had previously been determined by calibration based on experimental modal parameters). This fact has demonstrated once again that the supports exhibit a nonlinear behaviour. Their horizontal stiffness is different depending on whether they are solicited by low amplitude actions or by railway traffic.

The acceleration results provided by the dynamic test under the passage of real trains also allowed the identification of modal damping coefficients for vibration levels corresponding to the passage of trains. The same methodology presented in Chapter 5, based on the application of the logarithmic decrement method to the slab's acceleration records, after the passage of each train's axles group, was used. It was concluded that higher values of modal damping coefficients have to be used when higher vibration levels were considered, by comparison to those obtained with vibration levels close to the ambient ones. A scenario with values of 3.71 % and 5.08 % for all global and slab's local vibration modes, respectively, and 0.5 % for the remaining vibration modes related to the steel structure, was initially adopted. The comparison between numerical and experimental dynamic responses showed a better agreement when the modal damping coefficients used in numerical analyses are obtained through this alternative procedure.

The validated model was to be used in the calculation of internal efforts in the RC slab and, in turn, also in the calculation of the fatigue damage in that structural element. Therefore, it was important to analyse the structure response considering frequencies higher than 15 Hz. In fact, it is well known that the calculation of internal efforts has to be carried out considering the complete range of frequencies which effectively contribute to the structural response. Therefore, additional analyses and comparisons with experimental results were carried out, in order to investigate the implications of the adopted cut-off frequency (upper limit for the range of frequencies considered in the analysis of the structural response). The following conclusions could be drawn:

- In order to evaluate the suitability of the FE model to obtain a proper dynamic response in higher frequencies, new cut-off frequencies were considered, namely 20 Hz, 30 Hz and 60 Hz. The numerical modelling approach was the one previously described, considering damping ratios of 3.71 %, 5.08 % and 0,5 %. An excellent agreement (between measurements and calculations) was obtained in terms of displacement results, for all the cut-off frequencies. This is because frequencies higher than 15 Hz have a negligible contribution to the analysed displacement. Contrarily, significant differences were found between numerical and experimental responses, either in terms of deformations or accelerations, when frequencies higher than 15 Hz are considered in the responses.

- Deformation responses were measured in several positions of the slab. The measured results revealed that the time-history of deformations is characterized with a good approximation if a cut-off frequency of 15 Hz is adopted. The measured records for all of the deformation sensors also revealed some contribution of the frequencies approximately equal to 17 Hz and 19 Hz. The contribution of frequencies higher than 20 Hz is negligible in the measured deformations.

  The calculated deformations in the same positions also showed an influence of the frequencies approximately equal to 17 Hz and 19 Hz. However, the magnitude of the contribution of these frequencies is markedly higher in the calculation results, when compared to the measured ones. Besides that, the calculated deformations also included very important contributions of frequencies higher than 20Hz. This means that the dynamic responses provided by the FE model are being overestimated when higher frequencies are taken into account.

- In order to get additional conclusions regarding these differences between measurements and calculations, the following influencing parameters were investigated: train speed; track irregularities; and modal damping coefficients for the local vibration modes with highest frequencies.

- It is known that a small variation in the train speed can give rise to a relevant decrease in the structure response. Such variation can be enough to avoid resonance with a certain vibration mode. This issue was analysed in this structure. However, it was concluded that, in this case, small variations in the train speed do not have a significant effect to prevent the higher excitation around the frequencies equal to 17 Hz and 19 Hz. Only slight changes in the dynamic responses could be noted for frequencies higher than 15 Hz, which are particularly visible in the auto-spectra responses.

- Then, the influence of track irregularities was assessed. It was concluded that, even if track irregularities are ignored in the TBI analyses, the calculated deformations and accelerations overestimate the measured ones for frequencies higher than 15 Hz.

  The consequences of using different track irregularities profiles in the TBI analyses were also studied. It was found that, for frequencies up to 20 Hz, different track irregularities profiles gave rise to minor differences in the numerical responses. For higher frequencies, distinct track irregularities profiles resulted in different structural responses, which are especially noticeable in the accelerations records. They are a consequence of the way how these different profiles contribute to the excitation of some local vibration modes of the RC deck slab.

  However, the calculated results provided by frequencies higher than 15 Hz were still overestimating the measured ones.

- Because of that, further analyses were made to study the influence of the modal damping coefficient for high-frequency vibration modes. A new scenario, based on higher damping coefficients (3.71 % for global vibration modes, 5.08 % for all local vibration modes up to a frequency equal to 17.5 Hz and 10 % for all the remaining vibration modes), revealed to be preponderant to reach a better approximation between numerical and experimental responses up to 20 Hz. It has to be pointed out that these higher modal damping ratios are not unrealistic. Investigations carried out

by the ERRI Commission D 214 (1999) revealed that some railway bridges exhibit damping ratios as high as 10 % even for the first vibration mode. Those values were obtained by the ERRI Commission for vibration levels corresponding to the passage of real trains.

Even for this last scenario of damping coefficients, the calculated deformations overestimate the measured ones for frequencies higher than 20 Hz. Further investigations should be conducted in the future for clarification of the reasons for these differences.

- The previous conclusions can be summarized as: i) the last scenario for damping coefficients provided a good agreement with measured deformations for frequencies up to 20 Hz; ii) the measured deformations caused by the train passage revealed a negligible contribution of frequencies higher than 20 Hz; iii) therefore, the calculation of internal forces and fatigue damage in this structure should be conducted considering that scenario for damping coefficients and a cut-off frequency of 20 Hz.

The validated numerical model, with the aforementioned scenario for damping coefficients, was then used to analyse the transverse bending behaviour of the RC slab of the Alcácer viaduct. It was also used to perform the fatigue analysis of that structure, focusing on the fatigue damage on the transverse reinforcement bars.

In the analysis of transverse bending moments, it was found that track irregularities have a minor effect. This is a consequence of considering frequencies up to 20 Hz in the analyses. These frequencies correspond to vibration modes with high wavelengths. For the high speeds under evaluation, the dynamic response associated with these vibration modes has not been excited by the usually small irregularities wavelengths. The train speed has proved to be an important influencing parameter: the maximum hogging transverse bending moment increases approximately 258 % when the train speed increases from 180 km/h to 260 km/h.

Dynamic amplification factors, φ' and φ'', were also quantified based on the results of these sagging and hogging transverse bending moments in the slab, provided by TBI analyses. These dynamic analyses allowed the calculation of realistic dynamic factors because numerical models of the bridge and the train, calibrated based on experimental results, were used. All the

calculated values of φ' are higher than those suggested by EN1991-2, which means that, in this specific case, the dynamic amplifications proposed by this code are not in the safe side for the evaluation of the local dynamic behaviour of the RC deck slab.

Regarding the fatigue damage, in this slab structure it was calculated only for the top transverse reinforcement. This was due to the fact that, considering the sum of the effects of dead and live loads, the concrete's upper layer of the slab was always in tension while the concrete's lower layer of the slab was always in compression. Therefore, transverse internal efforts induce concrete cracking in the upper slab surface only. These cracks cannot be easily inspected because this slab surface is covered by the railway track components. Consequently, the verifications of fatigue safety of the top reinforcement cannot be relaxed.

The fatigue analysis was performed for the passage of AP trains at different speeds and considering the effect of track irregularities. As expected, after the previously drawn conclusions, the track irregularities only led to small increases in the calculated fatigue damage, in comparison with the results for a track without irregularities. Contrarily, it was found that the train speed is an important variable. The calculated fatigue damage increases considerably when the train speed increases from 180 km/h to 260 km/h.

The area of transverse reinforcement required to prevent a fatigue failure of the reinforcement was calculated considering a traffic scenario of 30 AP trains per day. It was concluded that, for this scenario, fatigue failure of the transverse reinforcement of the RC slab will not occur throughout the design life of the bridge.

7.2 Future research

Some research topics, which should be developed in the future, in line with the work conducted on this thesis, are presented below.

- **Further development of numerical models to accurately reproduce the measured structural response considering high cut-off frequency values**

  The accurate simulation of the structure response, during the passage of real trains, considering the contribution of a high range of frequencies (high cut-off frequency)

is a major challenge. Accurate characterization and modelling is needed for the structure, track and vehicle. Further developments are needed aiming at getting improved numerical predictions of the structure response.

- **Experimental validation based on strain measurements in reinforcement bars**

  In the structures analysed in the present thesis, it was not possible to install sensors to measure strains in the reinforcing bars. In structures where there are not access restrictions to take measurements in the slab reinforcement bars, either in the construction phase or later when the structure is in service, strain gages can be installed. These measurements would be very important for further validation of methodologies for calculation of fatigue damage due to local effects in railway bridges' RC slabs.

- **Influence of cracking in the dynamic behaviour of the RC slab**

  It is well known that the occurrence of cracking in concrete elements strongly influences the structure's stiffness and, consequently, its dynamic behaviour. In the specific case of railway bridges, the repetitive and continuous loading to which they are subjected gives rise to a modification of the structure response throughout time, namely because of the degradation of the bond action between concrete and reinforcement. The detailed assessment of the consequences of concrete cracking, in this type of structure, should be conducted in the future.

- **Probabilistic analysis of fatigue safety**

  The fatigue safety may be analysed based on a probabilistic assessment of the structural reliability, looking for a more realistic characterization of both the structural response and the actions to which the structure is subjected. The uncertainty associated to these aspects can be characterized by random variables associated to both the parameters of the numerical model (material densities, modulus of elasticity, S-N curves that characterise the fatigue resistance of the materials, among others) and the parameters that characterise the traffic (axle loads,

wheelbase, among others). The reliability analysis can be based on the Monte Carlo or Latin Hypercube methods, generating samples, according to the probability distributions of the random variables. The structural response of the generated samples may be obtained based on the calibrated numerical model and the fatigue damage may be evaluated based on the damage accumulation method. Then the final fatigue safety assessment might be carried out by estimating the probability of failure using statistical measures that better reflect the distribution of the structural response.

The success of probabilistic fatigue analyses is strongly dependent on the quality of the characterization of the various variable parameters. This thesis provided relevant indications about parameters such as the modal damping coefficients, the horizontal stiffness of the supports, the cut-off frequencies and the track irregularities.

- **Influence of different trains and traffic scenario in the dynamic behaviour and fatigue resistance**

  In both structures analysed in Chapters 5 and 6, the effects of different track irregularities, damping coefficients and train speeds in the dynamic behaviour or fatigue phenomenon, were evaluated for the passage of only one AP passenger train. Furthermore, the total fatigue damage over the design life of those bridges was evaluated considering a constant traffic throughout time.

  Since the fatigue damage is extremely sensitive to the stress amplitudes, it is important to carry out analyses for different types of trains. Different trains, either passenger or freight trains, have different characteristics and, consequently, different aggressiveness to the structure. TBI analyses can only be performed if the train properties are characterized (both for the power cars and remaining wagons). The characterization available is still insufficient.

- **Determination of λ factors for local fatigue verifications using the damage equivalent stress method**

  The European standard EN1992-2 provides fatigue-resistance verification procedures for structural elements in reinforced or prestressed concrete, namely the damage accumulation method and the damage equivalent stress method. The latter allows, in

a simplified way, to carry out such verification based on the determination of the stress amplitude caused by the load model LM71 and considering correction factors (λ factors) that take into account the structural typology, the type of traffic, the total life of the structure and the number of existing tracks.

The λ factors related to the structural typology were calibrated to provide good results for a limited number of structural configurations, especially those with a preponderant global behaviour. Thus, in order to obtain realistic results through this method in the study of the fatigue phenomenon in deck slabs, it is important to correctly evaluate these corrective factors, considering different structural topologies.

Bibliography

Albuquerque, C., Calçada, R. and Delgado, R. (2010). Resonant effects on a bowstring railway bridge with orthotropic deck. *Bridge Maintenance, Safety, Management and Life-Cycle Optimization.* Philadelphia, USA: CRC Press, Taylor & Francis Group.

Allemang, R. J. (2003). The modal assurance criterion - twenty years of use and abuse. *Journal of Sound and Vibration,* 37**,** 14-21.

Alves costa, P. (2011). *Vibrações do sistema via-maciço induzidas por tráfego ferroviário. Modelação numérica e validação experimental.* PhD Thesis (in Portuguese), Faculty of Engineering of the University of Porto.

Ansys. (2007). Structural Analysis Guide - Release 11.0. *In:* ANSYS (ed.).

Antrim, J. (1965). A study of the Mechanism of Fatigue in Cement Paste and Plain Concrete. Joint Highway Research Project, Indiana Department of Transportation and Purdue University.

Aparicio, A. (2004). Differences in designing high-speed railway bridges and highway bridges. *In: Bridges for High-Speed Railways.* Faculty of Engineering of the University of Porto, Porto, Portugal.

Arora, V. (2011). Comparative study of finite element model updating methods. *Journal of Vibration and Control,* 17**,** 2023–2039.

Artemis. (2009). ARTeMIS Extractor Pro - Academic Licence. User's Manual. *In:* SVS (ed.). Aalborg, Denmark.

Baeβler, M., Bronsert, J., Cuéllar, P. and Rucker, W. (2012). The stability of ballasted track supported on vibrating bridge decks, abutments and transition zones. *Railways 2012 - 1st International Conference on Railway Technology: Research, Development and Maintenance.* Las Palmas de Gran Canaria, Spain.

Barbero, J. (2001). *Dinámica de puentes de ferrocarril para alta velocidad: métodos de cálculo y estudio de la resonancia.* PhD Thesis (in Spanish), Universidad Politécnica de Madrid.

Benedettini, F. and Gentile, C. (2011). Operational modal testing and FE model tuning of a cable-stayed bridge. *Engineering Structures,* 33**,** 2063–2073.

Bogaert, P. V. (2009). Fatigue due to concrete compression in bridges compared to practice. *The Annual International fib Symposium - Concrete: 21st century superhero - Building a sustainable future.* London.

Brehm, M. (2011). *Vibration-based model updating: Reduction and quantification of uncertainties.* PhD Thesis, Bauhaus Universitat Weimar.

Brehm, M., Zabel, V. and Bucher, C. (2010). An automatic mode pairing strategy using an enhanced modal assurance criterion based on modal strain energies. *Journal of Sound and Vibration,* 329**,** 5375-92.

Brincker, R., Ventura, C. and Andersen, P. (2001). Damping estimation by frequency domain decomposition. *IMAC XIX Conference.* Kissimmee, USA.

Brincker, R., Zhang, L. and Andersen, P. (2000). Modal identification from ambient responses using frequency domain decomposition. *IMAC XVIII Conference.* San Antonio, USA.

Brown, J. and Kunnath, S. K. (2004). Low-Cycle Fatigue Failure of Reinforcing Steel Bars. *Materials Journal,* 101**,** 457-466.

Brownjohn, J., Magalhães, F., Caetano, E. and Cunha, A. (2010). Ambient vibration re-testing and operation modal analysis of the Humber bridge. *Engineering Structures,* 32**,** 2003-2018.

Cabboi, A., Magalhães, F., Gentile, C. and Cunha, A. (2017). Automated modal identification and tracking: application to an iron arch bridge. *Structural Control and Health Monitoring*, 24.

Cachim, P. (1999). *Experimental and numerical analysis of the behaviour of structural concrete under fatigue loading with applications to concrete pavements.* PhD Thesis, Faculty of Engineering of the University of Porto.

Calçada, R. (1995). *Efeitos dinâmicos em pontes resultantes do tráfego ferroviário a alta velocidade.* Faculdade de Engenharia da Universidade do Porto.

Calçada, R., Cunha, A. and Delgado, R. (2002). Dynamic analysis of metallic arch railway bridge. *Journal of Bridge Engineering*, 7, 214-222.

Cantero, D., Arvidsson, T., Obrien, E. and Karoumi, R. (2016). Train–track–bridge modelling and review of parameters. *Structure and Infrastructure Engineering*, 12**,** 1051–1064.

Cantieni, R., Brehm, M., Zabel, V., Rauert, T. and Hoffmeister, B. (2008). Ambient modal analysis and model updating of a twin composite filler beam railway bridge for high-speed trains with continuous ballast. *IMAC-XXVI Conference on Structural Dynamics.* Orlando, USA.

CEB. (1988). Fatigue of concrete structures - State of the art report - Bulletin 188. Comite Euro-International du Beton.

CEN. (2002). EN1991-1-1. Actions on structures – Part 1-1: General actions – Densities, self-weight, imposed loads for buildings. Brussels: Europeean Committee for Standardization.

CEN. (2003). EN1991-2. Actions on Structures - Part 2: General Actions - Traffic loads on bridges. Brussels: Europeean Committee for Standardization.

CEN. (2004). EN1992-1-1. Eurocode 2: Design of concrete structures. Part 1-1: General rules and rules for buildings. Brussels: European Committee for Standardization.

CEN. (2005 a)). EN1990-A2. Basis of structural design - Annex A: Applications for bridges. Brussels: Europeean Committee for Standardization.

CEN. (2005 b)). EN1992-2. Eurocode 2: Design of concrete structures. Part 2: Concrete bridges - Design and detailing rules. Brussels: European Committee for Standardization.

Chellini, G., Nardini, L. and Salvatore, W. (2011). Dynamical identification and modelling of steel–concrete composite high-speed railway bridges. *Structure and Infrastructure Engineering,* 7**,** 823-841.

Chen, X., Omenzetter, P. and Beskhyroun, S. (2013). Dynamic Testing and Long Term Monitoring of a Twelve Span Viaduct. *Key Engineering Materials,* 570, 342-349.

Chopra, A. K. (1995). *Dynamics of Structures: Theory and Applications to Earthquake Engineering,* Berkeley, Prentice Hall International.

Clough, R. and Penzien, R. (1993). *Dynamics of Structures, Second Edition,* New York, McGraw-Hill International Editions.

Costa, C., Ribeiro, D., Jorge, P., Silva, R. and Arêde, A. (2016). Calibration of the numerical model of a stone masonry railway bridge based on experimentally identified modal parameters. *Engineering Structures,* 123**,** 354-371.

Cruz, S. (1994). *Comportamento dinâmico de pontes ferroviárias em vias de alta velocidade.* MSc Thesis (in Portuguese), Faculty of Engineering of the University of Porto.

Cunha, A. and Caetano, E. (2006). Experimental modal analysis of civil engineering structures. *Journal of Sound and Vibration,* 40**,** 12-20.

Cunha, A., Caetano, E. and Magalhães, F. (2007). Output-only dynamic testing of bridges and special structures. *Structural Concrete - Journal of FIB,* 8**,** 67-85.

Cunha, A., Caetano, E., Calçada, R., Roeck, G. D. and Peeters, B. 2003. Dynamic measurements on bridges: design, rehabilitation and monitoring. *Bridge Engineering*, 156, 135-148.

D216, E. (2000). ERRI D216/DT386 - Fatigue in concrete railway bridges. Independent verification of the correction factors used in the fatigue design in Eurocode 2, Part 2. Ultrecht, European Rail Research Institute.

D216, E. (2002). ERRI D216/RP1 - Fatigue of railway bridges. State of the art report. Ultrecht, European Rail Research Institute.

D216, E. (2003). ERRI D216/RP3 - Fatigue in concrete railway bridges. FInal report. Ultrecht. European Rail Research Institute.

De Roeck, G. (2010). Exploring the limits and extending the borders of structural health monitoring. VIADINTEL Project Kick-off. Madrid, Spain.

Deng, L. and Cai, C. S. (2010). Bridge model updating using response surface method and genetic algorithm. *Journal of Bridge Engineering,* 15**,** 553-564.

Dieleman, L. and Fournol, A. (2003). Dynamic behaviour of the short railway bridges. *IABSE - Structures for high-speed railway transportation.* Antwerp, Belgium.

ECORYS. (2014). The Economic Footprint of Railway Transport in Europe. Brussels, Belgium.

ERRI D183/DT346. (1997). Fatigue design of concrete railway bridges. Utrecht, Netherlands: European Rail Research Institute (ERRI).

ERRI D214/RP9. (2001). Railway bridges for speeds >200 km/h. Final Report. Utrecht, Netherlands: European Rail Research Institute (ERRI).

ERRI D202/DT363. (1997). Improved knowledge of forces in CWR track (including switches). Measurements of lateral resistance, longitudinal resistance and change of neutral rail temperature (NRT) for ballasted track. European Rail Research Institute, Utrecht, Netherlands.

European Commission. (2008). Modern Rail, Modern Europe - Towards an Integrated European Railway Area. Directorate-General for Energy and Transport - European Commission. Luxembourg.

Evangelista, L. and Vedova, M. (2004). The Italian High Speed Network: Design and Construction of the Reinforced Concrete Bridges. *In: Bridges for High-Speed Railways.* Faculty of Engineering of the University of Porto, Porto, Portugal.

Figueira, D., Sousa, C., Calçada, R. and Neves, A. S. (2016 a)). Push-Off Tests in the Study of Cyclic Behavior of Interfaces between Concretes Cast at Different Times. *Journal of Structural Engineering (United States),* 142.

Figueira, D., Sousa, C., Calçada, R. and Neves, A. S. (2016 b)). Design recommendations for reinforced concrete interfaces based on statistical and probabilistic methods. *Structural Concrete,* 17**,** 811-823.

Figueiredo, H. (2007). *Dinâmica de pontes mistas aço-betão em linhas de alta velocidade* MSc Thesis (in Portuguese). Faculty of Engineering of the University of Porto.

Fluorseals. (2006). Material specification - PTFE. *In:* FLUORSEALS (ed.). Italy.

Fortunato, E. (2005). *Renewal of railway platforms - Studies related to the load capacity (in Portuguese).* Faculdade de Engenharia da Universidade do Porto.

Fryba, L. (1996). *Dynamics of railway bridges*. London: Thomas Telford.

Fryba, L. (2002). Resistance of reinforced and prestressed concrete structures to repeated dynamic loads. *High Performance Structures and Composites.* Southampton.

Gabaldón, F., Goicolea, J. M., Navarro, J. A., Riquelme, F. and Domínguez, F. (2004). Dynamic analysis of hyperestatic structures under high speed train loads. *Bridges for High-Speed Railways.* Porto, Portugal.

Gentile, C. and Cabrera, F. (2001). Dynamic assessment of a curved cable-stayed bridge at the Malpensa airport. *Structural Engineering International,* 1**,** 52-58.

Gentile, C. and Saisi, A. (2011). Ambient vibration testing and condition assessment of the Paderno iron arch bridge. *Journal of Construction and Building Materials,* 25**,** 3709-3720.

Geoview. (2011). http://pt.geoview.info/ponte_da_variante_ferroviaria_de_alcacer,50013563p. 2011 (accessed at 18/10/2017).

Goicolea, J. M., Gabaldón, F., Dominguez, J. and Navarro, J. A. (2004). Dynamic loads in new engineering codes for railway bridges in Europe and Spain. *Bridges for High-Speed Railways.* Faculty of Engineering of the University of Porto, Porto, Portugal.

Goicolea, J. M. and Gabaldón, F. (2012). Dynamics of high-speed railway bridges: Methods and design issues. *Bridge Vibration and Controls: New Research*. Pages 89-111.

Guo, W. W., Xia, H., De roeck, G. and Liu, K. (2012). Integral model for train-track-bridge interaction on the Sesia viaduct: Dynamic simulation and critical assessment. *Computers & Structures,* 112-113**,** 205–216.

Hanson, N. W. (1960). Precast-Prestressed Concrete Bridges 2: Horizontal Shear Connections. *Journal of the PCA Research and Development Laboratories,* 2**,** 38-58.

Henriques, A. (1998). *Application of new safety formats in the design of structural concrete*. PhD Thesis (in Portuguese), Faculty of Engineering of the University of Porto.

Herwig, A. and Bruhwiler, E. (2011). In-situ dynamic behavior of a railway bridge girder under fatigue causing traffic loading. *In: Proc. ISCAP'11 - International Conference on Applications of Statistics and Probability in Civil Engineering*. Zurich.

Hess, P., Bruchman, D., Assakkaf, I. and Ayyub, B. (2002). Uncertainties in Material Strength, Geometric and Load Variables. *Naval Engineers Journal*.

Holmen, J. O. (1982). Fatigue of concrete by constant and variable amplitude loading. ACI Special Publication SP75, Fatigue of concrete structures, S.P. Shah, Ed.

IAPF. (2010). Instructions of actions to consider in railway bridges (in Spanish). Ministerio de Fomento – Gobierno de España.

Jafarkhani, R. and Masri, S. F. (2011). Finite element model updating using evolutionary strategy for damage detectio. *Computer-Aided Civil and Infrastructure Engineering,* 26**,** 207-224.

Jaishi, B. and Ren, W. (2005). Structural finite element model updating using ambient vibration test results. *Journal of Structural Engineering,* 45**,** 617-628.

JCSS. (2001). Probabilistic Model Code Part 2: Load Models. Joint Committee on Structural Safety.

Johansson, U. (2004). *Fatigue tests and analysis of reinforced concrete bridge deck models.* Royal Institute of Technology. Stockholm. Sweden.

Knothe, K. and Wu, Y. (1998). Receptance behavior of railway track and subgrade. *Archive of Applied Mechanics,* 68**,** 457-470.

Leander, J. and Karoumi, R. (2013). Dynamics of thick bridge beams and its influence on fatigue life predictions. *Journal of Constructional Steel Research*, 89, 262–271.

Lei, X. and Noda, N. (2002). Analyses of dynamic response of vehicle and track coupling system with random irregularity of track vertical profile. *Journal of Sound and Vibration,* 258**,** 147-165.

Li, Q., Xu, Y., Wu, D. and Chen, Z. (2010). Computer-aided Nonlinear Vehicle-bridge Interaction Analysis. *Journal of Vibration and Control*, Volume 16**,** 1791–1816.

Lin, W., Yoda, T. and Taniguchi, N. (2015). Effects of bridge accessories in steel–concrete composite railway bridges in service condition. *Journal of Bridge Engineering*, 10.1061/(ASCE)BE.1943-5592.0000809.

Liu, K., Reynders, E., De roeck, G. and Lombaert, G. (2009). Experimental and numerical analysis of a composite bridge for high-speed trains. *Journal of Sound and Vibration*, 320**,** 201-220.

Lou, P. (2007). Finite element analysis for train-track-bridge interaction system. Arch Appl Mech.

Magalhães, F. (2004). *Identificação modal estocástica para validação experimental de modelos numéricos.* MSc Thesis (in Portuguese), Faculty of Engineering of the University of Porto.

Majka, M. and Hartnett, M. (2008). Effects of speed, load and damping on the dynamic response of railway bridges and vehicles. *Computers & Structures*, 86, 556-572.

Man, A. D. (2002). *DYNATRACK. A survey of dynamic railway track properties and their quality.* PhD Thesis, Delft University.

Manterola, J. (2006). *Bridges notes for design, calculation and construction* (in Spanish), Colegio de Ingenieros de caminios, canales e puertos.

Martínez-Rodrigo, M. D. (2009). *Atenuación de vibraciones resonantes en puentes de ferrocarril de alta velocidad mediante amortiguadores fluido-viscosos.* PhD Thesis, Universidad Politecnica de Valencia.

Meixedo, A., Ribeiro, D., Calçada, R. and Delgado, R. (2014). Global and local dynamic effects on a railway viaduct with precast deck. *In Railways'2014.* Corsica, France.

Miner, M. A. (1945). Cumulative damage in fatigue. *Journal of Applied Mechanics*, 12**,,** 159-164.

Mirza, S., Kikuchi, D. and Macgregor, J. (1979). Statistical descriptions of strength of concrete. *Journal of the Structural Division*, 105**,** 1021-1037.

Moller, P. and Friberg, O. (1998). Updating large finite element models in structural dynamics. *AIAA Journal*, 36 (10)**,,** 1861-1868.

Morassi, A. and Tonon, S. (2008). Dynamic testing for structural identification of a bridge. *Journal of Bridge Engineering*, 13**,** 573–585.

Murdock, J. and Kessler, C. E. (1960). The mechanism of fatigue failure in concrete. Report No 587. University of Illinois, Illinois.

Museros, P., Castillo-Linares, A. and Alarcón, E. (2004). Wheel-Rail Contact Forces in High-Speed Simply Supported Bridges at Resonance. *Procedings of the 7th International Conference on Computational StructuresTechnology.* Lisboa, Portugal.

Museros, P., Romero, M. L., Poy, A. and Alarcon, E. (2002). Advances in the analysis of short span railway bridges for high-speed lines. *Computers & Structures*, 80**,** 2121-2132.

Neves, S., Azevedo, A. and Calçada, R. (2012). A direct method for analyzing the vertical vehicle-structure interaction. *Engineering Structures*, 34**,** 414-420.

Nguyen, K., Goicolea, J.M., Galbadón, F. (2014). Comparison of dynamic effects of high-speed traffic load on ballasted track using a simplified two-dimensional and full three-dimensional model. *Proceedings of the Institution of Mechanical Engineers, Part F: Journal of Rail and Rapid Transit*, 228 (2), 128-142.

Norris, P. (2005). Recent advances in the understanding of bridge dynamic behaviour on the West Coast main line route modernisation project. *In: Dynamics of High-Speed Railway Bridges.* Porto, Portugal.

Nunes, M. (2014). *Fatigue Behaviour of Steel Reinforcement Bars at Very High Number of Cycles.* Phd Thesis, École Polytechnique Fédérale de Lausanne.

Optislang. (2008). OptiSLang – the optimizing Structural Language, 3.0 edition. *In:* GMBH, D. (ed.). Weimar, Germany.

Paz, M. (1980). *Structural Dynamics: Theory and Computation*, New York, Van Nostrand Reinhold.

Pimentel, M., Bruhwiler, E. and Figueiras, J. (2008). Fatigue life of short-span reinforced concrete railway bridges. *Structural Concrete - Journal of FIB*, 9,**,** 215-222.

Pimentel, M., Figueiras, J. and Bruhwiler, E. (2008). Dynamic analysis for fatigue safety examination of existing short span concrete railway bridges. EURODYN 2008 - 7th European Conference on Structural Dynamics. Southampton, UK.

Pinto, N. M. P., Ribeiro, C. A., Mendes, J. and Calçada, R. (2009). An optical system for monitoring the vertical displacements of the track in high speed railways. *3rd International Conference on Integrity, Reliability and Failure.* Portugal.

Pombo, J. (2004). *A Multibody Methodology for Railway Dynamics Applications.* PhD Thesis, Instituto Superior Técnico.

Infraestruturas de Portugal. 2017. *Mapa da refe ferroviária portuguesa* (Online). (Accessed in 25/06/2017).

Pruijssers, A. (1988). *Aggregate interlock and dowel action under monotonic and cyclic loading.* PhD Thesis. Delft University of Technology.

Rae, P. and Dattelbaum, D. 2004. The properties of poli(tetrafluoroethylene) (PTFE) in compression. *Polymer Journal*, 45, 7615-7625.

REFER. (2010). Variante de Alcácer. REFER, Lisboa.

Ren, W. and Chen, H. (2010). Finite element model updating in structural dynamics by using the response surface method. *Engineering Structures,* Volume 32**,** 2455-2465.

Ren, W.-X., Peng, X.-L. and Lin, Y.-Q. (2005). Experimental and analytical studies on dynamic characteristics of a large span cable-stayed bridge. *Engineering Structures,* 27**,** 535-548.

Reynolds, P., Pavic, A. and Ibrahim, Z. (2004). Changes of modal properties of a stadium structure occupied by a crowd. *IMAC XXII Conference.* Dearborn, USA.

Ribeiro, D. (2012). *Efeitos dinâmicos induzidos por tráfego em pontes ferroviárias: modelação numérica, calibração e validação experimental.* PhD Thesis (in Portuguese). Faculty of Engineering of the University of Porto.

Ribeiro, D., Calçada, R., Delgado, R., Brehm, M. and Zabel, V. (2012). Finite element model updating of a bowstring-arch railway bridge based on experimental modal parameters. *Engineering Structures,* 40**,** 413-435.

Ribeiro, D., Calçada, R., Delgado, R., Brehm, R. and Zabel, V. (2013). Finite-element model calibration of a railway vehicle based on experimental modal parameters. *Vehicle System Dynamics,* 51**,** 821-856.

Rigueiro, M. (2007). *Avaliação dos Efeitos Dinâmicos em Pontes Ferroviárias de Alta Velocidade de Pequeno e Médio Vão.* PhD Thesis (in Portuguese). Faculdade de Ciências e Tecnologia da Universidade de Coimbra.

RILEM. (1984). Long term random dynamic loading of concrete structures. RILEM COMMITEE 36-RDL report: Matériaux et Constructions.

Rinde, J. (1970). Poisson's ratio for rigid plastic foams. *J. Applied Polymer Science*, 14, 1913-1926.

RIVAS (2013). Overview of Methods for Measurement of Track Irregularities Important for Ground-Borne Vibration: Railway Induced Vibration Abatement Solutions Collaborative project.

Rocha, J., Henriques, A. and Calçada, R. (2012). Safety assessment of a short span railway bridge for high-speed traffic using simulation techniques. *Engineering Structures*, 40, 141-154.

Rocha, J. M., Henriques, A. A. and Calçada, R. (2014). Probabilistic safety assessment of a short span high-speed railway bridge. *Engineering Structures*, 71**,** 99-111.

Rodrigues, J. (2004). *Identificação modal estocástica - métodos de análise e aplicações em estruturas de engenharia civil. Tese de Doutoramento.* PhD Thesis (in Portuguese). Faculty of Engineering of the University of Porto.

Sarmadi, H., Karamodin, A. and Entezami, A. (2016). A new iterative model updating technique based on least squares minimal residual method using measured modal data. *Applied Mathematical Modelling*, 40**,** 10323-10341.

Schlafli, M. and Bruhwiler, E. (1998). Fatigue of existing reinforced concrete bridge deck slabs. *Engineering & Structures*, 20, 991-998.

Sogabe, M., Furukawa, A., Shimoura, T., Iida, T., Matsumoto, N. and Wakui, H. (2005). Deflection limits of structures for train speed-up. *QR of RTI* 46**,** 130-136.

Sousa, C. (2012). *Analysis of cyclic and long-term effects in continuous precast railway bridge decks.* PhD Thesis. Faculty of Engineering of the University of Porto.

Sousa, C., Calçada, R. and Serra Neves, A. (2015). Numerical evaluation of the non-linear behaviour of cracked RC members under variable-amplitude cyclic loading. *Materials and Structures*, 48(9), 2815-2838.

Tepfers, R. (1979). Tensile fatigue strength of plain concrete. *ACI Structural Journal*, 78**,** 919-933.

Teughels, A., De roeck, G. and Suykens, J. (2003). Global optimization by coupled local minimizers and its application to FE model updating. *Computers & Structures*, Volume 81**,** 2337-2351.

Tilly, G. P. (1979). Fatigue of steel reinforcement bars in concrete: a review. *Fatigue of Engineering Materials and Structures*, 2**,** 251-268.

Tomioka, T. and Takigami, T. (2010). Reduction of bending vibration in railway vehicle carbodies using carbody–bogie dynamic interaction. *Vehicle System Dynamics*, Volume 48 467-486.

Toolbox, T. E. (2011). *The Engineering Toolbox. www.engineeringtoolbox.com/* (Accessed in 4/2015)

TSI. (2002). Technical Specification for Interoperability. Official Journal of the European Communities.

UIC. (2008). UIC 719R. Earthworks and track bed for railway lines.

Ülker-Kaustell, M. and Karoumi, R. (2012). Influence of non-linear stiffness and damping on the train-bridge resonance of a simply supported railway bridge. *Engineering Structures*, 41, 350–355.

Walraven, J. C. (1994). Rough cracks subjected to earthquake loading. *Journal of Structural Engineering ASCE*, 120 (5), 1510-1524.

Wang, H., Li, A. and Li, J. (2010). Progressive finite element model calibration of a long-span suspension bridge based on ambient vibration and static measurements. *Engineering Structures*, 32**,** 2546-2556.

Wisniewski, D. (2007). *Safety Formats for the Assessment of Concrete Bridges.* PhD Thesis, University of Minho.

Wu, Y., Yang, Y. and Yau, J. (2010). Three-dimensional analysis of train-rail-bridge interaction problems. *Vehicle System Dynamics,* 36**,** 1-35.

Xia, H. and Zhang, N. (2005). Dynamic analysis of railway bridge under high-speed trains. *Computers & Structures,* 83.

Xia, H., Zhang, N. and Guo, W. W. (2006). Analysis of resonance mechanism and conditions of train-bridge system. *Journal of Sound and Vibration,* 297, 810-822.

Xiankun, L., Lingmi, Z., Qintao, G. and Yufeng, Z. (2009). Dynamic finite element model updating of prestressed concrete continuous box-girder bridge. *Earthquake Engineering and Engineering Vibration,* 8**,** 399-407.

Yang, F. and Fonder, G. (1996). An iterative solution method for dynamic response of bridge-vehicles systems. *Earthquake Engineering & Structural Dynamics,* 25**,** 195-215.

Yang, Y. and Chen, Y. (2009). A new direct method for updating structural models based on measured modal data. *Engineering Structures,* Volume 31**,** 32-42.

Yang, Y. B. and Y.S.Wu. (2001). A versatile element for analyzing vehicle-bridge interaction response. *Engineering Structures,* 23**,** 452-469.

Yang, Y. B., Yau, J. D. and Wu, Y. S. (2004). *Vehicle-Bridge Interaction Dynamics: with applications to high-speed railways,* World Scientific Publishing Company.

Zabel, V. and Brehm, M. (2009a). Stochastic model updating methods. *IMAC XXVII.* Orlando, USA.

Zabel, V. and Brehm, M. (2009b). System identification of high-speed railway bridges. *In:* DYNARDO (ed.) *Weimar Optimization and Stochastic Days.* Weimar.

Zacher, M. and Baeβler, M. (2009). Dynamic behaviour of ballast on railway bridges. *Dynamics of High-Speed Railway Bridges.* Taylor & Francis.

Zanuy, C., Fuente, P. and Albajar, L. (2007). Effect of fatigue degradation of the compression zone of concrete in reinforced concrete sections. *Engineering & Structures,* 29, 2908-2920.

Zanuy, C., Albajar, L. and Fuente, P. (2009). Sectional Analysis of Concrete Structures under Fatigue Loading. *ACI Structural Journal,* 106, 667-677.

Zanuy, C., Maya, L. F., Albajar, L. and Fuente, P. (2011). Transverse fatigue behaviour of lightly reinforced concrete bridge decks. *Engineering & Structures*, 33, 2839-2849.

Zhai, W., Wang, S., Zang, N., Gao, M., Xia, H., Cai, C. and Zhao, C. (2013). High-speed train–track–bridge dynamic interactions – Part II: experimental validation and engineering application. *International Journal of Rail Transportation*, 1**,** 25-41.

Zhou, L., Wang, L., Chen, L. and Ou, J. (2016). Structural finite element model updating by using response surfaces and radial basis functions. *Advances in Structural Engineering*, 19**,** 1446–1462.

Zordan, T., Briseghella, B. and Liu, T. (2014). Finite element model updating of a tied-arch bridge using Douglas-Reid method and Rosenbrock optimization algorithm. *Journal of Traffic and Transportation Engineering*, 1**,** 280-292.

Zwolski, J. and Bien, J. (2011). Modal Analysis of Bridge Structures by Means of Forced Vibration Tests. *Journal of Civil Engineering and Management*, 17**,** 590-599.

Annex A

Numerical and experimental deformation responses throughout the RC deck slab

This annex shows a comparison between numerical and experimental deformation responses, obtained in the locations 1 to 4 depicted in Figure 6.26. Cut-off frequencies equal to 15 Hz, 20 Hz and 60 Hz were adopted, which were obtained through the application of Chebyshev (type II) low-pass digital filters of order 11, 13 and 20, respectively, and stopband attenuation equal to 45 dB.

In the numerical calculations a time step equal to 0.001 s and a train speed equal to 220 km/h were considered. Only the initial track irregularities profile was taken into account. The damping scenario was adopted as follows: 3.71 % and 5.08 % for all global and slab's local vibration modes, respectively, and 0.5 % for the remaining vibration modes related to the steel structure. In the following figures, the time-history records correspond to the figures presented on the left-hand side while the respective auto-spectra are presented in the right-hand side.

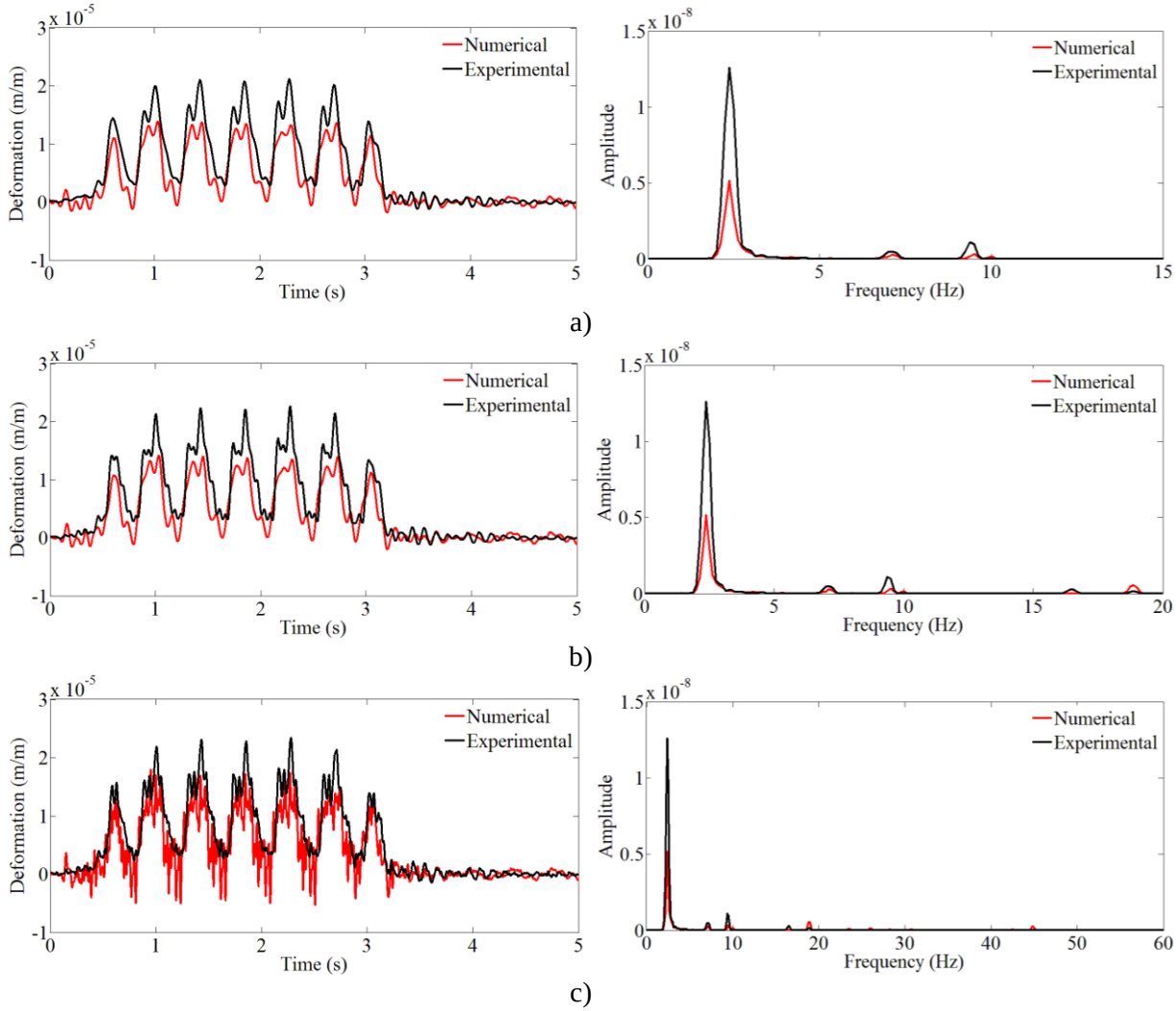

Figure A.1 – Comparison between measured and calculated deformation records, obtained in the position 1, for different cut-off frequencies: a) 15 Hz; b) 20 Hz; c) 60 Hz

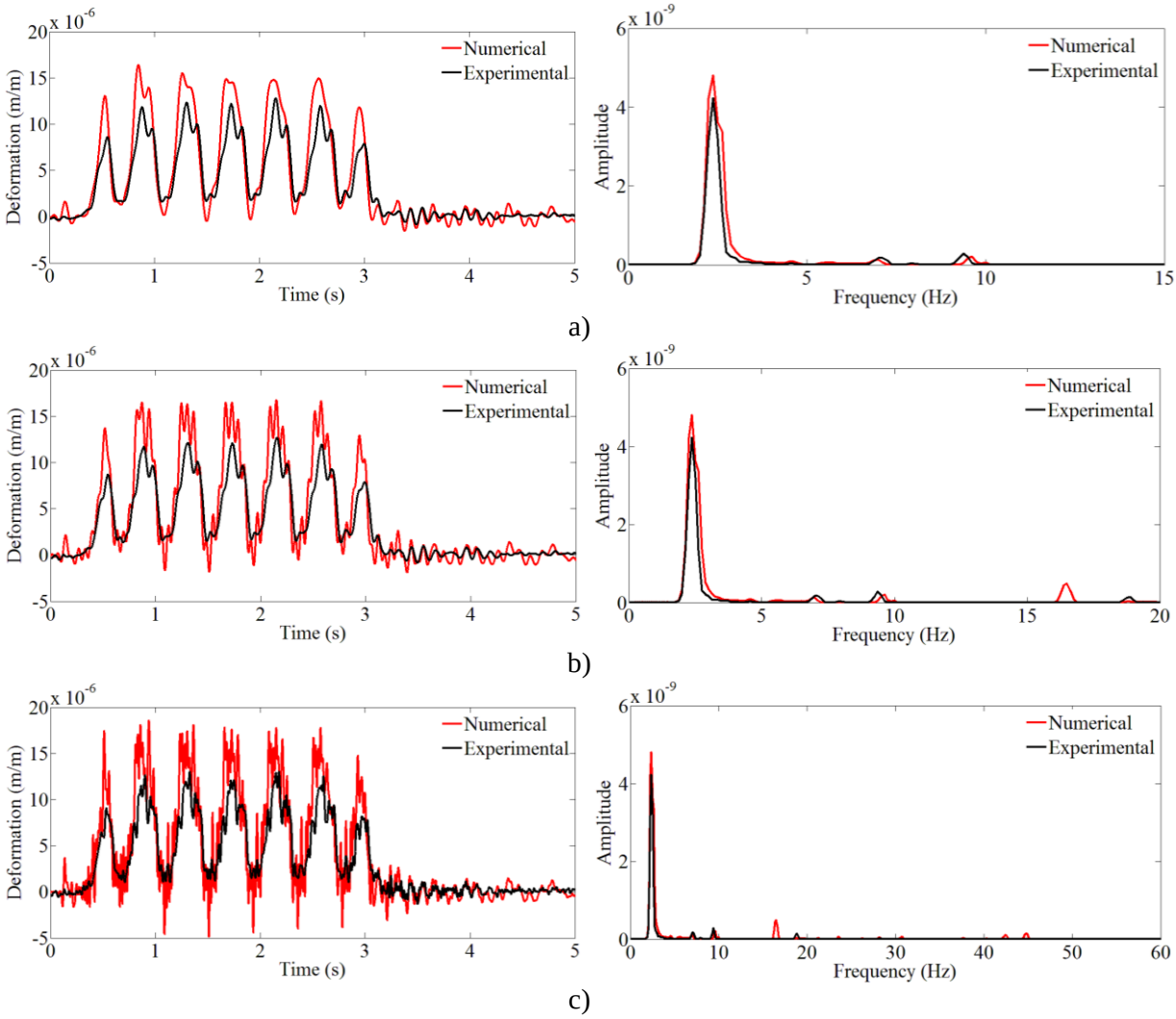

Figure A.2 – Comparison between measured and calculated deformation records, obtained in the position 2, for different cut-off frequencies: a) 15 Hz; b) 20 Hz; c) 60 Hz

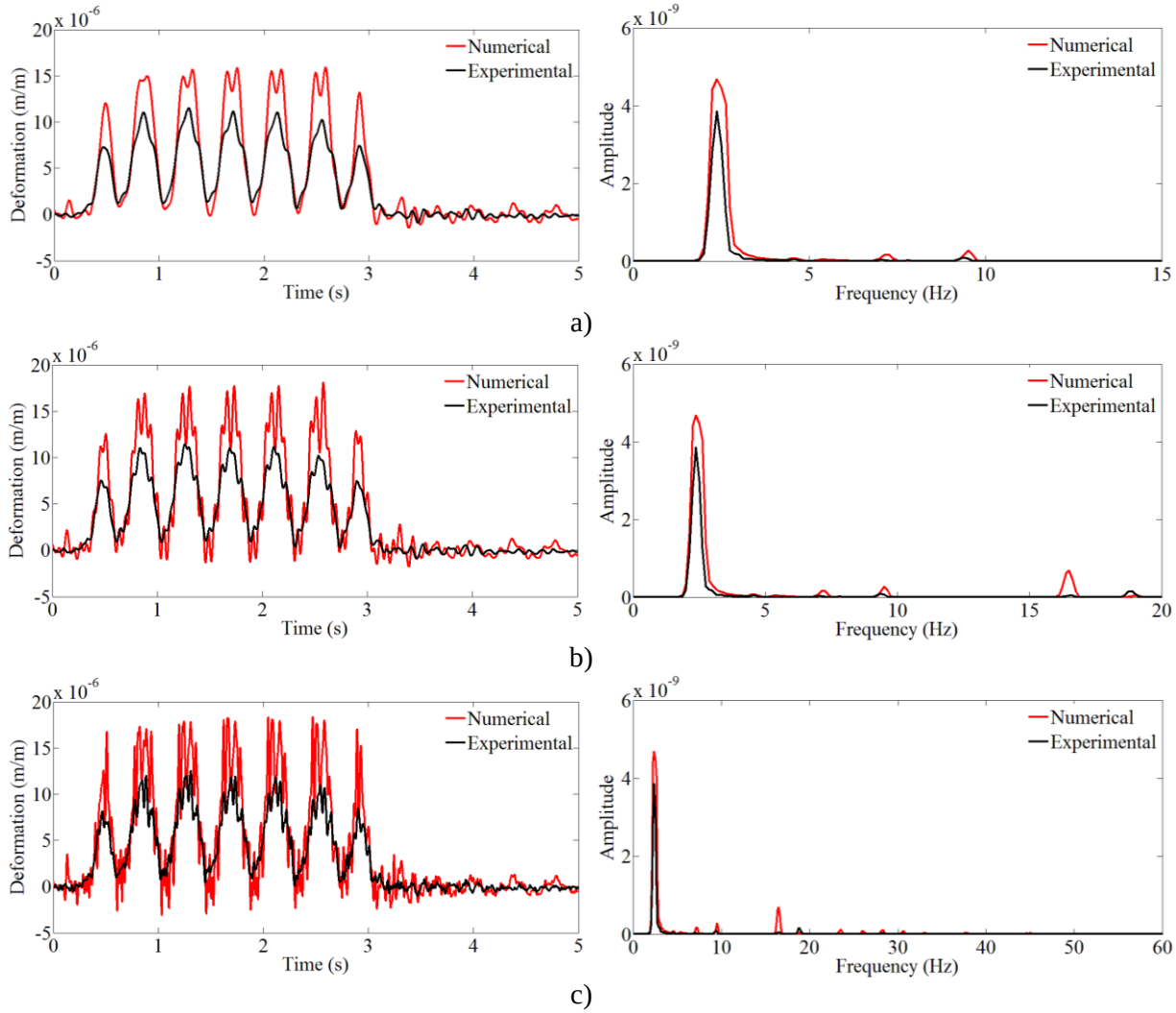

Figure A.3 – Comparison between measured and calculated deformation records, obtained in the position 3, for different cut-off frequencies: a) 15 Hz; b) 20 Hz; c) 60 Hz

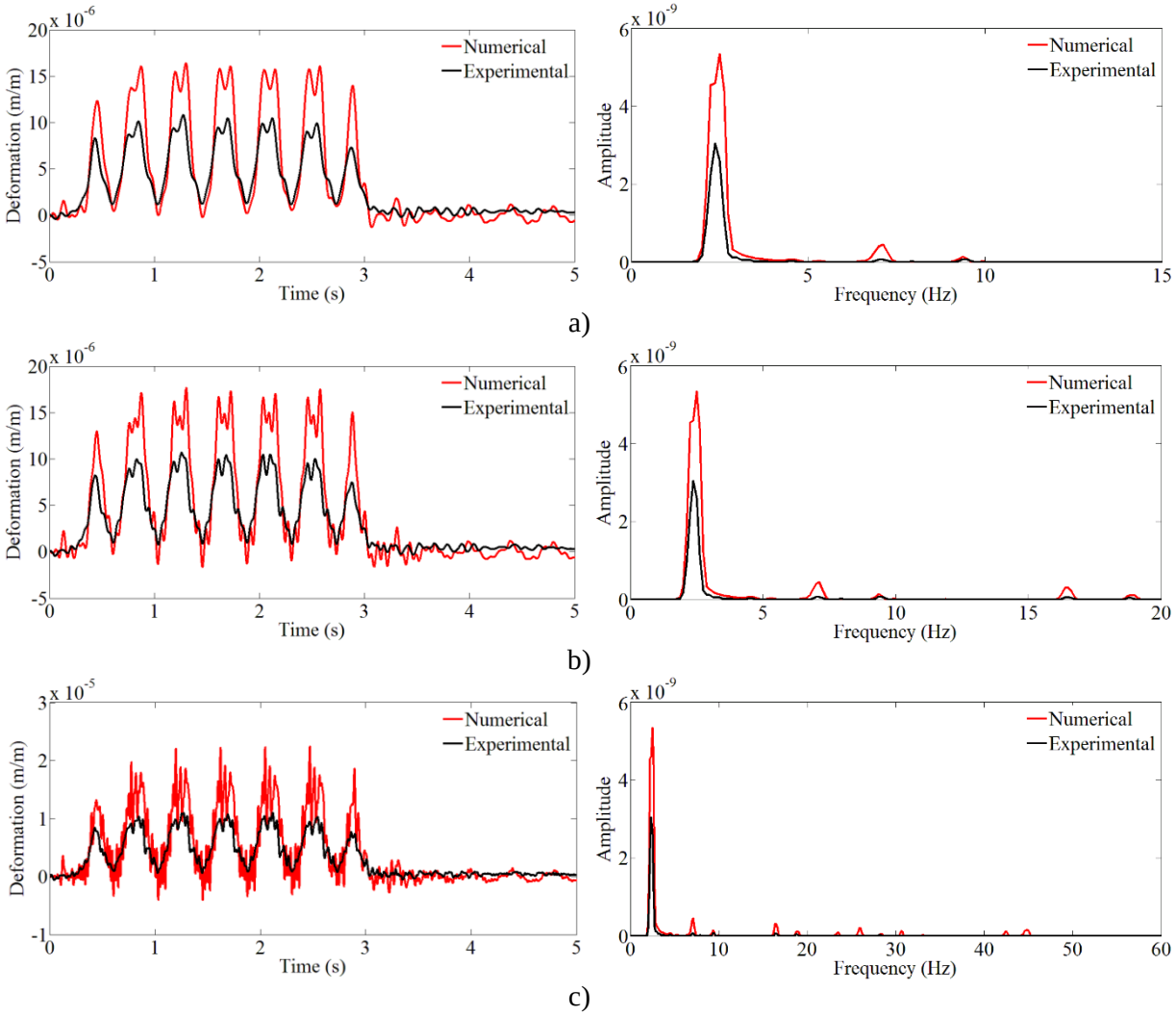

Figure A.4 – Comparison between measured and calculated deformation records, obtained in the position 4, for different cut-off frequencies: a) 15 Hz; b) 20 Hz; c) 60 Hz